Technische Universität München
TUM School of Engineering and Design

Optimal heuristic strategies for risk- and reliability-based inspection and maintenance planning

Elizabeth Yolande Lidia Bismut

Vollständiger Abdruck der von der TUM School of Engineering and Design der Technischen Universität München zur Erlangung des akademischen Grades einer

Doktorin der Ingenieurwissenschaften (Dr.-Ing.)

genehmigten Dissertation.

Vorsitz: Prof. Dr.-Ing. Christian Große

Prüfer*innen der Dissertation:

1. Prof. Dr. sc. techn. Daniel Straub
2. Prof. Matteo Pozzi, PhD
3. Assoc. Prof. Dr. Jannie Sønderkær Nielsen, PhD

Die Dissertation wurde am 28.06.2022 bei der Technischen Universität München eingereicht und durch die TUM School of Engineering and Design am 28.11.2022 angenommen.

Abstract

Well-planned inspection and maintenance (I&M) is essential to infrastructure management, to delay or prevent catastrophic failure and provide information about the health of the system. The cost of I&M typically represents a large share of the operating costs of infrastructure systems and, as the proportion of ageing infrastructure increases, there is a need to quantify the efficiency of I&M strategies and ultimately optimize I&M decisions.

In this thesis, we formulate the optimization of I&M actions as a sequential decision problem under uncertainty. In theory, the optimal I&M strategy perfectly balances the expected cost of I&M actions with the lifetime risk of system failure. However, this problem becomes intractable as the dimension of the system state and action space increases. We provide a description of the mathematical framework applied to I&M and give an overview of the state of the art in approximate dynamic programming solvers. We highlight limitations of existing methods for I&M planning problems, discuss the complexity of optimal strategies as identified by these methods and the problems linked to their practical implementation.

To overcome these limitations, we propose a framework for optimal risk- and reliability-based I&M planning for complex, multi-component systems. We describe I&M strategies with a heuristic, i.e., a parametrized set of rules. The optimal heuristic strategy minimizes the total expected cost within the explored set of strategies. In an adaptive feature, we show that parametrized strategies are quantifiably improved as more information on the system is collected and included in the decision framework. We discuss possible heuristics for I&M planning and assess their efficiency based on the value of information concept. The assessment of heuristic strategies relies on sampling I&M histories to compute the lifetime risk of failure and the time-dependent reliability of the system. Stochastic optimization methods for finding the optimal heuristic parameter values are suggested based on the cross-entropy method and surrogate-based optimization.

The modeling choices and assumptions for the framework implementation are discussed, along with their impact on the resulting optimal I&M decisions. First, we interpret and connect different probabilistic models for inspection quality within a unifying framework and provide insight into how these models should be learned, calibrated, and applied. Then, we provide the building blocks for constructing the stochastic models of deterioration for multi-component systems. We review time-dependent reliability analysis methods and present an approximation using a hierarchical dynamic Bayesian network model.

With two numerical examples of risk- and reliability-based I&M optimization – a steel frame subject to fatigue and a nuclear feeder system with 480 pipes subject to corrosion, we demonstrate the versatility and usability of the heuristic optimization framework. It enables the inclusion of operational constraints, fosters the improvement of current I&M practice and yields explainable strategies.

Inhaltsangabe

Eine gut geplante Inspektion und Wartung (I&M) ist für das Infrastrukturmanagement von wesentlicher Bedeutung, um katastrophale Ausfälle zu verzögern oder zu verhindern und Informationen über den Zustand des Systems zu liefern. Die Kosten für I&M machen in der Regel einen großen Teil der Betriebskosten von Infrastruktursystemen aus. Da der Anteil der alternden Infrastruktur zunimmt, besteht die Notwendigkeit, die Effizienz von I&M-Strategien zu quantifizieren und letztendlich I&M-Entscheidungen zu optimieren. In dieser Arbeit formulieren wir die Optimierung von I&M-Maßnahmen als ein sequentielles Entscheidungsproblem unter Unsicherheit. In der Theorie balanciert die optimale I&M-Strategie die erwarteten Kosten der I&M-Maßnahmen mit dem Risiko eines Systemausfalls. Dieses Problem wird jedoch unlösbar, wenn die Dimension des Systemzustands- und Aktionsraums wächst. Wir beschreiben die mathematischen Grundlagen des Entscheidungsproblems im Kontext von I&M und geben einen Überblick über den Stand der Forschung zu Lösungsansätzen, welche auf approximativer dynamischer Programmierung beruhen. Wir zeigen die Grenzen der bestehenden Methoden für I&M-Planungsprobleme auf und besprechen die Komplexität der durch diese Methoden gefundenen optimalen Strategien sowie die mit deren praktischer Umsetzung verbundenen Probleme.

Um diese Einschränkungen zu überwinden, schlagen wir einen neuen Ansatz zur optimalen risiko- und zuverlässigkeitsbasierten I&M-Planung für komplexe Mehrkomponentensysteme vor. Wir beschreiben I&M-Strategien mit einer Heuristik, d.h. mit einem parametrisierten Satz von Regeln. Die optimale heuristische Strategie minimiert die erwarteten Gesamtkosten innerhalb der untersuchten Menge von Strategien. Wir entwicklen einen adaptiven Ansatz und zeigen, dass dieser parametrisierte Strategien quantifizierbar verbessert, wenn mehr Systemnformationen verfügbar und in die Lösung miteinbezogen werden. Wir erörtern mögliche Heuristiken für die I&M-Planung und bewerten deren Effizienz basierend auf dem value-of-information-Konzept. Die Bewertung heuristischer Strategien beruht auf der Simulation zufälliger I&M-Verläufe, anhand derer das Ausfallrisiko und die zeitabhängige Systemzuverlässigkeit geschätzt werden. Wir entwickeln Lösungsverfahren zur Ermittlung optimaler Strategie-Parameter, welche auf der Cross-Entropy-Methode und Ersatzmodell-basierter Optimierung fußen.

Wir diskutieren die unserem Ansatz zugrunde liegenden Modellannahmen und deren Einfluss auf die resultierenden optimalen I&M-Entscheidungen. Wir entwickeln eine vereinheitlichte Formulierung und Interpretation verschiedener probabilistischer Modelle für die Inspektionsqualität und leiten hieraus ab, wie diese Modelle gelernt, kalibriert und angewendet werden sollten. Anschließend diskutieren wir die Komponenten stochastischer Schädigungsmodelle für Mehrkomponentensysteme. Wir geben einen Überblick über Methoden der zeitabhängigen Zuverlässigkeitsanalyse und formulieren eine auf hierarchisch aufgebauten dynamischen Bayes'schen Netzwerken basierende Approximation.

Wir demonstrieren die Vielseitigkeit und Anwendbarkeit unseres heuristischen Optimierungsansatzes anhand zweier numerischer Beispiele für risiko- und zuverlässigkeitsbasierte I&M-Optimierung – einem Stahlrahmen unter Ermüdung und einem nuklearen Versorgungssystem mit 480 Rohren, welche Korrosion ausgesetzt sind. Unser Ansatz ermöglicht die Einbeziehung operationeller Randbedingungen, fördert die Verbesserung der gegenwärtigen I&M-Praxis und liefert interpretierbare Strategien.

Acknowledgements

This thesis concludes six years of research within the Engineering Risk Analysis group. Behind this work, I must acknowledge and thank an entire scientific family, without whom this achievement would not have been possible.

To Daniel, thank you for welcoming me into this group and for six years of weekly supervision and conversations. I am grateful for your patience, encouragements and guidance, and for challenging me in periods of doubt. I could not have wished for a better supervisor.

I thank Matteo Pozzi for the warm reception within his research group at Carnegie Mellon University – I hope I will have the opportunity to visit Pittsburgh again under kinder temperatures – and for awakening my interest in research fields which enriched my understanding of my own topic.

I thank Mahesh Pandey for sharing his knowledge and for the very enjoyable and fruitful collaboration. I also gratefully acknowledge the discussions and resulting collaborations with Jorge Mendoza, who completed the frightful task of reading, understanding and improving thousands of uncommented lines of code.

This research adventure would not have been as enjoyable without the moral, technical and scientific support of my colleagues, office-companions and now enduring friends, Felipe, Sebastian, Max E and Jonas. I cannot do justice to all your contributions. Truly, thank you.

To the ERA family, 2016 to 2022: Thank you for being there, for finding my thesis title, for the yoga lessons, and for the good advice.

I thank my Mom and Dad for thinking of me (it works!) and for the corrections and advice, and my brothers David & Gab for watching over me from Paris.

You come last, but you are first. Thank you, Lukas, for your love and eternal patience. I will come home now.

Finished in Senigallia, June 2022

Contents

List of Publications vi

1. Introduction 1
   1.1. Context 1
   1.2. Motivation 3
   1.3. Scope of work 4
   1.4. Structure of the thesis 5

I. The foundations 7

2. Sequential decision problems under uncertainty 9
   2.1. I&M planning is a sequential decision problem 9
   2.2. Bayesian decision analysis: a generic decision problem 10
   2.3. Optimal I&M planning and SDP under uncertainty 20
   2.4. A classical approach to SDPs: MPD, POMPD and belief-MDP 25
   2.5. Limitations of the POMDP formulation for I&M planning of large infrastructure 35

3. Heuristic adaptive planning 39
   3.1. Peering into the black box 39
   3.2. Heuristic approach to direct policy search 41
   3.3. Adaptive planning 42
   3.4. Heuristics for I&M planning 43
   3.5. Stochastic computation of strategy cost 48
   3.6. Noisy optimization method for optimal heuristic planning approach 53
   3.7. Summary and future investigations 57

4. A unifying review of models of NDE quality 61
   4.1. NDE models for I&M planning 61
   4.2. A unifying framework for NDE quality 63
   4.3. NDE systems and decision analysis 72
   4.4. Example 1: Hypothetical NDE system 73
   4.5. Example 2: Half-cell potential measurement for corrosion detection 82
   4.6. Summary 89

5. Time-dependent reliability of deteriorating systems 93
   5.1. Time to failure of a maintainable, non-repairable system 93
   5.2. Models of deterioration processes 96
   5.3. Models at the system level 101
   5.4. Time-variant reliability analysis: methods and case studies 103
   5.5. Summary and limitations 111

II. Heuristic methods for infrastructure planning: Applications 115

6. Adaptive I&M planning of a steel frame subject to fatigue 117
   6.1. Introduction 117
   6.2. Structural model 118
   6.3. Deterioration model 118
   6.4. Inspection and repair model 119
   6.5. Costs of I&M actions 120
   6.6. Heuristic parameter choice 120
   6.7. Optimization set up and computation 121
   6.8. Results 122
   6.9. Summary 126

7. Reliability-based I&M planning of a nuclear feeder piping system 129
   7.1. Introduction 129
   7.2. Inspection and maintenance of a piping system 131
   7.3. Reliability-constrained I&M strategy 133
   7.4. Reliability-based heuristic planning 137
   7.5. Models of pipe deterioration and inspection and repair models 140
   7.6. Piping system reliability 142
   7.7. Numerical investigation: I&M planning at the beginning of service life 145
   7.8. Summary 154

8. Conclusion and outlook 157
   8.1. Conclusion 157
   8.2. Originality of work 159
   8.3. Outlook 159

III. Appendices 161

A. Prioritization Index for component inspection 163

B. Estimation of the annual risk of failure 165

C. Solution of the two-step decision problem 169

D. Hierarchical DBN inference algorithm 175

E. Effect of the discretization scheme on the accuracy of the DBN 181

F. Parameters of the fatigue deterioration model 185

G. Simplified flow accelerated corrosion predictive model 189

H. Nomenclature 191

References 193

List of publications

This thesis contains excerpts from articles that were published or submitted for publication as part of Elizabeth Bismut's doctoral research. Elizabeth Bismut is the main author of these articles, which are listed below:

(1) Bismut, E., Straub, D., and Pandey, M. (2022). "Inspection and maintenance planning of a feeder piping system". In: *Reliability Engineering & System Safety* 224, p. 108521.

(2) Bismut, E. and Straub, D. (2022). "A unifying review of NDE models towards optimal decision support". In: *Structural Safety* 97, p. 102213.

(3) Bismut, E. and Straub, D. (2021). "Optimal adaptive inspection and maintenance planning for deteriorating structural systems". In: *Reliability Engineering & System Safety* 215, p. 107891.

Article (3) appears in Chapters 2, 3, 5 and 6, (2) appears in Chapters 2 and 4 and (1) is present in Chapter 7.

Despite not being included in this thesis, other works and collaborations are listed below:

– as first author

  - Bismut, E. and Straub, D. (2019). "Direct policy search as an alternative to POMDP for sequential decision problems in infrastructure planning". In: *13th International Conference on Applications of Statistics and Probability in Civil Engineering, ICASP13*. ISBN: 9791196712501.
  - Bismut, E. and Straub, D. (2018b). "Inspection and maintenance planning in large monitored structures". In: *Proc 6th International Symposium on Reliability and Engineering Risk Management (ISRERM)*.
  - Bismut, E. and Straub, D. (2018a). "Adaptive Direct Policy Search for Inspection and Maintenance Planning in Structural Systems". In: *Sixth International symposium on Life-Cycle Civil Engineering 2018, IALCCE*.
  - Bismut, E., Luque, J., and Straub, D. (2017). "Optimal prioritization of inspections in structural systems considering component interactions and interdependence". In: *12th International Conference on Structural Safety & Reliability, ICOSSAR 2017*, pp. 2260–2269.

– as co-author

  - Holdorf Lopez, R., Bismut, E., and Straub, D. (2022). "Stochastic efficient global optimization with high noise variance and mixed design variables". In: *Journal of the Brazilian Society of Mechanical Sciences and Engineering* 45.1, p. 7. ISSN: 1806-3691.

- Mendoza, J., Bismut, E., Straub, D., and Köhler, J. (2022). "Optimal life-cycle mitigation of fatigue failure risk for structural systems". In: *Reliability Engineering & System Safety* 222, p. 108390. ISSN: 0951-8320.
- Mendoza, J., Bismut, E., Straub, D., and Köhler, J. (2021). "Risk-Based Fatigue Design Considering Inspections and Maintenance". In: *ASCE-ASME Journal of Risk and Uncertainty in Engineering Systems, Part A: Civil Engineering* 7.1, p. 04020055. ISSN: 2376-7642.
- Straub, D., Bismut, E., Depina, I., and Papaioannou, I. (2021). "Stochastische Optimierung mittels Cross Entropy: Methodik und Anwendungen". In: *Proc. Baustatik-Baupraxis 14*.
- Straub, D., Schneider, R., Bismut, E., and Kim, H.-J. (2020). "Reliability analysis of deteriorating structural systems". In: *Structural Safety* 82, p. 101877. ISSN: 0167-4730.
- Mendoza, J., Köhler, J., Bismut, E., and Straub, D. (2019). "Integrated Life-cycle Decision Framework for Structural Systems". In: *Structural Health Monitoring 2019*.
- Straub, D., Chatzi, E., Bismut, E., Courage, W., Döhler, M., Faber, M. H., et al. (2017). "Value of information: A roadmap to quantifying the benefit of structural health monitoring". In: *12th International Conference on Structural Safety & Reliability, ICOSSAR 2017*.

Chapter 1

Introduction

1.1. Context

Civil and structural assets naturally deteriorate due to mechanisms such as corrosion or fatigue. These can decrease the structural performance and potentially lead to structural failure. Timely interventions on the structure, such as maintenance, repair or replacement of structural components, can offset the effects of deterioration and aging, at a cost to the operator. These intervention costs can represent a significant part of the operation and maintenance budget, especially if not properly planned. As an example, for wind turbines, Nielsen and Sørensen (2010b) and Röckmann et al. (2017) report that up to 30% of the cost of energy is spent on operation and maintenance of the structure.

The optimal planning of these interventions is hindered by the large uncertainty associated with deterioration processes. The main reasons are the variable and uncertain production and environmental factors and material properties (Irving and McCartney, 1977; Wirsching and Chen, 1988; King, 1998; Newman Jr, 1998; Melchers, 2003a). Inspection and monitoring data can reduce this uncertainty and inform future maintenance decisions (Thoft-Christensen and Sørensen, 1987; Enright and Frangopol, 1999; Straub, 2004; Straub and Faber, 2005, 2006; Nielsen and Sørensen, 2015). Hence, inspection and maintenance (I&M) is an essential part of the structural integrity management.

We can identify three main approaches to I&M planning. *Rule-based* (or systematic) planning is the most common approach to I&M. It constrains the operator to follow certain principles and leaves little leeway in modifying the prescribed I&M actions. In *reliability-based* planning, the interventions must ensure that a certain reliability level is maintained. In *risk-based* planning, an I&M plan must trade-off the uncertainty and consequences of failure (i.e., collapse of the structure) for the costs of mitigating actions. Overall, a good I&M plan would maximize the expected rewards (e.g., increase in system reliability) while minimizing the expected I&M cost over the lifetime of the asset.

I&M strategies for infrastructure have been around long before decision making under uncertainty was formalized in the middle of the 20^{th} century (Raiffa and Schlaifer, 1961). Covello and Mumpower (1985) give a fascinating and detailed account on risk perception and risk-mitigating strategies among Mesopotamian civilizations in 3200 BC until the emergence of probabilistic and uncertainty concepts in the 17^{th} century, applied to a range of topics such as epidemic management, natural hazards protection and structural safety. During the Roman empire, records show that the development of extensive infrastructure (e.g., aqueducts, sewage

systems) was accompanied by the assignment of maintenance teams, usually slaves, that performed routine inspections and repairs (Deming, 2020). One could argue that the principle of maximum utility, central to decision analysis, existed before Bernoulli's work in a primitive form since the 4$^{\text{th}}$ century within the maxim by Augustine of Hippo: "*Quod amplius nos delectat, secundum id operemur necesse est*; Act we must in pursuance of what gives us most delight" (Arnold, 1883). Risks were, however, not quantified as such. Covello and Mumpower (1985) show that modern probability and decision theories anchored themselves firmly with the "increasing prevalence of the idea that injuries, deaths, and diseases are not acts of God to be fatalistically accepted, but avoidable events subject to some degree of human control". In an analogy with game theory, Luce and Raiffa (1989) imagine Nature as a player behind the realization of these random events.

The 1940s witnessed the emergence of operations research (OR) and, with it, a new field of study focusing on the optimization of decisions under uncertainty. Duff (2002), Powell (2011), and Sutton and Barto (2018) comprehensibly retrace the history of the body of research stemming from the works of Bernoulli and Wald (1947). Notably, this optimization problem has been approached with different research perspectives and different fields of application in mind, such as scheduling problems or stochastic sequential decision problems (SDPs) (Raiffa and Schlaifer, 1961; Benjamin and Cornell, 1970; Straub, 2004; Kochenderfer, 2015). While I&M planning clearly belongs to such types of problems, I&M interventions on infrastructure have traditionally been based on industry standards, expert knowledge and empirical studies of the underlying mechanisms of deterioration. Until today, I&M plans are developed in an ad-hoc manner, with little harmonization of practice and risk quantification in place (European Commission, 2020). Among the reasons why this is the case, we must acknowledge that deterioration can only be predicted to a limited extent in engineering practice, even though the scientific literature abounds with stochastic models of deterioration, from corrosion to fatigue (e.g., Southwell et al., 1979; Yang, 1994; Newman Jr, 1998; Melchers, 2003a). Furthermore, the sheer size of the infrastructure, impacting the dimension of the associated I&M planning problem, is a significant computational obstacle to the implementation of classical decision theory. Finally, efforts towards a formal decision analysis had not been economically motivated until the end of the 20$^{\text{th}}$ century, simply because aging infrastructure was not as widespread an issue.

However, rule-based I&M plans currently implemented may no longer be cost-efficient nor sufficient to ensure an appropriate safety level. Increasing trends in specialized labor and material costs are fast changing the dynamics of the planning problem. The reliability requirements on infrastructure cannot be addressed solely in the design phase in a cost-efficient manner, and large infrastructure systems are expected to be operated over a longer period of time. Similarly, aging infrastructure is required to be maintained and operated past their intended service life. The past decades have also seen changes in regulations, often through fatal accidents, which have triggered stricter or new I&M regulations and have pushed towards targeted mitigating actions: The Alexander L. Kielland offshore platform collapse in 1980 called for including fatigue failure in reliability analysis and motivated the development of

risk-based inspection (RBI) planning in that field (Straub, 2004); The nuclear accident at Surry Point in 1986 led to a review of corrosion management in nuclear power plants (Wu, 1989). Recently, the catastrophic collapse of the Genoa bridge in 2018 raises the question of how to control and approve I&M plans. It highlights a misunderstanding of standards of maintenance and a lack of rigorous assessment of inspection information (Morgese et al., 2020). More generally, there is a real risk of misinterpretation (or inconsistent interpretation) of inspection and monitoring signals and too much reliance on past observation of no failure when dealing with structures designed to be highly reliable. An example situation of such a misled operation is the cable-car failure in North Italy in May 2021, where triggered alarm systems were deactivated to avoid disruption of operations, instead of the source of the alarm being thoroughly investigated (Giuffrida, 2021). Such imprudent misjudgments may be symptomatic of a lack of accessible decision tools for I&M planning.

1.2. Motivation

Numerous algorithms have been proposed towards the general solution of stochastic SDPs, to which I&M planning belongs. The founding algorithms were developed in the 1950s in the field of OR to tackle the growing demand in storage associated with production automation, but also for a large variety of problems, such as the management of a baseball team (Howard, 1960). Bellman and Howard described solution strategies for a specific class of SDP, the (fully observable) Markov decision processes (MDPs), based on Bellman's dynamic programming tool (Bellman, 1957a,b; Howard, 1960). Raiffa and Schlaifer (1961) formally included the uncertainty associated with the information acquired during the decision process, paving the way to the study of partially observable Markov decision processes (POMDPs) (Åström, 1965; Kaelbling et al., 1998). The MDP and POMDP approaches attempt to provide a universal plan for decision problems where the process is Markovian, and, in theory, accounts for all possible scenarios (Kochenderfer, 2015). The I&M planning problem can be formulated within the POMDP framework, although the dimensions of the resulting problem are typically very large for multi-component systems. Unfortunately, finite-horizon POMDP become intractable as the time and space dimensions of the problem increase (Papadimitriou and Tsitsiklis, 1987).

Approximate and tractable offline and online solutions for POMDPs are available and have been applied to selected I&M planning problems (Durango and Madanat, 2002; Nielsen and Sørensen, 2014; Papakonstantinou and Shinozuka, 2014; Memarzadeh and Pozzi, 2016; Schöbi and Chatzi, 2016; Papakonstantinou et al., 2018). These approaches perform well when the dynamics of the problem are smooth, and where the dimensionality of the problem remains moderate. However, they scale poorly for large multi-component systems reliability problems, since this assumption cannot be ensured for real-life structural reliability problems where the state-space can be larger than 10^{100} (Bismut et al., 2017).

Significant advances have recently been made in the field of deep reinforcement learning, in particular using deep neural networks, which promises to address the complexity of SDPs and the I&M planning problem in a computationally efficient manner (e.g., Andriotis and

Papakonstantinou, 2019). However, as for the POMDP-based solvers, there remains the challenge of interpreting the optimal strategies as identified by these methods, which can hinder its applicability and lead operators to deviate from it, however misguided they may be.

1.3. Scope of work

To overcome these limitations, we propose in this work a rigorous framework for optimal risk-based and reliability-based I&M planning, which relies on a parametrized description of I&M strategies. In the context of I&M planning, the engineering understanding allows the identification of suitable functional forms of the rules underlying I&M decisions. We call these *heuristics*. For example, a simple heuristic is to perform an inspection campaign whenever the reliability of the structure falls below a threshold. In the proposed framework, the optimization of the I&M strategy is performed over a few heuristic parameters associated with the chosen heuristics.

Most existing RBI planning methodologies are based on such heuristic strategies, mostly in an ad-hoc manner (see, e.g., Thoft-Christensen and Sørensen, 1987; Lam and Yeh, 1994; Faber et al., 2000; Straub, 2004; Moan, 2005; Nielsen and Sørensen, 2014). In the context of optimizing inspections for single structural components, it has been found that heuristics lead to solutions that are very close to the optimum POMDP solutions in terms of the resulting expected total life-cycle costs (Nielsen and Sørensen, 2011; Luque and Straub, 2013). However, these methodologies perform the optimization component-by-component, without considering the interaction among components. Hence it cannot be ensured that the resulting plans are optimal at the system level. In fact, Luque and Straub (2019) show that component-based optimization can lead to strongly sub-optimal I&M plans. Straub (2004) and Straub and Faber (2005) consider an extension to address system effects in a simplified manner.

Luque and Straub (2019) extended the heuristic approach to a system-level I&M planning, which accounts for the interdependence among components. The methodology relies on the computation of the system reliability by means of a dynamic Bayesian network (DBN) model developed in (Straub, 2009; Luque and Straub, 2016). They evaluate the expected cost of selected system-level I&M plans, however, without performing a formal optimization. The heuristic framework in presented in this work provides optimized heuristic I&M strategies for multi-component deteriorating systems. It also enables an adaptive feature, whereby re-optimizing the heuristic parameters, once new information is available, leads to quantifiably improved I&M plans.

Throughout this work, we strive to highlight the wide range of interdisciplinary resources in order to motivate the reader and analyst to learn and take inspiration from approaches to sequential decision making, that have been developed for a specific field of application. These various perspectives help one understand the diversity in terminology pointing to similar concepts, thus, they facilitate our reading and interpretation of existing methods. Finally, we

hope that this thesis contributes to provide tools directed to the practitioner for a rigorous but flexible analysis of the decision context.

1.4. Structure of the thesis

This thesis is structured in two parts. In the first part (Chapters 2 to 5), we progressively introduce the elements of the proposed heuristic optimization framework to address the sequential decision problem that is I&M planning. In the second part, (Chapters 6 and 7), we demonstrate the framework and find optimal heuristic I&M strategies for two types of deteriorating systems.

Chapter 2 presents the premises of the general planning problem, the equations associated with the optimization, then, reviews the existing POMDP approximations for its solution. While this last part is not required to understand the methodology introduced in Chapter 3, it motivates the proposed heuristic description of the strategy space.

The heuristic planning methodology then described in Chapter 3 is applicable to multi-component systems. It additionally enables adaptive planning, whereby the I&M plan is modified as new information becomes available through inspections and monitoring. The I&M plans are evaluated in terms of expected total life-cycle I&M cost and failure risk. Heuristic parameters are proposed that prescribe inspection and repair times, and locations. The heuristic strategies are optimized by means of stochastic optimization methods, such as the cross-entropy method (Rubinstein and Kroese, 2017).

The proposed methodology requires that probabilistic models of the evolution of the deteriorating system and for the propagation of inspection information are available to the analyst. Chapters 4 and 5 address these model choices and discuss how they affect the resulting optimized I&M plan. In Chapter 4, we review the existing models of inspection quality, focusing on non-destructive evaluation (NDE). These models include probability of detection curves and receiver operating characteristic curves. We interpret the models within a unifying framework and show how they are connected. This framework provides insights into how these models should be learned, calibrated, and applied. We investigate and highlight how the choice of the model can affect the maintenance decisions taken on the basis of NDE results. In addition, we analyze the impact of experimental design on the performance of a given NDE system in a decision-making context.

Chapter 5 lays down the different pieces of the probabilistic model representing the system evolution, in order to evaluate the risk of system failure over time, updating it as more inspection results are obtained and mitigating actions are performed. First, the various descriptions of deterioration processes at the component level are introduced, then, the relationships between system and components are established. In this chapter, we review time-variant reliability methods and focus in particular on the hierarchical DBN model for multi-component systems originally presented by Luque and Straub (2016), which demonstrates good computational performance in the strategy optimization problem.

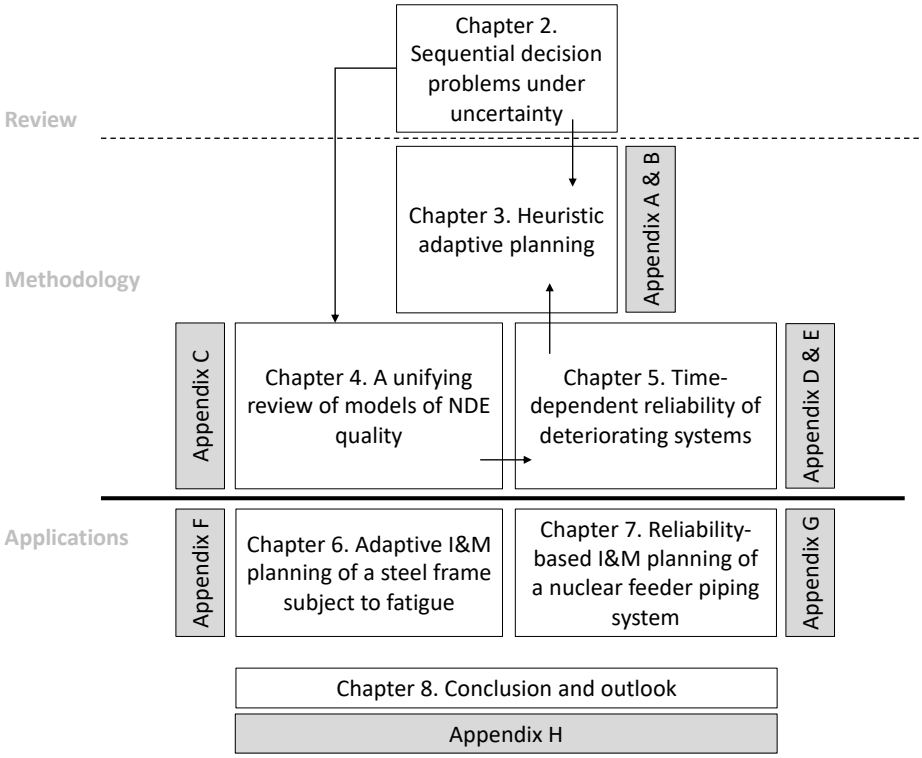

Figure 1.1 Structure of the thesis

In the numerical investigation part of the thesis, we apply the heuristic planning methodology to two problems. Risk-based I&M planning for a structural steel frame subject to fatigue is investigated in Chapter 6. In Chapter 7, we develop a reliability-based assessment for strategies of I&M planning for a nuclear feeder piping system with 480 pipes and we apply the heuristic approach to improve current I&M practice.

Finally, conclusion and outlook are summarized in Chapter 8. The connection between the different chapters is succinctly illustrated in Figure 1.1.

Part I.

The foundations

Chapter 2

Sequential decision problems under uncertainty

> As they say in Ekumenical School, when action grows unprofitable, gather information; when information grows unprofitable, sleep.
>
> *The Left Hand of Darkness*
> Ursula K. Le Guin

Parts of this chapter originate from Bismut, E. and Straub, D. (2021). "Optimal adaptive inspection and maintenance planning for deteriorating structural systems". In: *Reliability Engineering & System Safety* 215, p. 107891.

2.1. I&M planning is a sequential decision problem

Inspection and maintenance (I&M) planning is a crucial aspect of operating civil engineering infrastructures. Consider an offshore platform, which can be described as a superstructure supported by a steel frame anchored to the seabed. The operator must ensure the good functioning of the platform during its design service life and in particular the structural integrity of the support structure. Structural decay is a natural phenomenon, which has been extensively described in the literature (see Chapter 5). It can lead to cracks in critical points and eventually to the collapse of the platform. The operators of such structures can decide to repair (e.g., retrofitting, reinforcing, replacing) once, or with some regularity (e.g., every 5 years), parts of the structure in the hope that it mitigates the decay, at least locally. They also have at their disposal a team of expert inspectors who check for cracks in the structural members and report back their assessment of the integrity of the elements. If the offshore structure collapses, loss of life can ensue, as well as very high financial costs (e.g., contract penalties, reconstruction costs, legal consequences). On the other hand, inspection campaigns and maintenance operations involve paying for adequate workforce and materials, as well as possible loss of revenue from discontinued operations on the platform. The operator must decide when to schedule I&M campaigns, as well as what type of inspection and maintenance is carried out, and where in the structure. This decision-making scenario can be translated to all types of structures, such as bridges, wind turbines or power plants.

It is clear that early I&M decisions affect the state of the structure and the decisions at a later point of the structure's life. One must consider the full sequence of decisions over the service

life to evaluate their impact on operational costs and on the integrity of the structure. This planning problem is a *sequential decision problem* (SDP). A notorious difficulty associated with I&M planning is that the environment in which the decisions are taken is uncertain. This uncertainty affects the knowledge about the past, present and future state of the structure, the effect of an action on the system, and the information collected about the system.

These types of planning problems, also referred to as "stochastic optimal control", have been extensively studied in operations research (OR), including inventory planning (Strack and Pochet, 2010), hospital facility planning (Vora, 1974) and farm and livestock management (Yaron and Horowitz, 1972; Pourmoayed and Nielsen, 2019). SDPs are also at the core of game theory, motion planning in robotics and optimal stopping in economy. Each field of research has contributed approaches to finding solutions to the planning problem, which has led to a difference in terminology to designate the same entities.

In risk-based planning, a good I&M plan must trade-off the uncertainty and consequences of failure (e.g., collapse of the structure) against the actions and associated costs taken to reduce uncertainty and mitigate the occurrence of failure, and thus needs to account for changes in the uncertainty through inspection information. This chapter provides the fundamental concepts and tools to formulate the risk-based I&M planning optimization problem. Section 2.2 covers Bayesian decision analysis and the concepts of expected utility and value of information, applied to a generic decision problem. In Section 2.3, we set the premises of the SDP for I&M planning and extend the previous concepts to introduce the general equation. Section 2.4 gives a comprehensive overview of a major class of solvers for SDPs, based on the classical mathematical framework of Markov decision processes, and their associated computational complexity. Section 2.5 concludes on the challenges specific to the I&M planning problem and the limitations of existing solvers and motivates the methodology presented in Chapter 3.

2.2. Bayesian decision analysis: a generic decision problem

Before diving deeper into the complexity of SDPs, the trade-off in I&M planning is illustrated with a generic decision problem. The notations in this section are adopted from Raiffa and Schlaifer (1961).

2.2.1. The variables of the problems

The premises of the problem are introduced below.

- $\boldsymbol{\Theta}$ represents the state of the environment, or state of nature (Benjamin and Cornell, 1970). In Chapter 4, $\boldsymbol{\Theta}$ is also called the *condition*. It affects the consequences of decisions and is typically not known with certainty at the point of making a decision. For a structural system, it includes the structural capacity and the loads. When the state of a system depends on the state of multiple sub-systems, or components, $\boldsymbol{\Theta}$ also includes the state of the components.

- It can be practical to introduce F, which explicitly links the state $\mathbf{\Theta}$ to the actual consequences, for instance the failure of the system. This link can be deterministic (e.g., $\mathbf{\Theta}$ exceeds a threshold, a limit state is exceeded) or probabilistic. In this work, F is used to distinguish the binary states "failed" and "safe". In I&M planning, the failure event is often meant as structural failure (e.g., bridge collapse) but can also express non-compliance of the infrastructure with specific regulations or unfulfilled function.
- e designates the decision to collect information about the state $\mathbf{\Theta}$. Decision e includes what is inspected (e.g., the length of a crack, the presence of corrosion, the stress in a material), the manner this information is collected (e.g., in-situ visual inspection, a strain-gauge communicating with an information center), and the location in the system where this information is collected (e.g., specific welded connections in the structure). This characterization of e makes it a *non-destructive evaluation (NDE) system*, which is chosen by the decision maker. As the name suggest, NDE systems do not affect the state of the system $\mathbf{\Theta}$. e_0 – the "null experiment" – denotes the case when no information is collected.
- The outcome of the inspection defined by e is summarized in Z, the *observation*. The relationship between Z and state $\mathbf{\Theta}$ is affected by the choice e. Chapter 4 provides the framework of this relationship. Z is typically a multi-dimensional vector, where each entry corresponds to the inspection outcome of a component in a multi-component system.
- With information Z, the operator (decision-maker) can choose action A, among a (preset, or not) number of actions $a_0, a_1, ...a_m$, typically to mitigate the risk of failure. These actions include the "do nothing" action, a_0. In OR, actions are also termed "controls". The state of the system $\mathbf{\Theta}$ and action A both influence the failed or safe state of the system, F.

For example, the NDE system e is a human visual inspection for a crack of size $\mathbf{\Theta}$, the failure F occurs when the crack exceeds a threshold a_{cr}, the outcome Z is "detection" or "no detection" of a crack, and the possible actions A "repair" or "no repair".

> A quantity X is qualified as uncertain, when its value is unknown: either because it cannot be measured exactly; it cannot be or has not been observed in the present; or its value depends on a chain of events which are yet to occur. This quantity can be modeled by a random variable, X. It is associated with a probability measure, which is in general denoted by $p(x)$. If the domain of X is continuous, the probability density function (PDF) is denoted by $f_X(x)$; if X takes discrete states, the probability mass function (PMF) is denoted by $\Pr(X = x)$. Some graphical models such as the Bayesian network (see Section 2.2.2.3) traditionally use the discrete notation without necessarily implying that the variable is discrete. When the distinction is necessary to the application of a method, the continuous or discrete properties of the variables are clearly stated. When a conditioning variable Y is introduced, the corresponding conditional probability objects are denoted by $p(x|y)$, $f_{X|Y}(x)$, and $\Pr(X|Y)$.

Choices on e and A are fully known to the decision maker. In contrast, there is uncertainty associated with $\mathbf{\Theta}$. Thus, $\mathbf{\Theta}$ is modeled as a random variable with probability distribution

$p(\boldsymbol{\theta})$. The information Z is known at the point it is obtained, however at the point of planning the decision, the observation Z is a-priori unknown and is also modeled as a random variable, with probability distribution $p(z)$. The fact that uncertainty is expressed with a probabilistic model is essential to Bayesian decision theory. In this work, it is assumed that a probabilistic model for $\boldsymbol{\Theta}$ and Z is available to the decision maker. This model and its implications are further discussed in Section 2.2.3.2. Chapter 4 addresses the relationship between $\boldsymbol{\Theta}$ and Z.

2.2.2. Utility and graphical representations

2.2.2.1. Decision tree

We can represent the possible sequence of events and decision with a *decision tree*, a graphical representation stemming from game theory (Raiffa and Schlaifer, 1961; Luce and Raiffa, 1989). In Figure 2.1, the round nodes indicate random variables and the square nodes the decisions.

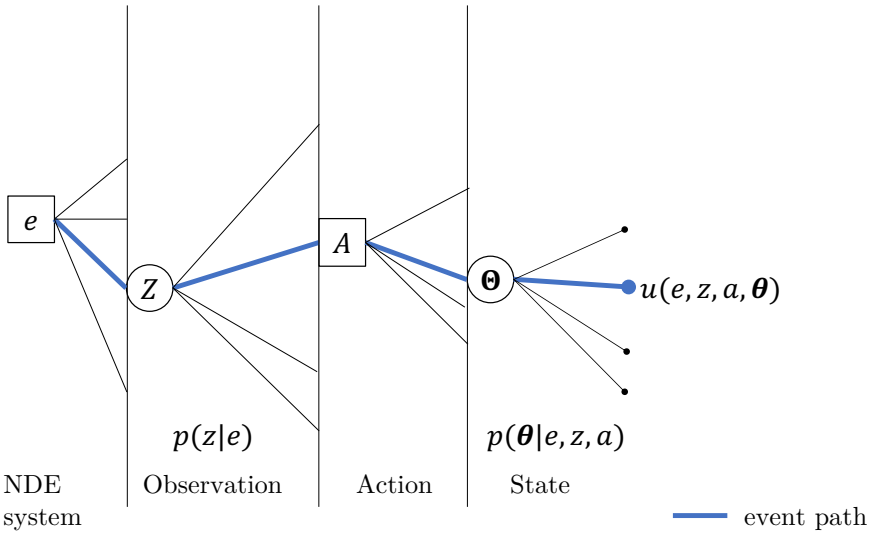

Figure 2.1 Decision tree for a simple decision problem. The square nodes indicate choices made by the decision maker. The round nodes denote the quantities with uncertain outcome. An event path connects the root of the tree with a terminal leaf. Each leaf specifies the utility associated with the event path (see Section 2.2.2.2)

An *event path* is obtained by starting from the root of the tree and ending at a terminal leaf. The tree structure ensures that a unique path connects a leaf to the root. The number of paths can in principle be infinite –non-countable or countable– or finite. In general, not all event paths have the same probability of occurrence. To represent this fact, each branch is accompanied by its probability of occurrence, which depends on the branches it originates from. Therefore, in this tree, the probabilities of the branches associated with a realization of $\boldsymbol{\Theta}$ are expressed as a function of the parent branches, e, a, and z, in the form of a conditional probability $p(\boldsymbol{\theta}|e, z, a)$ (see Section 2.2.2.4).

2.2.2.2. Utility, loss and costs

To complete the decision tree, the end leaf is attributed a quantity, the *utility* of the associated root-to-leaf path, $u(e, z, a, \boldsymbol{\theta})$. The concept of utility was introduced by Von Neumann and Morgenstern (1953) as a metric of the preference of a decision maker and is fundamental to decision theory. In general, the determination of the utility function u is a complex endeavor, as it aims to describe the behavior of the decision-maker in different situations. For more details on utility theory and axioms, the reader can refer to the text by Luce and Raiffa (1989). In the context of I&M planning, the utility associated with a path can be expressed as a loss in monetary terms, which reflects the costs of I&M actions and the consequence of failure of the system (Benjamin and Cornell, 1970).

In this work, the utility function is given the following attributes. Firstly, we assume that the utility function is linear over the monetary range considered, which characterizes the decision-maker as risk-neutral. Secondly, the utility of an event path can be decomposed into the sum of independent utilities, namely the loss incurred directly from decisions e and a and the loss due to the consequences of failure. The linear additive property of utility is commonly assumed in engineering applications, including in RBI planning (Benjamin and Cornell, 1970; Straub, 2004) and is advantageous when applying linear operators, such as the expectation operator, see Section 2.2.3. It is furthermore assumed that the benefits generated by the correct functioning of the system are not affected by how it is operated and are therefore omitted from the evaluation of the total cost. The path utility is

$$u(e, z, a, \boldsymbol{\theta}) = u_e(e, z) + u_a(a) + u_{\boldsymbol{\theta}}(\boldsymbol{\theta}) \tag{2.1}$$

To facilitate the interpretation of the results, the term *cost* is adopted as synonym of negative utility. A *cost model* consists of all the costs resulting directly from a decision and from failure (or any consequence related to the state of the system). Each action a_m is assigned a cost of execution, c_{a_m}, such that $u_a(a_m) = -c_{a_m}$; action a_0 "do nothing" has an associated cost of 0. When the state F is explicitly introduced, the consequence of failure is c_F. $c_e = -u_e(e, z)$ is the direct cost (or investment) of implementing NDE system e (e.g., cost of mobilizing a team of inspectors), and typically does not depend on the inspection outcome z. Notably, we assume that the cost of not collecting information is zero, $c_{e_0} = 0$. For simplicity of notation, we write $u(e, z, a, \boldsymbol{\theta}) = u(e, a, \boldsymbol{\theta})$.

For an event path, the notation $C_{\text{tot}}(e, a, \boldsymbol{\theta})$ replaces $-u(e, a, \boldsymbol{\theta})$. The cost C_{tot} is therefore the sum of cost components corresponding to the negative additive utilities of Equation (2.1). These costs correspond to the monetary loss associated with the implementation of NDE system e (e.g., cost of inspecting the system), with executing actions a (e.g., repairing a component) and with the consequences associated with state $\boldsymbol{\theta}$ (e.g., the cost of failure).

2.2.2.3. Bayesian network and influence diagram

Raiffa and Schlaifer (1961) recognize that the decision tree representation can very quickly become cumbersome, as the number of event paths increasing polynomially with the number of

possible states and observed values. The interactions and relationships between the parameters of the decision problem can be represented more compactly with an *influence diagram* (ID), also called decision network. The features of an ID are detailed in (Kochenderfer, 2015), and summarized below.

An ID is based on a Bayesian network (BN), which represents the probabilistic relationship between random variables, here $\boldsymbol{\Theta}$, Z and F (Jensen et al., 2007). A BN is a directed acyclic graph, in which the random variables are represented as round nodes (chance nodes). Directed edges (called conditional edges) connect the variables and represent the probabilistic dependence structure between variables. Parent nodes are those from which emerges at least one edge; children nodes have at least one parent. Typically, but not necessarily, the arrows indicate a causal relationship. A BN with nodes X_i, $i \leq N$, is associated with conditional probabilities of the nodes X_i given their parent nodes $pa(X_i)$. The joint probability distribution of all random variables in the BN is obtained by applying the chain rule:

$$\Pr(X_1, X_2, ..., X_N) = \prod_{i=1}^{N} \Pr(X_i|\text{pa}(X_i)), \tag{2.2}$$

where $\Pr(X_i|pa(X_i))$ is conditional probability of variable X_i given its parent variables in the network $\text{pa}(X_i)$. If $\text{pa}(X_i) = \emptyset$, $\Pr(X_i|\text{pa}(X_i)) = \Pr(X_i)$. Marginal probabilities can thereafter be computed from the joint probability:

$$\Pr(X_i) = \sum_{j \neq i} \Pr(X_1, X_2, ..., X_N). \tag{2.3}$$

The dependence structure of the variables is read in the BN by applying d-separation rules (Jensen et al., 2007). These rules state that two nodes X_i and X_j ($i \neq j$) are d-separated, i.e., probabilistically independent, if for all (non-directed) paths between the nodes, there is an intermediate node V, distinct from X_i and X_j, such that either (i) the connection is serial or diverging and the state of V is known (ii) or the connection is converging and the states of V and the children of V are not known. The types of connections are shown in Figure 2.2. The dependence structure directly influences the complexity of computing the joint, marginal or conditional probability distributions.

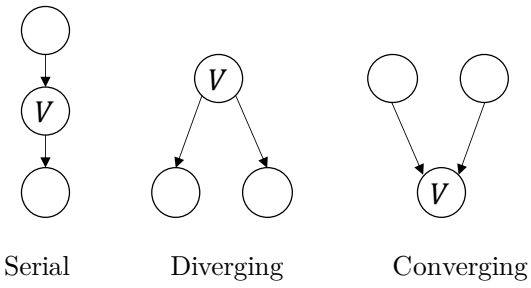

Figure 2.2 The three types of connections in a Bayesian network.

Posterior probabilities conditional on the observation of a node of the BN can be computed

using Bayes' rule. When the BN variables have a discrete and finite number of states, the BN probabilities $\Pr(X_i|\text{pa}(X_i))$ are summarized in conditional probability tables (CPT) and the inference operations correspond to the multiplication of multi-dimensional matrices. The use of a BN in I&M planning is detailed in Chapter 5 and for the application in Chapter 6.

To complete the ID, square decisions nodes are connected to the BN with arrows, either to indicate their effect on the chance nodes (conditional edge), or to indicate that the decision is made with the knowledge of the parent nodes (informational edge). Finally, the value of diamond-shaped utility node is determined by the outcomes of its parents, decision or chance nodes. The ID for the basic decision problem is shown in Figure 2.3. With multiple utility nodes, the diagram displays the additive decomposition of the utility discussed in Section 2.2.2.2, into cost of actions and consequence of failure.

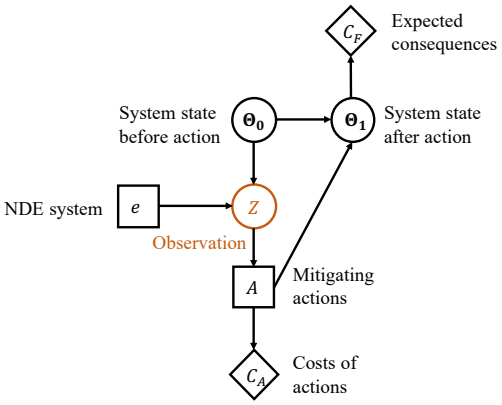

Figure 2.3 Influence diagram for a simple decision problem. This ID distinguishes explicitly the initial system state $\boldsymbol{\Theta}_0$, from which observation Z is obtained, and the system state affected by action A, $\boldsymbol{\Theta}_1$.

2.2.2.4. Bayesian analysis: effect of an observation z

The decision tree described in Section 2.2.2.1 requires the evaluation of the posterior probability of the state conditional on the observation and after the action has been carried out. Adopting the notation of the ID in Figure 2.3, this probability corresponds to $p(\boldsymbol{\theta}_1|e,z,a)$. It is obtained by integrating out the initial state $\boldsymbol{\Theta}_0$,

$$p(\boldsymbol{\theta}_1|e,z,a) = \mathbf{E}_{\boldsymbol{\Theta}_0|e,z}\left[p(\boldsymbol{\theta}_1|\boldsymbol{\theta}_0,a)\right], \tag{2.4}$$

where $\mathbf{E}_{\boldsymbol{\Theta}_0|e,Z}[\cdot]$ is the expectation with respect to $p(\boldsymbol{\theta}_0|e,z)$.

We examine the case when $a = a_0$, i.e., when the action "do nothing" does not affect the system state and $\boldsymbol{\theta}_1 = \boldsymbol{\theta}_0$. Equation (2.4) is reduced to $p(\boldsymbol{\theta}_1|e,z,a) = p(\boldsymbol{\theta}_0|e,z)$. In the following Equations (2.5) to (2.7), a and e are omitted[1] for clarity and $\boldsymbol{\theta} = \boldsymbol{\theta}_0$.

The amount of information provided by observation z about a certain $\boldsymbol{\theta}$ is given by a *likelihood function*, denoted by $\mathcal{L}(\boldsymbol{\theta};z)$. The likelihood corresponds to the conditional probability $p(z|\boldsymbol{\theta})$.

[1] The omission of e is not trivial and can cause a bias in the estimation of the conditional probability in sequential decision problems. A brief discussion on this selection bias is provided in Section 3.5.5.

Assuming that a probabilistic model, $p(\boldsymbol{\theta})$, is available, the posterior probability distribution of the condition $\boldsymbol{\Theta}$ is obtained with Bayesian analysis, as

$$p(\boldsymbol{\theta}|z) \propto \mathcal{L}(\boldsymbol{\theta}; z)p(\boldsymbol{\theta}). \tag{2.5}$$

The normalizing constant of Equation (2.5) is the model evidence, $p(z)$:

$$p(z) = \mathbf{E}_{\boldsymbol{\Theta}}\left[\mathcal{L}(\boldsymbol{\theta}; z)\right], \tag{2.6}$$

where $\mathbf{E}_{\boldsymbol{\Theta}}[\cdot]$ is the expectation with respect to $p(\boldsymbol{\theta})$.

One is typically interested in identifying a critical condition, or failure, F (see Figure 4.7). Conditional on the NDE outcomes, one obtains the posterior probability of this critical condition $\Pr(F|Z = z)$ as

$$\Pr(F|Z = z) = \frac{1}{p(z)}\mathbf{E}_{\boldsymbol{\Theta}}\left[\Pr(F|\boldsymbol{\theta})\mathcal{L}(\boldsymbol{\theta}; z)\right]. \tag{2.7}$$

Such reliability updating with likelihoods from NDE models was first investigated by Tang (1973), and many studies integrating reliability analysis with inspection models have been published (e.g., Madsen, 1987; Sindel and Rackwitz, 1996; Onoufriou and Frangopol, 2002; Straub, 2011). Chapter 4 reviews the different types of likelihood functions for NDE methods under a unifying framework.

It is important to note that Bayesian analysis can be performed only when a probabilistic model of the system state is available. The significance of this prior probabilistic model $p(\boldsymbol{\theta})$ for the decision analysis is discussed in Section 2.2.3.2.

2.2.3. The general optimization problem

Raiffa and Schlaifer (1961) formalized the decision problem under uncertainty[1] using expected utility theory and Bayesian analysis. Paraphrasing Bernoulli, the solution to the decision problem can be expressed as follows:

Rational decision making relies on the principle of maximizing the expected utility.

In this work, this is equivalent to minimizing the expected total costs (see Section 2.2.2.2).

It is common to find alternative formulations of the decision problem that combine the minimization of the expected cost as well as the variance of the cost. In reality, these formulations attempt to model the risk-avoidance of the decision-maker, while adopting a risk-neutral (linear) utility function. Strictly, the risk-avoidance should be reflected in the

[1] Luce and Raiffa (1989) use the term "risk" instead of "uncertainty" to designate the type of problems described in this chapter, and refer to decision-making under uncertainty where the probability of the outcomes is completely unknown, following the definitions by Knight (1921). Here a probabilistic model is assumed to be available to the decision maker, see Section 2.2.3.2.

utility function introduced in Section 2.2.2.2, and the above principle should remain untouched (Pozzi and Der Kiureghian, 2011).

2.2.3.1. Extensive and normal form

Raiffa and Schlaifer (1961) distinguish two ways to formulate the solution of the decision problem, also called the *preposterior analysis*: the extensive form (or backward induction) and the normal form.

In the *extensive form*, the optimization progresses from the leaves backwards to the root of the decision tree: the action is first optimized, for a given e and observation outcome z. The optimal action $a_{opt,e}(z)$ minimizes the conditional expected cost given e and z:

$$a_{opt,e}(z) = \arg\min_{a} \mathbf{E}_{\boldsymbol{\Theta}|Z,e,a}[C_{\text{tot}}(e, a, \boldsymbol{\theta})], \tag{2.8}$$

where a is chosen from the available actions. The loss is represented by the total cost C_{tot} and includes the action costs and the consequences of failure. $\mathbf{E}_{\boldsymbol{\Theta}|Z,e,a}[\cdot]$ is the expectation with respect to $p(\boldsymbol{\theta}|z, e, a)$ obtained from Equation (2.5). The optimal choice e_{opt} is then selected among the possible e, the condition on $a_{opt,e}(z)$ is omitted for clarity:

$$e_{opt} = \arg\min_{e} \mathbf{E}_{Z}\left[\mathbf{E}_{\boldsymbol{\Theta}|Z,e}[C_{\text{tot}}(e, a_{opt,e}(z), \boldsymbol{\theta})]\right]. \tag{2.9}$$

The preposterior analysis for the basic decision problem and the optimal selection of the NDE systems is demonstrated in Chapter 4.

In the *normal form*, the optimization is carried out simultaneously on e and on function d, or action rule, such that $a = d(e, z)$, instead of doing so sequentially. With this formulation the problem consists of a single optimization operation, even though it does not reduce the effort required to perform it (Luce and Raiffa, 1989). The problem in the normal form is expressed as

$$[e_{opt}, d_{opt}] = \arg\min_{e,d} \mathbf{E}_{\boldsymbol{\Theta},Z|e,d}\left[C_{\text{tot}}(e, d(e, z), \boldsymbol{\theta})\right] \tag{2.10}$$

Raiffa and Schlaifer (1961) prove that both forms of the problem are equivalent and lead to the same sequence of decisions. They are important to understand the different approaches proposed in the literature for solving decision problems and specifically the sequential decision process introduced in Section 2.3.

2.2.3.2. Effect of the prior model in decision analysis

The decision analysis as presented in this work supposes that an a-priori probability distribution of state $\boldsymbol{\Theta}$, the *prior model* $p(\boldsymbol{\theta})$ is available to the analyst. The prior model includes a prior probabilistic model of uncertain parameters and the dynamics of the system (deterioration, loads, structural response). The typical structure of the prior model for I&M planning of deteriorating systems is described in Chapter 5. Model-free, non-Bayesian methods also exist (Luce and Raiffa, 1989) but will not be addressed here.

It is obvious from Equations (2.8) to (2.10) that the optimal decisions e_{opt}, a_{opt} or $[e_{opt}, d_{opt}]$ are dependent on this prior model. The prior model can be interpreted as the carrier of all previous knowledge, experience or expertise, and reflects a confidence about this knowledge. Since omniscience about past and future is not achievable, the "perfect" prior model, which accurately predicts the event path with the lowest cost, is not known. Instead, the prior should be carefully selected to reflect our state of knowledge at the time of solving the decision problem. The effect of the choice of the prior model on the resulting optimal strategies is investigated for a specific case study in Chapter 7.

In one-step decision problems, there are no opportunities to learn and act upon additional information about the prior model. However, in sequential decision problems (see Section 2.3), information about the state of the environment is collected progressively. This opens the possibility to revise our state of knowledge during the execution of the decision process, hence update the prior probabilistic model. When a hierarchical structure is attributed to the prior model, i.e., uncertainties about the model are included as random variables, a posterior probabilistic model can be obtained with Bayesian analysis during the decision process. This approach belongs to *Bayesian reinforcement learning* methods (Ross et al., 2011), and is the basis of the adaptive planning methodology presented in Chapter 3.

2.2.4. Value of information

2.2.4.1. General expression

The conditional expected value of the utility, or costs, $\mathbf{E}_{\boldsymbol{\Theta}|Z,e,a}[\cdot]$ weighs the possible paths of the decision tree with their respective probability of occurrence.

In the extensive form, the expected cost associated with implementing the NDE system e, C_e, is defined according to Equation (2.9) as

$$C_e = \mathbf{E}_{Z|e}\left[\mathbf{E}_{\boldsymbol{\Theta}|Z,e}[C_{\text{tot}}(e, a_{opt,e}(z), \boldsymbol{\theta})]\right] . \tag{2.11}$$

Note that this expected cost includes c_e, the direct investment required to implement the NDE system (see Section 2.2.2.2).

In the normal form, the expected cost of a strategy $[e, d]$ is defined similarly as

$$C_{e,d} = \mathbf{E}_{\boldsymbol{\Theta},Z|e,d}[C_{\text{tot}}(e, d(e, z), \boldsymbol{\theta})] \tag{2.12}$$

Under the null experiment e_0, no information is collected (at cost $c_{e_0} = 0$) and the decisions are based on the prior knowledge of the system, $p(\boldsymbol{\theta})$. Thus, the optimal action and expected cost under e_0 are obtained from Equation (2.8) as

$$a_{e_0} = \arg\min_a \mathbf{E}_{\boldsymbol{\Theta}}[C_{\text{tot}}(e_0, a, \boldsymbol{\theta})] \tag{2.13}$$

$$C_{e_0} = \mathbf{E}_{\boldsymbol{\Theta}}[C_{\text{tot}}(e_0, a_{e_0}, \boldsymbol{\theta})] \tag{2.14}$$

The *value of information* (VoI) (also called expected value of sample information) for an NDE system e is the gain evaluated as the difference between the total expected prior cost associated with e_0 and the total expected cost associated with e. The VoI typically does not include the cost c_e of implementing the NDE system. If c_e is included, then the net VoI (NVoI) is obtained.

$$\text{VoI}(e) = C_{e_0} - (C_e - c_e) \tag{2.15}$$

$$\text{NVoI}(e) = \text{VoI}(e) - c_e = C_{e_0} - C_e \tag{2.16}$$

Notably, if for any outcome z obtained through e, the optimal action $a_{opt}(z) = a_{e_0}$, then $\text{VoI}(e) = 0$. In other terms, an NDE system only brings value if it changes the decision on which action to take.

An upper bound of the VoI is the value of perfect information, where the perfect information collection process, e_P, provides full knowledge of $\boldsymbol{\Theta}$ (Raiffa and Schlaifer, 1961). The VoI of an NDE system e is thus linked to the reduction in uncertainty provided by the NDE system.

Solving the decision problem of Equation (2.8) for a given e is equivalent to maximizing the VoI and solving Equation (2.9) is equivalent to maximizing the NVoI.

Decision problems involving systems with N components, which can all be inspected, become significantly more complex. One can consider the 2^N NDE systems collecting information on any subset of components $\{1, ..., N\}$, and their associated VoI as per Equation (2.15). However, one can also consider that the inspection decisions are done sequentially: The observation about the first component informs the decision about the second component, and so on. This is illustrated by Straub and Faber (2004) in a so-called extended decision tree. Establishing the VoI for all possible sequences of observation is typically impractical and computationally demanding.

Nevertheless, the VoI concept enables the comparison and ranking of selected NDE systems. This approach is used in Chapter 4 to evaluate the performance of NDE. For the multi-component system mentioned above, the individual components' VoI can be used as a metric to prioritize the order in which the components are inspected, although this greedy selection may not be optimal (Kochenderfer, 2015).

Furthermore, since only the VoI ordering is required, and not its absolute value, it is convenient to find a proxy for the VoI, such that the ranking according to that proxy reflects the ranking according to the VoI. For this reason, several studies have focused on linking the VoI with specific system or component characteristics. Konakli and Faber (2014) show that the VoI of component inspection in a structural system is linked to the uncertainty associated with structural properties, the quality of the inspection and the components' interdependence. Malings and Pozzi (2016) use conditional entropy to optimize sensor placement in infrastructure. In Chapters 3 and 6 we propose a prioritization index as a proxy for the VoI of component inspection in a structural system, which combines different contributions to the VoI.

2.3. Optimal I&M planning and SDP under uncertainty

The decision problem under uncertainty as formulated by Raiffa and Schlaifer (1961) in Equations (2.8) to (2.10) is not easy to manipulate when a temporal sequence of decisions must be optimized. In the 1950s, around the time when fundamental game theory equations were derived, RAND corporation scientist Richard Bellman was studying the optimal inventory problem, an OR classic and an SDP problem, in his words a "multi-stage process" (Bellman, 1953). He introduced the term *dynamic programming* to designate the process of solving SDP problems. The word "dynamic" is an explicit reference to time, which plays an important part in the problem complexity (see Section 2.4). Howard (1960) followed by developing the founding algorithms to tackle a large variety of problems, from optimizing the location of warehouses in order to minimize transportation costs, to the management of a baseball team.

2.3.1. Time, history, policy and strategy

The I&M planning problems considered in this work are limited to a *finite time-horizon* T, which is typically the anticipated service life of the system. A finite service life is a reasonable assumption since the durability of materials, technological advances, changing user demands and requirements are likely to make the structure obsolete eventually. The service life is in general subject to uncertainty; the effect this could have on the results is not further investigated in this work. Time is discretized; i indicates the i^{th} time step between times t_{i-1} and t_i, where $t_0 = 0$ is the beginning of the system service life. n_T denotes the last time step between times t_{n_T-1} and $t_{n_T} = T$. In this discrete-time setting, it is reasonably assumed that the effects on the system of one I&M action carried out at a point in time are indistinguishable from the effects of the same action carried out within the same time step.

In sequential decision-making, a *history* (or *trajectory*) contains all the information gathered during the lifetime of the structure, including inspection decisions and outcomes, maintenance and repair actions, and eventual failures. We adapt the notations of the generic decision problem from Section 2.2.1 to describe an I&M history:

- $\boldsymbol{\Theta} = \{\boldsymbol{\Theta}_0, ..., \boldsymbol{\Theta}_{n_T}\}$ describes the state evolution over the considered time horizon. $p(\boldsymbol{\theta}_i)$ represents the joint probability distribution of the random vector state $\boldsymbol{\Theta}_i$.
- $\boldsymbol{Z} = \{Z_1, ..., Z_{n_T}\}$ are the vectors containing the inspection and monitoring outcomes collected during the service life of the structure. $\boldsymbol{Z}_{1:i}$ denotes the outcomes collected up to time step i.
- $\boldsymbol{e} = \{e_1, ..., e_{n_T}\}$ are the inspection (information collection) decisions during the service life. The notation $\{I_1, ..., I_{n_T}\}$ will be used interchangeably.
- We consider the actions that affect the system reliability $\boldsymbol{A} = \{A_1, ..., A_{n_T}\}$ during the service life, such as repair or other maintenance actions. The notation $\{R_1, ..., R_{n_T}\}$ will be used interchangeably.

- For a given history, the *total life-cycle cost* C_{tot} is calculated by recording the inspection and repair actions and consequences of failure during the lifetime, and aggregating their cost. $C_{\text{tot},i:j}$ designates the total (discounted) cost between time steps i and $j > i$.
- A discount factor $\gamma(t)$ is applied to the costs incurred at time t and gives more importance to the short-term costs than to the long-term costs. It expresses the influence of time on the utility of an action and its consequences. A typical expression for the discount factor in discrete time is $\gamma(t_i) = \frac{1}{(1+r)^t_i}$, with r the *discount rate*.

Figure 2.4 shows the sequence of decisions for I&M of a deteriorating system. The decision tree grows exponentially with the considered number of time steps and with the number of system components, and it grows polynomially with the number of available actions and with the number of deterioration states and observations.

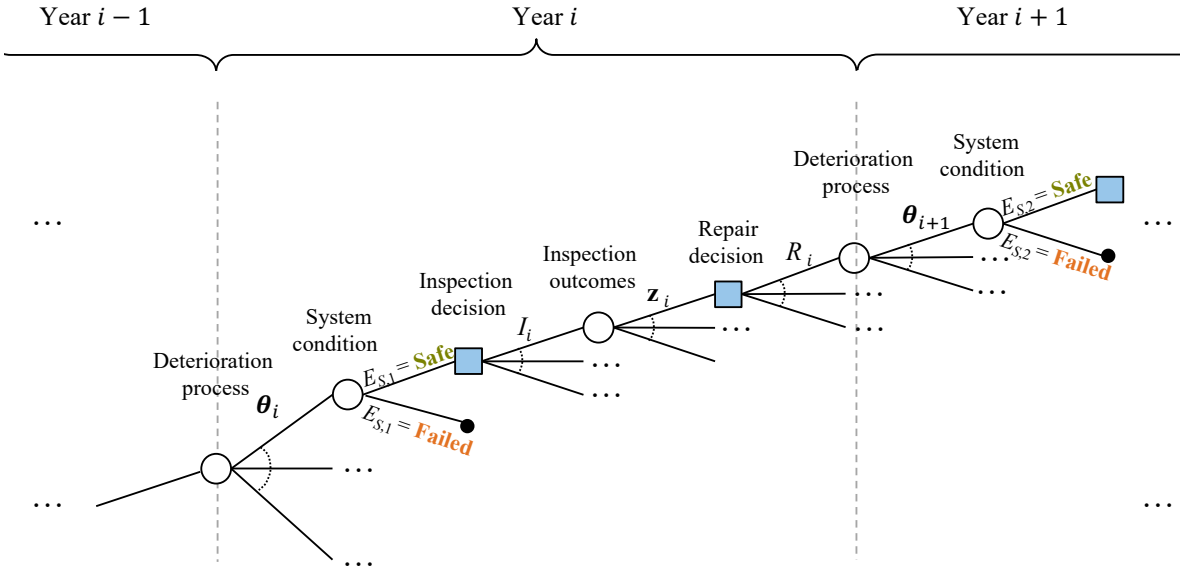

Figure 2.4 Detail of a decision tree for a deteriorating system which can be inspected and repaired. Random events and outcomes are represented by round nodes, and decisions by square nodes. The deterioration process includes all possible states of damage that the system components can take. Similarly, the inspection outcomes and repair decisions collect all the data and actions for all system components.

A *policy* π_i is the set of rules adopted at time step i guiding the decision process based on the information available at that time (Jensen et al., 2007). When considering a deteriorating multi-component system, the policy takes as input all or part of the current knowledge on the state of the system, and gives the answer to the questions "Inspect?" {yes, no}, "Where?" {component j, k, ...}, "What to look for?" {corrosion, fatigue,...} , "How?" {visually, ultrasonic inspection, thickness measurements, ...}, "Repair?" {yes, no, how}. The system knowledge includes the history of inspection outcomes, monitoring data, repairs and component failures. A policy is *stochastic* if it assigns an action following a probability distribution; it is otherwise *deterministic*[1]. This work considers deterministic policies, but the general methodology is applicable to either type of policies. A policy specifies both information collection e_i (I_i)

[1] This also depends on the space in which the policy operates. A deterministic policy mapping from the observation space to the action space can correspond to a stochastic policy in belief space (see Sections 2.4.2 and 2.4.3.1), and vice-versa. For an example, refer to the study by Bismut and Straub (2019).

and mitigating (repair) action decisions A_i (R_i) at the time step i considered, possibly in a sequential manner. This sequence of decisions within a single time step is not explicit in the decision trees or influence diagrams but in theory, there are no limitations as to how a policy operates and reacts immediately to information. The only limitation posed on a policy as defined here is that it cannot take as an input information obtained in the future.

A *strategy* $\mathcal{S} = \{\pi_1, \pi_2, \cdots \pi_{n_T}\}$ is the set of policies for all time steps. $\mathscr{S}$ is the space of all strategies. A strategy is *stationary* if its policies are identical for all time steps, i.e., $\pi_1 = \pi_2 = ... = \pi_{n_T} = \pi$. It is common to find the terms policy and strategy used interchangeably in the literature or find that a policy designates the rules adopted for a certain number of (but not all) time steps (Gittins, 1979).

2.3.2. The general I&M optimization problem: extensive and normal forms

The extensive form of an SDP does not appear naturally from Equations (2.8) and (2.9), since the optimal information collection process for the full duration of the decision problem is determined dynamically as more information is acquired. Bellman (1957a) proposes to divide the optimization problem time-wise into sub-problems. In this formulation, the solution of the extensive form is the reversed policy sequence, $\pi_{n_T}, ..., \pi_i, ..., \pi_1$, where for each time step i, the policy π_i is obtained with Equation (2.9). As stated above, the policy π_i addresses both decisions of information collection e_i and associated action a_{opt} at time step i and can thus be interpreted as the solution of the normal form of the sub-problem, $[e_i, d_i]$ (see Section 2.2.3.1). The decision tree of Figure 2.4 is translated into a decision tree at the policy level in Figure 2.5. For each sub-problem at time step i, the "prior" models of the state of the environment, $p(\boldsymbol{\theta}_i)$,

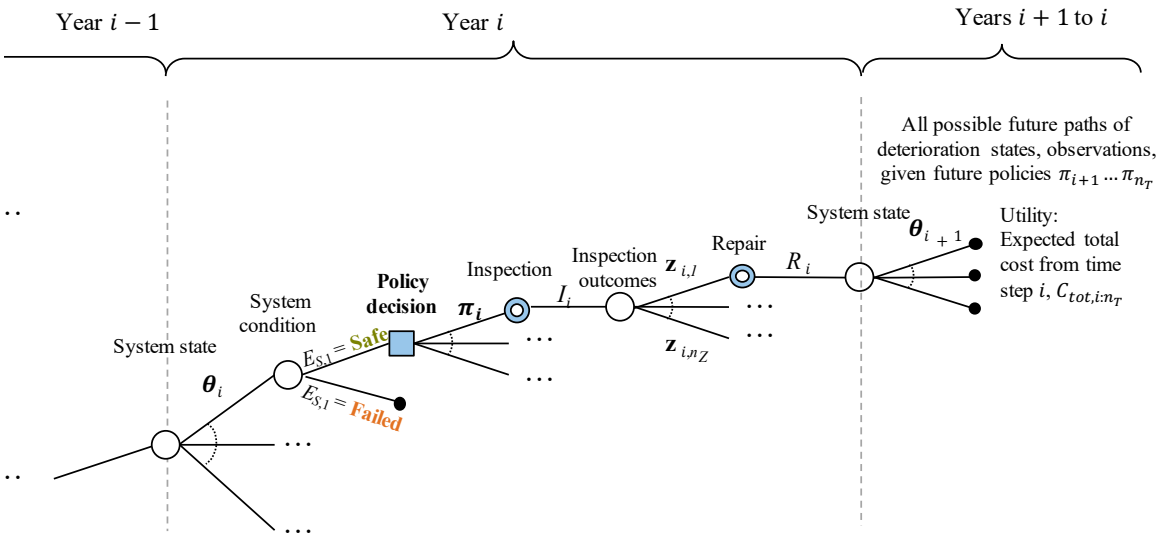

Figure 2.5 Modified decision tree of the SDP described by Figure 2.4, in the extensive form. The decision at time step i is on the policy π_i. The subsequent inspection (information collection) and action are fully determined by the chosen policy and the inspection outcomes. They are indicated by the double oval nodes, out of which only one branch emerges. The future policies $\pi_{i+1}, ...\pi_{n_T}$ are set and the future costs are compressed into a terminal utility, which depends on the future policies and corresponds to the expected cost from that time step onwards.

and the total cost function, $C_{\text{tot},i:n_T}$, are different : the "prior" $p(\boldsymbol{\theta}_i)$ is in fact conditioned on

the outcomes and decisions at past time steps, and the cost $C_{\text{tot},i:n_T}$ depends on the future sequence of actions and outcomes, i.e., on the policies $\pi_{i+1}, ..., \pi_{n_T}$. This mechanism where the policy accounts for future decisions is also called "closed-loop planning", as opposed to "open-loop planning" (e.g., a maintenance policy prescribing replacement of the system at regular time intervals, regardless of its state) (Kochenderfer, 2015).

The backward induction method proposed by Bellman would therefore require that the optimal policy π_i be computed for (i) all possible (or reachable) models $p(\boldsymbol{\theta}_i)$, and (ii) the future expected cost is determined from the future optimal policies $\pi_{i+1}, ..., \pi_{n_T}$. It is clear that condition (i) is equivalent to performing an extremely large, at the limit even infinite, number of optimizations to build up the optimal strategy, which makes this problem intractable in general. The complexity of an SDP is formally analyzed in Section 2.4. The backward induction method is demonstrated on a generic two-step problem in Chapter 4.

It is also possible to formulate the SDP in the normal form. This reduces the problem to exactly one choice: one must select among the available strategies. This formulation directly affects the characteristic of the methods used to approximate a solution to the problem, as discussed in Section 2.4.4 below. Adopting the normal form, the optimization of the SDP aims to identify the decision strategy $\mathcal{S}^*$ that minimizes the expected total life-cycle cost:

$$\mathcal{S}^* = \arg\min_{\mathcal{S} \in \mathscr{S}} \mathbf{E}[C_{\text{tot}}|\mathcal{S}], \tag{2.17}$$

where C_{tot}, also written as $C_{\text{tot},1:n_T}$, is the discounted total life-cycle cost, including inspections, repairs and possible failures of the system occurring within the time horizon T. $\mathbf{E}[C_{\text{tot}}|\mathcal{S}]$ is the expected total life-cycle cost when strategy $\mathcal{S}$ is implemented. Its computation for I&M planning applications is described in Chapter 3.

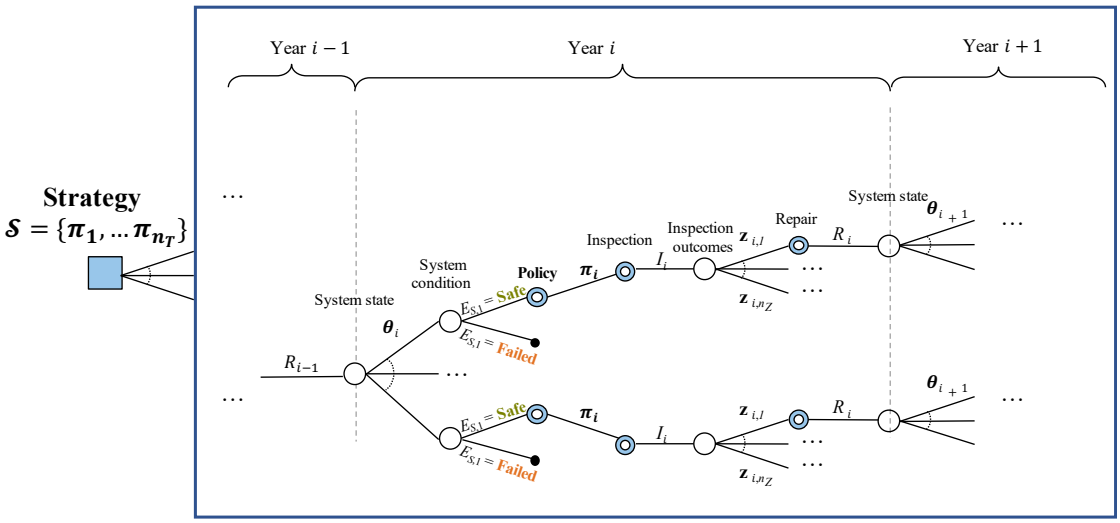

Figure 2.6 Decision tree where the only decision is the strategy. The policies are fully determined by the strategy $\mathcal{S}$.

2.3.3. Reliability-based planning and other constraints

It is common for I&M strategies to obey to certain constraints: these can be (i) operational (e.g., inspections can only take place at regular time intervals, there are annual budget constraints) (ii) regulatory (e.g., inspection intervals cannot exceed 5 years) or (iii) linked to standard practice. These constraints can significantly increase the complexity of the optimization problem.

Ideally, these constraints should be represented in the utility (cost) function, in the form of ranked preferences. One approach is to assign a penalty, i.e., a very high cost, to all strategies that do not comply with the constraints. These constraints can be made explicit under Equation (2.17), but the equation is in fact left unchanged.

A special case appears when the cost of failure c_F cannot be quantified. For civil engineering infrastructure, it can be difficult to estimate, since the types of consequence can be financial (loss of revenue) as well as societal, for instance loss of life. Attributing a monetary value to loss of life remains a controversial topic. However, economists have conceptualized and derived values of statistical life from a society's willingness to pay for reducing the probability of a death (Viscusi and Aldy, 2003). While in most countries the value of statistical life remains an implicit quantity, in the U.S. an official value is readily available for the risk assessment of engineering projects (e.g., Viscusi and Aldy, 2003; National Center for Environmental Economics, 2010). A discussion on the topic can be found in (JCSS, 2001; Straub, 2004; Colmer, 2020).

One could also simply assess the expected total life-cycle I&M cost, i.e., excluding the total life-cycle risk of failure from Equation (2.17), but this assessment presents an obvious flaw: if the strategy considered prescribes no inspections and no repairs during the entire service life, this cost is simply zero, hence this "do-nothing" strategy would always be the one with minimal cost, even if this strategy is clearly undesirable. If the consequences of failure, thus the risk, cannot be included in the objective function, a constraint, typically a minimum requirement on the system performance, ensures the optimization trade-off.

In *reliability-based planning*, the optimal strategy minimizes the total expected I&M costs, while ensuring that the system always complies with a reliability criterion. The objective function thus excludes any costs associated with consequences of system failure, as the occurrence of failure is represented through the reliability criterion. In Chapter 7, we propose a formulation of the reliability-based I&M planning problem and investigate how the chosen reliability criterion influences the outcome of the strategy optimization, by demonstrating the proposed reliability-based framework on I&M planning for a nuclear feeder piping system. A general discussion on the choice of the reliability criterion for I&M of structure is found in (Mendoza et al., 2021). The rest of Chapter 2 focuses on the complete, risk-based planning problem.

2.3.4. VoI in SDPs

The VoI concept can also be extended to SDPs. The VoI of a single observation at a given time step can in theory be computed. In fact, finding the VoI of an inspection (or combinations of inspections, for a multi-component system) at each time step leads to solving the optimization problem in its extensive form.

The VoI can also be quantified for a structural health monitoring (SHM) system, as detailed in (Kamariotis et al., 2022). Assuming that monitoring data are obtained at every time step at no extra cost, and that the likelihood function associated with the SHM system is available to the analyst, the optimal I&M strategy can be computed with Equation (2.17), where additional (and costly) inspections can be carried out and maintenance can be carried out on the basis of the information from both the SHM and inspection data. The expected cost of the obtained optimal strategy with SHM can be compared to that of the optimal strategy without SHM.

2.4. A classical approach to SDPs: MPD, POMPD and belief-MDP

A special class of SDP has been extensively studied and a complete mathematical framework developed for their resolution. These are the *fully observable Markov decision processes* (MDPs) and the more general *partially observable MDPs* (POMDPs). In the earlier years, Bellman (1957a,b) and Howard (1960) described solution strategies for MDPs based on Bellman's dynamic programming tool. Raiffa and Schlaifer (1961) and preposterior analysis paved the way to the study of POMDPs (Åström, 1965; Kaelbling et al., 1998).

In this section we describe the properties and structures of MDPs and POMDPs and show the challenges and limitations of translating a general SDP to this framework. Finally, we give an overview of the MDP and POMDP approximate solvers. The reader is referred to (Kochenderfer, 2015) for more details.

A detailed understanding of the intricacies of the MDP and POMDP formulation is not required to comprehend the heuristic adaptive planning methodology presented in Chapter 3 following. However, they reveal the complexity associated with SDPs in general and the I&M planning problem and motivate the focus of this work on the heuristic approach.

2.4.1. The Markov assumption

Section 2.3.2 formulates the SDP for the general case without specifying the probabilistic model of the sequence of system states $\boldsymbol{\Theta} = \{\boldsymbol{\Theta}_0, ..., \boldsymbol{\Theta}_{n_T}\}$.

A particular class of SDP is such that the system state evolution is formulated so that the *Markov assumption* is verified: the next state $\boldsymbol{\Theta}_{i+1}$ at time step $i+1$, conditional on the current state $\boldsymbol{\Theta}_i$ at time step i, does not depend on any states $\boldsymbol{\Theta}_{j<i}$ prior to the current time.

The system evolution is thus described by a *Markov process*: the joint probability distribution $\Pr(\boldsymbol{\Theta})$[1] is fully determined by the transition probabilities from state $\boldsymbol{\Theta}_i$ at time step i to state $\boldsymbol{\Theta}_{i+1}$ at time step $i+1$, $\Pr(\boldsymbol{\Theta}_{i+1}|\boldsymbol{\Theta}_i)$, and the distribution of the initial state at time $t=0$, $\Pr(\boldsymbol{\Theta}_0)$. The joint probability distribution of variables $\boldsymbol{\Theta}_i$ is obtained by applying the chain rule:

$$\Pr\left(\boldsymbol{\Theta}_1, ..., \boldsymbol{\Theta}_{n_T}\right) = \Pr(\boldsymbol{\Theta}_0) \cdot \prod_{i=0}^{n_T-1} \Pr(\boldsymbol{\Theta}_{i+1}|\boldsymbol{\Theta}_i). \tag{2.18}$$

The BN of a Markov process follows the pattern of Figure 2.7. When the transition probabilities for $i \geq 0$ do not depend on the time step i, the Markov process is said to be stationary. Moreover, the Markov assumption is interesting at the computational level, notably for Bayesian inference.

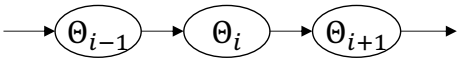

Figure 2.7 Section of the Bayesian network associated with a Markov process. The states $\boldsymbol{\Theta}_i$ can aggregate the values of other random variables, here not shown.

2.4.2. MDP, POMDP and belief-MDP

In a fully observable *MDP*, the state evolution is described by a Markov process where the state transition probability between time steps i and $i+1$ is determined by the action taken at time step i, A_i. We use the corresponding notation $\Pr(\boldsymbol{\Theta}_{i+1}|\boldsymbol{\Theta}_i, A_i)$. By definition, the state $\boldsymbol{\Theta}_i$ is perfectly observed at every time step, corresponding to NDE system e_P (see Section 2.2.4.1) implemented at no cost. Figure 2.9 shows the typical ID for an MDP.

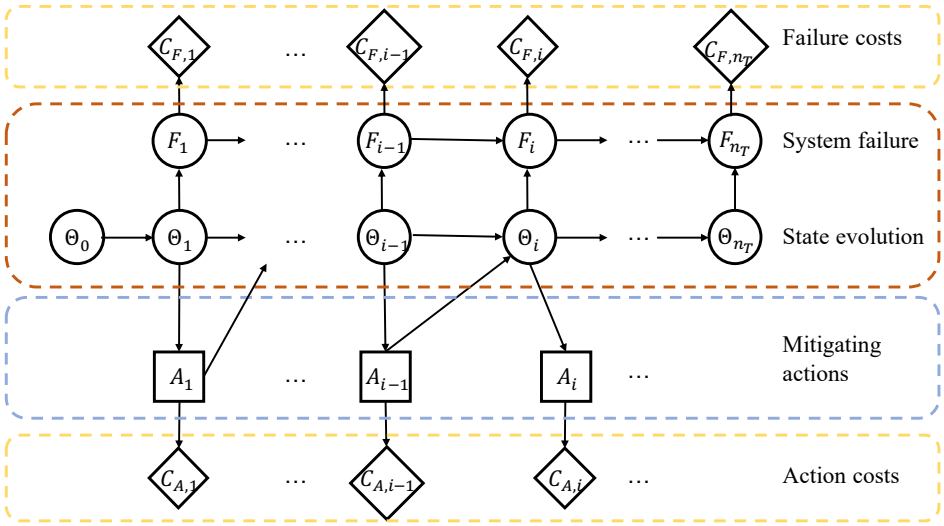

Figure 2.8 Influence diagram typical of an MDP. The actions A_i are taken based on the perfect knowledge of the system $\boldsymbol{\Theta}_i$.

The *POMDP* generalizes the MDP to the case where the observation is partial or imperfect

[1] It is usual to adopt the discrete variable notation for MDPs and POMDPs. Continuous variable domains add a layer of complexity to the problem, as discussed in Section 2.4.3.2.

and the state $\boldsymbol{\Theta}_i$ is only known with uncertainty (Sondik, 1971). The observations, Z_i, are typically assumed to be conditionally independent given the states, $\boldsymbol{\Theta}_i$. The corresponding likelihoods are determined by $\Pr(Z_i|\boldsymbol{\Theta}_i, I_i)$[1]. It is important to note that while the process at the state level is Markovian, the Markov property does not hold when conditioning the future states only on the current observation, i.e., $\Pr(\boldsymbol{\Theta}_{i+1}|\boldsymbol{Z}_{1:i}, \boldsymbol{A}_{1:i}) \neq \Pr(\boldsymbol{\Theta}_{i+1}|Z_i, A_i)$. Figure 2.9 illustrates the ID of a POMDP.

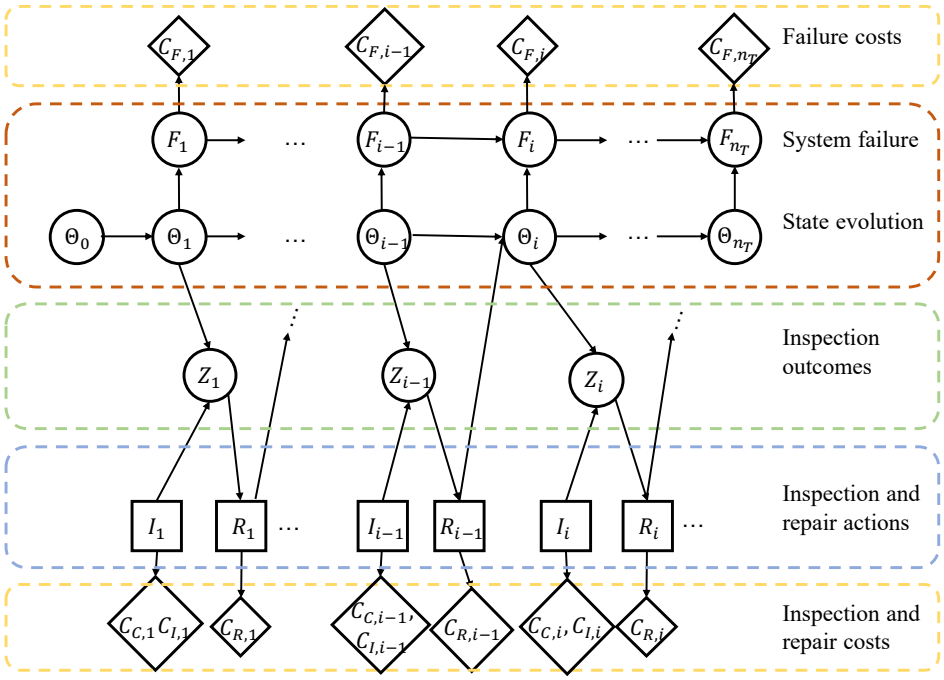

Figure 2.9 Influence diagram typical of a POMDP. It is implied that all past observations $\boldsymbol{Z}_{1:i-1}$ and inspection decisions $\boldsymbol{I}_{1:i-1}$ and repair actions $\boldsymbol{R}_{1:i-1}$ influence the decisions I_i and R_i. The corresponding edges are typically omitted for clarity.

It can be shown that POMDPs are MDPs over the *belief* $\boldsymbol{B}_i$, called *belief-MDPs*. The belief is defined as the probability distribution over the state of the system given all the past information collected and all previous actions, i.e., for all $\boldsymbol{\theta} \in \Omega_{\boldsymbol{\Theta}_i}$ $B_i(\boldsymbol{\theta}) = \Pr(\boldsymbol{\Theta}_i = \boldsymbol{\theta}|\boldsymbol{Z}_{1:i}, \boldsymbol{A}_{1:i-1}, \boldsymbol{I}_{1:i})$ (Kaelbling et al., 1998). Therefore, the belief condenses all the knowledge about the system at time step i into a function of $\boldsymbol{\theta}$ and this function is fully known and observed at every time step. With $|S|$ the number of states in $\Omega_{\boldsymbol{\Theta}_i}$, the belief $\boldsymbol{B}_i$ is a random vector of dimension $|S|$ with $|S| - 1$ degrees of freedom (since $\sum_{\Omega_{\boldsymbol{\Theta}_i}} \boldsymbol{B}_i(\boldsymbol{\theta}) = 1$). The belief-MDP is illustrated in Figure 2.10. The transition from $\boldsymbol{B}_i$ to $\boldsymbol{B}_{i+1}$, or *belief updating*, involves the observation Z_{i+1} of system state $\boldsymbol{\Theta}_{i+1} = \boldsymbol{\theta}$ (Pineau et al., 2006), such that:

$$B_{i+1}(\boldsymbol{\theta}) = \frac{\Pr(Z_{i+1}|\boldsymbol{\Theta}_{i+1} = \boldsymbol{\theta}, I_{i+1})}{\Pr(Z_{i+1}|\boldsymbol{B}_i, A_i, I_{i+1})} \Pr(\boldsymbol{\Theta}_{i+1} = \boldsymbol{\theta}|\boldsymbol{\Theta}_i, A_i)^\top \cdot \boldsymbol{B}_i, \tag{2.19}$$

where $\Pr(\boldsymbol{\Theta}_{i+1} = \boldsymbol{\theta}|\boldsymbol{\Theta}_i, A_i)$ is an $|S|$-dimensional vector. The denominator $\Pr(Z_{i+1} = z|\boldsymbol{B}_i, A_i, I_{i+1})$ is the normalizing constant ensuring that $\sum_{\Omega_{\boldsymbol{\Theta}_{i+1}}} \boldsymbol{B}_{i+1}(\boldsymbol{\theta}) = 1$. This normalizing constant can be evaluated for any given observation $Z_{i+1} = z$. The transition

[1] The observation likelihood is determined by the inspection decision I_i (e.g., inspect or not, how), see Figure 2.9. The dependence is often omitted in the notation in the classical POMDP formulation but is always implied.

probabilities for the belief-MDP, $\Pr(\boldsymbol{B}_{i+1}|\boldsymbol{B}_i, A_i, I_{i+1})$, are then determined by integrating $\Pr(Z_{i+1} = z|\boldsymbol{B}_i, A_i, I_{i+1})$ over the domain of Z_{i+1} where $B_{i+1}(\boldsymbol{\theta})$ is equal to the value obtained with Equation (2.19).

The complexity associated with solving the belief-MDP is discussed in Section 2.4.3. The formulation of POMDP as a belief-MDP is central to many solvers described in the literature, which we briefly review in Section 2.4.4.

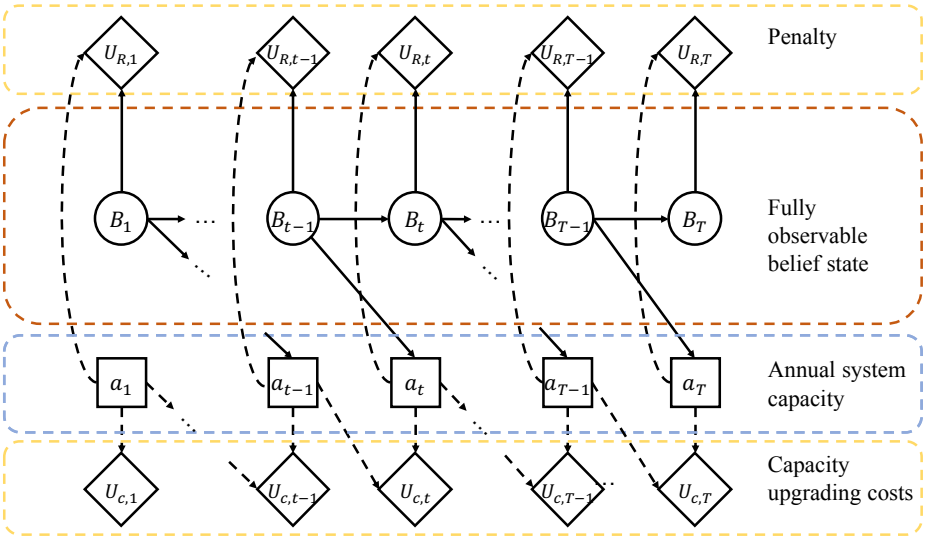

Figure 2.10 Influence diagram for the planning problem translated into the belief space. Here it is assumed that the state is observed at each time step at no cost, and the inspection decision node is omitted for clarity (Bismut and Straub, 2019).

2.4.3. Solving a sequential decision problem: a cursed problem

2.4.3.1. Principle of dynamic programming

The MDP and POMDP formulations attempt to provide a universal plan for decision problems where the process is Markovian, and, in theory, account for all possible scenarios. Thanks to the Markov property, the optimal policies can be evaluated with dynamic programming. At time step i, the optimal policy π_i^* attributes deterministically for an MDP an action to each system state $\boldsymbol{\Theta}_i = \boldsymbol{\theta}$ (Equation (2.20)), and for a POMDP an action to each belief state $\boldsymbol{B}_i = \boldsymbol{b}$ (Equation (2.21)), such that[1] (Kaelbling et al., 1998)

$$\pi_i^*(\boldsymbol{\theta}) = \arg\min_a \left[C_i(\boldsymbol{\theta}, a) + \gamma \sum_{\boldsymbol{\Theta}_{i+1}} \Pr(\boldsymbol{\Theta}_{i+1}|\boldsymbol{\theta}, a) V_{i+1}^*(\boldsymbol{\Theta}_{i+1}) \right], \tag{2.20}$$

$$\pi_i^*(\boldsymbol{b}) = \arg\min_a \left[C_i(\boldsymbol{b}, a) + \gamma \sum_{\boldsymbol{B}_{i+1}} \Pr(\boldsymbol{B}_{i+1}|\boldsymbol{b}, a) V_{i+1}^*(\boldsymbol{B}_{i+1}) \right]. \tag{2.21}$$

[1] For simplicity in the notation, we write $\Pr(\boldsymbol{\Theta}_{i+1}|\boldsymbol{\theta}, a)$ for $\Pr(\boldsymbol{\Theta}_{i+1}|\boldsymbol{\Theta}_{i+1} = \boldsymbol{\theta}, A_i = a, I_{i+1})$ and $\Pr(\boldsymbol{B}_{i+1}|\boldsymbol{b}, a)$ for $\Pr(\boldsymbol{B}_{i+1}|\boldsymbol{B}_i = \boldsymbol{b}, A_i = a, I_{i+1})$.

Here, $\boldsymbol{b} = [b_1, ..., b_{|S|}]^\top$ indicates the $|S|$-dimensional belief state, such that $\sum b_s = 1$. $C_i(\boldsymbol{\theta}, a)$ and $C_i(\boldsymbol{b}, a)$ are the expected costs incurred at time step i (immediate costs). In particular $C_i(\boldsymbol{b}, a) = \sum_{s=1}^{|S|} C_i(\boldsymbol{\theta}_s, a) b_s$. γ is the discount factor. The *Q-value* at time step i is defined for a pair $(\boldsymbol{\theta}, a)$ or $(\boldsymbol{b}, a)$ as the quantity within the square brackets in Equations (2.20) and (2.21). The *optimal value function* V_i^* at time step i[1] evaluated in $\boldsymbol{\theta}$ or $\boldsymbol{b}$ is equal to the Q-value at time step i evaluated in $(\boldsymbol{\theta}, \pi_i^*(\boldsymbol{\theta}))$ or $(\boldsymbol{b}, \pi_i^*(\boldsymbol{b}))$. The process of evaluating V_i^* recursively is called *value iteration*[2] (Bellman, 1957a).

Equation (2.20) shows that finding the optimal policies for a finite time horizon with n_T steps and discrete-, finite-state MDP requires in total $|S| \cdot n_T$ optimization operations, where $|S|$ is the number of possible states at each time step. For the infinite-horizon case, asynchronous value iteration converges to the stationary optimal value function $V_i^* = V^* \; \forall i \in \mathbb{N}$ without requiring a full state sweep (Kochenderfer, 2015).

To understand the complexity of a finite time horizon POMDP, consider a system with N components that can be inspected, then potentially repaired, at every time step i. There are three possible courses of action: either one does nothing, or inspects and based on the inspection result either repairs or does not repair. The total number of possible actions at each time step is $n_{actions} = 3^N$. All observations from inspection and monitoring during a time step i are summarized in $\boldsymbol{Z}_i$, which has a discrete outcome space of size n_{obs}. In the simplest case, the inspection outcome for each component is either no inspection, or inspection and no detection, or inspection and detection, in which case $n_{obs} = 3^N$.

A deterministic policy π_i at time step i chooses an action among the 3^N options, in function of the belief state. The belief state can also be represented by the observation history, which can take n_{obs}^i distinct realizations. Hence, the total number of potential policies at time step i is $3^{N n_{obs}^i}$. It follows that there are $\prod_{i=1}^{n_T} 3^{N n_{obs}^i} = 3^{N \frac{n_{obs}^{n_T} - 1}{n_{obs} - 1}}$ distinct strategies. This illustrates how the space of strategies $\mathscr{S}$ increases double-exponentially with the number of time steps n_T and with the number N of system components. Papadimitriou and Tsitsiklis (1987) showed that the exact solution of the finite-horizon POMDP cannot be found in polynomial time and is indeed PSPACE-complete. Bellman (1957b) coined the term *curse of dimensionality* and Pineau et al. (2006) added the term *curse of history* to describe this complexity.

Nevertheless, the solution of a discrete-state POMDP has an interesting property when formulated in belief space. The optimal value function at time step i V_i^* is piece-wise linear concave in belief space (Sondik, 1971), and is

$$V_i^*(\boldsymbol{b}) = \min_a \boldsymbol{\alpha}_{i,a}^\top \cdot \boldsymbol{b}, \tag{2.22}$$

[1] Literature treating of MDP and POMDP often omits the time step indices in the policy, Q-value and value function for problems with infinite-horizons, due to the stationary property of the solution strategy in this case.

[2] The time step index is here consistent with a forward time description, as in previous sections. Most references on this topic, however, use the index to indicate the remaining time steps in the decision process, such that V_i^* denotes the optimal value function for a horizon of i time steps.

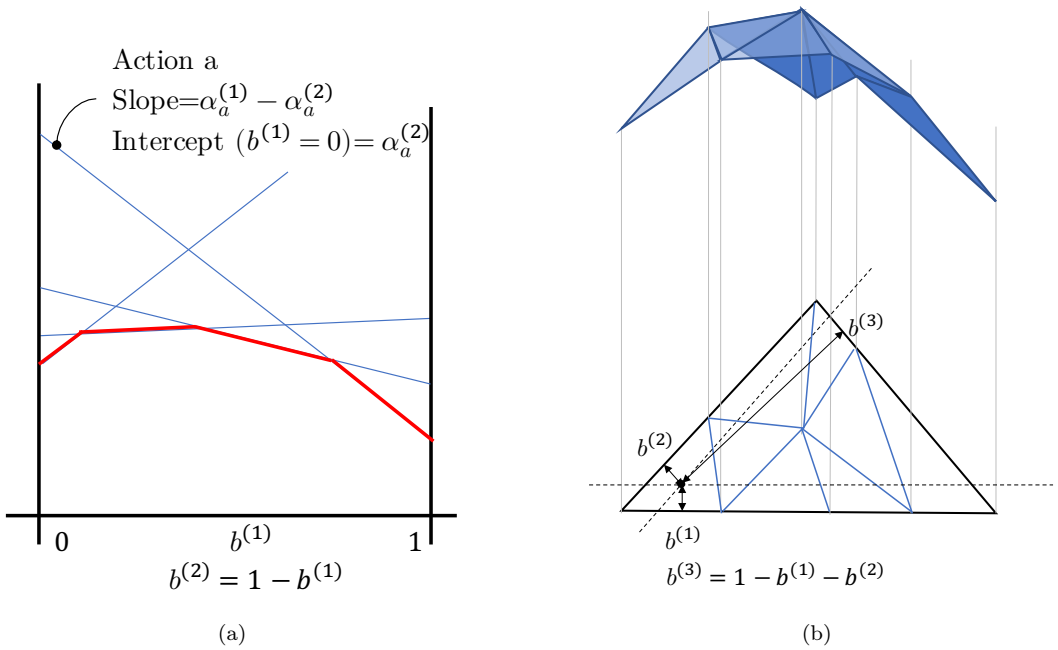

Figure 2.11 (a): Depiction of the concave optimal value function V^* (in red) at a given time step, for $|S| = 2$ in function of belief state $\boldsymbol{b} = [b^{(1)}\ b^{(2)}]$. (b): When $|S| = 3$, it is convenient to represent the belief state as a point within an equilateral triangle (here drawn in perspective), applying Viviani's theorem. The hyperplanes of the concave optimal value function and the optimal action zones in belief space are depicted. After (Papakonstantinou and Shinozuka, 2014).

where the $\boldsymbol{\alpha}_{i,a}$ are vectors of same dimension as $\boldsymbol{b}$, each associated with an action a. Finding the finite set of so-called $\boldsymbol{\alpha}$*-vectors* and solving Equation (2.22) is equivalent to solving Equation (2.21). The concavity of the optimal value function can be illustrated with hyperplanes of dimension $|S| - 1$ characterized by the $\boldsymbol{\alpha}$-vectors, as shown in Figure 2.11.

Here again, we note that in finite-horizon $\boldsymbol{\alpha}$-vectors must be evaluated at every time step. Exact solution algorithms for POMDP based on value iteration to find the sets of $\boldsymbol{\alpha}$-vectors have been proposed (e.g., Smallwood and Sondik, 1973) and applied to toy problems, but they are no match for higher dimensional problems. For this, approximate solution algorithms have been developed. We review these algorithms in Section 2.4.4 below.

2.4.3.2. Challenges

The dynamic programming solution given in Section 2.4.3.1 above is very attractive in theory. However, there are several challenges associated with transforming an SDP into an MDP or a POMDP.

In the classic definition of MDPs and POMDPs, the number of states and observations is discrete and finite and so is the action space (Bellman, 1957b). This does not hold in general for real-life planning problems, in which the decision maker evolves typically in a continuous environment and receives continuous information (e.g., spatial position, crack length, audio signal). Instructions for a robotic arm consists of angles, speed, location, which are actions in continuous space. This increases the difficulty of the problem as the belief is defined in an infinite-dimension space and, in general, does not have a closed form (Coquelin et al., 2008;

Ross et al., 2011). This is reflected in the belief updating operation Equation (2.19), where the scalar product $\Pr(\boldsymbol{\Theta}_{i+1} = \boldsymbol{\theta}|\boldsymbol{\Theta}_i, A_i)^\top \cdot \boldsymbol{B_i}$ translates into an integral, which must be computed for an infinite number of system states. The belief can be approximated with particle filters (Coquelin et al., 2008; Silver and Veness, 2010), the simplest of which is the Kalman filter when the dynamics are linear and the noise Gaussian. Another approach is to discretize the state space and describe the probabilistic model with a discrete BN and associated CPTs (see Section 2.2.2.3) and obtain the updated belief through matrix operations (Andriotis and Papakonstantinou, 2019). Roy et al. (2005) proposed a *belief compression* method, where one finds a low-dimensional representation of the belief, such that the distribution described by the belief is approximated within a fixed class of distributions. They note that the POMDP solution with belief compression loses its concavity property and cannot be resolved with the classical PBVI solvers (see Section 2.4.4.1); therefore, they propose to operate on a discrete grid of the parameters of the belief, resolve the discrete MDP at the grid points using value iteration (Equation (2.21)) and obtain the optimal value function at any point with a local approximation (Kochenderfer, 2015). In I&M planning applications, Nielsen and Sørensen (2015) used a Weibull distribution approximation; in infrastructure planning, Bismut and Straub (2019) discretized the parameters of the Gaussian belief. Alternatively, Porta et al. (2004, 2005) proposed a framework, in which the belief is represented as a Gaussian mixture, which was adapted by Schöbi and Chatzi (2016) for I&M planning with non-linear dynamics.

Another great challenge lies with the Markov assumption. This assumption is valid for certain fully observable games such as Go or chess, where an action (or move) is made only considering the current state. However, some decision processes require to store the memory of past states, which therefore violates the Markov assumption. A classic illustration is arcade game, where the current state observed consists of the frame pixels, but the optimal action (e.g., move right, left, stop) must consider the information given by previous frames, e.g., to obtain direction or speed (Mnih et al., 2013).

State-space augmentation is a modeling technique that, in theory, allows to transform any (discrete-time) SDP into an MDP or POMDP. Essentially, it replicates at the next time step the variables (the states) that must be stored in memory, such that the process is Markovian. In the general case, the dimensionality of the problem transformed with state-space augmentation increases exponentially with the time horizon, as more variables are stored and replicated over time. In Figure 2.12 we consider an SDP where the transition between states at time steps i and $i+1$ depends on all past states and the number of possible states at each time step is $|S|$. The number of system states of the equivalent MDP at time step i is $|S|^i$; and the dimension of the belief state in the associated POMDP is $|S|^i$. Although the depicted configuration presents the worst-case scenario, this exponential increase of the size and dimension of the state and belief space with time is a major obstacle to solving SDPs with the MDP and POMDP approach.

State-space augmentation can however be practical to convert MDPs and POMDPs with uncertain transition and observation models, parametrized by invariant but unknown parameters $\boldsymbol{\Lambda}$. Bayesian model-based approaches address this uncertainty by modeling $\boldsymbol{\Lambda}$ as

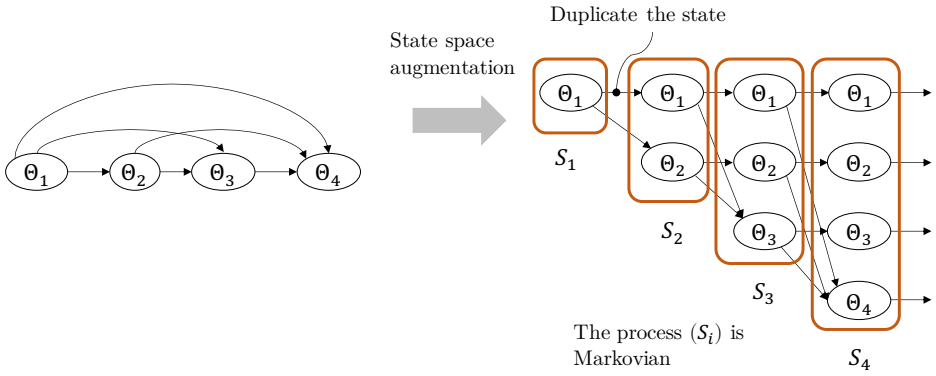

Figure 2.12 Transforming a non-Markovian process into a Markovian process by state space augmentation.

a random variable and assigning it a prior distribution, $f_{\boldsymbol{\Lambda}}(\boldsymbol{\lambda})$ (Kochenderfer, 2015). As illustrated in Figure 2.13, the invariant unknown parameters are replicated over time and the new process $(\boldsymbol{\Lambda}_i, \boldsymbol{\Theta}_i)$ verifies the Markov assumption. The configuration of the network obtained is that of a hidden Markov model, since only the states $\boldsymbol{\Theta}_i$ are then observed in the MDP or POMDP. Hierarchical Bayesian modeling of model uncertainty has been formulated

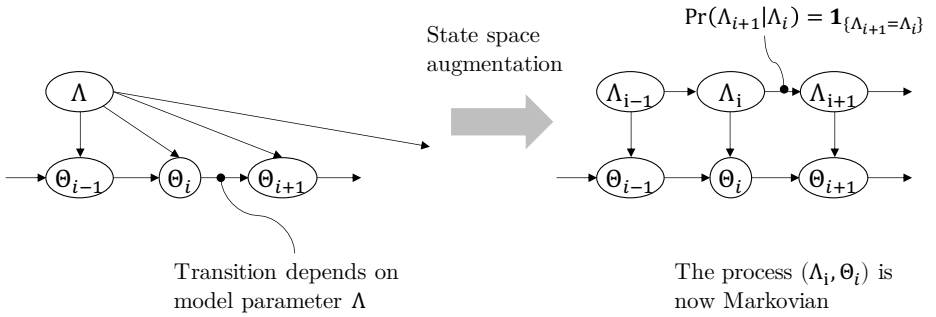

Figure 2.13 Applying state space augmentation to model parameters.

with so-called *Bayes-adaptive MDPs and POMDPs*, which explicitly consider the belief state of the unknown parameters (Duff, 2002; Poupart et al., 2006; Ross et al., 2007). As we will see in Chapter 5, such a hierarchical structure is not only useful for a POMDP formulation, but also to facilitate the computation of the reliability of a system with multiple component (Luque and Straub, 2016).

We note that integrating the uncertainty in the variables of the problem has an interesting effect on the optimization: the optimal strategy, reacting to the information it acquires, and optimally performing with this information, balances the *exploration*, by which one learns about the parameters of the model and decreases the uncertainty on the model by actions which do are not necessarily optimal according to the current knowledge of the model; and the *exploitation*, by which one acts optimally according to what has been learned about the model so far. This mechanism is highlighted in the case study of Chapter 7.

2.4.4. Review of approximate solutions for POMDP

The complexity and challenges associated with solving MDPs and POMDPs described in Section 2.4.3 have motivated the development of numerous methods and algorithms to provide approximate solutions to MDPs and POMDPs, belonging to what Powell (2011) calls *approximate dynamic programming*. In this section, we review the existing methods and summarize their limitation. Kochenderfer (2015) is an excellent reference for an introduction to the main approaches.

There are many ways to classify and rank MDP and POMDP solution methods. One can distinguish between offline and online methods: for the former, the proposed solution strategy is computed once for the entire duration of the lifetime before it is executed; for the latter the strategy is optimized for a number of time-steps, executed and updated as new information is obtained from the environment (e.g., Silver and Veness, 2010). Model-free or model-based is another possible algorithm classification.

In this section, we choose to divide the methods in two main categories in view of the methodology presented in the following Chapter 3: *value function* methods, in which the algorithms output the cost corresponding to a state or state-action pair (value function or Q-value); and *direct policy search* methods, where the algorithms explore directly the space of policy functions. Table 2.1 gives an overview of the main MDP and POMDP solvers.

We strive to mention here the most important methods using the POMDP formulation. However, the research on dynamic programming and approximate dynamic programming has branched out into many fields of application (Duff, 2002) and other methods may have been developed that would deserve to be added to the following review.

2.4.4.1. Value function methods

Point-based value iteration (PBVI) is the approach behind most well-known POMDP approximation algorithms, such as SARSOP (Kurniawati et al., 2008). A review of the performance of PBVI algorithms is available in Shani et al. (2013). The basic idea is described by Pineau et al. (2006). In essence, PBVI solvers exploit the concavity of the optimal value function (Equation (2.22)) and focus the search of $\boldsymbol{\alpha}$-vectors by sampling belief states (the "points") and associating a vector to each point. The resulting set of $\boldsymbol{\alpha}$-vectors can then be used to estimate the optimal value function at any belief point with Equation (2.22). The PBVI algorithms specify how the belief state vectors are generated and how the points are selected. Typically, the algorithms operate on most probable (or reachable) belief points for increased efficiency, such that the approximation error of the optimal value function is less likely to be large in the belief zones where most decisions are taken (Schöbi and Chatzi, 2016).

Most of the existing algorithms are designed for infinite-horizon POMDP, where the resulting value function and strategy are stationary in belief space (see Section 2.4.3.1). The finite-horizon optimal strategy is typically not stationary in the belief space, although time discounting through factor γ attenuates this effect. Walraven and Spaan (2019) showed that these PVBI

algorithms do not easily generalize to finite-horizon problems and proposed the algorithm FiVI to address the added complexity.

Reinforcement learning (RL) algorithms have also been proposed. For infinite-horizon MDP with large state spaces, Q-learning (Watkins, 1989) and SARSA (Rummery and Niranjan, 1994) algorithms learn the Q-values by sampling states, actions and rewards from the environment, by following some exploration policy. These methods are model-free, insofar as the learning algorithm does not require the explicit knowledge of the model transition probabilities. However, they typically suppose that the model is available to sample the trajectories. Unfortunately, SARSA-type algorithms do not ensure convergence when applied to POMDP due to the high state uncertainty. However, they form the basis of more sophisticated RL algorithms, where the value functions are approximated by weighted combinations of linear or non-linear function approximators, also known as artificial neural networks (Williams, 1992). Each layer of the network performs specific operations, as decided by the designer of the network, on successive multidimensional inputs. The weight of each layer is optimized during the training phase. The trained network approximates the optimal value function and thus provides a policy. Deep Q-learning, with non-linear function approximators, has been successfully implemented for relatively large POMDPs (Mnih et al., 2013).

Certain algorithms get around the curses of dimensionality and history by approximating the optimal value function for the current belief state with an online computation. Monte Carlo tree search algorithms (MCTS) for POMDP use a roll-out policy (i.e., an exploration policy) to sample future actions and observations histories from the current belief state over a small number of time steps. In the MCTS algorithm proposed by (Silver and Veness, 2010), the roll-out policy uses random action selection. Each distinct action visited from the initial belief state is associated with an expected cost and the action with the lowest expected cost is executed in real life. As a real observation is obtained, the new belief state is then computed and the roll-out and action selection procedure repeated. The particularity of this method is that, even though the roll-out policy is not optimal, the executed plan demonstrates a very good performance on benchmark problems (Silver and Veness, 2010). MCTS methods have notably been combined with deep RL to greatly improve the performance of trained neural networks (Silver et al., 2017).

2.4.4.2. Direct policy search methods

An alternative to belief- and value function-based solvers is a *direct policy search* (Ng et al., 2000; Rosenstein and Barto, 2001; Powell, 2011), in which one aims at identifying directly and jointly the optimal set of rules for all decisions. This is analogous to the normal form of the decision analysis. The idea behind this approach stem from the observation that policies that are compactly defined can perform very well (Ng et al., 2000), and the effort required to approximate Q-values and value functions in PBVI methods is converted into a parametrized search in policy space.

The policy gradient approach developed by (Sutton et al., 2000) implements a direct policy search, in which the policies are allowed to be stochastic, contrary to PBVI methods. To illustrate, we consider a finite-horizon MDP, and parameters $\boldsymbol{\zeta}_1 ... \boldsymbol{\zeta}_{n_T}$ such that the policy at time step i attributes to each state $\boldsymbol{\theta}$ an action a with a certain probability, parametrized by $\boldsymbol{\zeta}_i$:

$$\pi_i(\boldsymbol{\theta}, a, \boldsymbol{\zeta}_i) = p(A_i = a | \boldsymbol{\Theta} = \boldsymbol{\theta}, \boldsymbol{\zeta}_i). \tag{2.23}$$

The conditional probability distribution belongs to a chosen class and $\boldsymbol{\zeta}_i$ is the distribution parameter. The policies thus defined are improved, through the parameters $\boldsymbol{\zeta}_i$, according to the gradient of the value function, which is typically approximated. Allowing the policies explored to be stochastic effectively relaxes the discrete-domain Equations (2.20) and (2.21).

Sutton et al. (2000) have shown that direct policy search implemented with policy-gradient methods, for infinite-horizon MDPs, presents algorithmic and convergence advantages over PBVI solvers.

Policy search algorithms using deep neural networks can handle finite time horizon and, to a certain extent, POMDPs. These algorithms are popular in the field of motion planning and robotics (e.g., Deisenroth et al., 2013; Montgomery and Levine, 2016; Chebotar et al., 2017). In the actor-critic approach, two neural networks are trained in parallel, emulating the policy gradient method: the *actor* network improves the policy parameters, and the *critic* network approximates the value function. An implementation of such an algorithm for I&M planning is found in (Andriotis and Papakonstantinou, 2019).

The direct policy search approach, by which policies and strategies are parametrized, can be extended beyond the classic POMDP formulation. In the following Chapter 3 we present an approach, which does not require Markovian assumptions on the model, nor the explicit computation of the belief states.

2.5. Limitations of the POMDP formulation for I&M planning of large infrastructure

In this chapter, we have formulated the general I&M planning problem as a SDPs. We have also reviewed the different elements of the POMDP framework, and we have shown how it provides a rigorous mathematical expression of the optimal I&M strategy.

As explained in Section 2.4.3, POMDPs can in theory be solved exactly by dynamic programming with Equation (2.21). The main advantage of this so-called closed-loop, complete solution is that even if one deviates from the prescribed policy, the solution strategy remains optimal for the remaining time horizon. Additionally, the approach is less sensitive to error in the assumptions of the prior model (Section 2.2.3.2) than an open-loop approach (Durango and Madanat, 2002; Kochenderfer, 2015). In practice, however, the equivalent belief-MDP has uncountably infinite state spaces (Kaelbling et al., 1998), and such exact solutions are computationally prohibitive (Papadimitriou and Tsitsiklis, 1987).

Table 2.1 Exact and approximate solutions of MDPs and POMDPs

	EXACT SOLUTIONS	APPROXIMATE SOLUTIONS
MDP	Discrete state space (Kochenderfer, 2015): • Value iteration (finite- and infinite-horizon) • Asynchronous value iteration (infinite-horizon) • Policy iteration (infinite-horizon) continuous state space: • with linear Gaussian dynamics (finite-horizon)	Offline (see Section 2.4.4.1): • Local approximation: optimize only for some states (or belief states) and compute the Q-values and value functions, assuming that states close to each other yield similar costs and actions. • Global approximation • Q-learning • SARSA • Policy gradient methods (Sutton et al., 2000) Online: • Monte Carlo tree search (MCTS) (e.g., Fu, 2016) • sparse sampling (Wang et al., 2005)
POMDP	Discrete state space • Value iteration in belief space using the PLC property Build the set of $\boldsymbol{\alpha}$-vectors One-pass, Witness (e.g., Smallwood and Sondik, 1973) Valid for toy problems with small state space **(Durango and Madanat, 2002)**. Exact belief updating • discrete state space. • continuous state with linear Gaussian model dynamics. Belief updating approximation • particle filter (Coquelin et al., 2008; Silver and Veness, 2010)	Offline • Belief compression and grid approximation (not using convex property) (Roy et al., 2005; **Nielsen and Sørensen, 2015**) • Point-based value iteration Infinite-horizon: SARSOP **(Memarzadeh and Pozzi, 2016)**, PERSEUS **(Papakonstantinou and Shinozuka, 2014)**. For finite-horizon see (Walraven and Spaan, 2019) • Model approximation with Gaussian linear dynamics (Porta et al., 2004, 2005; **Schöbi and Chatzi, 2016**) Online • MCTS-based POMCP (Silver and Veness, 2010) Learning • Reinforcement learning (Kumar, 1985) • Deep Q-learning (Mnih et al., 2013; **Andriotis and Papakonstantinou, 2019**)

Studies relevant to I&M planning are indicated in bold.

Approximate and tractable offline and online solutions for POMDPs using the PBVI solvers and belief state approximations reviewed in Section 2.4.4 and summarized in Table 2.1 have been applied to selected I&M planning problems. However, a review of numerical applications using these approaches reveals that the considered problems have a moderate number of states and actions, and the system is modeled as a single entity (Durango and Madanat, 2002; Papakonstantinou and Shinozuka, 2014; Nielsen and Sørensen, 2015; Schöbi and Chatzi, 2016). Papakonstantinou et al. (2018) compare the efficiency of POMDP algorithms applied to the I&M planning of a deteriorating bridge with few states and conclude that the reviewed solvers cannot handle state spaces larger than 10^4. Therefore, these approaches scale poorly for large multi-component systems such as those described in Chapters 6 and 7, which can easily have a state-space of size 10^{100} or larger (Bismut et al., 2017).

When the system components are explicitly modeled, the interdependence and correlation effects on the components and the system cannot be accounted for due to the unmanageable size of the POMDP (Memarzadeh et al., 2016), and Luque and Straub (2013) showed that this effect cannot be ignored.

As discussed in Section 2.4.3.2, implementing POMDP solvers present significant computational challenges, whether it is the hurdle of transforming the non-Markovian processes in the SDP by state space augmentation or belief updating and approximation (e.g., Nielsen and Sørensen, 2015).

Additionally, overcoming these modeling challenges and using a POMDP representation may not even be worth the effort. In the case of a single component subject to fatigue, Nielsen and Sørensen (2015) find that, while the step-by-step policy description provides interesting insights about the optimal strategy, the belief approximation is time consuming and the POMDP approach does not perform better than the simpler threshold-based strategy description.

The POMDP approach implemented with deep neural networks has, however, shown promising result and could be extended to handle the optimization I&M planning for large, multi-component systems (Andriotis and Papakonstantinou, 2019). Nevertheless, the optimal strategy yielded by the POMDP approach is typically more elaborate than with a simple strategy parametrization (Papakonstantinou and Shinozuka, 2014), and may not be intuitively understandable by the decision-maker. This could result counterproductive, as we discuss in the next Chapter 3, where we address optimal I&M planning with a different approach.

Chapter 3

Heuristic adaptive planning

> Le grand art, c'est de changer pendant la bataille. Malheur au général qui arrive au combat avec un système.
>
> *Le mémorial de Saint Helène*
> Emmanuel de Las Cases

Parts of this chapter originate from Bismut, E. and Straub, D. (2021). "Optimal adaptive inspection and maintenance planning for deteriorating structural systems". In: *Reliability Engineering & System Safety* 215, p. 107891.

3.1. Peering into the black box

In Chapter 2, we have established that finding the optimal strategy for I&M planning is an intractable problem. The dynamic programming approach, although in principle providing the exact solution, cannot cope with its complexity. Many algorithms have attempted to get around this obstacle and provided approximate dynamic programming solutions. However, the output of these algorithms, in the form of a mapping between belief state and actions, are typically hard to interpret: While the output strategy will assign inspection decisions and maintenance actions at any moment it is prompted to do so, *it will not explain why it is doing so*. This black-box effect, which leaves the decision-maker oblivious to the inner workings of the strategy, can in real-life lead to distrust and eventually dismissal of this strategy (Zhou et al., 2017). The planning approach presented in this chapter aims to reconnect the decision-maker with the strategy optimization and to make use of expert knowledge.

In the context of I&M planning, the engineering understanding allows the identification of suitable functional forms of the policies. We call these *heuristics*. For example, a simple heuristic is to perform an inspection campaign whenever the reliability of the structure falls below a threshold (Bloch et al., 2000). Through such heuristics, the implementation of a direct policy search (see Section 2.4.4.2) is straightforward. The optimization is performed over a few heuristic parameters to search the space of policies. The heuristic formulation to the decision problem is presented in Section 3.2.

When optimizing inspections for structural components, it has been found that heuristics lead to solutions that are close to the optimum POMDP solutions in terms of the resulting expected

total life-cycle costs (Nielsen and Sørensen, 2015). Heuristics for I&M at the component level are usually simple to define. However, for multi-component systems, I&M decision rules must handle a much wider choice of actions, and in particular the question of prioritization of actions. More importantly, assessing the performance of I&M plans in multi-component systems requires the evaluation of the effects of component-level actions on the system reliability.

Most RBI planning methodologies in the literature are based on such heuristic strategies, mostly in an ad-hoc manner (e.g., Thoft-Christensen and Sørensen, 1987; Lam and Yeh, 1994; Faber et al., 2000; Straub, 2004; Moan, 2005; Nielsen and Sørensen, 2014). These methodologies perform the optimization component-by-component, without considering the interaction among components. Hence it cannot be ensured that the resulting plans are optimal at the system level. In fact, (Luque and Straub, 2019) show that component-based optimization can lead to strongly sub-optimal I&M plans. (Straub, 2004; Straub and Faber, 2005) consider an extension to address system effects in a simplified manner. Other studies have proposed a heuristic-based maintenance planning for series and parallel systems with independent or fully correlated failure modes, but do not account for the effect of inspection results on the components and system reliability (Barone and Frangopol, 2014).

Luque and Straub (2019) have proposed a methodology to assess heuristic strategies for system-level I&M planning, which accounts for the interdependence among components. The methodology relies on the computation of the time-variant system reliability by means of a dynamic Bayesian network (DBN) model developed in (Straub, 2009; Luque and Straub, 2016). This system model and the relevant reliability methods are presented in Chapter 5.

In their study, Luque and Straub (2019) evaluate the expected cost of selected system-level I&M plans without performing a formal optimization. In Section 3.2, we expand on this this methodology and formalize the heuristic optimal planning approach.

A further contribution of this work is the introduction of adaptive planning, whereby the heuristic I&M plan is modified as new information through inspections and monitoring becomes available (Section 3.3). We show that re-optimizing the heuristic parameters once new information is available leads to better I&M plans.

It ensues from the heuristic formulation that the choice of heuristics directly affects the efficiency of the strategy found. Section 3.4 discusses the relevance of the selection of heuristics for I&M planning and proposes heuristic parameters that prescribe inspection times and locations. Notably, the heuristic approach allows the decision-maker to include operational constraints. In the numerical investigations of Chapters 6 and 7, we also show how to identify I&M plan sensitivities in the expected total life cycle cost, through the heuristic parametrization.

In the presented heuristic planning methodology, the I&M plans are evaluated in terms of expected total life-cycle I&M cost and failure risk, as described in Section 3.5. The I&M plans are optimized by means of the cross-entropy method (Rubinstein and Kroese, 2017) (Section 3.6).

3.2. Heuristic approach to direct policy search

We examine the planning problem example with N components presented in Section 2.4.3.1. Going through each of the $3^{N\frac{n_T^{n_{obs}}-1}{n_{obs}-1}}$ strategies is clearly impossible. Instead, the solution space $\mathscr{S}$ can be reduced by choosing a suitable heuristic. A heuristic is defined by a set of rules with a set of parameters $\boldsymbol{w} = \{w_1, ..., w_h\}$ so that an I&M strategy is fully defined by the heuristic and the values of its parameters. A simple (although likely suboptimal) example of a heuristic is: Inspect all components of the structure whenever the reliability estimate is below a threshold, then repair all components at which defects are found. In this case, the heuristic parameter is the reliability threshold. A heuristic strategy is well defined when every decision can be resolved, such that the questions when and where to inspect and repair are clearly answered (see Section 3.4). The strategies $\mathcal{S}_{\boldsymbol{w}}$ resulting from such a heuristic form a subspace of $\mathscr{S}$. A major appeal of this approach resides in the fact that one can explicitly include operational constraints in the definition of a suitable plan.

The solution $\mathcal{S}^*$ to the optimization problem in Equation (2.17) is therefore approximated by $\mathcal{S}_{\boldsymbol{w}^*}$, where

$$\boldsymbol{w}_0^* = \arg\min_{\boldsymbol{w}} \left(\mathbf{E}\left[C_{\text{tot}} | \mathcal{S}_{\boldsymbol{w}} \right] \right). \tag{3.1}$$

From this point forward, we use $\mathbf{E}[\cdot|\boldsymbol{w}]$ to denote $\mathbf{E}[\cdot|\mathcal{S}_{\boldsymbol{w}}]$ for the sake of simplicity in the notation.

The heuristic parametrization of Equation (2.17) naturally reduces the solution space of strategies. In addition, the chosen heuristic parameters can take discrete values, e.g., "*3* components must be inspected" or continuous values, e.g., "repair if the measured crack is larger than *10.5* mm". In the example cited above, the space of distinct strategies is discrete and finite, although very large. In such a case, a heuristic parametrization of a subset of strategies with continuous values has two consequences: distinct parameter values could describe the same strategy in $\mathscr{S}$; and the subset explored also includes strategies with stochastic policies in the belief space (see Sections 2.4.4.2 and 3.7).

The proposed optimization method for this heuristic formulation of the I&M planning problem relies on the stochastic computation of the expected life-cycle cost of a strategy presented in Section 3.5 and is developed in Section 3.6. A key aspect of this approach is that the transformation of the SDP into a POMDP and, hence, the Markov property, is not required for the optimization procedure. The Markov property is nonetheless useful to improve the computational efficiency, as we discuss in Chapter 5.

One challenge is the selection of the heuristic, so that the strategies explored are close enough to the exact solution of Equation (2.17). In the context of machine learning, this selection is controlled by hyperparameters that can in turn be optimized, or "tuned". For optimal training of neural networks, (Diaz et al., 2017) propose a derivative-free algorithm for the optimization of these tuning parameters. This tuning aspect and more generally optimizing the choice of heuristic is not formally investigated in this work but initial studies have been carried out on the goodness of heuristics (Bismut and Straub, 2019).

In I&M planning problems, the choice of heuristics is often driven by operational constraints, such as the need for regular inspection intervals. The heuristic can also include reliability criteria that need to be fulfilled (Tsang, 1995; Nielsen and Sørensen, 2014). The heuristics are also not required to incorporate information about the system. For instance, a valid strategy is one that prescribes to replace a system every 10 years, regardless of its actual state of deterioration or of any prior collected information. Such systematic plans are typically adopted for non-crucial components of a system (e.g., air filters of an air handling unit); they are rarely based on a quantitative optimization, however. We discuss appropriate heuristics for I&M planning in deteriorating structures in Section 3.4.

3.3. Adaptive planning

Following Equation (3.1), the optimal heuristic is found initially and kept throughout the system lifetime T. However, as new observations $\boldsymbol{Z}_{1:i}$ become available, the initially optimal strategy may no longer be optimal. Therefore, we suggest to adapt the strategy during the lifetime of the structure by adding an on-line computation which accounts for the new observations $\boldsymbol{Z}_{1:i}$.

Initially, one performs the optimization with the prior model following Equation (3.1) to obtain the optimal parameters $\boldsymbol{w}_0^*$. The actions (e.g., inspections and eventual repairs) are performed as dictated by $\boldsymbol{w}_0^*$ until a time step j_1, typically when new information is available. At t_{j_1}, the decision maker has the opportunity to improve the strategy.

By updating the prior model with information obtained up to time t_{j_1}, $\boldsymbol{Z}_{1:j_1}$, a strategy heuristic optimization is again performed for the rest of the service life of the structure, and a new heuristic parameter value $\boldsymbol{w}_1^*$ and its associated strategy are obtained, as

$$\boldsymbol{w}_1^* = \arg\min_{\boldsymbol{w}} \mathbf{E}\left[C_{\text{tot},j_1:n_T} | \boldsymbol{w}, \boldsymbol{Z}_{1:j_1}\right]. \tag{3.2}$$

$C_{\text{tot},j_1:n_T}$ is the total cost evaluated from time step j_1 onwards, as opposed to $C_{\text{tot},1:n_T}$, evaluated from time step 1 onwards. $\mathbf{E}\left[\cdot | \boldsymbol{w}, \boldsymbol{Z}_{1:j_1}\right]$ is the expectation operator conditional on the observation and repair history up to time step j_1, applying strategy parameters $\boldsymbol{w}$.

It follows from Equation (3.2) that

$$\mathbf{E}\left[C_{\text{tot},j_1:n_T} | \boldsymbol{w}_0^*, \boldsymbol{Z}_{1:j_1}\right] \geq \mathbf{E}\left[C_{\text{tot},j_1:n_T} | \boldsymbol{w}_1^*, \boldsymbol{Z}_{1:j_1}\right]. \tag{3.3}$$

Our aim is to show that the adaptive planning decreases the expected total life-cycle cost. For this purpose, we decompose the expected total life-cycle cost of strategy $\boldsymbol{w}_0^*$ into

$$\mathbf{E}\left[C_{\text{tot},1:n_T} | \boldsymbol{w}_0^*\right] = \mathbf{E}\left[C_{\text{tot},1:j_1} | \boldsymbol{w}_0^*\right] + \mathbf{E}_{\boldsymbol{Z}_{1:j_1}}\left[\mathbf{E}\left[C_{\text{tot},j_1:n_T} | \boldsymbol{w}_0^*, \boldsymbol{Z}_{1:j_1}\right]\right], \tag{3.4}$$

where $C_{\text{tot},1:\tau_1} | \boldsymbol{w}_0^*$ is the cost incurred until time t_{j_1} following strategy $\mathcal{S}_{\boldsymbol{w}_0^*}$. The expectation $\mathbf{E}_{\boldsymbol{Z}_{1:j_1}}[\cdot]$ operates on the observation and repair history up to time step j_1. This operator

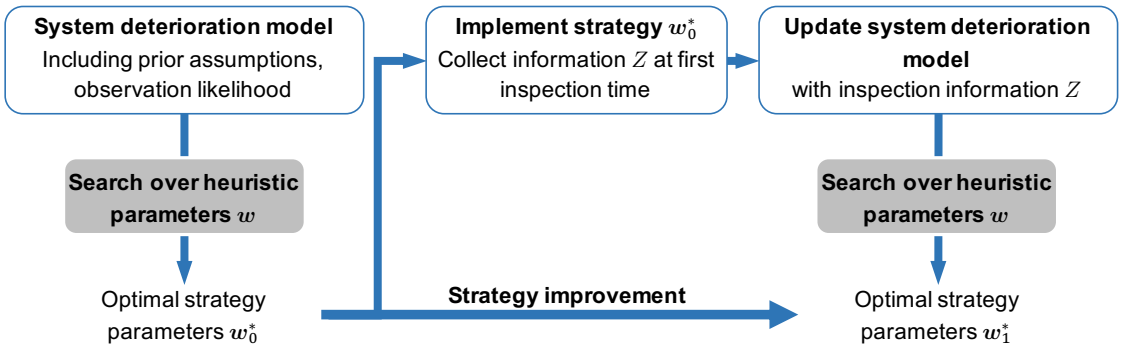

Figure 3.1 One-step adaptive I&M planning with heuristic search (Bismut and Straub, 2021).

preserves the inequality in Equation (3.3), hence by combining Equations (3.3) and (3.4), we obtain that

$$\mathbf{E}\left[C_{\text{tot},1:n_T}|\boldsymbol{w}_0^*\right] \geq \mathbf{E}\left[C_{\text{tot},1:j_1}|\boldsymbol{w}_0^*\right] + \mathbf{E}_{\boldsymbol{Z}_{1:j_1}}\left[\mathbf{E}\left[C_{\text{tot},j_1:n_T}|\boldsymbol{w}_1^*, \boldsymbol{Z}_{1:j_1}\right]\right]. \tag{3.5}$$

The difference between the left- and right-hand side of Equation (3.5) quantifies the expected gain by adapting the strategy at time t_{j_1}. Figure 3.1 retraces the steps of this strategy improvement.

In the context of production and supply optimization, a similar approach is known as model predictive control (MPC) (Pooya and Pakdaman, 2018). The principle is also adopted to improve reinforcement learning algorithms (Kahn et al., 2017), and is key to the MCTS POMCP algorithm presented in (Silver and Veness, 2010).

The strategy adaptation can be repeated every time new information is collected. The array $\boldsymbol{W}^*$ stores the successively adapted heuristic parameters values:

$$\boldsymbol{W}^* = \{\boldsymbol{w}_0^*, \boldsymbol{w}_1^*, \boldsymbol{w}_2^*, \ldots, \boldsymbol{w}_{n_{ADAPT}}^*\}, \tag{3.6}$$

Algorithm 1 summarizes the adaptive planning method.

The proposed adaptive planning is an on-line optimization at the level of array $\boldsymbol{W}^*$ and is greedy since the strategy optimization is always performed assuming that it is the last opportunity to optimize the strategy. Multi-step-based improvement greedy techniques have demonstrated to perform much better than a single initial optimization, as shown empirically with several algorithms (Silver and Veness, 2010; Efroni et al., 2018; Pooya and Pakdaman, 2018).

3.4. Heuristics for I&M planning

The proposed approach requires the definition of appropriate heuristics. The heuristic should be flexible enough to ensure that a sufficiently high number of strategies can be explored and that it can define a near-optimal strategy. This last goal is ambitious due to the intractable

Algorithm 1: Procedure for adaptive I&M planning

input : heuristic, number of times steps n_T for time horizon T, adaptation times $\boldsymbol{j} = \{j_1, \ldots, j_{n_{ADAPT}}\}$, $prior\_model$

output : $\boldsymbol{W}^*$

$l \leftarrow 0$;
$model \leftarrow prior\_model$;
repeat
  $\boldsymbol{w}_l^* \leftarrow \arg\min_{\boldsymbol{w}}(\mathbf{E}[C_{\text{tot},j_{l+1}:n_T}|\boldsymbol{w}, model])$; ▷ `find optimal heuristic parameters, e.g., with alg. 3`
  $l \leftarrow l + 1$;
  if no system failure before t_{j_l} **then**
    Perform inspections and repairs following $\boldsymbol{w}_{l-1}^*$ until t_{j_l}
    $model \leftarrow update\_model(model, \boldsymbol{z_{1:j_l}})$; ▷ `update deterioration model with` $\boldsymbol{z}_{1:j_l}$
  end
until $l > n_{ADAPT}$;
return $\boldsymbol{W}^* = \{\boldsymbol{w}_0^*, ..., \boldsymbol{w}_{n_{ADAPT}}^*\}$

nature of the planning problem. Nevertheless, choosing a suitable heuristic can lead to improving current I&M practice (e.g., Bismut et al., 2022) and revealing the value of SHM systems (Kamariotis et al., 2022) .

As an example, an overly simplistic heuristic is to never inspect and repair systematically at fixed time intervals ΔT. Finding the solution of Equation (3.1) is then equivalent to an optimization over one heuristic parameter $\boldsymbol{w} = \Delta T \in \{1, ..., T\}$. It is very likely that a heuristic strategy, which conditions the repair decision on observation outcomes, has a lower expected total life-cycle cost.

3.4.1. Choosing I&M heuristics

For I&M planning of a multi-component deteriorating system, the possible decisions must answer the elementary questions of "when", "where", "what" and "how" to inspect, and "when", "where", "what" and "how" to repair.

The answers to questions "what" and "how" to inspect and repair are dependent on the deterioration mechanism and are in general determined by expert knowledge of the system, and the availability of repair and inspection techniques. They are not within the scope of this work and are not further discussed. However, Chapter 4 provides the framework for comparing non-destructive evaluation (NDE) methods in the decision analysis context. The considerations addressed in the following sections can easily be applied to these questions.

For general I&M planning problems it is difficult to assess the efficiency of a chosen heuristic ahead of performing the heuristic optimization and obtaining the optimal expected cost for that heuristic. However, some guiding principles for building heuristic strategies can be hypothesized. Because they address information collection, the inspection-related questions are more complex to parametrize and are discussed in the following Sections 3.4.2 and 3.4.3.

They are treated sequentially, choosing first "when", then "where" to inspect. The repair rules are then addressed in Section 3.4.4.

3.4.2. "When" to inspect

An inspection can be planned to take place at specific times during the service life of the structure. It can also be triggered by exceeding a threshold p_{th}, for instance on the failure rate. This rate can usually be approximated by the annual probability of failure due to the high reliability of the structure. When a monitoring system is in place, an inspection might be triggered by the exceedance of a monitoring data threshold.

A number of scientific studies have focused on I&M planning for a single component, answering the question "when" to inspect (e.g., Thoft-Christensen and Sørensen, 1987; Grall et al., 2002; Straub and Faber, 2006; Nielsen and Sørensen, 2010b). By prescribing regular inspection times, or triggering inspections with a fixed threshold on the probability of failure of the component (Faber et al., 2000), these single-parameter heuristics have proven to yield a strategy that performs similarly in terms of cost and prescribed times of inspection as an optimal strategy found through POMDP or LIMID methods (Nielsen and Sørensen, 2010a; Luque and Straub, 2013).

The choice of a heuristic parameter prescribing an inspection campaign might be based on operational constraints, for instance inspections might have to be planned at regular time intervals ΔT. In other instances, they may arise from established practices.

3.4.3. "Where" to inspect: component prioritization and value of information

This question is specific to multi-component systems, where inspecting the entire system at every inspection campaign is suboptimal or not even feasible. Rather, one would typically inspect only a subset of all components during an inspection campaign. However, the optimal selection of components for inspection during an I&M campaign is a sequential decision problem in itself. Straub and Faber (2005) describe the intractability of the problem and propose instead to consider the solution through the VoI concept.

Because of the correlation among the components' deterioration (see Chapter 5), inspecting one component can provide information about the condition of other components. The value of this information can in theory be quantified, as demonstrated in (Straub and Faber, 2005). It seems reasonable to perform the component inspections with the highest VoI. An analogy to this heuristic can be found in the solution to the famous infinite horizon multi-armed bandit provided by Gittins (1979), in which a dynamic allocation index determines which arm to pull next based on the previous outcomes. However, estimating the VoI in multi-component systems is computationally challenging.

Instead, we propose a heuristic, where the first parameter n_I is the number of components to inspect at each campaign. We then introduce proxies for the VoI by recognizing fundamental contributions to this value: (a) the reduction of the uncertainty on the condition of the

inspected component and the corresponding effect on the system reliability; and (b) the reduction of the uncertainty on the condition of other components, through the components' interdependence.

These reductions are related to two quantities: the first is the probability of failure of component k, $\Pr(F_{c_k}|\boldsymbol{Z}_{1:i-1})$, conditional on all components' inspection outcomes up to that point. RBI planning revealed in particular that inspecting components with a higher probability of failure provides more information on the deterioration of other components than inspecting components with a lower probability of failure (Straub and Faber, 2005). Other characteristics of the distribution of the state of damage of the components can also be considered, such as the expected value or the coefficient of variation of the distribution.

The second quantity is the Single Element Importance measure for component k (SEI_k), defined as the difference between the probability of failure of the intact system and the probability of failure of the system when only component k has failed (Straub and Der Kiureghian, 2011):

$$SEI_k = \Pr(F_s|\overline{F_{c_1}},\dots,\overline{F_{c_{k-1}}},F_{c_k},\overline{F_{c_{k+1}}},\dots,\overline{F_{c_N}}) - \Pr(F_s|\overline{F_{c_1}},\dots,\overline{F_{c_N}}) \tag{3.7}$$

We introduce a Prioritization Index, PI_k, which combines these two contributions explicitly, serves as a proxy for the VoI, and prioritizes the components for inspection. The VoI of inspecting component k is linked to the reduction of the probability of system failure. This probability can be expressed approximately as a linear function of SEI_k and $\Pr(F_{c_k}|\boldsymbol{Z}_{1:i-1})$, as detailed in Appendix A. Hence, the VoI increases with increasing SEI_k and increasing $\Pr(F_{c_k}|\boldsymbol{Z}_{1:i-1})$.

It is not known in advance which contribution has the largest effect. For this reason, an adjustable exponent η serves as a heuristic parameter to combine the two effects within the Prioritization Index PI_k,

$$PI_k = (SEI_k)^{\eta} \cdot \Pr(F_{c_k}|\boldsymbol{Z}_{1:i-1}), \text{ with } \eta \geq 0. \tag{3.8}$$

This index is the proxy for the VoI used in the example of Chapter 6, where we show the effect of η on the resulting I&M strategy.

In the example of Chapter 7, all system components (the pipes) have the same SEI, hence the Prioritization Index thus defined ranks the components according to their probability of failure. This is a valid prioritization rule. However, numerical investigations for this example show that a better proxy for selecting n_I components for inspection is to rank them according to the coefficient of variation of their damage state. This chosen proxy is compatible with point (a) raised above, which links VoI with uncertainty on the condition of the inspected component.

Other factors could be considered for the prioritization, such as the effect of varying component correlations, inspection quality, and cost of inspection. For instance, an underwater part

of an offshore structure is more difficult and costly to inspect with the same accuracy as a part of the superstructure. In the applications of Chapters 6 and 7, we limit the study to equi-correlated components, with equal inspection quality and cost. Additional factors with corresponding exponents (i.e., additional heuristic parameters) could however be introduced into Equation (3.8).

3.4.4. "When" and "where" to repair

The questions "when" and "where" to repair can be classified according to the type of maintenance (Figure 3.2); for example, in corrective maintenance, repair or replacement occurs upon failure of the system; in systematic preventive maintenance, repair or replacement occurs at times fixed in advance, irrespective of any observation on the state of the system. (Barlow and Hunter, 1960; Nielsen and Sørensen, 2010b).

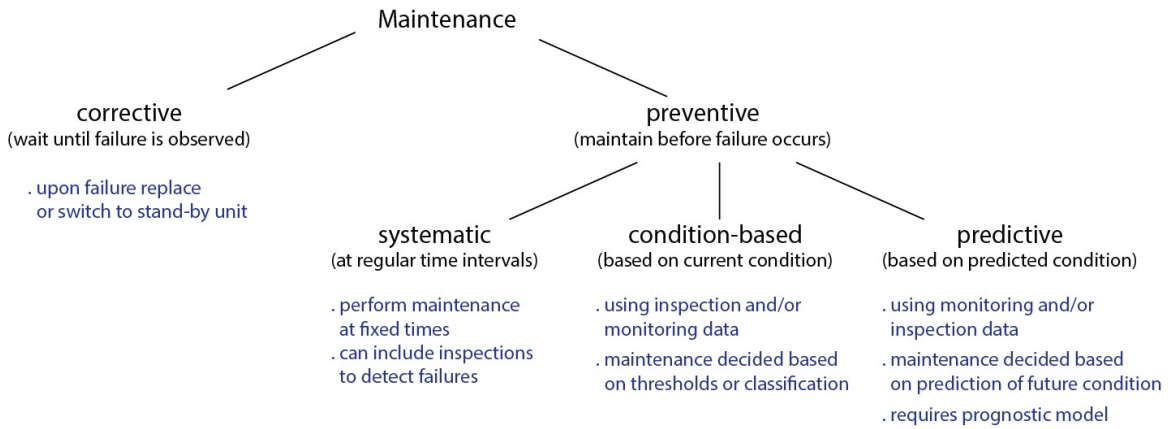

Figure 3.2 Types of maintenance (Straub and Bismut, 2019).

Corrective system maintenance is, by definition, unplanned: it is only triggered by the complete failure of the system. Therefore, there is no need to define a specific heuristic to account for this maintenance type. However, in the case of hidden system (or component) failures, e.g., for standby safety systems in a nuclear power plant, it is beneficial to optimize the inspection strategy (Rausand and Høyland, 2004). To this end, the heuristics introduced in Sections 3.4.2 and 3.4.3 above are relevant.

This work focuses mainly on preventive maintenance, whether condition-based or predictive. The efficiency of such maintenance actions is tightly linked with the means of collecting information on the system, which we addressed above in Sections 3.4.2 and 3.4.3. With this information one can refine a prognostic model, on which to base repair rules, but simpler heuristic can also be defined.

Component repair can be directly linked to inspection decisions, such that repair can only occur on components that have been inspected. In the numerical application of Chapter 6, the heuristic strategies investigated are relevant for a condition-based preventive maintenance, where repair actions are decided based on an estimate of the current condition of the system

using inspection and monitoring data. In this approach, a component repair is triggered by an inspection result. With some generality, this repair decision can be parametrized by a threshold D_{rep}: Whenever the identified defect exceeds D_{rep}, a repair is triggered.

In contrast, in the case study of Chapter 7, the maintenance decision is encoded in a more complex manner in the heuristic description of the strategies and is triggered based on a threshold p_{th} applied to the system annual probability of failure. The components are first selected preventively for repair according to their individual probability of failure. With such a heuristic it is possible for components to be repaired even though they have not been inspected. If this is not acceptable to the decision-maker, the heuristic can always be amended to incorporate practical constraints.

3.5. Stochastic computation of strategy cost

The heuristic approach requires the computation of the objective function $\mathbf{E}[C_{\text{tot}}|\boldsymbol{w}]$ in Equation (3.1). The influence diagram of Figure 2.9 shows the decision process and all the costs incurred during the service life of the structure.

3.5.1. Cost breakdown

We assume that a model describing the dynamics of the system (deterioration, loads, structural response), including a prior probabilistic model of uncertain parameters, is available to the analyst (see Chapter 5).

The expectation $\mathbf{E}[C_{\text{tot}}|\boldsymbol{w}]$ of the total cost of a strategy operates on the state of the system $\boldsymbol{\Theta}$, which includes the time varying system capacity and the applied loads, and on the observation outcomes $\boldsymbol{Z} \in \Omega_{\boldsymbol{Z}}$.

$$\mathbf{E}[C_{\text{tot}}|\boldsymbol{w}] = \mathbf{E}_{\boldsymbol{\Theta},\boldsymbol{Z}}[C_{\text{tot}}|\boldsymbol{w}] = \int_{\Omega_{\boldsymbol{\Theta}}} \int_{\Omega_{\boldsymbol{Z}}} C_{\text{tot}}(\boldsymbol{w}, \mathbf{z}, \boldsymbol{\theta}) f_{\boldsymbol{\Theta},\boldsymbol{Z}|\boldsymbol{w}}(\boldsymbol{\theta}, \mathbf{z}|\boldsymbol{w}) \mathrm{d}\mathbf{z}\mathrm{d}\boldsymbol{\theta}, \tag{3.9}$$

where $f_{\boldsymbol{\Theta},\boldsymbol{Z}|\boldsymbol{w}}(\boldsymbol{\theta}, \mathbf{z}|\boldsymbol{w})$ is the joint probability distribution of $\boldsymbol{\Theta}$ and $\boldsymbol{Z}$ conditional on the strategy parameters $\boldsymbol{w}$.

This expectation can be approximated with crude Monte Carlo simulation (MCS). However, when the expected costs involve the risk of failure, and if the underlying probability of failure is small, then the Monte Carlo (MC) sampling over both $\boldsymbol{\Theta}$ and $\boldsymbol{Z}$ is computationally expensive because a large number of samples is necessary to achieve an acceptable accuracy. Therefore, following (Luque and Straub, 2019) we propose to first evaluate the expected costs conditional on $\boldsymbol{Z}$ (Equation (3.11)), and then perform an MCS over the observation history $\boldsymbol{Z}$. To this end, Equation (3.9) is rewritten as

$$\mathbf{E}[C_{\text{tot}}|\boldsymbol{w}] = \int_{\Omega_{\boldsymbol{Z}}} \mathbf{E}_{\boldsymbol{\Theta}|\mathbf{z}}[C_{\text{tot}}(\boldsymbol{w}, \mathbf{z}, \boldsymbol{\Theta})|\boldsymbol{w}, \mathbf{z}] f_{\boldsymbol{Z}|\boldsymbol{w}}(\mathbf{z}|\boldsymbol{w}) \mathrm{d}\mathbf{z}, \tag{3.10}$$

where $f_{\boldsymbol{Z}|\boldsymbol{w}}(\mathbf{z}|\boldsymbol{w})$ is the probability distribution of the service life observations $\boldsymbol{Z}$ conditional on $\boldsymbol{w}$. The corresponding MC estimate and its computational advantage over the crude MCS are discussed in Section 3.5.4.

The total life-cycle cost $C_{\text{tot}}(\boldsymbol{w}, \boldsymbol{Z}, \boldsymbol{\Theta})$ is the sum of the inspection campaign costs $C_C(\boldsymbol{w}, \boldsymbol{Z}, \boldsymbol{\Theta})$, component inspection costs $C_I(\boldsymbol{w}, \boldsymbol{Z}, \boldsymbol{\Theta})$, repair costs $C_R(\boldsymbol{w}, \boldsymbol{Z}, \boldsymbol{\Theta})$ and failure costs $C_F(\boldsymbol{w}, \boldsymbol{Z}, \boldsymbol{\Theta})$ over the lifetime of the structure. All these costs are present values, i.e., they are discounted to time 0. Hence the expected total life-cycle cost conditional on the observation outcomes $\boldsymbol{Z}$ for given heuristic parameters $\boldsymbol{w}$ is

$$\mathbf{E}_{\boldsymbol{\Theta}|\boldsymbol{Z}}[C_{\text{tot}}|\boldsymbol{w}, \boldsymbol{Z}] = \mathbf{E}_{\boldsymbol{\Theta}|\boldsymbol{Z}}[C_C|\boldsymbol{w}, \boldsymbol{Z}] + \mathbf{E}_{\boldsymbol{\Theta}|\boldsymbol{Z}}[C_I|\boldsymbol{w}, \boldsymbol{Z}] + \mathbf{E}_{\boldsymbol{\Theta}|\boldsymbol{Z}}[C_R|\boldsymbol{w}, \boldsymbol{Z}] + \mathbf{E}_{\boldsymbol{\Theta}|\boldsymbol{Z}}[C_F|\boldsymbol{w}, \boldsymbol{Z}]. \tag{3.11}$$

The following sections detail how the individual terms in Equation (3.11) are evaluated.

3.5.2. Computing the conditional risk of failure

Failure is here considered a terminal event. This means that if failure of the system occurs before the end of the service life, no further inspection and repair actions are explicitly considered from that point on. This simplifying assumption does not significantly affect the estimate of the expected total life-cycle cost, due to the high reliability of infrastructure systems (Kübler and Faber, 2004). The fixed cost c_F in case of failure includes replacement costs and future life-cycle costs of the new structure. When failure occurs at time t, the associated cost expressed as present value is $\gamma(t) \cdot c_F$, where $\gamma(t)$ is the discount factor.

The conditional risk of failure over the lifetime of the structure $\mathbf{E}_{\boldsymbol{\Theta}|\boldsymbol{Z}}[C_F|\boldsymbol{w}, \boldsymbol{Z}]$ can be defined in terms of T_F, the time to failure of the system. T_F is a random variable and is dependent on the implemented strategy $\mathcal{S}_{\boldsymbol{w}}$ and the system history $\boldsymbol{Z}$. Its PDF is denoted by $f_{T_F|\boldsymbol{w},\boldsymbol{Z}}(t)$. It is

$$\mathbf{E}_{\boldsymbol{\Theta}|\boldsymbol{Z}}[C_F|\boldsymbol{w}, \boldsymbol{Z}] = \mathbf{E}_{T_F|\boldsymbol{Z}}[C_F|\boldsymbol{w}, \boldsymbol{Z}] = \int_0^T c_F \cdot \gamma(t) \cdot f_{T_F|\boldsymbol{w},\boldsymbol{Z}}(t)\mathrm{d}t. \tag{3.12}$$

As time is discretized in n_T time steps (years), the integration in Equation (3.12) is approximated by

$$\mathbf{E}_{\boldsymbol{\Theta}|\boldsymbol{Z}}[C_F|\boldsymbol{w}, \boldsymbol{Z}] \simeq c_F \cdot \sum_{i=1}^{n_T} \gamma(t_i) \cdot \left[F_{T_F|\boldsymbol{w},\boldsymbol{Z}}(t_i) - F_{T_F|\boldsymbol{w},\boldsymbol{Z}}(t_{i-1})\right], \tag{3.13}$$

where $F_{T_F|\boldsymbol{w},\boldsymbol{Z}}$ is the CDF of the conditional T_F. In particular, $[F_{T_F|\boldsymbol{w},\boldsymbol{Z}}(t_i) - F_{T_F|\boldsymbol{w},\boldsymbol{Z}}(t_{i-1})]$ is the annual probability of failure for year i. The significance of the variable T_F and the methods of computation of these conditional probabilities are detailed in Chapter 5.

3.5.3. Computing the conditional expected inspection and repair costs

Since failure is a terminal event, the evaluations of expectations $\mathbf{E}_{\boldsymbol{\Theta}|\boldsymbol{Z}}[C_C|\boldsymbol{w}, \boldsymbol{Z}]$, $\mathbf{E}_{\boldsymbol{\Theta}|\boldsymbol{Z}}[C_I|\boldsymbol{w}, \boldsymbol{Z}]$ and $\mathbf{E}_{\boldsymbol{\Theta}|\boldsymbol{Z}}[C_R|\boldsymbol{w}, \boldsymbol{Z}]$ consider that an observation or repair action at a time t_i can occur only if the system has survived until that time. For instance, the conditional expected life-cycle

inspection campaign costs are calculated as

$$\mathbf{E}_{\boldsymbol{\Theta}|\boldsymbol{Z}}[C_C|\boldsymbol{w},\boldsymbol{Z}] = \sum_{i=1}^{n_T} \gamma(t_i) \cdot c_C(t_i,\boldsymbol{w},\boldsymbol{Z}) \cdot \left[1 - F_{T_F|\boldsymbol{w},\boldsymbol{Z}}(t_i)\right], \tag{3.14}$$

where $c_C(t_i,\boldsymbol{w},\boldsymbol{Z})$ is the inspection campaign cost incurred at time t_i as prescribed by strategy $\mathcal{S}_{\boldsymbol{w}}$ and inspection history $\boldsymbol{Z}$, and $1 - F_{T_F|\boldsymbol{w},\boldsymbol{Z}}(t_i)$ is the probability of survival of the system up to time t_i.

Similarly, the conditional expected life-cycle component inspection cost and life-cycle repair cost are evaluated as

$$\mathbf{E}_{\boldsymbol{\Theta}|\boldsymbol{Z}}[C_I|\boldsymbol{w},\boldsymbol{Z}] = \sum_{i=1}^{n_T} \gamma(t_i) \cdot c_I(t_i,\boldsymbol{w},\boldsymbol{Z}) \cdot \left[1 - F_{T_F|\boldsymbol{w},\boldsymbol{Z}}(t_i)\right], \tag{3.15}$$

$$\mathbf{E}_{\boldsymbol{\Theta}|\boldsymbol{Z}}[C_R|\boldsymbol{w},\boldsymbol{Z}] = \sum_{i=1}^{n_T} \gamma(t_i) \cdot c_R(t_i,\boldsymbol{w},\boldsymbol{Z}) \cdot \left[1 - F_{T_F|\boldsymbol{w},\boldsymbol{Z}}(t_i)\right], \tag{3.16}$$

3.5.4. Monte Carlo simulation over inspection history Z

In Equation (3.9), the conditional expectation $\mathbf{E}_{\boldsymbol{\Theta}|\boldsymbol{Z}}[C_{\text{tot}}|\boldsymbol{w},\boldsymbol{Z}]$ must be integrated over all possible outcomes $\boldsymbol{Z}$. The integral over $\boldsymbol{Z}$ cannot be easily computed analytically, as the probability distribution of all possible inspection outcomes $f_{\boldsymbol{Z}|\boldsymbol{w}}(\mathbf{z})$ is not readily available.

However, sampling from this distribution is possible, by first generating deterioration histories from the model, and then generating inspection outcomes $\mathbf{z}^{(q)}$ conditional on the deterioration and the adopted strategy. Algorithm 2 outlines the steps for obtaining sample I&M histories for a given strategy $\mathcal{S}$.

Algorithm 2: Generating a deterioration and I&M history

input : Strategy $\mathcal{S}_{\boldsymbol{w}}$, prior model, model dynamics, observation likelihood

for $0 \leq i < n_T$ **do**
- Sample system deterioration state $\boldsymbol{D}_i$ from $\boldsymbol{D}_{i-1}$ with prior model and model dynamics;
- Apply strategy $\mathcal{S}_{\boldsymbol{w}}$: inspection decision I_i;
- Sample observations $\boldsymbol{Z}_i$ from $\boldsymbol{D}_i$ and the observation likelihood as required by inspection decision I_i;
- Apply strategy $\mathcal{S}_{\boldsymbol{w}}$: maintenance decision R_i;
- Resample/modify $D_{i,k}$ for component k if affected by R_i (e.g., perfect repair);

end

output : $\boldsymbol{Z}_{1:n_T}$, $\boldsymbol{I}_{1:n_T}$, $\boldsymbol{R}_{1:n_T}$

Equation (3.9) can then be approximated by MCS:

$$\mathbf{E}[C_{\text{tot}}|\boldsymbol{w}] \simeq \frac{1}{n_{MC}} \sum_{q=1}^{n_{MC}} \mathbf{E}_{\boldsymbol{\Theta}|\mathbf{z}^{(q)}}[C_{\text{tot}}|\boldsymbol{w},\mathbf{z}^{(q)}]. \tag{3.17}$$

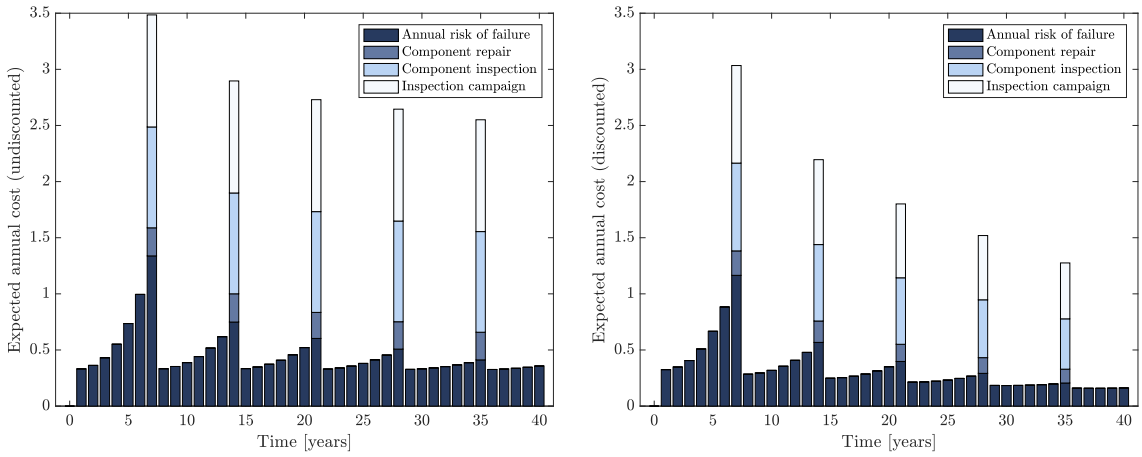

(a) undiscounted (b) discounted

Figure 3.3 Expected annual costs for strategy $\mathcal{S}_{\boldsymbol{w}_0^*}$ (see Chapter 6), evaluated with 200 samples, undiscounted (a), and discounted (b) with annually compounded discount rate $r = 0.02$ (Bismut and Straub, 2021).

Notably, estimating the expected cost, hence the risk of failure, using MCS over $\boldsymbol{Z}$ conditional on a strategy $\mathcal{S}_{\boldsymbol{w}}$, does not require to generate underlying trajectories of $\boldsymbol{D}_{1:n_T}$ that lead to the failure of the system. The probability of failure is included in the risk of failure $\mathbf{E}_{\boldsymbol{\Theta}|\mathbf{z}^{(q)}}[C_F|\boldsymbol{w}, \mathbf{z}^{(q)}]$, which is calculated directly conditional on each sample history $\mathbf{z}^{(q)}$ as per Equation (3.13).

A higher number of samples n_{MC} leads to more accurate estimation of the expected total life-cycle cost. In general, the computational efficiency of the conditional MC integration described by Equation (3.17) depends on the variance of $\mathbf{E}_{\boldsymbol{\Theta}|\boldsymbol{Z}}[C_{\text{tot}}|\boldsymbol{w}, \boldsymbol{Z}]$ with respect to the observation history $\boldsymbol{Z}$. In particular, to ensure that this conditional MC integration method is indeed more efficient than crude MCS (see Section 3.5.1), the variance of the conditional risk of failure $\mathbf{E}_{\boldsymbol{\Theta}|\boldsymbol{Z}}[C_F|\boldsymbol{w}, \boldsymbol{Z}]$ needs to be small. Appendix B discusses the variance of the estimator of the conditional risk of failure and details variance reduction techniques.

It should be noted that the need for accuracy in the MC estimator of the expected total life-cycle cost depends on the use case. In the numerical investigations of Chapter 6, it was found that a small number of samples is sufficient to obtain a good approximation of the expected total life-cycle cost, in the order of 200 samples. However, a smaller sampler size, such as $n_{MC} = 10$ might be sufficient for evaluating the cost during an optimization procedure, as described in Section 3.6.

One can also break down the expected costs into annual values. Figure 3.3a shows this breakdown for a selected strategy from the numerical application presented in Chapter 6, evaluated with $n_{MC} = 200$ samples. Figure 3.3b shows the effect of the discount factor $\gamma(t)$ on the distribution of the costs for the same strategy.

For the adaptive planning method presented in Section 3.3, the deterioration histories $\boldsymbol{D}_i$ in Algorithm 2 must be generated starting from time t_{j_1} conditional on the past inspection outcomes $\boldsymbol{Z}_{0:j_1}$. The model used for generating the deterioration histories in Algorithm 2

is the updated posterior model conditional on $\boldsymbol{Z}_{0:j_1}$. It is then necessary to resort to a Bayesian sampling method. When the posterior distributions can be obtained analytically (see Chapter 7), the sampling is performed as described above. Otherwise, the Bayesian updating with structural reliability methods (BUS) methodology with subset simulation (SUS) (Straub and Papaioannou, 2015) has been successfully utilized to compute the reliability of systems conditional on data (Schneider et al., 2017; Schneider, 2019). With BUS, drawing samples from a posterior distribution conditional on observations, $f(\boldsymbol{x}|\boldsymbol{z})$, is performed through a sampling rejection algorithm, in which samples $\boldsymbol{x}^{(q)}$ are drawn from the prior distribution $f(\boldsymbol{x})$ along with samples $p^{(q)}$ drawn from the uniform distribution $\mathcal{U}[0,1]$. A limit state function $g(\boldsymbol{x}, p, \boldsymbol{z})$, containing the likelihood function, is evaluated for each $\boldsymbol{x}^{(q)}$ and $p^{(q)}$. The samples $\boldsymbol{x}^{(q)}$ for which $g(\boldsymbol{x}, p, \boldsymbol{z}) \leq 0$ are accepted and distributed according to the posterior distribution. In high dimensions, the acceptance rate degenerates. SUS uses a sequence of Markov chain Monte Carlo (MCMC) steps to generate samples of $\boldsymbol{X}$ and p that fall within the domain $g(\boldsymbol{x}, p, \boldsymbol{z}) \leq c$, where throughout the sequence c is decreased until $c = 0$. Samples falling within $g(\boldsymbol{x}, p, \boldsymbol{z}) \leq 0$ are distributed according to the posterior distribution. SUS is particularly efficient in higher dimensions. BUS-SUS is the methodology employed in Chapter 6 for the adaptive optimization part.

3.5.5. Selection bias in posterior estimate

The conditional CDF $F_{T_F|\boldsymbol{w},\boldsymbol{Z}}$ is the probability of system failure conditional on observation outcomes, which is evaluated with Bayesian analysis described in Equation (2.7). The observation likelihood in this computation is given by the model of NDE quality (see Chapter 4). For instance, if the measured quantity is a crack length θ and the measuring device introduces an unbiased, normally distributed error ϵ, then the likelihood function is the normal PDF with mean θ and standard deviation σ_ϵ. However, this is an approximation, due to the selection bias (Nie et al., 2018). Strictly, the likelihood function also depends on the I&M strategy $\mathcal{S}$, since an observation Z is collected according to $\mathcal{S}$.

We demonstrate this effect with a simple example. Let us consider 10 random variables $X_1, ..., X_{10}$. The variables are i.i.d conditional on a parameter κ, such that $X_k \sim \mathcal{N}(\kappa, 3)$. κ is uncertain and is normally distributed with mean 2 and standard deviation 1. An imperfect observation of X_k, Z, is such that $Z|X_k \sim \mathcal{N}(X_k, 0.5)$. Finally, we draw 30 observations $Z_1, ..., Z_{30}$ sequentially from selected X_k, such that the variable k selected for the $(i+1)^{th}$ observation is the one for which the posterior mean $\mathbf{E}[X_k|\boldsymbol{Z}_{1:i}]$ is the highest. The posterior distribution of Y is also computed sequentially, conditional on the observations obtained at each time step, using the likelihood $Z|X_k$ defined previously. We repeat this procedure, generating observations $\boldsymbol{Z}^{(q)}$, $1 \leq q \leq 10^4$ and computing the posterior means $\mathbf{E}[Y|\boldsymbol{Z}_{1:i}]$. We then compute the sample average at each time step i, $\hat{Y}_i = 1/10^4 \sum_{q=1}^{10^4} \mathbf{E}[Y|\boldsymbol{Z}_{1:i}^{(q)}]$, shown in Figure 3.4a. If the observations are drawn purely randomly, the sample average corresponds to the prior mean of Y. Here, the selection heuristic de-randomizes the observations and the likelihood function does not take this effect into account, thereby introducing a negative bias in the estimation of Y. However, this example is an extreme case since, in the limit, the same

variable is always inspected, which is not representative of typical inspection strategies in infrastructure management.

Nevertheless, it is in general difficult to anticipate the magnitude of the effect of the selection bias on the computation of the life-cycle risk for any given I&M strategy. In the application described in Chapter 7, the strategy representative of the current I&M practice introduces a positive bias in the estimation of the posterior mean of deterioration parameter μ (Figure 3.4b), hence an error is likely introduced in the estimation of its expected cost; In comparison, we find that the bias induced by the I&M strategies described by the chosen heuristic is not significant, thus the estimation of their expected cost and the resulting optimization are not affected by the selection bias.

In this work, the strategies investigated typically do not rely on strongly informative characteristics (as in the simple example above), thus we do not correct this bias, as it is not expected to significantly affect the numerical results.

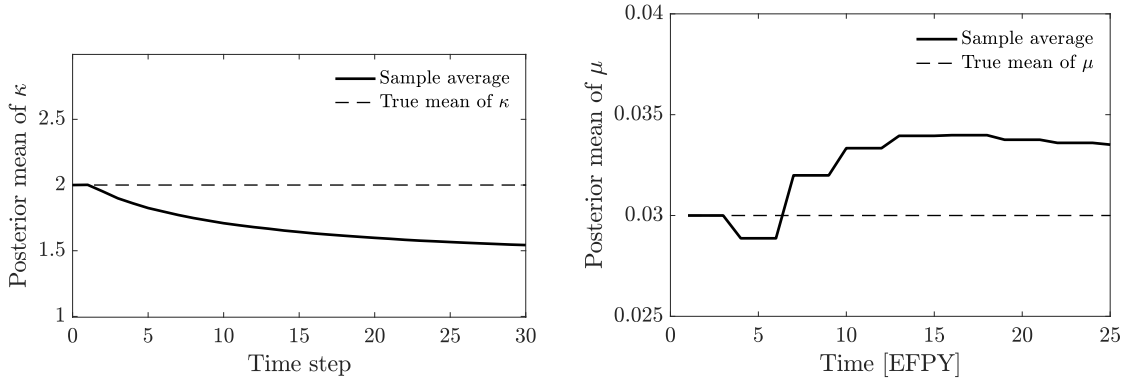

Figure 3.4 Effect of the selection bias on the Bayesian estimation of model parameters. (a): Selecting components based on the highest posterior mean. (b): Following representative strategy of Chapter 7.

3.6. Noisy optimization method for optimal heuristic planning approach

The optimization problem over the entire policy space has been reduced to a search of optimal heuristic parameter values. Several difficulties remain: The objective function consists of an integral, the evaluation of which is time-consuming. The proposed MC integration of Equation (3.17) provides an estimate of the objective function at a given point in the strategy space, but this estimate is associated with uncertainty, which decreases with increasing MC sample histories. However, when performing an optimization, it is typically desirable that the evaluation of the objective function remains cheap, thus contradicting the need for more samples for accurate estimation of the function. Another challenge resides in the nature of the optimization: the parameters can take discrete and/or continuous values. Discrete optimization is notoriously difficult. When only a few options are considered, an exhaustive

search is sufficient (Luque and Straub, 2019). When several parameters and a wider range of values are considered, this approach is no longer feasible in a reasonable time.

The optimization method must either handle expensive objective function evaluation – and find the minimum while exploring the fewest points possible – or account for the fact that the objective function evaluation is obtained for a low number of samples n_{MC} (see Section 3.5.4) and has a high associated noise.

The focus of this work has not been to find the best or most efficient stochastic optimization method. The reader is referred to the review papers of existing methods and their challenges by Spall (2012) and Hill (2013). After exploring different options, mainly motivated by the need to perform the optimization in a limited amount of time and the possibility of exploiting parallel computing capabilities, the proposed method is based on the cross-entropy (CE) method (De Boer et al., 2005) and is described in the following Section 3.6.1. Gaussian process regression (GPR) (Rasmussen, 2004) has also been utilized in combination with the CE method in the numerical investigations to provide a surrogate of the objective function. For the adaptive planning application in Chapter 6, optimum heuristic parameters are approximated from the surrogate using a deterministic optimization method. In Chapter 7, the sensitivities of the objective function to the different heuristic parameters are extracted from the GPR surrogate.

The presented optimization method can handle both continuous (e.g., a threshold) or discrete (e.g., inspection intervals) heuristic parameters.

3.6.1. Cross-entropy optimization

Algorithm 3 summarizes the steps of the CE method, inspired by (Kochenderfer, 2015). It generates n_{CE} samples $\boldsymbol{w}^{(m)}$ of heuristic parameters from an initial sampling density with parameters $\boldsymbol{\lambda}^*$. For each sample $\boldsymbol{w}^{(m)}$, n_{MC} observation and monitoring histories are generated and the expected total life-cycle cost is calculated through Equation (3.17). The samples $\boldsymbol{w}^{(m)}$ are then ranked in ascending order of their estimated expected life-cycle cost. The n_E best-ranked $\boldsymbol{w}^{(m)}$, also called elite samples, are used to update the CE sampling density parameter $\boldsymbol{\lambda}^*$ by cross-entropy minimization. This step is repeated until a convergence criterion has been met, or until a sufficient number n_{max} of strategies have been explored. The convergence speed of the CE method can be optimized by choosing n_{MC} adequately. In particular, the CE method can work with a single sample evaluation in Equation (3.17), i.e., $n_{MC} = 1$, and still converge towards the heuristic parameter values that minimize the exact expected total life-cycle cost (Rubinstein and Kroese, 2004).

The CE method is illustrated in one dimension in Figure 3.5. The initial sampling distribution is a truncated normal distribution, with mean 10[years] and standard deviation 10[years]. The samples of the first iteration and the estimated costs are shown with the blue dots. The updated sampling distribution has for mean 6.8[years] and standard deviation 0.95[years]. The red dots are the samples from the second iteration. The sampling density converges towards the minimum of the objective function, even though the estimations are noisy. The final

Algorithm 3: Pseudo-code for the CE-based stochastic optimization

in : CE sampling density $P(\cdot|\boldsymbol{\lambda}^*)$, initial sampling density parameter $\boldsymbol{\lambda}^*$, number of CE samples n_{CE}, number of elite samples n_E, number of observation history samples n_{MC}, maximum number of objective function evaluations n_{max}.

out : optimal heuristic parameters $\boldsymbol{w}^*$, minimum total life-cycle cost C^*, surrogate cost function f

$l \leftarrow 0$;
while $l \cdot n_{CE} < n_{max}$ **do**
  for $m \leftarrow 1$ **to** n_{CE} **do**
    $\boldsymbol{w}^{(m)} \sim P(\cdot|\boldsymbol{\lambda}^*)$; ▷ `generate random heuristic parameter values`
    $cost \leftarrow 0$;
    for $q \leftarrow 1$ **to** n_{MC} **do**
      generate an inspection and repair history $\mathbf{z}^{(q)}$ following strategy $\mathcal{S}_{\boldsymbol{w}^{(m)}}$;
      $cost \leftarrow cost + \mathbf{E}_{\boldsymbol{\Theta}|\mathbf{z}^{(q)}_{1:n_T}}[C_{\text{tot}}|\boldsymbol{w}^{(m)}, \mathbf{z}^{(q)}]$; ▷ `eqs. 3.11 to 3.16`
    end
    $q_m \leftarrow cost/n_{MC}$; ▷ `expected total life-cycle cost (eq. (3.17))`
  end
  Store $\boldsymbol{w}^{(m)}$, q_m;
  $\widehat{\boldsymbol{w}}^{(1)}, ..\widehat{\boldsymbol{w}}^{(n_{CE})} \leftarrow$Sort $(\boldsymbol{w}^{(1)}, ..\boldsymbol{w}^{(n_{CE})})$ in increasing order of q_m;
  $\boldsymbol{\lambda}^* \leftarrow \arg\max_{\boldsymbol{\lambda}} \sum_{m=1}^{n_E} \log P(\widehat{\boldsymbol{w}}^{(m)}|\boldsymbol{\lambda})$; ▷ `update` $\boldsymbol{\lambda}^*$ `with the elite samples`
  $l \leftarrow l + 1$;
end
$h \leftarrow GPR(\boldsymbol{w}^{(m)}, q_m)$; ▷ `build the surrogate function`
$\boldsymbol{w}^* \leftarrow \arg\min h$;
$C^* \leftarrow \min h$;
return $\boldsymbol{w}^*$, C^*, h

sampling distribution is centered around the found optimum and provides information on its associated uncertainty.

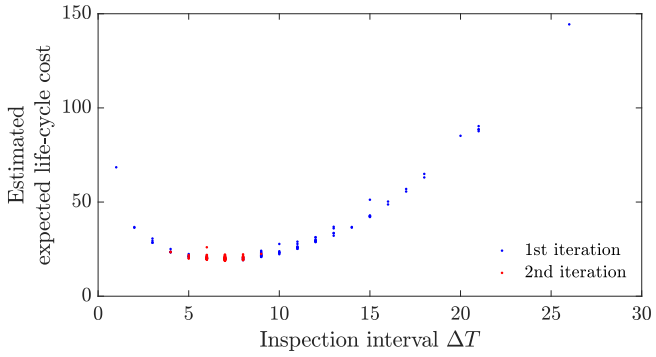

Figure 3.5 First iterations of the cross-entropy method for the example of Chapter 6 (Bismut and Straub, 2021).

The CE method for optimization can handle continuous and discrete variables (Rubinstein and Kroese, 2004). We note that in Figure 3.5 the samples are sampled from a continuous sampling density and rounded to the nearest integers to correspond to full years intervals for the I&M campaigns. While this is how we have proposed to handle discrete heuristic parameters, a parametrized PMF as the CE sampling density would strictly be more correct.

Nevertheless, this choice does not significantly affect the outcomes of the optimization.

In the numerical investigations of Chapters 6 and 7, we follow the recommendations from Geyer et al. (2019) and choose the multivariate Gaussian as the sampling density, truncated where needed to account for the feasible domain of the heuristic parameter values. Samples of heuristic parameters corresponding to a probability quantity (e.g., a probability threshold, see Sections 3.4.2 and 3.4.4) are obtained indirectly through sampling in the equivalent log-space.

The convergence of the CE method is illustrated in Figure 3.6 using the example of Chapter 7. The sampling progression is shown for two different initial sampling distribution. There is a variation in the obtained optimal heuristic parameter values, which reflects the higher or lower sensitivity of the objective function to the parameters.

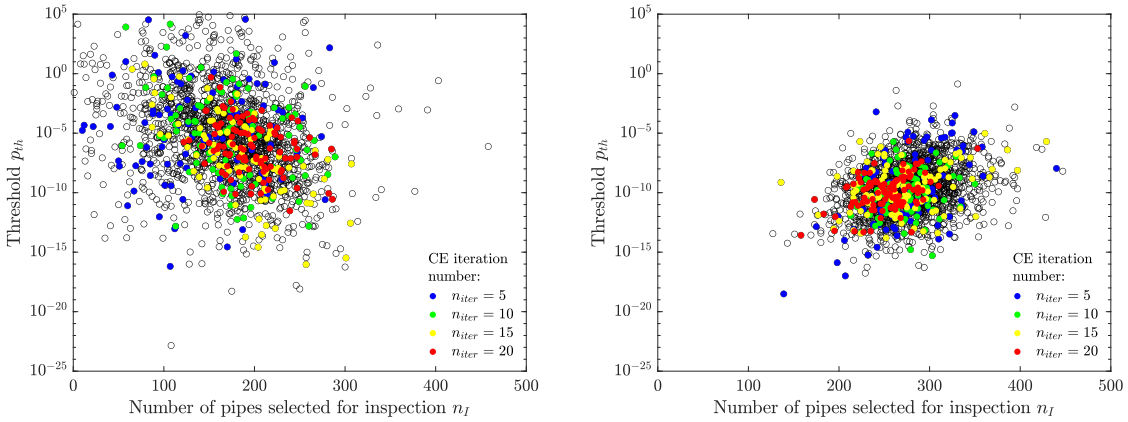

Figure 3.6 Influence of the initial sampling density in CE optimization. 2000 CE samples for the reliability-based optimization with $p_0 = 1.0 \cdot 10^{-2}$ (see Chapter 7) are obtained for two different initial sampling densities. Each point represents a specific I&M strategy, defined by parameters n_I and p_{th}. $\Delta T = 3$[yr] is fixed. The expected cost of each strategy is evaluated with 10 sample histories. Colored dots indicate samples belonging to selected CE iterations. a) The optimal heuristic strategy obtained from the last iteration is $n_I = 195$ and $p_{th} = 5.6 \cdot 10^{-7}$ with expected cost 379.1 (see Table 7.3). b) The optimal heuristic strategy obtained from the last iteration is $n_I = 246$ and $p_{th} = 2.5 \cdot 10^{-10}$. The resulting expected cost for this strategy is 388.9, which is close to the cost for the strategy obtained in a). From (Bismut et al., 2022).

In the proposed implementation of the CE method for stochastic optimization, we observe that the obtained minimum depends to a certain degree on the initial sampling distribution. The method as presented does not necessarily find the global minimum and its convergence relies on an appropriate tuning of the setting of the algorithm, such as the choice of the sampling distribution and its initial parameters but also on the shape of the objective function (Xu et al., 2015). Several algorithms based on the CE method have been developed to mitigate these effects and to give guarantees of convergence, such as the modified CE method proposed by Szita and Lörincz (2006) applied to learning strategies for playing Tetris, and the stochastic extension of model reference adaptive search (SMRAS) (Hu et al., 2008), which has also been applied to solving MDPs for inventory problems and queueing control (Hu et al., n.d.). These algorithms could replace the proposed CE method without changing the characteristics of the heuristic optimization framework.

3.6.2. Objective function surrogate through Gaussian process regression

In addition to the CE method, GPR, also known as Kriging, can be applied on estimations of the objective function for different heuristic parameter values, to obtain a surrogate approximating $\mathbf{E}[C_{\text{tot}}|\mathcal{S}_{\boldsymbol{w}}]$. A tutorial on Gaussian processes and GPR is found in (Rasmussen, 2004). Mathematical computing software, such as MATLAB, include GPR implementation packages.

The support points of the GPR where the expected cost is estimated (with n_{MC} sample I&M histories) can be chosen on a grid (see numerical investigations of Chapter 7). The surrogate function can confirm the location of the optimal heuristic parameter values $\boldsymbol{w}^*$ and provide information about the sensitivity of the expected cost to the heuristic parameters.

The support points can also be acquired using active learning, as in the stochastic efficient global optimization (SEGO) algorithm proposed by Holdorf Lopez et al. (2022). SEGO employs an acquisition function which populates the support of the learning algorithm with points which maximize an improvement function.

Another use of GPR is proposed in the numerical application of Chapter 6: the support points of the GPR consists of all the heuristic parameter values explored during the CE iterations along with their estimated expected costs. The surrogate function is then minimized to obtain the optimal heuristic parameter values $\boldsymbol{w}^*$. Coupling the CE method with GPR presents the advantage that the surrogate mean and standard error of the mean can be extracted for any point in the heuristic parameter space. This can be used to evaluate the sensitivity of the expected total life-cycle cost to the heuristic parameters. Furthermore, due to the CE sampling method, the standard error of the mean decreases towards the surrogate minimum.

3.7. Summary and future investigations

This chapter formalized an approach to I&M planning based on the concept of direct policy search, whereby a heuristic is chosen to describe and optimize I&M strategies. The approach enables adaptive planning, such that when new information is available, an improved heuristic may be found, which is more optimal under the a-posteriori model. As we prove in Section 3.3, this adapted strategy is always at least as good as the initially optimized strategy.

The steps to adaptive heuristic planning are summarized in Figure 3.7. The approach is applicable to any deteriorating system with multiple components. Just as POMDP solvers, the approach only results in an approximately optimal strategy. Unlike for POMDP solvers, the resulting optimal heuristic strategy does not explicitly give a mapping between belief state and action but provides a compact description of the policies through decision rules, the heuristics, and associated heuristic parameters.

The methods for the optimization or for the evaluation of the expected cost of a strategy can be chosen freely, as they will not affect the underlying principles of the methodology. For instance, the CE method described in Section 3.6.1 can be upgraded to include optimal computing

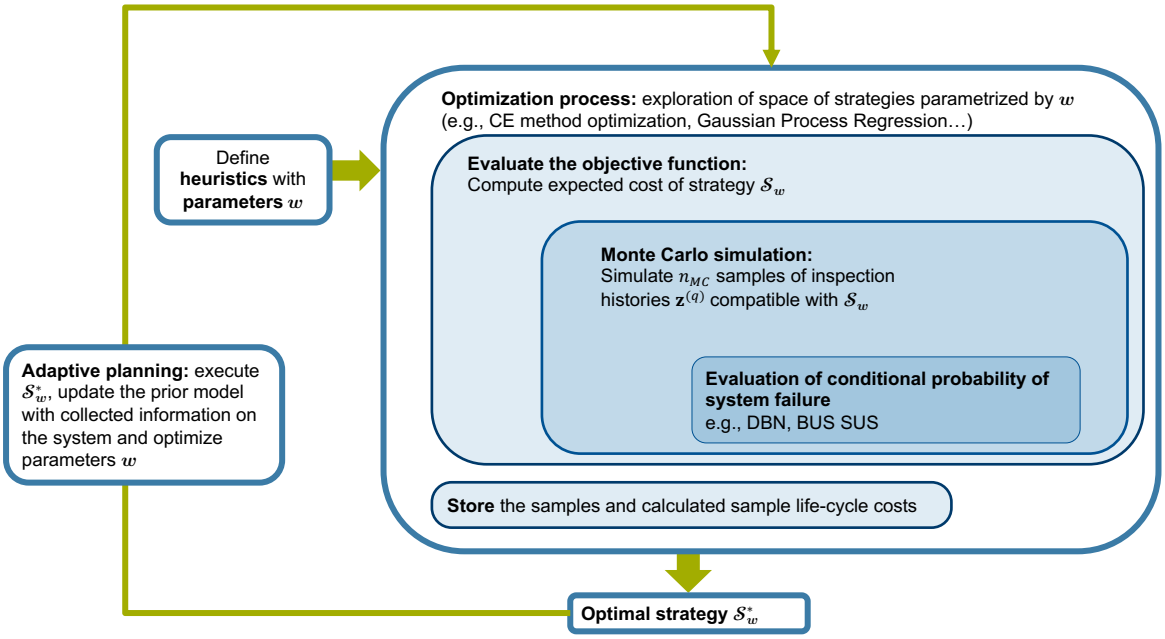

Figure 3.7 Steps of adaptive heuristic I&M planning, after (Bismut and Straub, 2021).

budget allocation (OCBA) (He et al., 2010; Chen and Lee, 2011), which identifies the strategies for which the number of MC samples n_{MC} should be increased, to increase the confidence in the selection of the elite parameters. The computational effort is thereby optimized, as is the efficiency of the chosen optimization method. This could be combined with modified CE-based methods, such as SMRAS (Hu et al., 2008), to further improve the convergence to the optimal parameter values. As an alternative to the CE method, Holdorf Lopez et al. (2022) proposed and applied the SEGO algorithm to an infrastructure planning problem, which employs Kriging and active learning to surrogate the noisy objective function.

The proposed approach for strategy optimization and evaluation is in principle simple to implement, as it only requires a model to generate I&M histories. The sequential decision problem must not be formulated in any particular way and does not require the Markov property characteristic of POMDPs. However, if the heuristics prescribe, for instance, that inspections of certain components be triggered by a system reliability requirement, such as a fixed threshold on the annual failure rate, a model describing the system, its components, the deterioration processes and interdependence or correlation effects must be available to the analyst. Modeling a deteriorating multi-component system and evaluating the associated time-variant reliability are addressed in Chapter 5.

In general, the approach is flexible with respect to adding new heuristic rules and parameters. It even enables reliability-based planning, by which only strategies, which comply with a heuristic-encoded reliability criterion, are explored. The reliability-based planning framework is presented and illustrated for a nuclear feeder piping system in Chapter 7.

The choice of heuristics is another optimization problem, which we do not formally address here. However, we propose some heuristics relevant to I&M planning, including prioritization

strategies for inspection and repair in a multi-component system. Other heuristics can be developed specifically for the planning problem considered. For inspiration, it is strongly encouraged to review old and recent scientific literature addressing OR-type problems in different disciplines (e.g., Yaron and Horowitz, 1972; Vora, 1974; Strack and Pochet, 2010; Russell and Norvig, 2016; Pourmoayed and Nielsen, 2019).

Further studies are required to understand the roles of the various characteristics of the model towards the goodness of the approximation. In a preliminary study, we investigated the efficiency of different heuristics in optimizing the capacity upgrading plan of a generic infrastructure and compared their performance to the exact solution of the associated POMDP (Bismut and Straub, 2019). We concluded that the best performing heuristics make use of the information available, and that the inclusion of observations in a probabilistic manner in the decision rules marginally improved the strategy. As for the adaptive planning approach, the question remains as to how heuristic parametrizations are best chosen adaptively.

There is no guarantee that any given heuristic is optimal, and this approach does not provide bounds on the expected cost. However, the heuristic approach offers the analyst the opportunity to explore methodically the mechanisms of optimal decision-making, and to select the best heuristic among the investigated ones through the computed expected total life-cycle cost. The more heuristics are investigated, the better. We conclude this chapter with these words on heuristic reasoning by George Polya (2004) in his book *How to solve it*: "[...] before obtaining certainty we must often be satisfied with a more or less plausible guess".

Chapter 4

A unifying review of models of NDE quality

> We use an audio signal or a light-flash. The subject presses a button and the elapsed time is measured. We try it a number of times, of course. Elapsed time varies in both the andy and the human. But by the time ten reactions have been measured, we believe we have a reliable clue.
>
> *Do androids dream of electric sheep?*
> Philip K. Dick

The paper: Bismut, E. and Straub, D. (2022). "A unifying review of NDE models towards optimal decision support". In: *Structural Safety* 97, p. 102213. constitutes this chapter.

4.1. NDE models for I&M planning

The methodology presented in Chapter 3 requires that probabilistic models for the propagation of inspection information are available to the analyst. In infrastructure maintenance problems, the information is generally acquired by means of non-destructive evaluation (NDE). The quality of this information is variable and the accuracy and reliability of NDE depends on environmental conditions (humidity, temperature, experimental setting) and inspector expertise, among other factors (e.g., Lentz et al., 2002). Probabilistic models have been developed to measure the quality and performance of non-destructive evaluation (NDE) methods. However, when used in a decision analysis context, they remain typically unchallenged, although they greatly influence the outcome of the analysis. The purpose of this chapter is to review and investigate these models for NDE quality by means of a unifying framework, which shows formally how they are connected. This enables us to provide insights into how they should be used and learned.

Probability of detection (PoD) curves, receiver operating characteristic (ROC) curves, or simply a probability of false positives/false negatives are the most commonly used models of NDE quality. In specific application domains, one of these models typically prevails (e.g., Packman et al., 1968; Hovey and Berens, 1988; Somoza et al., 1990; Sarkar et al., 1998), since

they historically emerged independently in different disciplines to address specific problems. PoD curve models were formulated in the 1950s as a statistical method to investigate the dose-response effect in biological tests (Finney, 1978; Rudemo et al., 1989; Ritz et al., 2015). ROC curve models grew out of the signal detectability theory developed in the 1940s (Shannon, 1948; Woodward and Davies, 1952; Peterson and Birdsall, 1953), aimed at measuring the capacity of a receiver to distinguish the presence of a signal from noise. In general, NDE quality models establish a probabilistic relationship between the condition of the structure and the testing outcome (or outcome assessment). They can be used to rate NDE methods and ensure their compliance with norms and standards in place (e.g., Pavlovic et al., 2008; Deutsches Institut für Normung, 2014).

Historically, a first major application of NDE was the identification of flaws with systematic inspections during the manufacturing process of parts. This was especially a concern in the nuclear industry, which strived to improve quality assurance in the fabrication of pressure vessel components (International Atomic Energy Agency, 1965). In the aeronautic industry, the high cost associated with discarding parts with small defects during manufacture motivated the use of NDE also during the service life. By the 1970s, the US Air Force had launched detailed investigations on quantifying the performance (also called reliability) of defect detection measures (Packman et al., 1968; National Materials Advisory Board, 1969). Its program "Have-Cracks-Will-Travel" laid the foundation for systematic I&M of aircrafts (Berens and Hovey, 1981; Hovey and Berens, 1988; Singh, 2000), where fatigue cracks are allowed to develop as long as they are monitored and repaired regularly. These studies provide the analytical framework to derive PoD curves from NDE data.

In parallel, the research on lifetime extension of aircraft structures (Graham and Tetelman, 1974; Yang and Trapp, 1974), nuclear reactor components (Harris and Lim, 1983), and large deteriorating civil infrastructures (Frangopol et al., 1997; Hong, 1997; Sheils et al., 2012) started to incorporate these probabilistic NDE models into Bayesian reliability analysis of the structure. As NDE models are now coupled with I&M plans, notably in RBI planning (Yang and Chen, 1985; Madsen et al., 1987; Straub, 2004), the focus of NDE studies has shifted to quantifying the added value of a specific NDE method on the expected total life-cycle cost.

While some existing literature does discuss relationships between two NDE quality models, we are not aware of any previous attempt to formalize the relationship between all these models. This unifying framework of NDE quality enables a better understanding of the assumptions associated with each model type and, as we demonstrate, can help in obtaining better models for NDE quality for specific applications. We particularly draw attention to the dependence of the NDE quality model on the experimental design and the risks of misinterpreting and generalizing quality indicators of NDE quality models from experimental studies. This formalization allows us to identify systematically issues and potential pitfalls when establishing and applying these models. The VoI concept sheds further light on the implications of not choosing the optimal model. The joint optimization of the calibration of the NDE system and the repair actions is formally addressed.

After some definitions in Section 4.2.1, Section 4.2.2 introduces the framework and the models, and their connections are reviewed and discussed in Sections 4.2.3 to 4.2.6. Considerations on model availability and uncertainty are made in Section 4.2.7. Section 4.3 focuses on the exploitation of the NDE data within decision analysis. The findings are illustrated with two examples: In Section 4.4, we apply the framework and solve a basic decision problem for a purely theoretical NDE system; In Section 4.5 we consider a real NDE technique, the half-cell potential, and we analyze the effect of model choice on the outcomes of optimal decision making for a one-step and a two-step decision problem.

4.2. A unifying framework for NDE quality

4.2.1. NDE systems

NDE quality models establish a relationship between the true *condition* and the measurement, which we call the *observed signal*. The latter includes noise. Figure 4.1 depicts this relationship, inspired by Shannon's diagram of a communication system (Shannon, 1948).

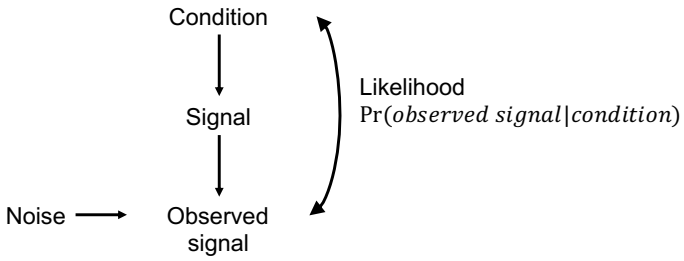

Figure 4.1 The observed signal measures the signal emitted by the condition and is also affected by noise. The model for NDE quality expresses the relationship between the observed signal and the condition, in the form of a likelihood.

The relationship between the true condition and the observed signal can be expressed probabilistically with *NDE quality models*. Here the term "NDE" covers all non-destructive information collection methods, ranging from visual inspection to automated data collection. An NDE quality model is defined by the conditional probability $\Pr(\textit{observed signal}|\textit{condition})$, which in statistics is known as the likelihood function. This relationship can be derived empirically by performing a number of tests (Packman et al., 1968; Berens and Hovey, 1981; Berens, 2000). While the primary purpose of these models was to establish a measure of reliability and performance of NDE techniques, they can be used for Bayesian analysis and decision analysis, see Section 4.3.

The *NDE system* encapsulates the process of collecting the data (type of data collected, inspection technique) and the interpretation of this data (Berens, 2000). The NDE system can encompass several measuring devices and data processors or interpreters (Sheils et al., 2010). The observed signal is the quantity on which the repair decision is taken. An example of an NDE system is an inspector going on-site, visually inspecting a wall, and appraising its state of damage (here, the condition) with a rating (here, the observed signal) (Quirk et al., 2018). The NDE quality model characterizes the NDE system.

4.2.2. Unifying NDE quality models

The NDE quality model probabilistically relates the observed signal with the condition. The condition can take continuous values (e.g., a crack size), or discrete values (e.g., "functioning" or "not functioning"). The observed signal can similarly take continuous (e.g., maximum vibration amplitude, measured crack length) or discrete values (e.g., "red" or "green", "suitable" or "not suitable"). Here, we limit the consideration of the discrete case to binary states. As the number of discrete states increases, the multinomial case approaches the continuous case.

We denote the continuous observed signal by S and the binary observed signal by I. Similarly, if the condition takes continuous values, it is denoted by X, and when it takes binary states, by Y. The condition can express a degree of damage or failure, although this remains an abstract concept and might not be related to anything failing as such. Here, the observed signal is considered as a scalar quantity, which can result from processing a multivariate signal, e.g., a time-series or an image (Kurz et al., 2012; Webb et al., 2015). Table 4.1 gives an overview of the four main NDE quality model categories for the possible combinations of continuous or binary condition X/Y and observed signal S/I.

Table 4.1 Monitoring models for binary or continuous signal and condition

		Condition	
		Continuous X	Binary Y
Signal	Continuous S	(1) $f_{S\|X=x}(s)$	(3) ROC curve
	Binary I	(2) PoD(x) curve	(4) PoD / PFA

The connection between the models comes from the fact that *the binary/discrete variables are the result of imposing one or more thresholds on the underlying continuous variables.* Specifically, a binary signal I is the result of a classification of the underlying continuous signal S, by means of a threshold s_{th}, that assigns $I = 1$ for $S > s_{th}$. A binary condition Y represents two domains of a continuous condition X, classified such that $Y = 1$ when $X > x_{th}$.

If one has access to the full continuous/continuous description of NDE quality, one can establish the link between all four models, as illustrated by Figure 4.2. Model (1) is the *base model.* Models (2–4) are derived by imposing thresholds s_{th} and x_{th} on continuous signal S and condition X, respectively. As we discuss in Section 4.2.7, almost all NDE systems and applications can be connected to the base model.

The mathematical formulation of this unifying framework is derived in Sections 4.2.3 to 4.2.6. Importantly, we show that the links between models require an understanding of the population of defects in the experimental design. This affects the validity of the NDE models outside of the experimental setting in which they are learned. This has ramifications on the optimal interpretation of data and the decisions taken based on NDE.

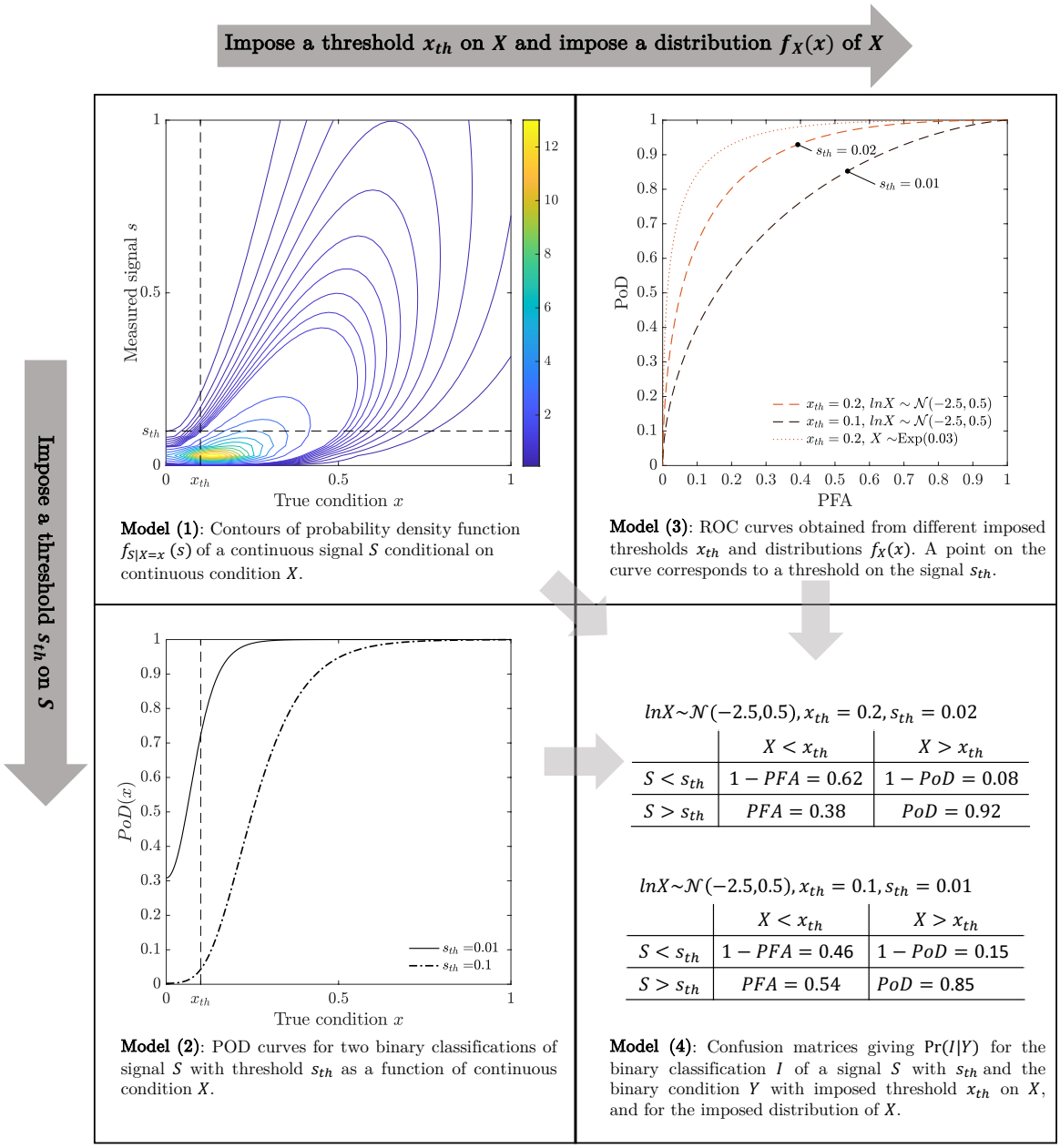

Model (1): Contours of probability density function $f_{S|X=x}(s)$ of a continuous signal S conditional on continuous condition X.

Model (3): ROC curves obtained from different imposed thresholds x_{th} and distributions $f_X(x)$. A point on the curve corresponds to a threshold on the signal s_{th}.

Model (2): POD curves for two binary classifications of signal S with threshold s_{th} as a function of continuous condition X.

	$X < x_{th}$	$X > x_{th}$
$S < s_{th}$	$1 - PFA = 0.62$	$1 - PoD = 0.08$
$S > s_{th}$	$PFA = 0.38$	$PoD = 0.92$

	$X < x_{th}$	$X > x_{th}$
$S < s_{th}$	$1 - PFA = 0.46$	$1 - PoD = 0.15$
$S > s_{th}$	$PFA = 0.54$	$PoD = 0.85$

Model (4): Confusion matrices giving $\Pr(I|Y)$ for the binary classification I of a signal S with s_{th} and the binary condition Y with imposed threshold x_{th} on X, and for the imposed distribution of X.

Figure 4.2 Unifying framework of models for NDE quality. Models (2–4) with a binary signal or condition can in principle be linked to Model (1). This link is established by fixing a threshold either on the signal, s_{th}, or on the condition, x_{th}, to classify the continuous signal or condition into binary states. The link between Models (1–2) to (3–4) requires additional information on the distribution of the continuous condition X. The specific NDE quality model depicted here is defined in Section 4.4.

4.2.3. Model (1): Base model – S continuous, X continuous

Many NDE methods relate a continuous condition to a continuous observed signal. For example, ultrasonic testing (UT) detects discontinuities inside a metal plate by emitting a high frequency ultrasonic pulse towards the plate and recording the echo. The amplitude of this echo (the observed signal) relates to the thickness (the condition) of defect-free material (Lavender, 1976). Another example described by this model is crack detection and measurement using magnetic particle inspection (MPI): MPI reveals the crack to the inspector who must then perform a visual inspection under UV lights and evaluate the crack size (Clark et al., 1987).

In the configuration of Model (1), the NDE system is fully characterized by the probability distribution of the observed signal S given the condition X, through the PDF, $f_{S|X}(s|x)$, or the associated CDF, $F_{S|X}(s|x)$. Figure 4.2 gives an example of such a conditional PDF.

This probabilistic model can be obtained from experimental data (experimental test blocks), if possible in different experimental settings. A traditional approach, which would allow to find such a model, is called "$\hat{a}$ *vs.* a," where $\hat{a}$ is the continuous observed signal and a the continuous condition (Berens, 2000). A relationship of the form $\hat{a} = f(a) + \epsilon(a)$ has been proposed, where f is the mean response function with some fixed parameters and $\epsilon(a)$ is a random variable representing the measurement noise. A linear log-logistic relationship is a common choice for the function f (Berens and Hovey, 1981; Annis, 2009). It originates from biological tests investigating the dose-response effect (Finney, 1978; Rudemo et al., 1989; Ritz et al., 2015). $\epsilon(a)$ is commonly modeled as a Gaussian random variable (e.g., Kurz et al., 2012; Goulet et al., 2015). Annis (2009) provides some guidance as to how the noise should be considered.

Simulation and meta-models of NDE processes have also given rise to model-assisted PoD (MAPOD) (Calmon, 2012; Aldrin et al., 2013; Calmon et al., 2016). In this procedure, physics-based models are used to determine the relationship f and are validated with the experimental data. One of the advantages of MAPOD is that it does not require large datasets and can include numerous experimental settings and influential parameters.

Our review of the existing literature on NDE models shows that continuous/continuous probabilistic models are often learned in an ad-hoc manner. An example is the probability of (correct) sizing (POS), which describes the error in the measurement by an inspector of the continuous condition (e.g., a crack length) (Visser, 2002; Silva and Padua, 2012; Brennan, 2013; Granville and Charlton, 2016; Nath, 2021). Models for POS are continuous/continuous, but definitions vary and no application to reliability analysis is documented in the literature.

For many NDE techniques, this model remains abstract, as a continuous signal or a continuous condition might not be easily identifiable. In this case, the NDE quality model is chosen among the other three categories described below.

4.2.4. Model (2): PoD curve – I binary, X continuous

The probability of detection curve, or *PoD curve*, has been adopted for many NDE techniques, such as UT, MPI, Eddy current testing, or impulse radar, which aim at identifying cracks or more generally defects in structures (Berens and Hovey, 1981; Hovey and Berens, 1988; Sarkar et al., 1998; Feistkorn and Taffe, 2011). It is

$$\mathrm{PoD}(x) = \Pr(I = 1|X = x). \tag{4.1}$$

As previously noted, one can interpret I as a classification of a continuous signal S by fixing a threshold s_{th}, i.e., $\{I = 1\} = \{S > s_{th}\}$. In NDE literature pertaining to PoD curves, s_{th} is

called the decision or detection threshold (Berens and Hovey, 1981; Sheils et al., 2012). The PoD function in Equation (4.1) can thus be written as a function of the continuous/continuous Model (1).

$$\mathrm{PoD}(x) = \Pr(S > s_{th}|X = x) = \int_{s_{th}}^{+\infty} f_{S|X}(s|x)\mathrm{d}s = 1 - F_{S|X}(s_{th}|x). \tag{4.2}$$

By changing the threshold s_{th}, the PoD curve changes (Sarkar et al., 1998); at the limit, it is $\mathrm{PoD}(x, s_{th} = -\infty) = 1$ and $\mathrm{PoD}(x, s_{th} = +\infty) = 0$ for any value x.

PoD curves have indeed been obtained from "$\hat{a}$ *vs.* a" models (Berens, 2000; Annis, 2009; Virkkunen et al., 2019). In aircraft integrity management, the threshold s_{th} is chosen so that a critical crack size fixed by expert judgement (Wood and Engle Jr, 1979) is detected with a 90% probability, with a 95% confidence level (Berens, 2000). According to Wood and Engle Jr (1979), the basis for these target probability and confidence level is arbitrary and relates to a required degree of conservatism and to the practical implementation of NDE testing programs. The characterization of a PoD curve with this 90/95 target value is considered best practice, until today (e.g., Annis, 2009; Tschöke et al., 2021). However, as we show below in Section 4.3, calibrating the PoD curve and fixing s_{th} in this way without a comprehensive decision analysis may not ensure that the test is exploited to its full potential. Furthermore, although the term decision threshold originally refers to the fact that a repair action systematically follows the detection of a defect with $S > s_{th}$, it may not be optimal to do so in all circumstances.

Equation (4.2) does not preclude the PoD curve from taking a non-zero value when $x = 0$. A PoD curve for which $\mathrm{PoD}(0) = 0.3$ is depicted in Figure 4.2 Model (2) for $s_{th} = 0.01$. Straub (2004) notes that PoD curves typically proposed in the literature, such as those obtained from the log-logistic model mentioned in Section 4.2.3, pass through the point $\mathrm{PoD}(0) = 0$, and thus do not include the possibility of false detection. (Packman et al., 1968; Berens and Hovey, 1981) have motivated this choice with damage tolerant design philosophy by presuming that unnecessary repairs can only improve the reliability of the system. However, Heasler and Doctor (1996) argue that for risk-based decision analysis it is more appropriate to consider PoD models for which $\mathrm{PoD}(0) > 0$ since unnecessary repairs lead to additional costs. Straub (2004) has proposed the term probability of indication (PoI) for PoD curves that include false alarms, i.e., those for which $\mathrm{PoD}(0) > 0$, which include the effect of noise on the indication of the condition. Nevertheless, we use the term PoD curve throughout this chapter.

4.2.5. Model (3): ROC curve – S continuous, Y binary

This model is commonly used to describe how the continuous observed signal S from NDE can be interpreted to discriminate between the absence ($Y = 0$) and presence ($Y = 1$) of a flaw. Most traditional NDE methods can be described by this model (Olin and Meeker, 1996), which can also be used to compare the ability of inspectors (human or machine) to interpret NDE results (Swets, 1983). Recently, image processing techniques for crack detection and

monitoring systems of pipe corrosion have been evaluated with this model (Pakrashi et al., 2010; Jarvis et al., 2018).

In this framework, the discrete condition Y is defined by setting a threshold on the continuous condition X such that $\{Y = 1\} = \{X > x_{th}\}$ and $\{Y = 0\} = \{X \leq x_{th}\}$. x_{th} is called the critical threshold (Sheils et al., 2010; Schoefs et al., 2012). The likelihood function is formed by the two conditional PDFs of the observed signal S. They are represented in Figure 4.3 and can be derived from the base Model (1):

$$f_{S|Y=1}(s) = \frac{1}{1 - F_X(x_{th})} \cdot \int_{x_{th}}^{+\infty} f_{S|X}(s|x) f_X(x) \mathrm{d}x, \tag{4.3}$$

$$f_{S|Y=0}(s) = \frac{1}{F_X(x_{th})} \cdot \int_{-\infty}^{x_{th}} f_{S|X}(s|x) f_X(x) \mathrm{d}x, \tag{4.4}$$

where $f_X(x)$ and $F_X(x)$ are the PDF and CDF of the condition X.

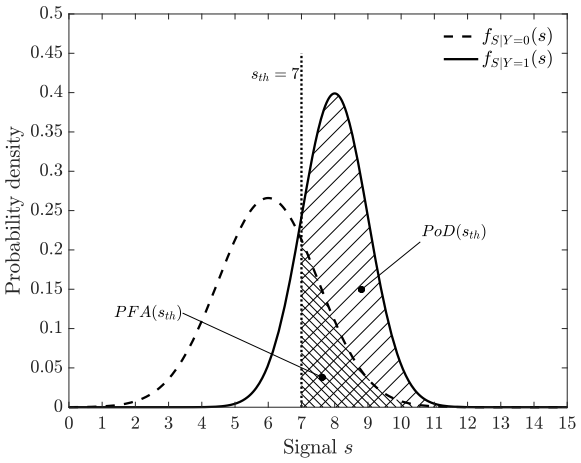

Figure 4.3 Conditional probability density functions. The areas under the two curves defined by the threshold s_{th} corresponds to a point PoD($s_{th} = 7$), PFA($s_{th} = 7$) on the ROC curve shown in Figure 4.4.

This model is commonly visualized by the corresponding receiver (or relative) operating characteristic (ROC) curve, which plots the PoD against the PFA. This curve is parametrized by a threshold on the signal s_{th}, also called the cut-off point (Fluss et al., 2005). Note that the PoD is not expressed as a function of the continuous condition X as in Section 4.2.4 above, but is here a function of s_{th}. The PoD and PFA as a function of s_{th} are

$$\mathrm{PoD}(s_{th}) = \Pr(S > s_{th}|Y = 1) = \int_{s_{th}}^{+\infty} f_{S|Y=1}(s) \mathrm{d}s, \tag{4.5}$$

$$\mathrm{PFA}(s_{th}) = \Pr(S > s_{th}|Y = 0) = \int_{s_{th}}^{+\infty} f_{S|Y=0}(s) \mathrm{d}s. \tag{4.6}$$

The ROC curve is illustrated in Figure 4.4, wherein the PoD and PFA for threshold values s_{th} are obtained from the conditional PDFs of Figure 4.3. Note that studies often derive the ROC curve for a single flaw size $X = x$, rather than for a domain defined by threshold

x_{th} (e.g., Rajesh, 1993). This can be useful to qualitatively compare NDE methods on a standardized flaw size but does not provide a complete model linking the observed signal with the condition.

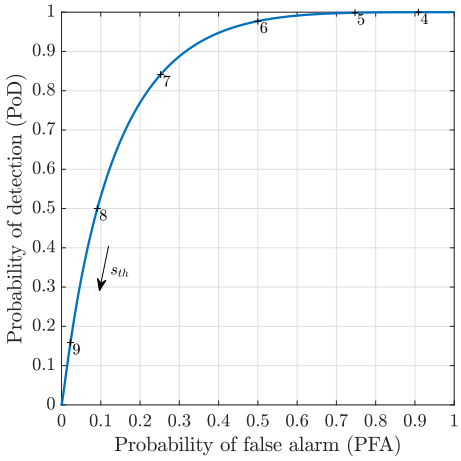

Figure 4.4 Each point on the ROC curve corresponds to a value of the signal threshold s_{th}.

One can alternatively express the PoD and PFA as a function of the conditional CDF $F_{S|X}$ from Model (1):

$$\mathrm{PoD}(s_{th}) = \Pr(S > s_{th} | X > x_{th}) = \frac{1}{1 - F_X(x_{th})} \cdot \int_{x_{th}}^{+\infty} \left(1 - F_{S|X}(s_{th}|x)\right) f_X(x) \mathrm{d}x, \quad (4.7)$$

$$\mathrm{PFA}(s_{th}) = \Pr(S > s_{th} | X < x_{th}) = \frac{1}{F_X(x_{th})} \cdot \int_{-\infty}^{x_{th}} \left(1 - F_{S|X}(s_{th}|x)\right) f_X(x) \mathrm{d}x. \quad (4.8)$$

Several indicators have been proposed to qualify the performance of an NDE system with a ROC curve (Greiner et al., 2000; Taner and Antony, 2000; Fluss et al., 2005). They include the *area under the curve* (AUC), the shortest distance between the curve and $(0, 1)$, also expressed in polar coordinates (Schoefs et al., 2012), and the *Youden Index* (Youden, 1950). The latter is computed as the maximum vertical distance between the ROC curve and the 45-degree line starting at $(0, 0)$.

Equations (4.3) to (4.8) show that the PoD and PFA on the ROC curve are a function of the distribution of the condition X. This signifies that even if the ROC curve is evaluated directly from experiments, it is only strictly valid for the distribution of the defects from which it is derived. Therefore, the ROC curve for the same NDE method can vary when applied to different situations. Boero et al. (2009) illustrates this effect for NDE of deteriorating structures, where the ROC curves change over time along with the distribution of the progressing damage condition. A problem appears when the given ROC curve is derived from a previous experiment because the distribution of X in the experiment, which we call *experimental design*, might not match the distribution of X in the specific application. To formally represent this, we distinguish between the PDF $f_X(x)$ and associated CDF $F_X(x)$ of the condition X for a specific application, and the PDF $f_{X,exp}(x)$ and associated CDF $F_{X,exp}(x)$ of X for the

experiment from which the ROC curve is derived. Although mentioned in earlier studies (Berens and Hovey, 1981), the effect of the experimental design has largely been ignored in the recent literature. To show this effect, we consider three experimental designs and show that the resulting ROC curves change significantly in Figure 4.5. An ROC curve from an NDE system provider should therefore be associated with information of the underlying experimental design.

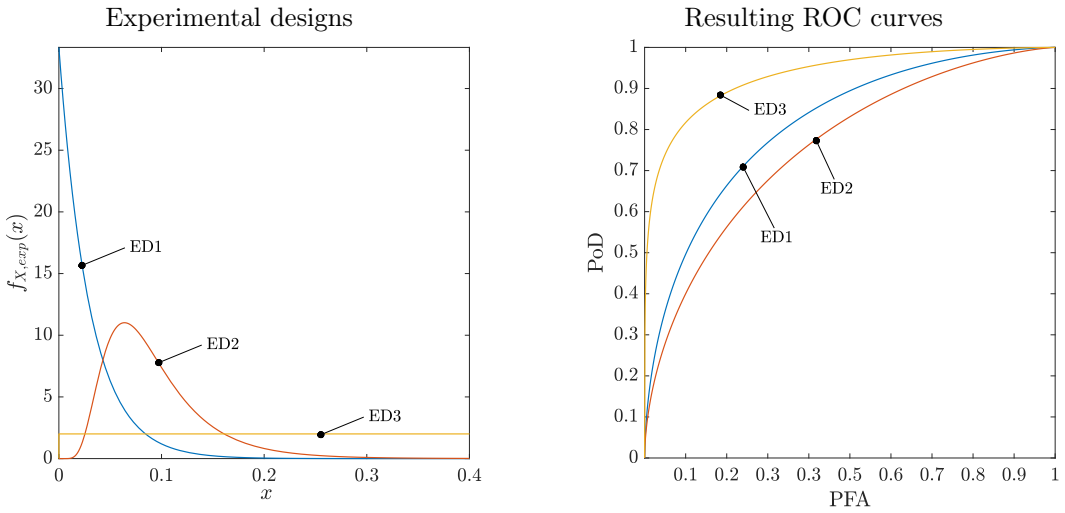

Figure 4.5 ROC curves for the same NDE derived for different experimental designs, ED1, ED2, and ED3. The model and distributions are presented in the example of Section 4.4 and their impact is investigated in Section 4.4.8. Here, $x_{th} = 0.1$.

4.2.6. Model (4): PoD/PFA – I binary, Y binary

This is the most elementary NDE quality model associated with an NDE, which identifies whether the system is in a certain state or not. It is obtained by fixing thresholds both on the condition X and the signal S. The associated likelihood is described by a confusion matrix, involving the operating PFA and PoD, as presented in Table 4.2.

Table 4.2 Likelihood of the binary-binary case: The confusion matrix $\Pr(I|Y)$.

	$Y = 0$	$Y = 1$
$I = 0$	$1 - \text{PFA}$	$1 - \text{PoD}$
$I = 1$	PFA	PoD

An example of a monitoring system that is described by such a model is ultrasonic flooded member detection, which detects the presence/absence of water in tubular steel members of underwater support structures as an indication of through-thickness cracks or other severe defects (Hayward et al., 1993; Visser, 2002). The performance of inspectors for visual inspection or using NDE devices is also typically represented through the PoD/PFA model (Swets, 1992; Sheils et al., 2010; Silva and Padua, 2012; Quirk et al., 2018).

The transition between Model (3) to Model (4) corresponds to calibrating the NDE system to an operating point on an ROC curve, by fixing the threshold s_{th}. The PoD and PFA are obtained from Equations (4.5) and (4.6).

The transition from Model (2) to (4) is obtained by combining Equations (4.7) and (4.8) with Equation (4.2). The PoD and PFA for Model (4) are

$$\mathrm{PoD} = \Pr(I = 1 | X > x_{th}) = \frac{1}{1 - F_X(x_{th})} \cdot \int_{x_{th}}^{+\infty} \mathrm{PoD}(x) f_X(x) \mathrm{d}x, \tag{4.9}$$

$$\mathrm{PFA} = \Pr(I = 1 | X < x_{th}) = \frac{1}{F_X(x_{th})} \cdot \int_{-\infty}^{x_{th}} \mathrm{PoD}(x) f_X(x) \mathrm{d}x. \tag{4.10}$$

The transition from Model (1) to (4) is obtained by transitioning from Model (1) to (3), then from Model (3) to (4), by fixing thresholds s_{th} and x_{th}. Depending on the nature of the condition and the observed signal, it is possible that both thresholds s_{th} and x_{th} are assigned the same value (Sheils et al., 2012), however they play very distinct roles in the NDE system and should not be confused with one another.

4.2.7. Some comments on learning the models

In the ideal case, one would learn the continuous/continuous Model (1) directly, giving a probabilistic relationship between condition X and signal S. From this base model, the three other model categories could be derived for specific applications. Surprisingly, review of the existing literature reveals that, when continuous/continuous probabilistic models are obtained from experimental or simulated data (see Section 4.2.3), they are often not used for reliability analysis, or for explicitly deriving PoD curves or other models.

Figure 4.6 summarizes how the four continuous or binary variables X, Y, S, and I interact through the four model types.

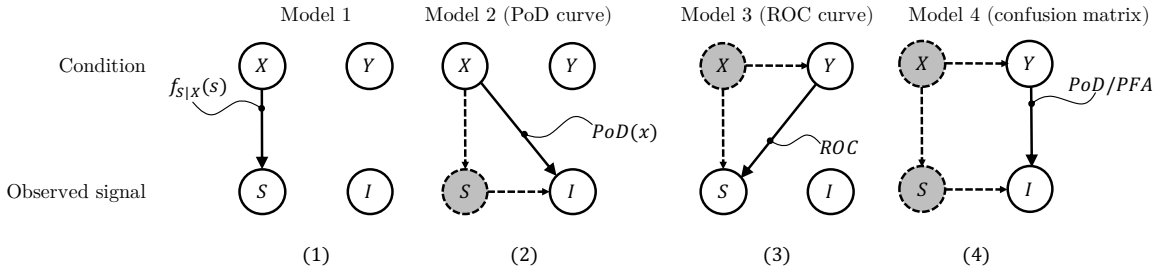

Figure 4.6 Interaction of the four continuous or binary variables X, Y, S, I through the NDE quality Models (1–4). The continuous edges illustrate the relationships between condition and observed signal described by the models. The grayed-out nodes designate the variables hidden when the models are directly evaluated from the experiments. For each model, the link between these hidden variables and the variables of the model can be expressed with Model (1) and an imposed threshold s_{th} or x_{th}.

It is not always possible to reveal a continuous condition or a continuous signal, in which case the NDE system is described by one of Models (2) to (4). Still, the base model linking X to S can be considered at an abstract level to ensure correct interpretation of the signal and good experimental design.

The correct interpretation of the observed signal is also affected by the uncertainties associated with the model of NDE considered. Several studies point to the fact that experimental data

and NDE performance obtained from this experimental data do not translate into similar performance once in-situ (e.g., Rouhan and Schoefs, 2003). The reasons given typically involve aleatoric and epistemic uncertainties in influential parameters affecting the NDE quality, which cannot always be reproduced in an experimental context (Wall and Wedgwood, 1994; Straub, 2004). For instance, temperature, humidity or lighting can affect the performance of an NDE technique (Annis, 2009) and introduce a bias in the model. Boero et al. (2009) investigated the spatial variability of NDE models. These model uncertainties can be partly quantified by assigning a probability distribution to the model parameters, thus explicitly accounting for the model uncertainty in the NDE quality model performance (Straub, 2004). This hierarchical dependence in the NDE models can also be used to update the models and their parameters with the information collected through Bayesian inference (Aldrin et al., 2013; Hamida and Goulet, 2020).

However, even if model uncertainties can be mitigated, the derivations in Sections 4.2.5 and 4.2.6 show that incorrect assumptions on the distribution of the true condition X lead to erroneous ROC curves and misinterpretation of the performance of NDE systems. In Section 4.4.8 we investigate the effect of such errors on the optimality of decisions.

4.3. NDE systems and decision analysis

Section 4.2 shows that several choices are made when modeling the performance of an NDE system. There is no unique description of NDE quality, and the quality models depend on threshold values on the measured signal and on the condition, s_{th} and x_{th}. These thresholds are set by either the designer or the user of the NDE system, often according to standard practice and predefined requirements (Wood and Engle Jr, 1979; Annis, 2009; Kurz et al., 2012). When the decision context is specifically considered for the choice of the thresholds, it is usually through the minimization of mis-classification rates or through minimum requirements on the detection performance of the NDE method (Rajesh, 1993). In some studies, the consequences of actions or failure are accounted for (e.g., Swets, 1992). In general, it is acknowledged that the thresholds affect the quality of the NDE system and that they should be calibrated (Kurz et al., 2012; Webb et al., 2015). Furthermore, the repair decision is often directly conditioned on the NDE outcome (recall the name "decision threshold" for s_{th}), and the quality of NDE systems is usually assessed without optimizing this decision (Berens and Hovey, 1981; Sheils et al., 2010). In this framework, we distinguish between the interpretation of observed signal S (or calibration of the NDE system) and the decision. We can scrutinize the choices of thresholds and repair decisions with a formal analysis.

As stated in Section 4.2.1, the probabilistic NDE quality models presented in Section 4.2.2 are likelihood functions, written as $\mathcal{L}(\boldsymbol{\theta}; z)$. $\boldsymbol{\Theta}$ is either X or Y depending on the setting. z is the measurement, which is either s or i. The posterior probability distribution of the condition $p(\boldsymbol{\theta}|z)$ is therefore obtained from Equation (2.5).

Additionally, the VoI concept can be used to quantify how NDE quality models affect the

decisions taken based on NDE results. While the methods developed in the NDE community focus on comparing inspection techniques, the actual value added is related to how the information from NDE leads to better decisions (Raiffa and Schlaifer, 1961; Straub, 2014). As explained previously in Section 2.2.3.1, it is assumed that the decision maker selects an action that maximizes the expected utility after obtaining information Z through NDE, as represented by the ID in Figure 2.3. The associated preposterior analysis is described by Equation (2.8).

Although the concept of VoI appeared in the mid-20th century, it is only recently that it has been introduced for assessing the performance of NDE, for example in SHM systems (e.g., Kamariotis et al., 2022). Reliance on established processes also explains why the concept of VoI was left aside. Historically, the primary focus of NDE performance evaluation has been to support systematic inspection plans or condition-based maintenance, where monitoring outcomes systematically result in one action of the "find nothing, do nothing" and "find a defect then repair" type (Berens and Hovey, 1981; Kerntechnischer Ausschuss, 2016). The performances of NDE techniques are codified by standards, based on traditional rule-of-thumb criteria, that are not specific to the problem. An example of NDE for systematic maintenance is the automated Eddy current inspection system for detecting and repairing cracks in engine components which has been used by the US air force since the 1980s (Berens, 2000). In the nuclear industry, standards prescribe fixed time intervals between inspections and the NDE techniques to adopt, assuming that any detected defect is systematically repaired (Kerntechnischer Ausschuss, 2016). The conservative conditions for inspection and repair are adopted without a risk-based decision analysis. In this context, false alarms and unnecessary repairs are judged as negligible when compared to preserving the safe operation of the system.

In Sections 4.4 and 4.5 we perform optimizations using Equations (2.8) to (2.15), where the decision maker can decide whether or not to repair the system based on observations provided by an NDE system. In the one-step decision problem, Equation (2.8) reduces to a simple condition that links the likelihood $\mathcal{L}(\boldsymbol{\theta}; z)$ with the different costs and prior probabilities. As is shown in the numerical results, employing Models (2) to (4) can lead to suboptimal decisions relative to using Model (1).

4.4. Example 1: Hypothetical NDE system

The purpose of this example is to demonstrate the unifying framework and investigate the impact of each of the four NDE models on the optimal decision outcome and cost in a basic decision problem. We highlight the effect of experimental design on the assessment of NDE performance.

4.4.1. Base model

We consider a hypothetical NDE system which measures a continuous condition and outputs a continuous signal, in analogy with crack detection systems such as UT.

The conditional PDF of the continuous measurement signal S given true condition X is

$$f_{S|X}(s|x) = \frac{1}{s\sqrt{2\pi}} \exp\left(-\frac{\left(\ln s - \ln\left(2x^3 + x^2 + 10^{-2}\exp(-1/2)\right)\right)^2}{2}\right). \tag{4.11}$$

This is the lognormal distribution with parameters $[\ln\left(2X^3 + X^2 + 10^{-2}\exp(-1/2)\right), 1]$. This conditional probability density is shown in Figure 4.2 (Model (1)).

In the following we consider a basic decision problem, where one needs to decide on a repair action. We adopt the four different NDE quality models described in Section 4.2.2 in turn and assess their impact on the repair decision. We additionally investigate the effect of learning the NDE models with different experimental designs.

4.4.2. Solution of the one-step decision problem

The decision problem consists in selecting a repair action to mitigate the consequence of failure, after obtaining imperfect NDE outcome Z on state $\boldsymbol{\Theta}$. It is illustrated in Figure 4.7. The condition $\boldsymbol{\Theta}$ is either X or Y. The observation variable is Z, which is either the continuous signal S or the binary signal I. $\mathcal{L}(\boldsymbol{\Theta}; z)$ indicates the likelihood function. In this setup, we consider two possible actions: either do nothing a_0, for a cost $c_A(a_0) = 0$, or repair a_R, for a cost $c_A(a_R) = c_R$. The probability of system failure F is defined conditional on the state $\boldsymbol{\Theta}$ and the action A. The consequence of failure is c_F.

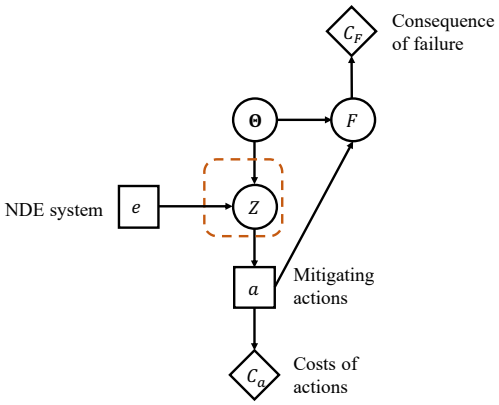

Figure 4.7 Influence diagram for the one-step decision problem.

The a priori optimal action a_{e_0} is the one that minimizes the total expected cost as given by Equation (2.14). Here,

$$\mathbf{E}_{\boldsymbol{\Theta}}[C_T(a, \boldsymbol{\Theta})] = c_A(a) + c_F \Pr(F|a) \text{ with } \Pr(F|a) = \mathbf{E}_{\boldsymbol{\Theta}}\left[\Pr(F|\boldsymbol{\Theta}, a)\right]. \tag{4.12}$$

From Equation (2.13), one finds that

$$a_{e_0} = a_R \iff c_F \Pr(F|a_0) > c_R + c_F \Pr(F|a_R). \tag{4.13}$$

As per Equation (2.8), the a posteriori optimal action is the one that minimizes the conditional expected total cost,

$$\mathbf{E}_{\mathbf{\Theta}|z}[C_T(a,\mathbf{\Theta})] = c_A(a) + c_F \Pr(F|Z=z,a), \text{ with } \Pr(F|Z=z,a) = \mathbf{E}_{\mathbf{\Theta}|z}\left[\Pr(F|\mathbf{\Theta},a)\right]. \tag{4.14}$$

Making the likelihood $\mathcal{L}(\mathbf{\Theta};z)$ explicit in the conditional expectation, one obtains that

$$a_{opt}(z) = a_R \iff \mathbf{E}_{\mathbf{\Theta}}\left[\mathcal{L}(\mathbf{\Theta};z) c_F \Pr(F|\mathbf{\Theta},a_0)\right] > \mathbf{E}_{\mathbf{\Theta}}\left[\mathcal{L}(\mathbf{\Theta};z)\left\{c_R + c_F \Pr(F|\mathbf{\Theta},a_R)\right\}\right]. \tag{4.15}$$

When the condition is binary, i.e., $\mathbf{\Theta} = Y$, $\mathcal{L}(Y;z)$ is the likelihood for Models (3) or (4). The condition of the above equation can be transformed into a condition on $\frac{\mathcal{L}(Y=1;z)}{\mathcal{L}(Y=0;z)}$, also called the "likelihood ratio test" (Peterson and Birdsall, 1953; Green and Swets, 1966). If $a_{e_0} = a_R$,

$$a_{opt}(z) = a_R \iff \frac{\mathcal{L}(Y=1;z)}{\mathcal{L}(Y=0;z)} > \frac{\left\{c_R + c_F \Pr(F|Y=0,a_R) - c_F \Pr(F|Y=0,a_0)\right\}\Pr(Y=0)}{\left\{c_F \Pr(F|Y=1,a_0) - \left[c_R + c_F \Pr(F|Y=1,a_R)\right]\right\}\Pr(Y=1)}. \tag{4.16}$$

The expected total cost associated with the optimal action following an NDE is given by Equation (2.11). When the observation is binary, i.e., $Z = I$ and $\{I=1\} = \{S > s_{th}\}$, the expected cost depends on the choice of threshold s_{th}.

4.4.3. Condition model and a priori optimal action

The prior PDF of X is the exponential PDF with mean 0.03.

$$f_X(x) = \frac{1}{0.03}\exp\left(-\frac{x}{0.03}\right). \tag{4.17}$$

We fix the cost of repair $c_R = 1$. Under the do-nothing action a_0, the probability of failure of the system is defined conditional on X (Figure 4.8),

$$\Pr(F|X=x) = 10^{-5} + (1-10^{-5}) \cdot \left(\frac{1}{2} + \frac{1}{2}\text{erf}\left(\frac{\log x - 0.1}{\sqrt{2}}\right)\right), \tag{4.18}$$

where erf is the error function.

When the system is repaired, the probability of failure is reduced such that $\forall x$, $\Pr(F|X = x, a_R) = p_{F|R} = 10^{-4}$. The cost of failure is $c_F = 800$.

Equation (4.13) gives the condition to identify the a priori best decision. The probability of failure of the system conditional on action a_0 is evaluated as $\Pr(F|a_0) = 1.2 \cdot 10^{-3}$, and the probability of failure conditional on action a_R is $\Pr(F|a_R) = p_{F|R} = 10^{-4}$. Since $c_F \Pr(F|a_0) = 0.94$ is smaller than $c_R + c_F p_{F|R} = 1.08$, the a priori best decision is therefore to do nothing, $a_{e_0} = a_0$, with associated cost 0.94.

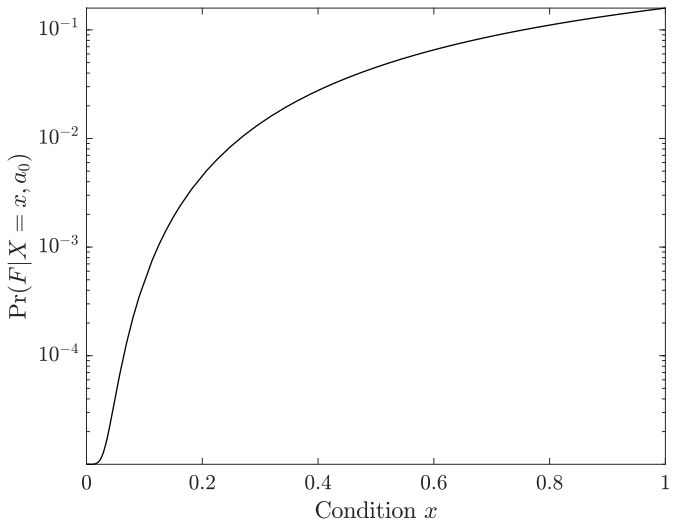

Figure 4.8 Probability of system failure conditional on the condition X.

4.4.4. A posteriori optimal action with Model (1)

The likelihood $\mathcal{L}(x;s)$ is given by Equation (4.11). By solving Equation (4.15) for $z=s$, we find that the optimal action is $a_{opt}(s)=a_0$ for $s<s_{th,1}=1.6\cdot10^{-2}$, and $a_{opt}(s)=a_R$ for $s>s_{th,1}$. Here, $s_{th,1}$ is effectively a repair threshold. The comparison of expected costs for both actions as a function of the measured signal S is depicted in Figure 4.9. The expected total cost computed with Equation (2.11) is 0.65. The VoI of this NDE system is $0.94-0.65=0.29$.

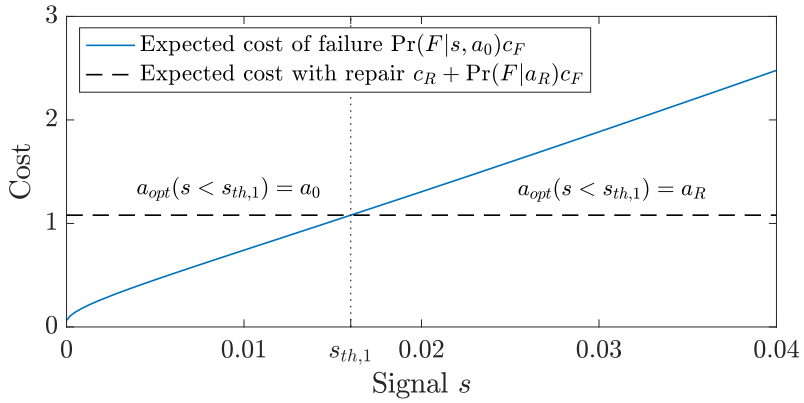

Figure 4.9 Expected cost for action a_0 and a_R conditional on the observed signal S.

4.4.5. A posteriori optimal actions for a given PoD curve

We now determine the optimal a posteriori action identified with the PoD curve (Model (2)) and the associated VoI. We remind that in Model (2), a binary signal I is considered, which is related to the continuous signal S by $\{I=1\}=\{S>s_{th}\}$. The likelihood $\mathcal{L}(x;I)$ is given by

the PoD curve of Equation (4.2), which depends on the fixed threshold s_{th}. PoD curves for different thresholds are depicted in Figure 4.10.

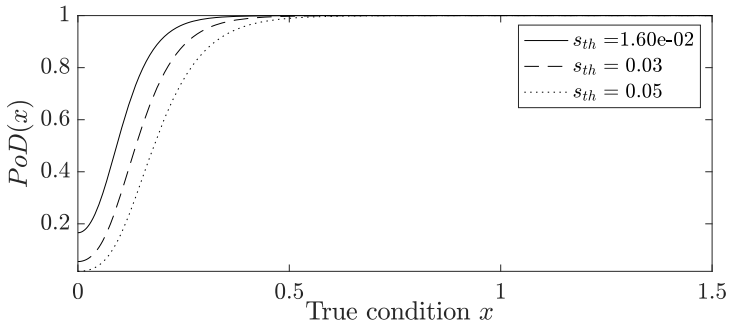

Figure 4.10 PoD curves for different thresholds s_{th}, including $s_{th,2}$.

PoD curves are typically given and not specific to the application, and hence are likely suboptimal for a given decision context. For example, if the given PoD curve is calibrated with $s_{th} = 0.03$, the optimal actions are $a_{opt}(I = 0) = a_0$, $a_{opt}(I = 1) = a_R$ and the expected cost is 0.70. The resulting the VoI is $0.94 - 0.70 = 0.24$, which is below the potentially achievable VoI= 0.29.

For each imposed threshold s_{th} and associated PoD curve, Figure 4.11 indicates the optimal actions $a_{opt}(I)$ and the expected cost calculated with Equation (2.11). A threshold exists that maximizes the VoI and minimizes the expected cost for this case study. It is the decision threshold $1.6 \cdot 10^{-2}$, with the associated expected cost of 0.65, which corresponds to the result obtained with Model (1). However, when describing the NDE by the PoD curve, this optimal solution will only be obtained by coincidence. In general, the PoD curve leads to a suboptimal decision.

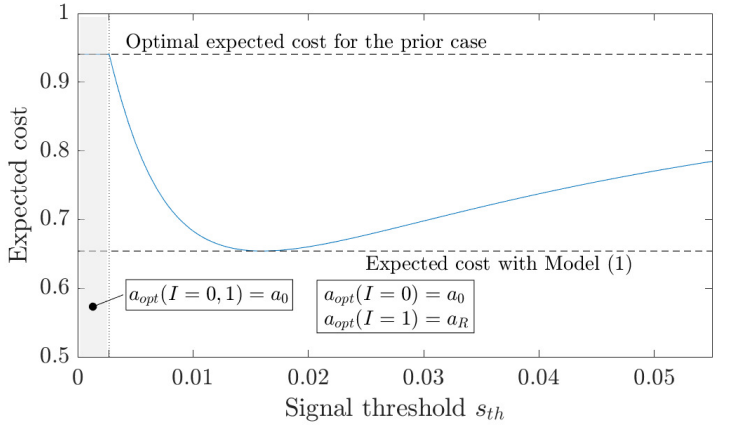

Figure 4.11 Expected cost using the PoD curve model as a function of the fixed signal threshold s_{th}.

4.4.6. A posteriori optimal actions for a given ROC curve

When ROC curves are utilized to represent the quality of NDE, the continuous condition X is replaced by the binary condition $\{Y = 1\} = \{X > x_{th}\}$. Here we fix $x_{th} = 0.1$. The corresponding ROC curve is depicted in Figure 4.5, where the distribution of X corresponds to the experimental design ED1.

To compare the performance of Models (1) and (3), we must first ensure that the relationships between binary condition Y and failure F are compatible with the relationship between continuous condition X and failure F. This compatibility is ensured by the following equations,

$$\Pr(Y = 1) = 1 - F_X(x_{th}) = 3.6 \cdot 10^{-2}, \tag{4.19}$$

$$\Pr(F|Y = 1, a_0) = \frac{\int_{x_{th}}^{+\infty} \Pr(F|X = x) f_X(x) \mathrm{d}x}{1 - F_X(x_{th})} = 1.7 \cdot 10^{-2}, \tag{4.20}$$

$$\Pr(F|Y = 0, a_0) = \frac{\int_{0}^{x_{th}} \Pr(F|X = x) f_X(x) \mathrm{d}x}{F_X(x_{th})} = 5.8 \cdot 10^{-4}. \tag{4.21}$$

Additionally, it is $\forall y \in \{0, 1\},\ \Pr(F|Y = y, a_R) = p_{F|R}$.

The solution of the decision problem is derived from Equation (4.16):

$$a_{opt}(s) = a_R \iff \frac{\mathcal{L}(Y = 1; s)}{\mathcal{L}(Y = 0; s)} = \frac{f_{S|Y=1}(s)}{f_{S|Y=0}(s)} > 1.31. \tag{4.22}$$

The likelihoods $\mathcal{L}(Y; s) = f_{S|Y}(s)$ are computed with Equations (4.3) and (4.4). Both Models (1) and (3) provide the same model evidence $p(s)$.

From Equation (4.22), we find the optimal action $a_{opt}(s)$ is a_0 when $s < 1.7 \cdot 10^{-2}$ and a_R otherwise. This threshold $s_{th,3} = 1.7 \cdot 10^{-2}$ is shown as the optimal operating point on the ROC curve in Figure 4.12. Furthermore, Figure 4.12 indicates that ROC performance indices, such as the Youden Index, are associated with certain operating points. But using either of these points, as proposed in some references (e.g., Schoefs and Clement, 2004), is not optimal in view of the specific decision.

The total expected cost for the optimal operating point is 0.76. The VoI of this NDE system is 0.18, lower than for Model (1). Even though the actions are optimized, their efficiency are limited by the fixed threshold x_{th} and associated "failure" domain of the NDE device, through Equation (4.22). Other values of x_{th} can yield a higher or lower VoI: E.g., with $x_{th} = 0.2$ the associated optimal expected cost is 0.91 and the VoI is only 0.03. However, the threshold x_{th} can typically not be influenced for a given NDE device.

4.4.7. A posteriori optimal actions for a given point on the ROC curve

Here, the NDE system is described by a point on the ROC curve defined above in Section 4.4.6, such that $\{I = 1\} = \{S > s_{th}\}$. The likelihood of Model (4) $\mathcal{L}(Y; I)$ is given by a confusion

matrix as per Table 4.2, with $\mathcal{L}(Y=1;I=1) = \text{PoD}$ and $\mathcal{L}(Y=0;I=1) = \text{PFA}$. As in Equation (4.22), the likelihood ratio verifies the conditions

$$a_{opt}(I=1) = a_R \iff \frac{\mathcal{L}(Y=1;I=1)}{\mathcal{L}(Y=0;I=1)} > 1.31 \iff \frac{\text{PoD}}{\text{PFA}} > 1.31, \tag{4.23}$$

$$a_{opt}(I=0) = a_R \iff \frac{\mathcal{L}(Y=1;I=0)}{\mathcal{L}(Y=0;I=0)} > 1.31 \iff \frac{1-\text{PoD}}{1-\text{PFA}} > 1.31. \tag{4.24}$$

For example, for $s_{th} = 1 \cdot 10^{-2}$ (and $x_{th} = 0.1$ as above), PoD = 0.82, PFA = 0.37, $a_{opt}(I=1) = a_R$, $a_{opt}(I=0) = a_0$ and the expected cost is 0.79.

Figure 4.12 shows the expected cost for any fixed PoD and PFA as well as the optimal actions $a_{opt}(I)$. Two zones can be distinguished: (a) for any (PFA, PoD) in the yellow zone, the optimal course of action is to do nothing, whatever the observation outcome; this is what the prior optimal action also prescribes, therefore the VoI at these points is 0; (b) for any (PFA, PoD) to the left of this yellow zone, detection triggers repair a_R, and no detection entails a_0.

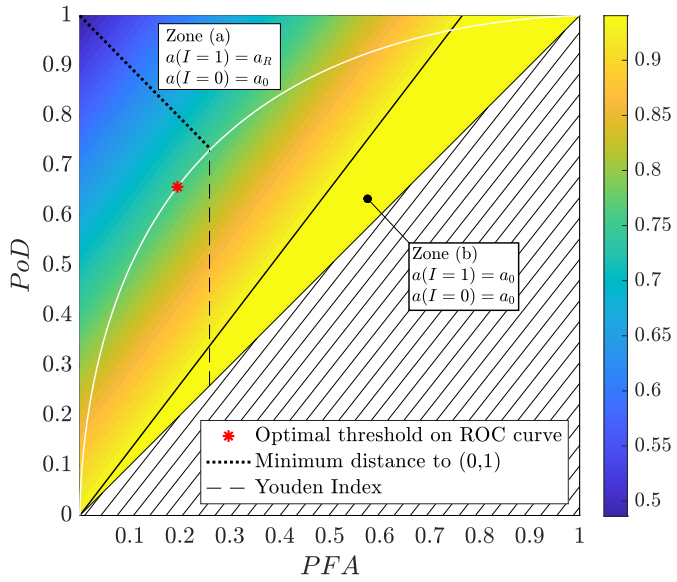

Figure 4.12 Optimal expected cost as a function of PFA and PoD. Zone (b) corresponds to $VoI = 0$: this means that for any decision threshold s_{th} on the ROC curve that falls within that zone, the best course of action is the prior optimal action, i.e., do nothing. The hatched area corresponds to the situation where the significance of $I = 0$ and $I = 1$ are inverted.

4.4.8. Influence of the experimental design

We investigate how the experimental design $f_{X,exp}$ used to learn the ROC curve can affect the decision taken and the resulting expected total cost and VoI. We consider three experimental designs ED1, ED2, and ED3, where the test conditions follow an exponential, lognormal, and uniform distribution, respectively (Equations (4.25) to (4.27)). The imposed threshold on the

condition remains $x_{th} = 0.1$ as above, with $\{Y = 1\} = \{X > x_{th}\}$.

$$f_{X,exp,1}(x) = \frac{1}{0.03} \exp\left(-\frac{x}{0.03}\right), \tag{4.25}$$

$$f_{X,exp,2}(x) = \frac{2}{x\sqrt{2\pi}} \exp\left(-2(\ln x + 2.5)^2\right), \tag{4.26}$$

$$f_{X,exp,3}(x) = 2, \quad \text{if } 0 \leq x \leq 0.5,\ 0 \text{ otherwise.} \tag{4.27}$$

The corresponding likelihoods $f_{S|Y,exp,i}(s)$ are obtained with Equations (4.3) and (4.4). The resulting ROC curves for $x_{th} = 0.1$ are plotted in Figure 4.5.

For each likelihood $f_{S|Y,exp,i}(s)$, the model evidence $p_{exp,i}(s)$ is evaluated with Equation (2.6), where the prior probability of the condition Y is obtained with Equation (4.19):

$$\begin{aligned} p_{exp,i}(s) = \sum_{y=0}^{1} f_{S|Y=y,exp,i}(s) \Pr(Y = y) = & \frac{1 - F_X(x_{th})}{1 - F_{X,exp,i}(x_{th})} \cdot \int_{x_{th}}^{+\infty} f_{S|X}(s|x) f_{X,exp,i}(x) \mathrm{d}x \\ & + \frac{F_X(x_{th})}{F_{X,exp,i}(x_{th})} \cdot \int_{-\infty}^{x_{th}} f_{S|X}(s|x) f_{X,exp,i}(x) \mathrm{d}x. \end{aligned} \tag{4.28}$$

The posterior probabilities $\Pr(Y|s)$ and $\Pr(F|s)$ are similarly computed with Equations (2.5) to (2.7).

The first experimental design ED1= $f_{X,exp,1}(x)$ corresponds to the distribution of the condition in this application $f_X(x)$ defined in Equation (4.17). Equation (4.28) shows that in this case the model evidence $p_{exp,1}(s)$ and the posterior probabilities coincide with the model evidence and posterior probabilities obtained by applying Model (1) and the continuous/continuous likelihood $f_{S|X=x}(s)$. $f_{S|Y,exp,1}(s)$ is therefore the true likelihood and provides the correct evaluation of expected costs. This case is examined in Sections 4.4.6 and 4.4.7 and is called the reference case here.

When the experimental design differs from the distribution in the application, i.e., when $f_{X,exp}(x) \neq f_X(x)$, the model evidence and posterior probabilities deviate from the reference case and the conditional expected costs calculated with Equation (4.14) are incorrect. This in turn affects the results of the decision problem and changes the optimal action attributed to each observation outcome by Equation (4.15). It also impacts the expected cost calculated with Equation (2.11).

One can evaluate this impact by overlaying the corresponding ROC curves on Figure 4.12 and by plotting the expected cost and optimal actions of the decision problem with binary observation $\{I = 1\} = \{S > s_{th}\}$ as a function of the fixed signal threshold s_{th}, as in Figure 4.13.

Figure 4.13 shows that each experimental design gives a different evaluation of the expected cost for a given s_{th}. The constant part of each curve corresponds to the portion of the ROC curve in zone (a), and the other part falls in zone (b) (see Figure 4.12). These action zones

differ for each ROC curve. For example, when the ROC curve is learned from experiments with ED2= $f_{X,exp,2}(x)$, one finds that imposing a threshold $3.5 \cdot 10^{-3} < s_{th} < 6 \cdot 10^{-3}$ leads to the action "do nothing," whatever the outcome s. In contrast, under the reference case the optimal action is to repair if the signal is higher than the fixed threshold and do nothing otherwise. By misevaluating the conditional expected costs, the experimental design leads to suboptimal actions.

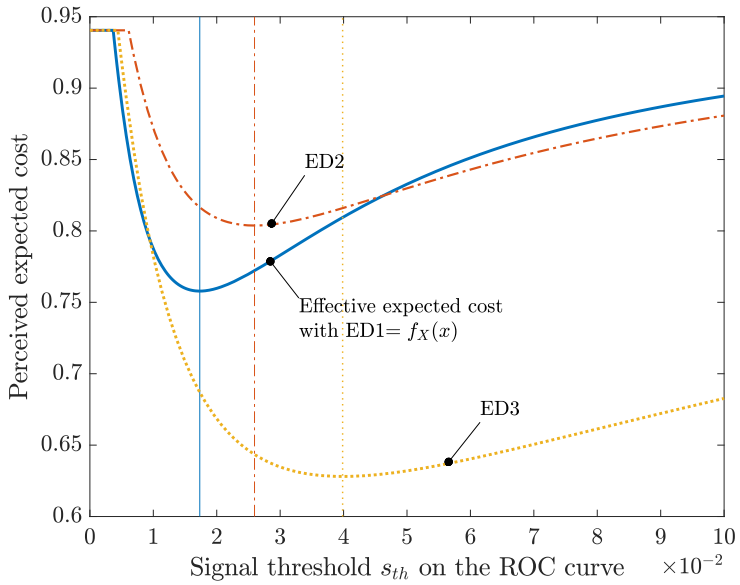

Figure 4.13 Expected cost calculated for experimental designs ED1, ED2, and ED3. ED1 corresponds to the distribution of the condition in this application $f_X(x)$. ED2 and ED3 differ from $f_X(x)$. For a fixed threshold s_{th}, only ED1 provides the correct values for PoD and PFA and the associated expected cost. ED2 and ED3 give wrong PoD and PFA, thus the perceived expected cost associated with s_{th} is also wrong. The vertical lines of corresponding style locate the perceived optimal threshold $s_{th,exp,i}$ for each experimental design, where optimal action a_{opt} is a_0 if $s < s_{th,exp,i}$ and a_R otherwise. The effective expected cost for these thresholds is read on the reference curve (ED1): The perceived expected cost for the optimal threshold for ED2 overestimates the effective expected cost; the perceived expected cost for the optimal threshold for ED3 underestimates it (see Table 4.3).

Another problem is that the optimal calibration, in the form of a threshold $s_{th,exp,i}$, minimizes the wrong expected cost function. The effective expected cost at this threshold, obtained with the reference case, can in fact be higher or lower. In Figure 4.13, the optimal threshold for ED2 is $s_{th,exp,2} = 2.6 \cdot 10^{-2}$. At this point, the effective expected cost given by ED1 is lower than the perceived expected cost for ED2. Table 4.3 summarizes these results for all investigated likelihoods.

Table 4.3 Effect of the experimental design on recommended actions and on the assessment of expected cost.

Experimental design	Optimal threshold	Perceived expected cost	Effective expected cost
$f_{X,exp,1}(x)$ - Reference	$1.7 \cdot 10^{-2}$	0.76	0.76
$f_{X,exp,2}(x)$	$2.6 \cdot 10^{-2}$	0.80	0.77
$f_{X,exp,3}(x)$	$4.0 \cdot 10^{-2}$	0.63	0.81

In summary, ignoring the underlying experimental design of a given ROC curve can lead to suboptimal decisions and to an NDE system that is not used to its full potential. Additionally,

the expected costs can be over- or underestimated, hence they affect the perceived VoI. Ultimately, this can lead the decision maker to favor one or another NDE system based on an erroneous evaluation of the NVoI of the NDE systems.

4.5. Example 2: Half-cell potential measurement for corrosion detection

The purpose of this example is the investigation of the effects of different model choices on a real NDE technique. We consider the half-cell potential measurement of reinforcement corrosion in concrete structures, and we analyze the effect of choosing Model (3) or Model (4), with different calibration choices, on the outcomes of optimal decision making for a one-step and a two-step decision problem.

4.5.1. Description and model of the inspection technique

Corrosion of reinforcement bars (rebars) in concrete structures is one of the leading deterioration mechanisms in civil infrastructure. Visible signs of corrosion on the concrete surface occur when corrosion of the rebars is already extensive and major repairs are needed. This demonstrates the need for early detection of rebar corrosion.

As the rebars are encased in the concrete, NDE methods are required to monitor their condition. Half-cell potential measurement is such a method, and it is used to detect whether corrosion has initiated. This test measures the difference of electric potential between an electrode, directly connected to an exposed rebar, and a half-cell (reference electrode) placed on the concrete surface. The intensity of the chemical reaction responsible for corrosion at the half-cell is translated into a negative potential. The higher the amplitude of this electric potential, the higher the probability that corrosion has initiated in the rebar under the concrete cover (Elsener et al., 2003).

Empirical testing has revealed that the amplitude of the signal is clearly affected by environmental factors including humidity, chloride content, temperature, concrete cover, or concrete strength (e.g., Lentz et al., 2002; Kessler and Gehlen, 2017). This is why obtaining relevant and accurate probabilistic models a priori is a challenge. In practice, the electric potentials are measured on a regular grid on the concrete structure and are summarized in a frequency plot. The measurement data is then classified into two sets, "corroded" and "not corroded," by applying a threshold on the potential. This is typically done by expert judgement. The downside of this method is that it relies on relatively few sample measurements and misclassification can occur at a high rate.

Some studies have proposed to model the performance of this NDE method with a non-site-specific likelihood (Faber and Sorensen, 2002; Lentz et al., 2002). Typically, the chosen model involves a continuous signal (the potential) and a binary measured condition (corrosion initiated/no corrosion), thus follows Model (3) described in Section 4.2.2. However, these

distributions are not used as such to perform Bayesian analysis. Instead, a threshold value on the potential is proposed, and the continuous signal transformed into a binary one (Lentz et al., 2002). Interestingly, the ROC representation is not common in this domain, even if it highlights best how the PoD and PFA vary with the chosen threshold.

This example uses the NDE quality model proposed by Faber and Sorensen (2002). The absence and presence of corrosion is represented by $Y = 0$ and $Y = 1$, respectively. We adopt normal PDFs for the likelihood after (Faber and Sorensen, 2002). The parameters of the normal distribution of the measured electric potential S given that no corrosion has initiated ($Y = 0$) are $\mu_0 = -0.207$[Volt] and $\sigma_0 = 0.0804$[Volt]. The parameters of the normal distribution given that corrosion has initiated ($Y = 1$) are $\mu_1 = -0.354$[Volt] and $\sigma_1 = 0.08$[Volt]. The distributions are shown in Figure 4.14a and the corresponding ROC curve in Figure 4.14b. These distributions are (where φ is the standard normal) PDF:

$$f_{S|Y=0}(s) = \mathcal{L}(Y = 0; s) = \varphi\left(\frac{s - \mu_0}{\sigma_0}\right), \tag{4.29}$$

$$f_{S|Y=1}(s) = \mathcal{L}(Y = 1; s) = \varphi\left(\frac{s - \mu_1}{\sigma_1}\right). \tag{4.30}$$

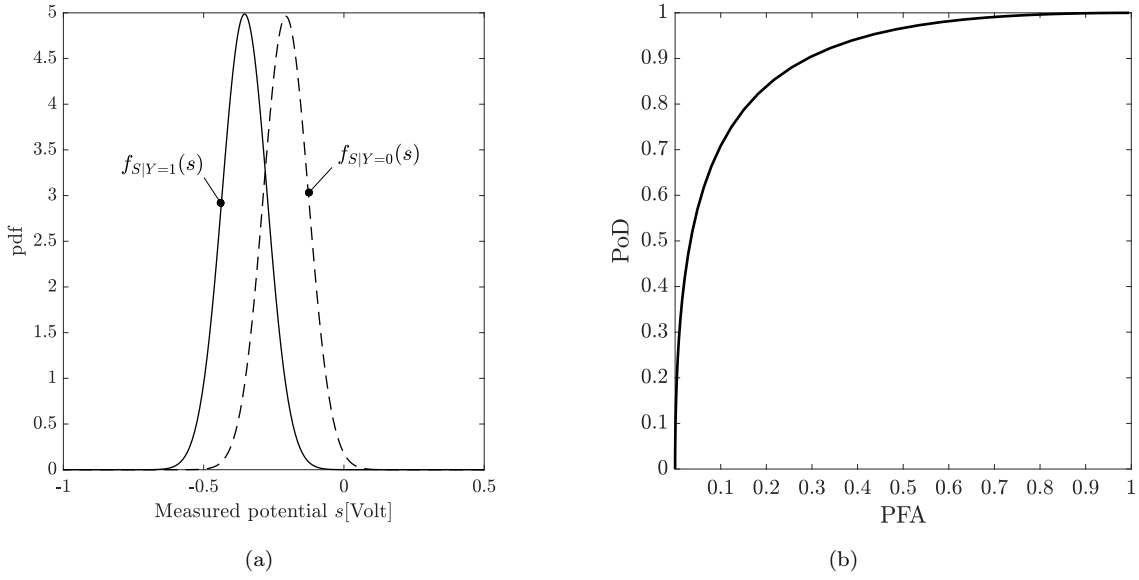

Figure 4.14 (a):The two likelihoods are depicted. (b): Corresponding ROC curve.

We first investigate the one-step decision problem, where a repair action is taken based on the NDE result. In the second part, we consider a two-step decision problem, where information about the condition of the rebar is collected in two separate instances and repairs can be carried out each time. For both problems, we find the optimal course of action considering the continuous signal with Model (3). We show that fixing a threshold for Model (4), irrespective of the specific application is not optimal, for instance the one recommended by Faber and Sorensen (2002). We demonstrate how this fixed threshold can be optimized for both problems.

4.5.2. One-step decision problem

4.5.2.1. Decision model and a priori optimal action

Corrosion of the system ($Y = 1$) can eventually lead to failure. The decision maker has the opportunity to repair, a_R, at a cost $c_R = €5$ million, or to do nothing, a_0, at cost of €0. If the system is repaired, there are no further consequences. If the system is corroded ($Y = 1$) but not repaired, the consequences are $c_F = €50$ million. If the system is not corroded ($Y = 0$), there are no consequences. The prior probability of corrosion is $\Pr(Y = 1) = 0.05$.

The results are obtained following Section 4.4.2. Without inspections, the expected total cost conditional on action a_0 is $c_F \Pr(Y = 1) = €2.5$ million. Conditional on action a_R, it is $c_R = €5$ million. Hence, the a priori optimal action is $a_{e_0} = a_0$, do nothing.

4.5.2.2. Optimal a posteriori action considering the continuous signal

Equation (4.16) applied with $Z = S$ is here adapted to

$$a_{opt}(s) = a_R \iff \frac{\mathcal{L}(Y = 1; s)}{\mathcal{L}(Y = 0; s)} > \frac{c_R \Pr(Y = 0)}{(c_{F,0} - c_{F,R} - c_R) \Pr(Y = 1)} = 2.11. \tag{4.31}$$

We derive

$$a_{opt}(s) = a_R \iff \left(\frac{s - \mu_0}{\sigma_0}\right)^2 - \left(\frac{s - \mu_1}{\sigma_1}\right)^2 > 2 \log\left(\frac{\sigma_1}{\sigma_0} \frac{1}{2.11}\right). \tag{4.32}$$

Finally,

$$a_{opt}(s) = a_R \iff s \in [s_1^* = -29.72[\text{Volt}]; s_2^* = -0.31[\text{Volt}]]. \tag{4.33}$$

We see here that the signal domain is divided into three action zones. This is due to a mathematical artefact caused by the fact that the likelihoods are normal PDFs with unequal (although very similar) standard deviations. In practice, it does not make sense not to repair when the observed potential is very negative. The unsuitability of normal likelihoods for some NDE systems has been highlighted by Green and Swets (1966). The left bound s_1^* in Equation (4.33) is, however, very far from the expected values of the signal S, and does not significantly affect the results.

The expected cost associated with the a posteriori optimal action is evaluated by numerical integration from Equation (2.11) and is €1.4 million.

The VoI of this NDE system is $2.5 - 1.4 = €1.1$ million, equivalent to a gain of 45% relative to the a priori expected cost.

4.5.2.3. Optimal a posteriori action for a binary signal with decision threshold s_{th}

Here, the continuous signal S is processed to a binary outcome $\{I = 0\} = \{S > s_{th}\}$ (no detection) and $\{I = 1\} = \{S < s_{th}\}$ (detection), i.e., $Z = I$, and $\mathcal{L}(Y = 1; I = 1) = \text{PoD}(s_{th})$

and $\mathcal{L}(Y=0;I=1) = \text{PFA}(s_{th})$. As in Equation (4.31), the optimal actions are determined by a condition on PoD and PFA:

$$a_{opt}(I=1) = a_R \iff \frac{\text{PoD}}{\text{PFA}} > 2.11, \tag{4.34}$$

$$a_{opt}(I=0) = a_R \iff \frac{1-\text{PoD}}{1-\text{PFA}} > 2.11. \tag{4.35}$$

Figure 4.15 shows the expected cost given by Equation (2.11) as a function of PFA and PoD. It also represents the ROC curve obtained from the PDFs of Equations (4.29) and (4.30).

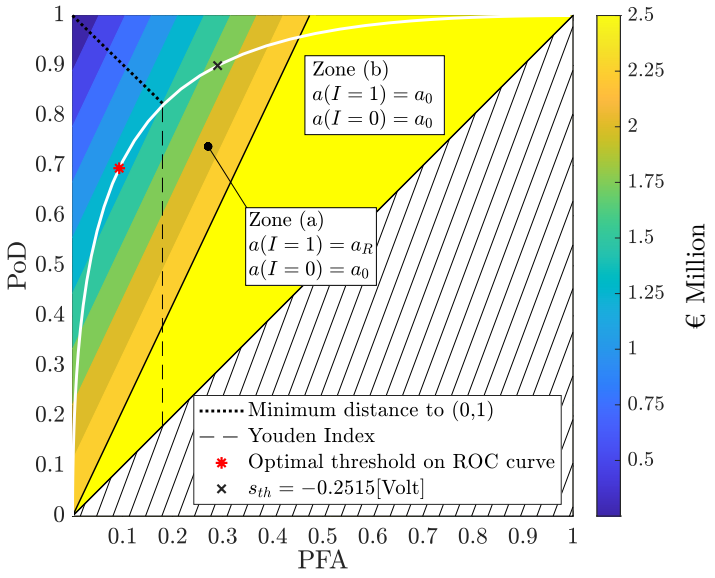

Figure 4.15 Expected cost as a function of PFA and PoD, corresponding optimal actions, and the ROC curve in white. In zone (b), the selected action is a_0, hence the VoI is 0. The hatched area corresponds to a monitoring system where the significance of $I=0$ and $I=1$ are inverted. The optimal point on the ROC curve obtained by Bayesian analysis differs from the Youden Index threshold and the point closest to (0,1). As a comparison, the threshold -0.2515[Volt] recommended by Faber and Sorensen (2002) is indicated.

Figure 4.15 also locates the cut-off point of the Youden Index, $s_{th} = -0.28$[Volt], which coincides for this ROC curve with the point closest to the origin. These are suboptimal operating points with an associated expected cost of €1.5 million, which is higher than the optimal cost found with Model (1).

The optimal threshold on the ROC curve that minimizes the expected cost is $s_{th,fix} = -0.31$[Volt], with associated cost €1.4 million. We note that this threshold is equal to bound s_2^* found in Section 4.5.2.2. For this setup, Model (3) and Model (4) achieve the same performance without loss of information if the threshold is optimized for the problem at hand.

We can also evaluate the NDE system with cut-off point -0.2515[Volt] that Faber and Sorensen (2002) directly apply on the measured potential for the repair decision criteria. It is shown on Figure 4.15. The expected total cost associated to that threshold is €1.9 million, which is 34% more than the cost found with Model (3). It still yields a non-zero VoI.

Table 4.4 Conditional probability $\Pr(Y_2|Y_1')$.

	$Y_1' = 0$	$Y_1' = 1$
$Y_2 = 0$	0.95	0
$Y_2 = 1$	0.05	1

4.5.3. Two-step decision problem

4.5.3.1. Decision model and a priori optimal actions

We now consider a two-step decision problem. The repair actions are taken at each step based on the NDE data obtained up to that step. Additionally, the actions affect the state of the system at the next step. The initial condition of the system is Y_1. The effect of the action $A_1 \in \{a_0, a_R\}$ at time step 1 on the state of the system is reflected in Y_1'. The condition of the system can evolve from Y_1' to Y_2 at time step 2. Both Y_1 and Y_2 are binary, with states "corroded" or "not corroded." Similarly, an action A_2 is taken that affects the state of the system, resulting in Y_2'. The immediate consequence of the concrete being corroded at time step i is $C_{F,i}(Y_i' = 1) = c_F$, where $c_F = €50$ million. If $Y_i' = 0$, there are no associated consequences, i.e., $C_{F,i}(Y_i' = 1) = €0$. The action cost is $C_{A,i}(a_R) = c_R = €5$ million and $C_{A,i}(a_0) = €0$.

The random variable Y_1 is characterized by $\Pr(Y_1 = 1) = 0.1$. The conditional probabilities reflecting the decision taken at time step i are given by $\Pr(Y_i'|A_i = a_0, Y_i \in \{0,1\}) = \mathbb{1}\{Y_i' = Y_i\}$, where $\mathbb{1}\{\cdot\}$ is the indicator function, and $\Pr(Y_i' = 1|A_i = a_R, Y_i \in \{0,1\}) = 0$. The transition from Y_1' to Y_2 is expressed by the conditional probability in Table 4.4.

We solve the two-step decision problem assuming three models of NDE quality. First, the NDE quality is described by Model (3) (Figure 4.16a) and the thresholds and actions are optimized sequentially. The second quality model is Model (4), where a fixed point on the ROC curve in Figure 4.14b is given (Figure 4.16b). Finally, we optimize the point on the ROC curve for this specific application (Figure 4.16c). The details of the derivations are available in Appendix C.

The optimal actions based only on prior knowledge are to first repair at time step 1, and then do nothing at time step 2, i.e., $(a_1, a_2)_{e_0} = (a_R, a_0)$. The associated expected cost is €7.5 million.

4.5.3.2. Optimal a posteriori actions considering the continuous signal

The actions are first optimized sequentially, based on the continuous half-cell potential measurements S_1 and S_2 at time step 1 and 2, respectively. This means that the NDE method is represented by Model (3).

This multi-step sequential decision problem with NDE results is in general difficult to resolve. A heuristic approach to the optimization can provide an approximate solution (Bismut and Straub, 2021). For this two-step problem, an analytical solution is obtained by backward induction (Bellman, 1957b).

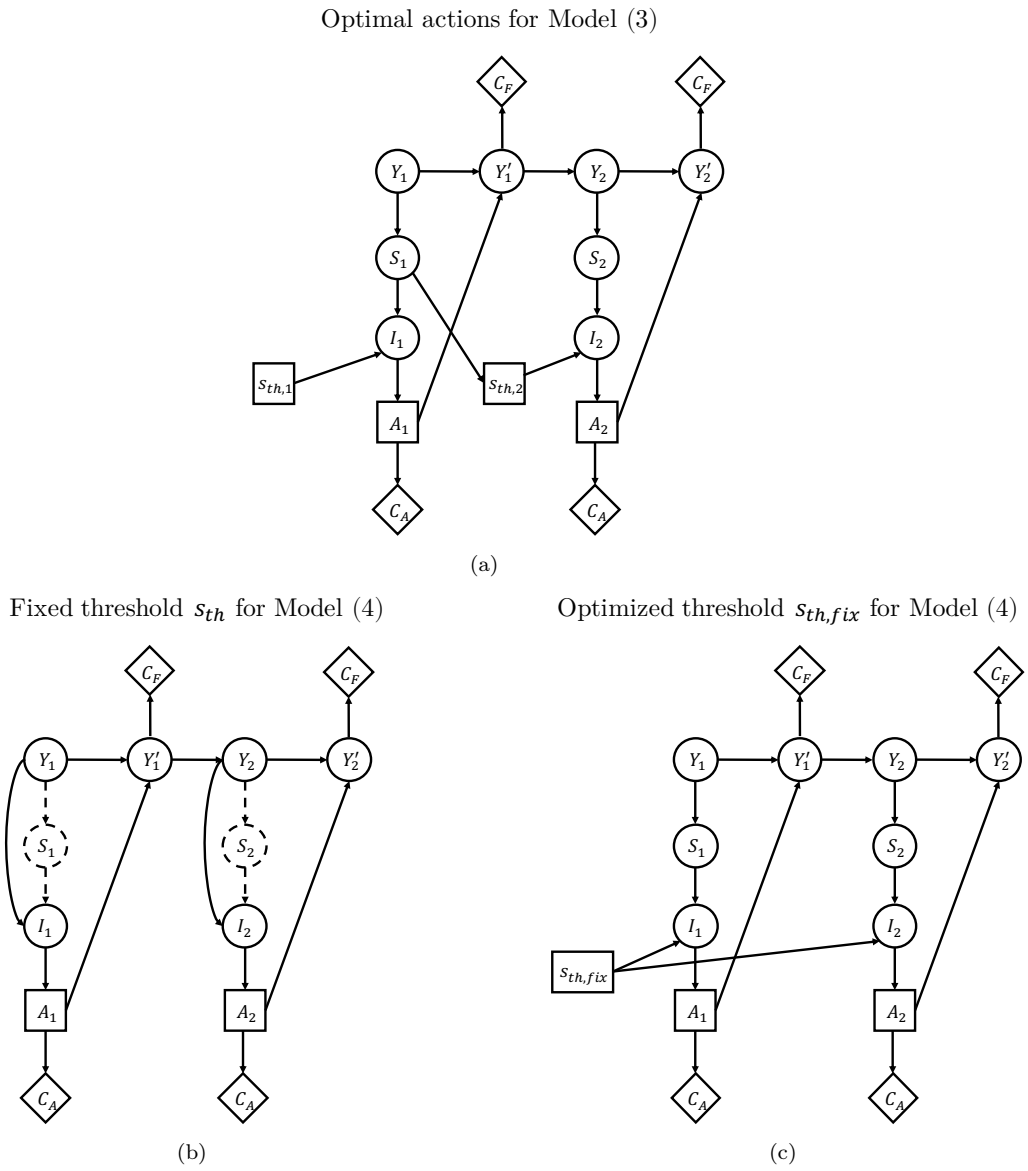

Figure 4.16 Influence diagrams of the two-step decision problem where the quality of NDE is described: (a) by Model (3), where the thresholds $s_{th,i}$ such that $\{I_i = 1\} = \{S_i < s_{th,i}\}$ are optimized sequentially; (b) by Model (4) with a given threshold defining the likelihood $\Pr(I|Y)$; and (c) by Model (4), where the fixed threshold is optimized for the specific application.

The optimal actions are shown in Figure 4.17, as a function of the measured signal S_1 and S_2 obtained sequentially. We can see that the optimal solution is equivalent to applying a threshold $s_{th,1} = -0.28$[Volt] on S_1, then a threshold $s_{th,2}$ on S_2 that depends on S_1, as illustrated by Figure 4.16a. We see that if $S_1 > s_{th,1}$, the optimal threshold at time step 2 depends on the outcome at time step 1. When the system is repaired at time step 1, the optimal decision $a_{2,opt}$ is independent of outcome S_1.

The expected total cost of reacting optimally at each time step to the continuous signal is €3.7 million. The VoI for this NDE system is $7.5 - 3.7 =$ €3.8 million. This result shows that considering the continuous signal is more optimal compared to classifying the signal according to a fixed rule.

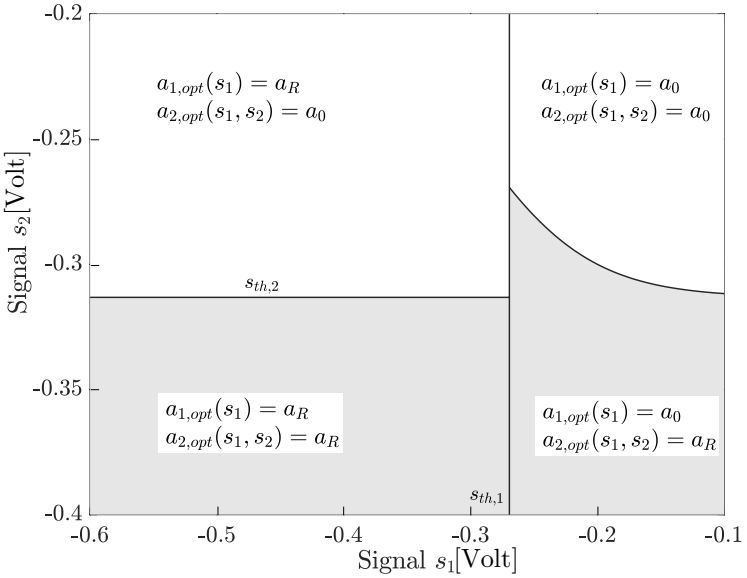

Figure 4.17 Optimal policy given monitoring history S_1 and S_2. The optimal threshold on signal S_1 is $s_{th,1} = -0.27$[Volt]. The optimal threshold $s_{th,2}$ on signal S_2 depends on the observation S_1.

4.5.3.3. Optimal a posteriori actions for a binary signal with decision threshold

In this configuration, the NDE system is described by Model (4). The corresponding influence diagram is drawn in Figure 4.16b. We investigate, for example, the fixed threshold -0.2515[Volt] from Faber and Sorensen (2002). The NDE system is described by the point PoD $= 0.90$ and PFA $= 0.29$ on the ROC curve (Figure 4.14b). The expected total cost is €4.2 million and the VoI is $7.5 - 4.2 =$ €3.3 million. This fixed threshold -0.2515[Volt] is not optimal when compared to the VoI of Model (3) above.

Using Model (3) for the considered NDE method provides the optimal actions for the two-step decision problem. However, one can optimize the fixed threshold and point on the ROC curve for Model (4), as illustrated by the modified influence diagram of Figure 4.16c. To do so, we first determine sequentially the optimal actions $a_{1,opt}(I_1)$ and $a_{2,opt}(I_1, I_2)$, for any PFA and PoD values. The resulting expected cost is depicted in Figure 4.18. The optimal threshold is found on the ROC curve that maximizes the expected cost along the curve. One finds $s_{th,fix} = -0.28$[Volt] and the associated expected cost is €3.8 million. The VoI for this NDE system is $7.5 - 3.8 =$ €3.7 million. The ROC curve and optimal operating point are also shown in Figure 4.18. As a comparison, the previously evaluated threshold -0.2515[Volt] is also plotted on the ROC curve.

For given PFA and PoD values, the optimal actions of the two-step problem with Model (4) are defined by the zone, numbered 1 to 5, to which the PFA and PoD values belong in Figure 4.18. In zone 1, the optimal actions are condition-based and memoryless, which corresponds to $a_{opt,i}(I_i = 1) = a_R$ and $a_{opt,i}(I_i = 0) = a_0$. This is not true when the PFA and PoD values belong to zones 2 to 5. It is therefore necessary to solve the decision problem, as any point on the ROC curve does not result in optimal actions that are condition-based

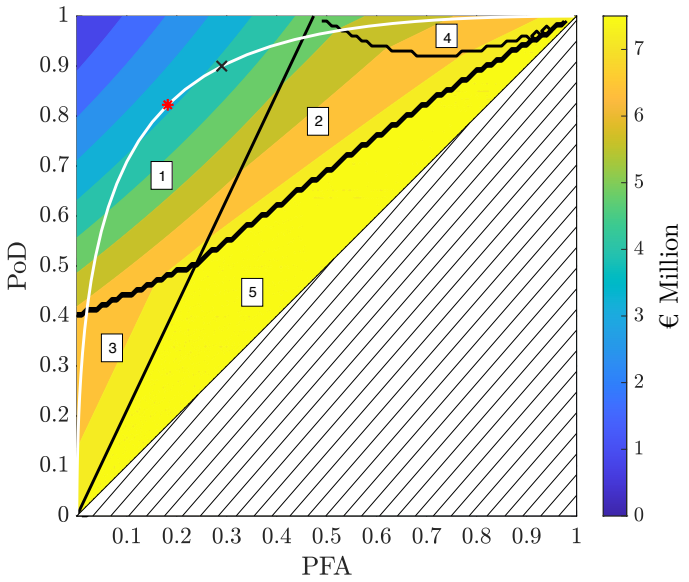

Figure 4.18 Expected total cost as a function of PFA and PoD. The ROC curve is in white. The areas numbered 1 to 5 correspond to action zones. In zone 1, $a_{i,opt}(I_i = 1) = a_R$, $a_{i,opt}(I_i = 0) = a_0$; in zone 2, $a_{1,opt}(I_1 = 1) = a_R$, $a_{1,opt}(I_1 = 0) = a_0$, $a_{2,opt}(I_2 = 1, I_1 = 0) = a_R$, $a_{2,opt}(I_2 = 0, I_1 = 0) = a_0$, $a_{2,opt}(I_1 = 1) = a_0$; in zone 3, $a_{1,opt} = a_R$, $a_{2,opt}(I_2 = 0) = a_0$, $a_{2,opt}(I_2 = 1) = a_R$; in zone 4, $a_{1,opt}(I_1 = 1) = a_R$, $a_{1,opt}(I_1 = 0) = a_0$, $a_{2,opt} = a_0$; in zone 5, $a_{1,opt} = a_R$, $a_{2,opt} = a_0$. Zone 5 corresponds to $VoI = 0$. The red asterisk locates the optimal fixed operating point with threshold $s_{th,fix} = -0.28$[Volt]. As a comparison, the cross locates the point for threshold -0.2515[Volt] from (Faber and Sorensen, 2002).

and memoryless. This conclusion echoes the results by Bertovic (2016), who warns that the outcomes of mechanized NDE are trusted too rapidly, where the results are interpreted as calling for action, to the detriment of information assessment.

The effect of ignoring the different action zones is illustrated in Figure 4.19. This figure compares the optimal expected total costs along the ROC curve and the expected total cost of following a condition-based and memoryless maintenance strategy (as in zone 1). The curve corresponding to the optimal expected cost along the ROC curve stays within the lower and upper bounds, which are respectively the optimal expected cost with Model (3) at €3.7 million (Section 4.5.3.2) and the optimal a priori expected cost of €7.5 million (Section 4.5.3.1). In contrast, implementing a condition-based and memoryless maintenance strategy with a fixed NDE threshold, for example -0.4[Volt] in zone 3, results in an expected cost of €8 million. This cost is higher than the expected cost of €6.9 million associated with the optimal actions for Model (4) with this same threshold, and even higher than the a priori expected cost.

4.6. Summary

This chapter reviews existing models of NDE quality in the context of a unifying framework. We have clarified the connection between the different models of NDE quality, such as PoD curves or ROC curves, through a base model in which both the condition and the NDE outcome are modeled continuously. The models with a binary observed signal or binary condition are derived by imposing thresholds on the observed signal and the condition. For

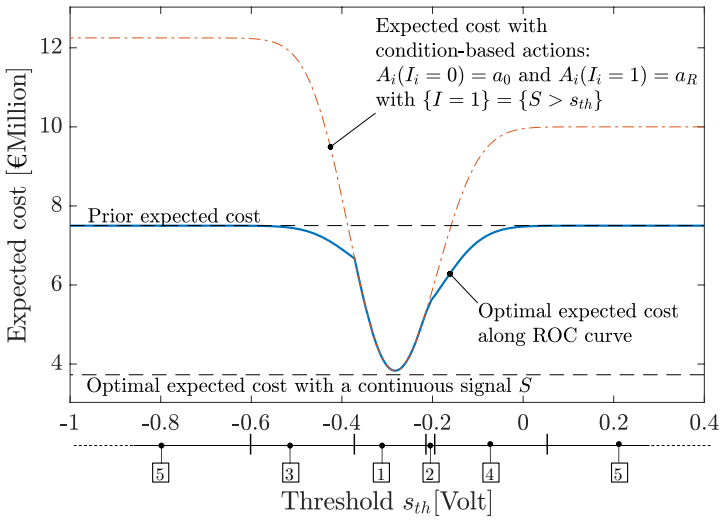

Figure 4.19 Expected cost associated with a condition-based and memoryless maintenance strategy and with the optimal actions for Model (4). The action zones, 1 to 5, of Figure 4.18 are indicated as a function of the threshold value. For certain threshold values, the expected cost associated with the condition-based memoryless maintenance strategy is higher than the prior expected cost.

models that use a binary condition, one must also impose a distribution on the underlying continuous condition.

In practice, there currently is no systematic approach to choose and calibrate NDE models and handle NDE data for reliability assessment or maintenance planning (Kurz et al., 2012). The presented framework can support the development and appropriate application of NDE models to real-life settings. Ideally, the base model is learned from experimental data and any other model can then be derived from this base model. When the base model is not available, it can still be considered at an abstract level to appraise the quality of given NDE models. As we demonstrate, the use of given PoD curves or ROC curves are likely to yield suboptimal actions for a specific decision context, since the signal and condition thresholds are fixed without considering of the decision problem. The framework also highlights the importance of explicitly accounting for the experimental design conditions that underlie ROC curve models, which should be assessed within the decision context.

Calibration of an NDE system in function of the decision settings (e.g., cost model) is beneficial. Such a calibration is often done implicitly. In particular, on-site inspectors tend to report a larger damage when the occurrence of failure is cost-critical, and vice-versa will be more cautious to diagnose damage when the costs of repair are very high (Silva and Padua, 2012; Bertovic, 2016). Bayesian decision analysis provides the means to compute the VoI, which allows direct comparison between NDE systems. This analysis gives the opportunity to calibrate an NDE system to suit the decision parameters such as the cost of mitigating actions and the expected consequences of failure. In Sections 4.4 and 4.5 we have evaluated the VoI in simple one-step and two-step decision problems. We find that using the model with continuous variables leads to the best decisions. In contrast, systematically associating NDE system outcomes with maintenance actions can lead to sub-optimal decisions and a detrimental use

of the inspection data. In order to keep the focus on the heuristic strategy optimization approach of Chapter 3, we do not address this aspect and potential savings in the numerical investigations described in Chapters 6 and 7. However, the methodology presented in this thesis easily enables the inclusion of additional decision parameters for the calibration of the NDE model.

Finding the VoI of NDE systems in sequential decision problems remains, however, an intractable task, as demonstrated in Chapter 2. As an alternative, the heuristic approach presented in Chapter 3 can be applied for the treatment of information, and some heuristic parameters optimized such that the information from NDE system is collected, interpreted and exploited in a good manner.

Chapter 5

Time-dependent reliability of deteriorating systems

> Quoi, à mon âge !!! Vous me prenez pour une vieille coque rouillée, bonne pour la ferraille ?...Vous allez voir, espèces de Bachi-Bouzouks, si je suis si vieux que cela !...Je pars, m'entendez-vous ?...Et de la Lune, je vous enverrai des cartes postales !...
>
> *Les aventures de Tintin: Objectif Lune*
> Hergé

Parts of this chapter originate from Bismut, E. and Straub, D. (2021). "Optimal adaptive inspection and maintenance planning for deteriorating structural systems". In: *Reliability Engineering & System Safety* 215, p. 107891.

5.1. Time to failure of a maintainable, non-repairable system

The risk-based heuristic planning approach presented in Chapter 3, and in particular Equations (3.13) to (3.16), require the evaluation of the probabilities associated with the failure branches of the decision tree of Figure 2.4, i.e., the distribution of the time to failure of the system T_F and its CDF $F_{T_F|\boldsymbol{w},\boldsymbol{Z}}$. Aside from this requirement, it is generally interesting to predict the evolution of the state of the system and of its components, for instance as part of a preventive predictive maintenance plan (see Figure 3.2), where repair is triggered by a threshold on system reliability, or to ensure that a reliability level is maintained during the service life in a reliability-based planning approach (see Chapter 7). This chapter lays down the assumptions for the type of systems considered in this work and presents the available methods to compute the required probabilities.

In the context of large infrastructure I&M planning, we explicitly consider multiple components (or sub-systems), indexed by $1 \leq k \leq N$, within the system. The components and the system are linked by a functional relationship, which we describe in Section 5.3.1. We define system failure as the event which leads to a major intervention, and high costs c_F (see Section 2.2.2.2). In the decision analysis problem for I&M planning, we consider system failure as a terminal event (see Section 3.5.2); thus, the system is non-repairable (Rausand and Høyland, 2004).

However, it is maintainable, in the sense that maintenance actions, for instance replacement, can be carried out on its components.

In this work, failure of the system originates from the deterioration processes, in conjunction with extreme load. This assumption notably ensures that the variance of $\mathbf{E}_{\boldsymbol{\Theta}|\boldsymbol{Z}}[C_F|\boldsymbol{w}, \boldsymbol{Z}]$ with respect to $\boldsymbol{Z}$ remains small (see Section 3.5.4), as the conditional probability of system failure is dominated by the effect of the extreme load.

The capacity R of the system decreases over time due to deterioration. In a multi-component system, this decrease is the result of local, progressive damage at component level (see Section 5.2). The deterioration processes thus reduce the ability of the system to resist the applied loading, S, where S can be a fixed load (e.g., an ultimate design load) or a variable load (e.g., wave impacts on an offshore structure). The dependence with time of the capacity and the load are denoted by $R(t)$ and $S(t)$, respectively. In a maintained system, the mitigating I&M actions on the system components can contribute to improving the capacity.

Identifying the time to failure of the system is therefore a first passage problem, illustrated by Figure 5.1. The components' states are affected by the deterioration processes and by eventual mitigating maintenance actions. This translates into the system capacity $R(t)$. The *time to failure*, T_F, is defined by Rausand and Høyland (2004) as "the time elapsing from when the item is put into operation until it fails for the first time." Here, the system fails at the first point in time when the load $S(t)$ exceeds $R(t)$.

We introduce the limit state function (LSF) $g(t) = R(t) - S(t)$. The time to failure T_F is

$$T_F = \min\{t, \text{ s.t. } g(t) < 0\}. \tag{5.1}$$

The *accumulated failure event* $F(t)$ {"the system is in the failed state at time t"} is

$$F(t) = \{T_F \leq t\}. \tag{5.2}$$

The evolution of $R(t)$ and $S(t)$ shown in Figure 5.1 is typically not known in advance, due to the uncertainties associated with the deterioration processes and the loading, but also with the future decisions on mitigating actions. Thus, T_F is unknown and can be modeled as a random variable. To account for the uncertainties, a probabilistic model of the system behavior, including deterioration and loads, can be provided, such that the distribution of T_F can be derived. The CDF of T_F is

$$F_{T_F}(t) = \Pr(T_F \leq t) = \Pr[F(t)]. \tag{5.3}$$

We now discretize time, where the i^{th} time step designates the time interval $[t_{i-1}, t_i]$, with $t_0 = 0$ (see Section 2.3.1). We denote by F_i the accumulated failure event $F(t_i)$, "failure of the system up to time t_i". Following (Straub et al., 2020), we introduce $F_i^* = \{g_i < 0\}$, such that $g_i = R_i - S_i$, where S_i represents the maximum load within time step i, and R_i is the system

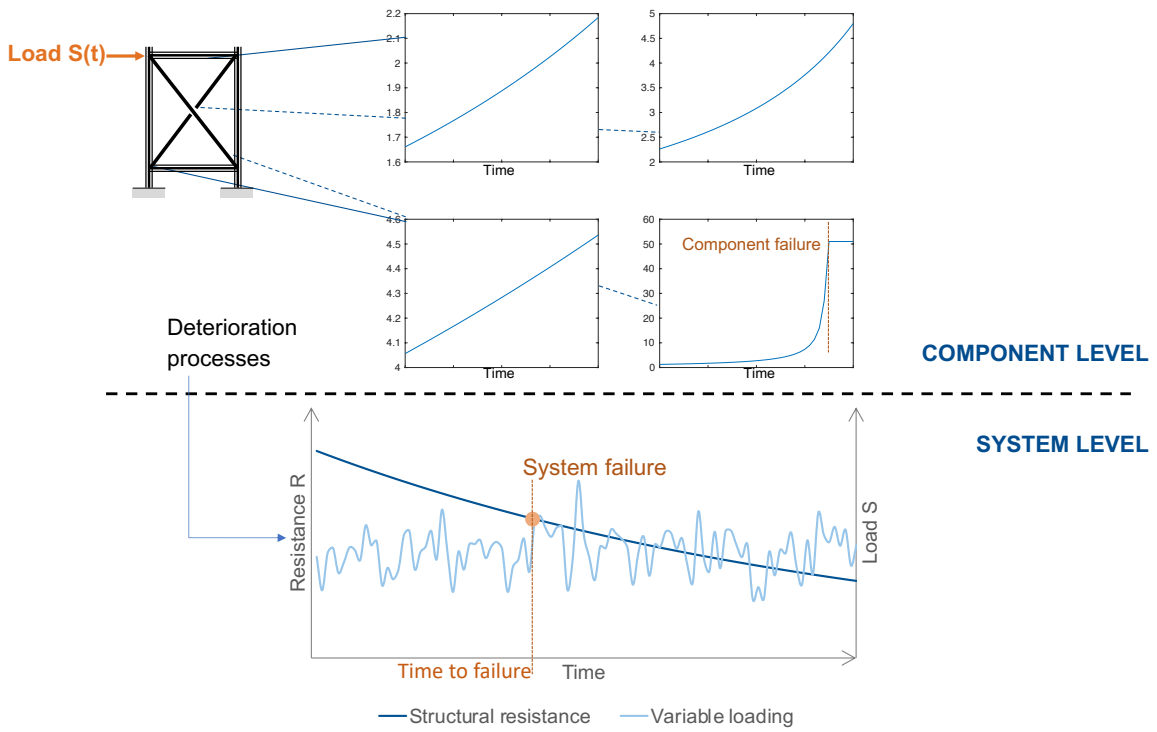

Figure 5.1 Failure of a deteriorating system expressed as a first passage problem. The deterioration is represented at the component level, where critical damage leads to the failure of the component. The dependence between the state of deterioration of the components and the evolution of the system capacity $R(t)$ is depicted schematically. System failure occurs when $R(t)$ is not sufficient to sustain the load $S(t)$. The time to failure T_F is indicated. $R(t)$, depicted here as decreasing, can very well increase due to maintenance operations on the components. The evolution of $R(t)$ and $S(t)$ is typically not known in advance, this shows a possible realization.

resistance at time t_i. The F_i^* are the *interval failure events* (Straub et al., 2020). When the time steps are small enough, one can approximate:

$$F_i = F_1^* \cup F_2^* \cup \ldots \cup F_i^*. \tag{5.4}$$

On its own, the interval failure event F_i^* can be interpreted as a hypothetical event, where the system has deteriorated, i.e., the resistance has decreased until time t_i, but it has not previously had the opportunity to fail, i.e., the system has not been loaded before time t_i. The successive accumulated failure events are nested, such that $F_1 \subset F_2 \subset ... \subset F_i$.

The basic structural reliability problem of the type $\Pr(g(\boldsymbol{X}) < 0)$, where g is an LSF of uncertain quantities $\boldsymbol{X}$, has been extensively investigated and several methods for its solution have been developed, including numerical integration methods, Monte Carlo methods, or the First Order Reliability Method (FORM). Details about these methods can be found in (Ditlevsen and Madsen, 1996; Melchers and Beck, 2018). However, the sought quantity in Equation (5.3) is a probability of the union of failure domains:

$$\Pr(F_i) = \Pr(F_1^* \cup F_2^* \cup \ldots \cup F_i^*) = \mathbf{E}_{\boldsymbol{X}}\left[\mathbb{1}\left\{\cup_{j\leq i}\left\{g_j(\boldsymbol{x}) < 0\right\}\right\}\right], \tag{5.5}$$

where $\mathbb{1}\{\cdot\}$ is the indicator function. Here, random variable $\boldsymbol{X}$ aggregates all the past, present

and future states of the system and its components. $\mathbf{E}_{\boldsymbol{X}}[\cdot]$ is the expectation over the joint distribution $p(\boldsymbol{x})$. g_j is a function of variable $\boldsymbol{X}$ is such that $g_j(\boldsymbol{X}) = R_j - S_j$. Through the functional relationship between system performance and components, the system capacity at time t_j, R_j, is a function of the variables describing the system components' states (see Section 5.3). The computation of $\Pr(F_i)$ is a *time-dependent reliability problem* and is nontrivial (Der Kiureghian, 2004). For deteriorating systems, the probabilistic model for $\boldsymbol{X}$, which describes both space- and time-dependent characteristics of the system, can be formulated to facilitate computations, e.g., using Markov chains. This is detailed in Section 5.4.2.

In addition, the reliability of the system changes over time as observations $\boldsymbol{Z}$ are obtained and maintenance actions are carried out during the execution of the chosen I&M plan $\mathcal{S}$. We distinguish three cases: The *filtered* probability at time step i is conditioned on all the information obtained up to and including time step i, it is $\Pr(F_i|\boldsymbol{Z}_{1:i})$. The *predicted* probability is conditioned on past information obtained up to and not including time step i, for instance $\Pr(F_i|\boldsymbol{Z}_{1:i-3})$. The *smoothed* probability is conditioned on information obtained after the considered time step, for instance $\Pr(F_i|\boldsymbol{Z}_{1:i+3})$. The expectation of Equation (5.5) is then with respect to $p(\boldsymbol{x}|\mathbf{z})$.

Computing these conditional probabilities supposes that a probabilistic model is available to the analyst, which allows for information and uncertainty propagation through the system components, the sub-systems and the system itself. In this chapter we lay down the principal parts of such a probabilistic model, such that the time-dependent reliability of a deteriorating multi-component system can be evaluated. First, the types of deterioration models at the component level are reviewed in Section 5.2. Then, the inter-components and components-system relationships are addressed in Section 5.3 such that the model at the system level is built. In Section 5.4 the available methods for computing the time-dependent reliability are compared and demonstrated on two case-studies, the Zayas frame and the nuclear piping system, which are the objects of numerical investigations in Chapters 6 and 7. The applicability and limitations of the methods are summarized in Section 5.5.

5.2. Models of deterioration processes

5.2.1. What is deterioration?

Deterioration is a monotonous, irreversible process, which is linked to the slow dissipation of energy contained in an organized atomic structure according to the second law of thermodynamics (Amiri and Modarres, 2014). Prigogine (1978) characterizes the deterioration process as the ability of a system to self-organize and reach thermodynamic equilibrium. The effect of deterioration in structural materials, such as concrete or steel, is a reduction of their strength and thus of their ability to perform as designed, until eventually the structural element cannot function, e.g., cannot sustain a certain load, and fails.

The progress of the deterioration process is influenced by numerous environmental factors, oxygen levels for corrosion, chloride concentration for chloride-induced corrosion, wind-induced

vibrations for fatigue, to only cite a few. These factors are associated with large uncertainty, which amplifies the uncertainty of atomic level phenomena. This is why probabilistic models of deterioration processes are suited to the analysis of deteriorating systems.

There is a long history of research and development of models for deterioration processes. Melchers (2003b) provides a review of empirical models for marine corrosion. Fatemi and Yang (1998) record over 50 models for fatigue damage since Palmgren's damage accumulation model (Palmgren, 1924). All agree that all models have limitations in the number of effects and factors they can account for and in their applicability.

It is convenient to classify the existing probabilistic models according to the level of detail that they provide, as in Figure 5.2. On the furthest right end of the spectrum, the models are

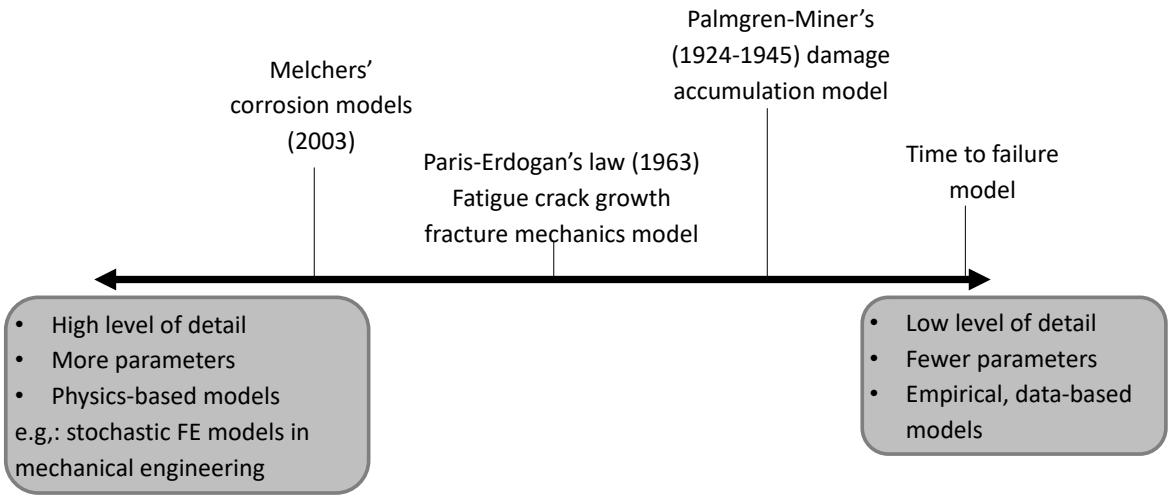

Figure 5.2 Examples of models of deterioration ordered according to their level of detail. On the right side, one finds empirical-based models, with low level of detailing. On the left side, physics-based models are defined from explicit equations with uncertain parameters.

derived from empirical data, and do not explain the process: The time to failure model only accounts for the final effect of deterioration, the failure and summarizes all the uncertainty in a single random variable; The damage accumulation model provides an abstract description of the path to failure (based on theory of equal works). At the other end of the spectrum, Melchers (2003b) motivates the development of physics-based models, mechanistic or chemical, because empirical models based on data are often too simple to represent the impact of environmental factors and to be used for reliability analysis. Such mechanistic models typically describe a quantity linked to the deterioration, such as the size of a crack, which evolves over time, until failure is reached, e.g., the crack size exceeds a critical value d_{cr}. In the following, we will show how this evolution can be modeled with stochastic processes or by physics-based equations with uncertain model parameters, or a combination of both.

In Sections 5.2.2 to 5.2.5, we introduce the four model types mentioned above and discuss their suitability for time-variant reliability analysis and I&M planning.

5.2.2. Time-to-failure model

The effect of the deterioration is represented by a random variable, $T_{F,c}$, the time to failure of the considered deteriorating component. This single random variable condenses all uncertainties (e.g., environmental factors). The accumulated failure event at time t is such that $T_{F,c} \leq t$.

$T_{F,c}$ is associated with a probability distribution, typically derived through laboratory testing or other historical failure records of similar components. Accelerated life testing is also used, where the part is subjected to amplified loads or environmental conditions, thus accelerating the deterioration process (Nelson, 2009). The Weibull distribution is a common choice for fitting failure data of deteriorating parts (Nelson, 2009). However, in the case of a very reliable component or system, there can be little to no data to derive the distribution of $T_{F,c}$.

This model cannot describe intermediate states of deterioration. The likelihood of the type $f_{T_F|Z}(t)$, where Z is an observation of a damage indicator such as crack depth, is typically not available. Consequently, updating the distribution of $T_{F,c}$ is not straightforward.

5.2.3. Palmgren-Miner damage accumulation model

Palmgren (1924), and later Miner (1945), proposed a rule to evaluate the fatigue life of a machine part subject to variable stress amplitude. This rule introduces the concept of damage contribution from a certain number of loading cycles n_1 at a constant stress amplitude S_1. The damage contribution is the ratio between n_1 and the total number of cycles, $N_{F,1}$, at that same amplitude S_1, which lead to the failure of the part. Miner (1945) defines the point of failure as "the [observed] inception of a crack." The Palmgren-Miner rule states that the sum of the damage contribution of n_q cycles at stress levels S_q until failure of the part is equal to 1. Therefore, if failure is reached after n cycles, and denoting $\Delta_q = 1/N_{F,q}$ the damage contribution of the q^{th} at stress level S_q, the total damage contribution after n cycles is

$$\delta_n = \sum_{q}^{n} \Delta_q = 1. \tag{5.6}$$

The relationship between the numbers of cycles to fatigue failure N_F for a constant stress amplitude S is better known as S-N curve. Murakami et al. (2021) retraces the history of these fatigue models. Since the mid-19^{th} century, S-N curves have been defined empirically for various materials (typically metals), geometries and environmental conditions (e.g., Gurney, 1976; Hobbacher, 2015). The basic equation for the S-N curve is an inverse power law, as in Equation (5.7):

$$N_F = C_1 S^{-m_1}, \tag{5.7}$$

and the S-N curve is typically bilinear in logarithmic scale, due to a fatigue (or endurance) limit, defined by a stress level under which loading cycles contribute no additional damage.

There are a few challenges associated with using Equation (5.6) for describing the deterioration process. The parameters of the S-N depend on the environmental conditions (Det Norske

Veritas, 2010). The experimental fatigue data also reveal a scatter, therefore an uncertainty about $N_F(S)$. Probabilistic S-N curves have been derived (e.g., Mansour et al., 1996). Furthermore, Miner (1945) observed in fatigue cycle experiments that the total accumulated damage at failure, computed as the left term of Equation (5.6) using S-N curves, does not exactly add up to 1. For this reason, it is appropriate to model the critical accumulated damage as a random variable, Δ. In the literature, Δ is typically assumed lognormally distributed with moments $(1, 0.3)$ (Faber et al., 2000; JCSS, 2001). A discussion on the uncertainties associated with the damage accumulation model is found in (Straub, 2004). The LSF associated with the accumulated damage at cycle n can be written

$$g_{SN}(n) = \Delta - \delta_n, \tag{5.8}$$

where the failure state at cycle n is given $\{g_{SN}(n) \leq 0\}$.

The Palmgren-Miner's rule relies on one fundamental, but simplifying, assumption: it is interaction-free, meaning that it assumes that the order of the stress cycles is not relevant. However, it is known that the fatigue crack size at a given time influences the shape of the S-N curve, in particular the endurance limit (Murakami et al., 2021). A more accurate model of deterioration would take into consideration the order of the stress cycles for the computation of the accumulated damage δ_n.

Fatemi and Yang (1998) observe that the Palmgren-Miner's model is predominantly used in design and not as a damage prediction model, while physics-based models (see Section 5.2.5 below) are more readily adopted because they are connected to the observed damage, for example a fatigue crack. Nevertheless, the Palmgren-Miner's is useful for estimating the remaining useful life – Morgese et al. (2020) recently applied it to the Genoa viaduct to estimate the remaining fatigue life at the point of its collapse – and for the calibration of fracture mechanics models (see Section 5.2.5), as outlined in Appendix F.2 for the numerical investigations of Chapter 6.

5.2.4. Random process models

In this model, the accumulated state of deterioration ΔD in a certain time interval is given by the sum of random increments. These random increments form an *additive random process*. In discrete time, the accumulated deterioration in Δt time steps is

$$\Delta D = \sum_{\tau=1}^{\Delta t} \Delta D_\tau \tag{5.9}$$

The random process model can implicitly express random temporal environmental effects, such as temperature fluctuations and other environmental shocks (Shafiee et al., 2015).

It is common to assume probabilistic independence of the increments, such that the evolution of the damage forms a Markov chain (Section 5.4.2). When the increments are independently

and identically distributed, the additive process is a Lévy process (Ken-Iti, 1999). The process is non-stationary when the distributions of the increments vary with time.

The quantity ΔD typically models a damage indicator, such as the crack depth, or the corrosion depth (Lin and Yang, 1985; Noortwijk, 2009; Shafiee et al., 2015). The Gamma process model, where the random increments are Gamma distributed with a common scale parameter, is often employed to model corrosion, creep or structural wear (Noortwijk, 2009; Pandey et al., 2009). Typically, the magnitude of the increments is time-dependent to represent the effect of damage acceleration, hence the increments are not identically distributed.

5.2.5. Physics-based models

Physics-based descriptions of deterioration processes are characterized by a relationship between the damage and time with an equation where time appears explicitly, for instance through a differential equation in which fixed but unknown parameters appear.

One example is the Paris-Erdogan's law, which describes the fatigue crack growth. It has been derived from empirical data but is consistent with physics-based models (Paris and Erdogan, 1963):

$$\frac{dD}{dn} = C[\Delta K^M], \tag{5.10}$$

where C and M are empirical material parameters, which are uncertain. ΔK is the range of the stress intensity factor. Paris and Erdogan (1963), Irving and McCartney (1977), Madsen et al. (1987), and Fatemi and Yang (1998) review the various models stemming from this equation, which include in particular the linear fracture mechanics relationship between ΔK and the crack depth $D(n)$ at cycle n. Contrary to the Palmgren-Miner damage accumulation model, this model is used for fatigue life prediction (Fatemi and Yang, 1998).

Another example is Fick's second law of diffusion (Fick, 1855) applied to chloride ingress. The solution of the one-dimensional differential equation gives the chloride concentration at a given time t and depth x, $C_l(x,t)$, as (Barone and Frangopol, 2014):

$$C_l(x,t) = C_{l0}\left[1 - \text{erf}\left(\frac{x}{2\sqrt{Dt}}\right)\right], \tag{5.11}$$

where C_{l0} and D are constant, unknown, parameters over time and space.

Compared to the other models presented thus far, physics-based models present the advantage of describing a physical quantity, which can be measured, thus facilitating the inclusion of inspection information. Furthermore physics-based models provide a higher level of detail as to the sources of uncertainty in the evolution of the damage. Melchers (2003a)'s marine immersion corrosion phenomenological model describes the different phases of corrosion, through a high number of uncertain parameters, which are themselves described by probability distribution with uncertain parameters.

This level of detail has some disadvantages. Learning a high number of uncertain parameters and modeling them as random variables requires a large amount of data. Implementing a high dimensional model can also become a computational burden. Furthermore, once the parameters are fixed, the evolution of the damage is fixed. These models cannot represent time-dependent random events. To remedy this limitation, physics-based models have been combined with random processes (e.g., Madsen et al., 1987; Straub, 2009).

5.3. Models at the system level

Modeling the deterioration effects at the system level has its challenges. Infrastructure systems are typically designed to have a high reliability and usually have a unique configuration. Therefore, it is difficult to obtain relevant failure data in order to characterize a time-to-failure model, as presented in Section 5.2.2. Furthermore, as stated previously, such a model does not enable the inclusion of observations indicating the progress of damage.

Several studies adopt models of deterioration at the system level similar to those presented in Sections 5.2.3 to 5.2.5, such that the system is considered as a single entity, and the state of damage is a quantity that aggregates local damage effects (e.g., Lam and Yeh, 1994; Frangopol et al., 1997; Durango and Madanat, 2002; Nielsen and Sørensen, 2014). In other studies, the system is modeled at the component level and system effects and components' interactions and interdependence are not explicitly considered (Straub, 2004; Moan, 2005; Straub and Faber, 2005; Bocchini et al., 2013).

In this section, we present the model structure proposed by Luque and Straub (2016), which is an extension of the component level model by Straub (2009). It accounts for the components interactions and interdependence and their effect on the system and allows the propagation of information collected at the component level throughout the system and the other components. This model combines deterioration models at the component level, a hierarchical structure to model the correlation in components' deterioration, and a functional relationship between the system and the components.

5.3.1. Effect of components on system

The functional relationship between system performance and components expresses how the capacity R of the system depends on the state of deterioration of its components. Finding this functional relationship is equivalent to identifying the different failure modes of the system and the existing redundancies. In the simplest cases, this functional relationship can be depicted through a system diagram, with a combination of series and parallel sub-systems. In structural systems, a physical model of system failure is typically available (e.g., for a pushover analysis) and can be used to obtain the ultimate capacity of the system for all possible combinations of components deterioration states.

5.3.2. Deterioration at the component level

Several deterioration processes can interact at the component level, for instance corrosion influences fatigue processes (Moan, 2005). Typically, I&M planning problems are designed for a dominant mode of deterioration. For instance, I&M plans in offshore support structures prioritize the identification of fatigue cracks. In bridges, corrosion progression is the main actor in capacity reduction. In this framework, the adopted model describes the dominant mode of deterioration, and the secondary processes can be represented through influencing parameters.

5.3.3. Correlation effects at the component level

The functional relationship described in Section 5.3.1 expresses the components' interactions within the system. However, interdependence also exist at the level of the deterioration processes. In the majority of real multi-component structural systems, components' deterioration processes are correlated due to common manufacturing conditions and similar environmental and load conditions (Straub, 2004). However, there is limited information available, which must be accommodated through engineering judgment (Schneider et al., 2017).

Accounting for this correlation in the system model enables the information propagation mechanism, by which an observation obtained at the component level reduces the uncertainty for that particular component but also for all other components. Schneider et al. (2017) investigates the effect of high to low correlation of the deterioration processes on the reliability of a maintained structural system.

In some cases, the interdependence between component-level deterioration processes is explicitly included through a common parameter, such that the deterioration processes are conditionally independent given this parameter (see the case study in Section 5.4.1.1). In other cases, the components interdependence is given through correlation coefficients between deterioration parameters (see the case study in Section 5.4.1.2). In this last case, it is convenient to represent this correlation by applying the Nataf transformation, which describes the joint distribution of the deterioration parameters with a Gaussian copula in the standard normal space (Der Kiureghian and Liu, 1986). Luque and Straub (2016) adopt this transformation to construct a hierarchical probabilistic structure to represent the joint distribution of correlated time-invariant deterioration parameters at the component level. Considering N invariant, uncertain deterioration parameters V_k, $1 \leq k \leq N$, identically distributed with marginal CDF $F_V(v)$ and equi-correlated with correlation coefficient ρ_V, a standard normal distributed hyperparameter α_V is introduced. Using the Nataf transformation, the V_k are conditionally independent on α_V and their marginal conditional distribution is given by the CDF:

$$F_{V_k|\alpha_V}(v) = \Phi\left(\frac{\Phi^{-1}(F_V(v)) - \sqrt{\rho_Y}\alpha_V}{\sqrt{1-\rho_Y}}\right), \tag{5.12}$$

where ρ_Y is the correlation in standard normal space equivalent to ρ_V in original space.

5.3.4. Environmental effects

The system is subject to an external load S as defined in Section 5.1. This load can be fixed and known or an uncertain quantity representing the impact of the environment on the system. The temporal dependence of the load must also be described. In the case studies presented in the following Section 5.4, it is assumed that the loads at every time step are independent. As we discuss in Section 5.5, temporal dependence of external loads and in general time-dependent correlation effects can greatly affect the computational complexity of the Bayesian analysis.

Aside from the load, other environmental factors (e.g., temperature) can affect the deterioration processes at the component level, the functional relationship between the system and its components, and the evolution of the external load. A hierarchical probabilistic structure can account for these influencing factors by modeling them as random variables and explicitly representing the dependence links in the equivalent Bayesian network.

5.3.5. System inspections

The state of the system is probed through inspections, performed at different points in time. The system probabilistic model should be such that the inspection observation outcomes are explicitly linked to the quantity being measured, and a likelihood function (or NDE model, see Chapter 4) available. The information obtained can in theory relate to any of the variables composing the system model: measure of the state of deterioration of the components (local response), monitoring of displacements (global system response), or monitoring of environmental effects, such as the applied load. In this work, we address the case when the information is collected only at the component level.

5.4. Time-variant reliability analysis: methods and case studies

The evaluation of expected costs of I&M strategies requires many reliability evaluations conditional on inspection results. This calls for methods that can efficiently compute conditional reliabilities and can handle a large number of random variables.

The annual probability of failure required for Equation (3.13) is computed for time step i as:

$$\Pr(F_i|\boldsymbol{Z}_{1:i-1}) - \Pr(F_{i-1}|\boldsymbol{Z}_{1:i-1}) \tag{5.13}$$

We derive from Equation (5.5) the predicted cumulative probability of system failure:

$$\Pr(F_i|\boldsymbol{Z}_{1:i-1}) = \mathbf{E}_{\boldsymbol{X}|\boldsymbol{Z}_{1:i-1}}\Big[\mathbb{1}\big\{\cup_{j\leq i}\{g_j(\boldsymbol{x})<0\}\big\}\Big]. \tag{5.14}$$

The conditional expectation $\mathbf{E}_{\boldsymbol{X}|\boldsymbol{Z}_{1:i-1}}[\cdot]$ is with respect to the conditional joint distribution $p(\boldsymbol{x}|\mathbf{z}_{1:i-1})$.

In this section, we present four main methods for evaluating Equation (5.14), following the review paper by Straub et al. (2020): the closed form solution with traditional numerical

integration; the sampling-based methods; the FORM approximation; and the upper bound approximation using a discretized dynamic Bayesian network (DBN) model. As we will see, the last two methods employ an approximation of Equation (5.14).

We illustrate the methods on two case studies, introduced in Section 5.4.1. The methods are then presented in Sections 5.4.3 to 5.4.6. Lastly, the challenges associated with time-variant reliability analysis and the advantages and limitations of each presented method are summarized in Section 5.5.

5.4.1. Case studies

5.4.1.1. Nuclear feeder piping system

The premises of the case study investigated in Chapter 7 are the following. We consider a nuclear feeder piping system consisting of identical $N = 480$ pipes with initial nominal (fixed) thickness W_0. These pipes are subject to corrosion. The thickness loss at time $t = 0$ is $D_0 = 0$[mm]. The pipes are indexed by $1 \leq k \leq N$. The loss of wall thickness resulting from corrosion of a pipe k at time t_i is denoted by $D_{i,k}$. The failure of pipe k at time t_i is defined by $\{D_{i,k} > d_{max}\}$, where d_{max} is a critical threshold. The piping system is a series system: the system failure at point in time t_i is defined by $F_i^* = \cup_k \{D_{i,k} > d_{max}\} = \{\max_k D_{i,k} > d_{max}\}$.

The loss of thickness in one pipe k due to corrosion is modeled by a discrete-time Gamma process with stationary increments ΔD_τ. One time step corresponds to 1 effective full power year (EFPY). The wall thinning ΔD occurring in a pipe in Δt time steps is written as the sum of i.i.d yearly increments ΔD_τ, according to Equation (5.9). Therefore, ΔD is also Gamma distributed.

The corrosion processes in the pipes are correlated through a common parameter, here the mean μ of the stationary increments. μ is uncertain and modeled as a random variable.

Pipe thickness measurements are obtained during I&M campaigns over the service life. Pipe thickness measurements are assumed to be perfect. The modalities of pipe inspection and repair are detailed in Sections 7.5.2 and 7.5.3.

The time-variant reliability problem consists in evaluating the probability of the accumulated failure event $\cup_{j \leq i} \cup_k \{D_{j,k} > d_{max}\}$, conditional on pipe measurements obtained up to time t_i.

5.4.1.2. The Zayas frame

The structure investigated in Chapter 6 is a steel frame composed of two vertical legs, braced by 13 tubular members; 22 fatigue hotspots located at the welds are identified as per Figure 6.1 and constitute the system components.

The crack growth at a fatigue hotspot is given by Paris-Erdogan's law, as employed by Ditlevsen and Madsen (1996) and Straub (2004):

$$\frac{dD}{dt} = C\left[\pi^{\frac{M}{2}} K^M \Gamma\left(1 + \frac{M}{\lambda}\right)\right] \cdot D(t)^{\frac{M}{2}}, \tag{5.15}$$

Details about the equation derivation and its parameters are found in Section 6.3. The initial, unknown, crack depth is noted D_0. K and M are unknown parameters and are assumed constant during the deterioration process. $ln(C)$ is here expressed as a linear function of M. The solution of Equation (5.15) gives the expression of the crack depth at time t, corresponding to νt fatigue cycles. Failure of a component is defined as the fatigue crack size exceeding a critical depth d_{cr}.

We denote by $D_{i,k}$ the deterioration of component k at time t_i. The states of deterioration of the components are correlated. The initial crack depths of all components $D_{0,k}$ are equi-correlated with factor ρ_{D_0}, as are the stress and material parameters, K_k and M_k with factors ρ_K and ρ_M respectively.

The frame is loaded laterally with a time-varying load, $S_{max,i}$, which represents the maximum load occurring within one time step, or year. We assume that the maximum annual loads are independently and identically distributed. Failure is determined by the system components deterioration states and the response of the damage structure to the applied load. The functional relationship between the system resistance at time t_i, R_i and the state of deterioration of the $N = 22$ components, $D_{i,1}, ..., D_{i,N}$, is determined by a complete pushover analysis. Thereby, it is assumed that a structural member fails if any of its hotspots fails. The ultimate lateral resistance of the frame is computed for all 2^{13} combinations of member failure.

The crack size is measured imperfectly during inspection campaign. The inspection likelihood and the repair assumptions are described in Section 6.4.

The interval system failure event at time step i is defined as

$$F_i^* = R_i\left(\{D_{i,1} \geq d_{cr}\}, ..., \{D_{i,N} \geq d_{cr}\}\right) \leq S_{max,i}. \tag{5.16}$$

The time variant reliability problem is given by Equation (5.14).

5.4.2. Markov chain model

The expected value in Equation (5.14) is with respect to the joint probability distribution of $\boldsymbol{X}$, which includes all the deterioration states at the component level at all time steps. The joint distribution can be decomposed time-wise through the chain rule, but without further assumptions or transformations of the model, the decomposition cannot be simplified further. Using Markov chain models for representing deterioration can enable efficient computation of the component or system time-variant reliability. The Markov chain model has been extensively used in I&M research (e.g., Rosenfield, 1976; Rausand and Høyland, 2004; Bocchini et al., 2013; Faddoul et al., 2013; Zhu et al., 2013).

In general, deterioration processes at the component level are non-Markovian, in that the damaged state is not independent of the past states. The fatigue deterioration process introduced for the Zayas frame in Section 5.4.1.2 falls within this case due to the constant parameters K and M. However, non-Markovian deterioration processes can be transformed into Markovian processes by state-space augmentation (Straub, 2009) (see Figure 2.12). For the Zayas frame example, this means introducing additional random variables $K_{0\leq i\leq n_T,k}$ and $M_{0\leq i\leq n_T,k}$, such that $K_{i+1,k} = K_{i,k} = K_{0,k}$ and $M_{i+1,k} = M_{i,k} = M_{0,k}$.

To represent deteriorating multi-component systems with interdependent components, standard Markov chain models are not suitable. In both case studies, the deterioration states of the components within the systems are correlated. This correlation can be represented in the model through a hyperparameter (see Section 5.3.3), which results in a hierarchical Markov chain. A depiction of this hierarchical model structure for the Zayas frame is given by the hierarchical DBN in Figure 5.4.

5.4.3. Numerical integration of a closed form expression

The integral operation required to compute the expected value in Equation (5.14) can be formulated with a closed form expression, if the dependence structure of $\boldsymbol{X}$ and its conditional probability distribution allows it.

In the nuclear piping system case study, we make use of the self-conjugacy of the Gamma distribution to obtain the filtered probability distribution of the model parameter. In addition, since we assume no measurement error, we show in Section 7.6 that the integrand of Equation (7.18) consists of a product of closed form expressions. The integral can be evaluated using numerical integration. The error on the evaluation of the cumulative probability of failure is therefore small.

If a measurement error is considered in the nuclear piping system example, the product of conditional probabilities of pipe survival in Equation (7.18) is a product of integrals which do not have a closed form. Equation (7.18) is then an integral in high-dimensional space involving complex PDFs, for which adapted integration methods must be considered, such as those presented in the sections that follow.

5.4.4. Sampling-based reliability methods

When a closed form integration is not available, the expected value of Equation (5.14) can be approximated with a sampling-based method. MC samples of $\boldsymbol{X}$ are generated from the conditional joint distribution $p(\boldsymbol{x}|\mathbf{z}_{1:i-1})$ and the filtered cumulative probability of failure is approximated by

$$\Pr(F_i|\boldsymbol{Z}_{1:i-1}) \simeq \frac{1}{n_S}\sum_{q=1}^{n_S} \mathbb{1}\{\cup_{j\leq i}\{g_j(\boldsymbol{X}^{(q)}) < 0\}\}. \tag{5.17}$$

The accuracy of the MC integration depends on the target probability of failure and the number of random samples n_S. In infrastructure, the structure is typically designed (and maintained)

so that there is a low probability of occurrence of failure, which requires a high number of samples n_S. However, the efficiency of this method does not depend on the dimensionality of the problem.

The simple MC integration method of Equation (5.17) is applicable if independent random samples from the conditional joint distribution are available. When this is not the case, other sampling-based methods must be considered. Luque and Straub (2016) reviewed the performance of MCMC methods for the computing the reliability of the Zayas frame. Schneider et al. (2017) applied BUS SUS (described in Section 3.5.4) to the Zayas frame problem, with good computational performance.

5.4.5. FORM approximation

Straub et al. (2020) review an approximation of the probability of union of failure domains using FORM, after Hohenbichler and Rackwitz (1981). The cumulative failure probability defined in Equation (5.14) is approximated as

$$\Pr(F_i) \simeq 1 - \Phi_i(\boldsymbol{\beta}, \boldsymbol{\rho}), \tag{5.18}$$

where $\Phi_i(\boldsymbol{\beta}, \boldsymbol{\rho})$ is the i-dimensional multivariate standard normal CDF evaluated in $\boldsymbol{\beta}$ with correlation matrix $\boldsymbol{\rho}$. $\boldsymbol{\beta}$ consists of the individual FORM reliability indices β_j for each LSF g_j at time step $j \leq i$, g_j. $\boldsymbol{\rho}$ is obtained from the FORM sensitivities $\boldsymbol{\alpha}_j$ associated with the limit states g_j, such that $\rho_{j,l} = \boldsymbol{\alpha}_j^\intercal \boldsymbol{\alpha}_l$.

We demonstrate this approximation for the Zayas frame example. The LSFs g_j are written in function of all the random variables describing deterioration at time step j. For the Zayas frame model, each interval LSFs g_j would involve 70 variables (variables D, K, M for each of the 22 components, 3 correlating variables and one load variable). However, the accuracy of FORM, therefore of the index β_j and sensitivity $\boldsymbol{\alpha}_j$, degrades in high dimensions. To improve the accuracy in this example, we choose to reduce the dimension of each interval reliability problem $g_j(\boldsymbol{X}) < 0$ in Equation (5.14) and rewrite the high-dimension interval LSFs as a function of only two random variables, such that (Wen and Chen, 1987),

$$g_j(p, r) = p - \Pr(F_j^* | R_j = r) < 0, \tag{5.19}$$

where p is an auxiliary variable, uniformly distributed over $[0, 1]$, and $\Pr(F_j^* | R_j = r) = \Pr(S_j > r)$. The transformation in standard normal space is straightforward, since p and R_j are independent. The transformation in standard normal space requires the knowledge of the posterior (smoothed) CDF of R_j, conditional on the inspection results $\boldsymbol{Z}_{1:i-1}$, denoted by $F_{R_j|\boldsymbol{Z}_{1:i-1}}(r)$. Here, we sample from the posterior using BUS-SUS (see Section 5.4.4 above).

The resulting LSF for one time step is plotted in Figure 5.3, where variables p and R_j are represented in standard normal space. The FORM design point, by definition closest to the origin point $(0, 0)$, is also shown. The resulting predicted cumulative probability of failure is compared to other methods in Figure 5.7.

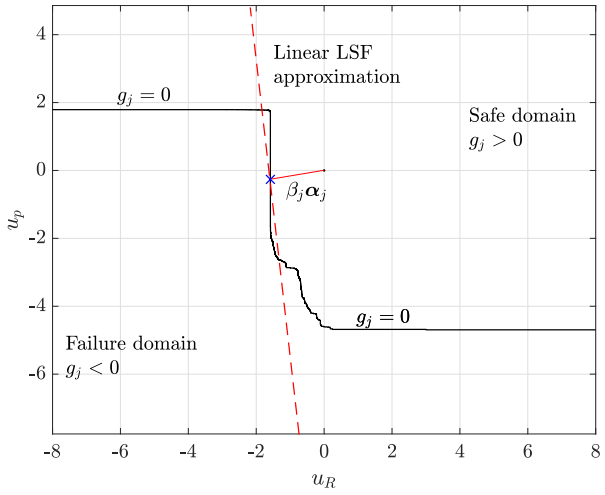

Figure 5.3 Limit state function $g_j(p, r)$ for the Zayas frame associated with an interval failure event F_j^* at a time step j, plotted in standard normal space for the equivalent parameters $u_R = \Phi^{-1}(F_{R_j|\boldsymbol{Z}_{1:i-1}}(r))$ and $u_p = \Phi^{-1}(p)$. The FORM design point is the point on the curve closest to the origin and is indicated with a cross. The linear LSF approximation does not capture the shape of the failure domain, and the associated error can be significant.

This approach has obvious limitations. Firstly, we transform a high-dimensional interval LSF into a 2-dimensional LSF, which requires samples from the posterior joint distribution to obtain the CDF of R_j. Directly implementing the sampling-based methods presented in Section 5.4.4 is probably more efficient. Secondly, the interval LSFs (see Figure 5.3) can be highly nonlinear around the FORM design point, and the evaluation of the interval probability of failure can be associated with a significant error, which ultimately propagates to the evaluation of the cumulative probability of failure. To remediate this non-linearity, it may be interesting to investigate using sampling-based FORM indices, which is a method suggested by Straub et al. (2020) when the FORM solution is not available but samples in the failure domain are. Finally, we note that the evaluation of the multivariate normal in Equation (5.18) is challenging as the dimension increases with the considered time step i. Accurate algorithms for the evaluation of Φ_i have been developed and can be employed in this case (Botev et al., 2013).

5.4.6. Discrete state DBN approach and upper bound approximation

Straub (2009) demonstrates the applicability of a DBN model to the computation of time-variant reliability at the component level for both random variable and stochastic process models, and Nielsen and Sørensen (2018) utilize such a model for the optimization of simple I&M rules. Luque and Straub (2016) extends this DBN model to represent a multi-component system through a hierarchical DBN, which accounts for the components' interdependence and correlations. We present here the different layers of this model, as well as the approximation necessary for the computation of the cumulative probability of system failure.

For the Zayas frame example, this hierarchical DBN model is depicted in Figure 5.4. It is a variant of the DBN model of (Luque and Straub, 2019).

Each component k is represented by its own DBN. As mentioned above in Section 5.4.2, in order

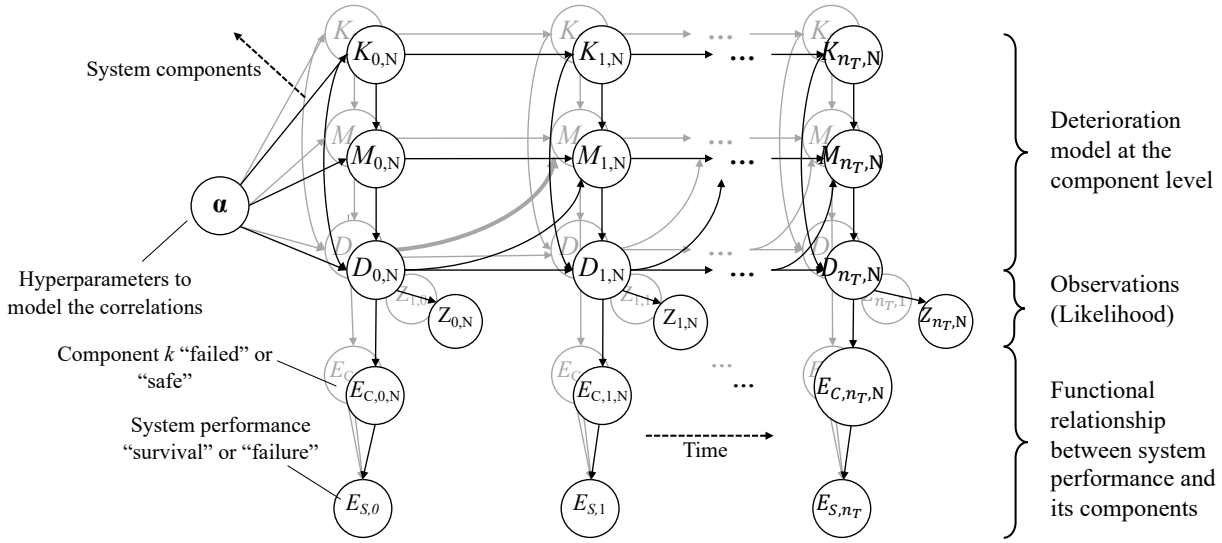

Figure 5.4 DBN for a deteriorating system with N components. The correlations between components are explicitly modeled through the hyperparameter vector $\boldsymbol{\alpha}$. The state of the system is described by nodes $E_{S,i}$, conditionally on the state of each component, $\boldsymbol{E}_{C,i,1:k}$, with a CPT obtained from a function relating components to system state, e.g., a pushover analysis, and from the uncertain annual load $S_{max,i}$. The loads $S_{max,i}$ are not explicitly represented in the network for clarity purposes. Evidence is set on the observation nodes $Z_{i,k}$ when the chosen I&M strategy prescribes it.

to preserve the Markovian assumption, the random variables $K_{0\leq i\leq n_T,k}$ and $M_{0\leq i\leq n_T,k}$ are introduced in the Bayesian network, such that $K_{i+1,k} = K_{i,k} = K_{0,k}$ and $M_{i+1,k} = M_{i,k} = M_{0,k}$. The transition from deterioration state at time step $i-1$ to time step i is obtained from Equation (5.15):

$$D_{i,k} = \left[\left(1 - \frac{M_{i,k}}{2}\right) \cdot C(M_{i,k}) \cdot K^{M_{i,k}} \cdot \Gamma\left(1 + \frac{M_{i,k}}{\lambda}\right) \pi^{M_{i,k}/2} \nu + D_{i-1,k}^{1-M_{i,k}/2}\right]^{(1-M_{i,k}/2)^{-1}} \tag{5.20}$$

The correlation between component deterioration parameters $D_{0,k}$, $M_{0,k}$ and $K_{0,k}$ is reflected through the hyperparameters $\boldsymbol{\alpha}$, following the procedure of (Luque and Straub, 2016). The conditional probability distributions $p(D_{0,k}|\alpha_D)$, $p(M_{0,k}|\alpha_M)$ and $p(K_{0,k}|\alpha_K)$ are obtained for each parameter by Equation (5.12). The component-level DBNs are therefore connected by the hyperparameters $\boldsymbol{\alpha}$ and the common system performance nodes, which here take states "survival" or "failure". Observations of deterioration state $D_{k,i}$ of component $0 \leq k \leq N$ from inspections or monitoring are represented by $Z_{k,i}$ and the associated likelihood function is given by Equations (6.3) and (6.4).

Therefore, the hierarchical DBN can be broken down component-wise; time-wise; or by distinguishing the deterioration model, the observation likelihood, and finally the function relating the system performance conditional on the state of its components. With this network structure, the information from observations $Z_{k,i}$ of deterioration state $D_{k,i}$ of component $0 \leq k \leq N$ can be propagated from the component level to the system level, and the impact on the system reliability can be evaluated. Furthermore, in the proposed model the states of all continuous random variables, i.e., $D_{i,k}$, $M_{i,k}$, $K_{i,k}$, $Z_{i,k}$, α_D, α_M,α_K, are discretized and the required conditional probability tables (CPT) are computed according to Straub

(2009). As with the discrete BN (see Section 2.2.2.3), Bayesian inference consists in performing operations with the CPT matrices, which are pre-computed. Exact inference algorithms are implemented to evaluate the probability distributions of all random variables conditional on the observations. For details on the modeling and computation in this hierarchical DBN model we refer to (Luque and Straub, 2016).

To improve the computational performance, the nodes $E_{S,i}$ represent the state of the system at time step i, if the system does not have to opportunity to fail earlier, thus, $\{E_{S,i} = \text{'failure'}\}$ is the interval failure event F_i^* introduced in Section 5.1. This is highlighted by the fact that no arrows link temporally the nodes $E_{S,i}$. The evaluation of the hierarchical DBN results in the conditional probability of F_i^* given the observation from all components.

This model does not include the accumulated failure event F_i, which would be done by including the temporal links mentioned above. Doing so would significantly increase the computational complexity of the inference operation. Instead, we use the bounds on the probability of the accumulated failure event, derived from Equation (5.4) by Straub et al. (2020), as

$$\max_{1\leq j\leq i} \Pr(F_j^*|\boldsymbol{w},\boldsymbol{Z}) \leq \Pr(F_i|\boldsymbol{w},\boldsymbol{Z}) \leq 1 - \prod_{1\leq j\leq i} 1 - \Pr(F_j^*|\boldsymbol{w},\boldsymbol{Z}) \tag{5.21}$$

The lower bound is trivial. The upper bound is obtained by observing that the annual loads S_j are mutually independent. The cumulative probability of failure is closer to one or the other bound depending on whether the reliability is dominated by the uncertainty in the system capacity R_j or by the uncertainty in the load S_j. For the Zayas frame example, we approximate the cumulative probability of system failure by the upper bound of Equation (5.21). This approximation has shown to be appropriate for this reliability problem (Straub et al., 2020). Further investigations are required to evaluate the goodness of this approximation when the annual load $S_{max,i}$ is measured and included in the inference operation.

The interval probabilities of failure $(\Pr(F_i^*|\boldsymbol{w},\boldsymbol{Z}))_{0\leq i\leq T}$ are computed with Bayesian inference in the DBN, involving Bayesian filtering, prediction and smoothing algorithms (Askar and Derin, 1981, 1983; Straub, 2009; Särkkä, 2013; Luque and Straub, 2016). The computational cost of this algorithm increases only linearly with the number of components, which makes it suitable for large systems (Luque and Straub, 2016). Figure 5.5 details the computational graph of the algorithm implemented to perform exact Bayesian inference in the DBN at the component level and propagate the information back to the hyperparameters, to finally compute the cumulative probability of failure with the upper bound approximation. In particular, it shows how intermediate results are stored to improve the computational efficiency of the algorithm. The exact inference algorithm is detailed in Appendix D.

Figure 5.6a depicts an example of the evolution of the computed probabilities for the Zayas frame described in Chapter 6. The corresponding evolution of the probability of failure of one hotspot is plotted in Figure 5.6b, for the same strategy $\mathcal{S}_{\boldsymbol{w}}$ and sample observation history.

It should be noted that the discretization scheme influences the accuracy of these computations, notably when performing Bayesian smoothing. The associated error is investigated in (Zhu

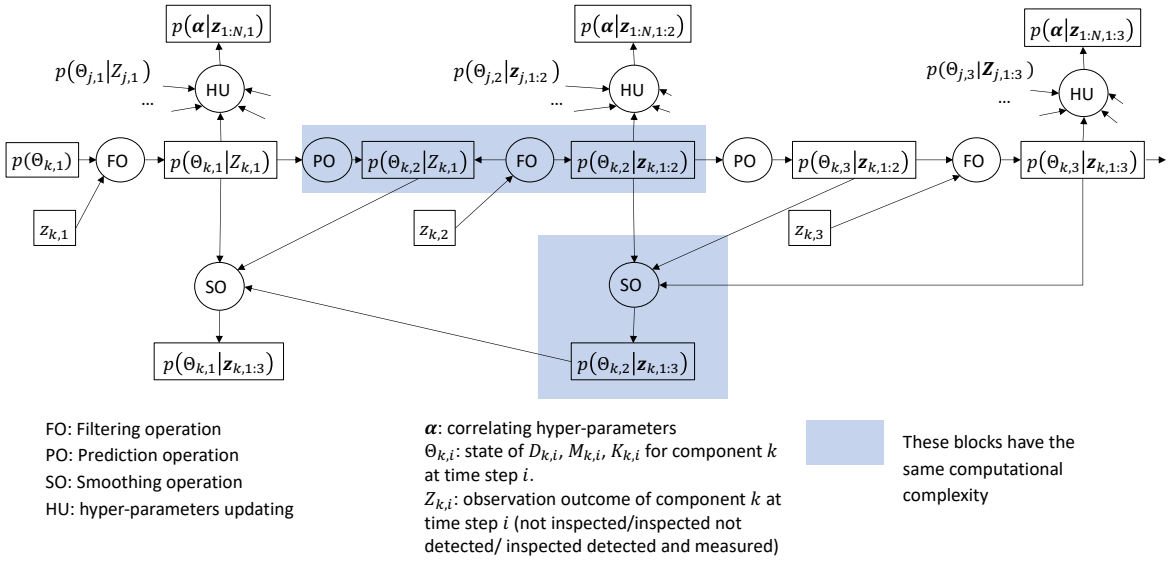

Figure 5.5 Computational graph at the component level – including updating of the hyperparameters (see Appendix D).

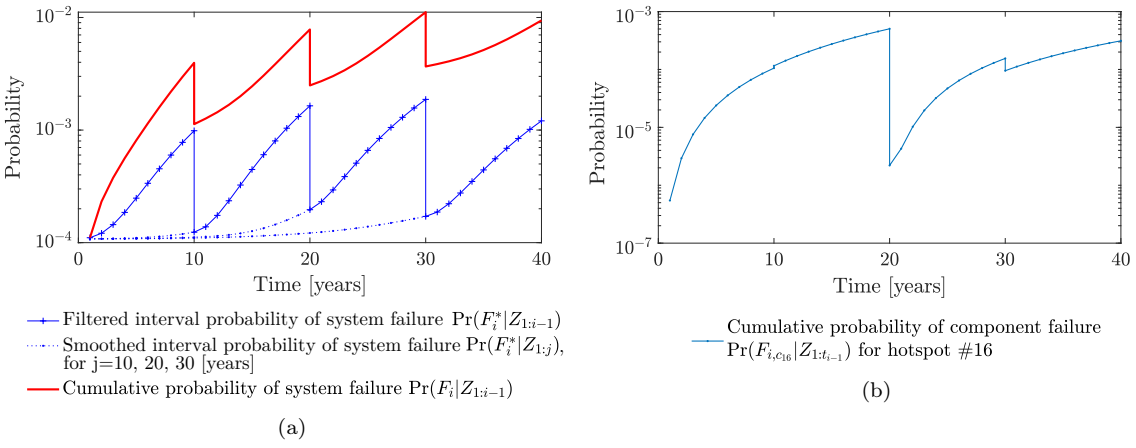

Figure 5.6 (a) Evolution of the interval probability and cumulative probability of system failure of the Zayas frame (see Chapter 6). The sample observation history follows heuristic strategy $\mathcal{S}_{\boldsymbol{w}}$, with $\boldsymbol{w} = \{\Delta T = 10,\ p_{th} = 1 \cdot 10^{-2},\ n_I = 4,\ \eta = 1\}$. The discontinuities indicate that an inspection is performed and the reliability is updated. The dotted blue lines represent the smoothed probabilities $\Pr(F_j^*|\boldsymbol{Z}_{1:t_i})$, for $j \leq i$, updated with the current system information; (b) corresponding evolution of the probability of failure for hotspot ♯16. The discontinuities at years {10, 30} are due to inspections on other components in the system. Hotspot ♯16 is inspected at year 20 and is never repaired in this simulation.

and Collette, 2015) and is mainly due to the rough discretization in the failure domain of the component. However, we have found that it does not significantly impact the evaluation of $\Pr(F_i^*|\boldsymbol{w}, \boldsymbol{Z})$. We illustrate the effect of the discretization scheme on a simple example in Appendix E.

5.5. Summary and limitations

The methodology presented in Chapter 3 requires a method that enables fast and efficient Bayesian analysis and reliability updating at the structural system level. In this chapter,

we described the layers of a multi-component deteriorating system model, which explicitly models deterioration at each component and includes the dependencies and interactions among multiple components within the structural system and their effect on the system reliability. This model structure enables the propagation of the information collected at individual component inspections to the rest of the system. However, setting up the probabilistic model of the structure and the deterioration is non-trivial in many cases (Papakonstantinou and Shinozuka, 2014). This first challenge is shared by all approaches that aim at using physics-based models for predictive maintenance.

We reviewed four different methods to evaluate the time-variant reliability, expressed in the form of an expected value. The first method, numerical integration of a closed form expression, can be utilized to compute the reliability of the system if the associated probabilistic model of the system possesses specific properties, in the assumed probability distributions (e.g., prior conjugacy) or in the dependence structure. However, in general, these assumptions are not met. The three remaining methods for the computation for the computation of the cumulative probability of system failure in the Zayas frame example are compared in Figure 5.7.

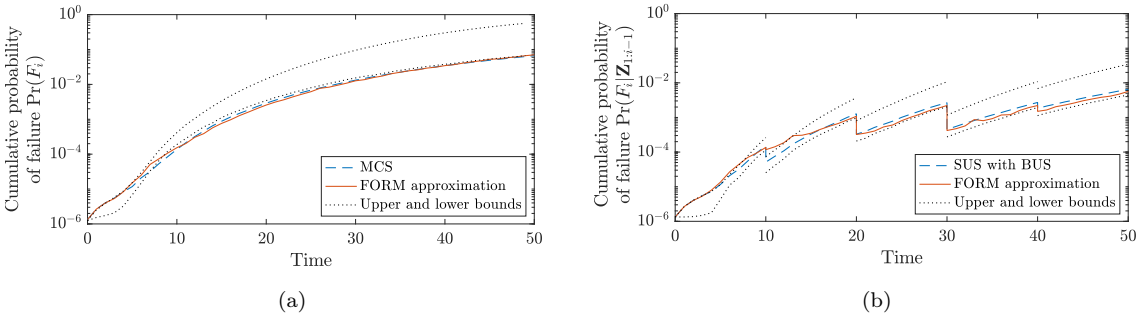

Figure 5.7 Evaluation of the filtered cumulative probability of failure for the Zayas frame example with three different methods, a): with no observations nor maintenance actions and b): integrating component inspection outcomes. The parameters of the model are here taken from (Schneider et al., 2017; Straub et al., 2020). The sampling-based integration methods with MCS and SUS with BUS are most accurate as long as a high number of samples are generated from the posterior. SUS with BUS is in particular computationally intensive. The FORM approximation matches closely the sampling-based approximation, but the obtained curve is not smooth and introduces a significant error in the evaluation of the annual risk. Finally, the lower and upper bounds from Equation (5.21) are computed with the hierarchical DBN model.

All three methods require the functional relationship between the system and its components (see Section 5.3.1) to be fully defined. For the Zayas frame example, the pushover analysis determining the ultimate lateral capacity of the frame for each combination of component state was performed with the Ultimate Strength for Offshore Structures (USFOS) software and took up to one hour per combination. Work-around strategies for a high number of components are discussed in (Luque and Straub, 2016).

The FORM approximation of Equation (5.18) requires that the predicted, filtered and smoothed posterior distributions of the components' states are available at every time step. Samples from these distributions can be obtained through the approaches mentioned in Section 5.4.4. Furthermore, as the performance of FORM degrades when applied to high dimensional LSFs, a computationally intensive dimension reduction had to be implemented, thus canceling its primary advantage over BUS-SUS and the DBN approach. Lastly, we can see in Figure 5.7

that the resulting FORM approximation closely matches that of BUS-SUS, but the resulting curve is not smooth and may introduce inconsistencies in the evaluation of the annual risk. Therefore, the FORM approximation for the computation of the accumulated failure event is not better than the sampling-based approaches, neither in terms of computational complexity nor in terms of accuracy.

In contrast, sampling-based reliability methods are not sensitive to the number of random variables in the deterioration model. However, they rely on the generation of many samples. The computational cost of MCMC algorithms increases with the number of inspection outcomes (Luque and Straub, 2016; Schneider et al., 2017), with the hierarchical DBN inference achieving a similar performance for a fraction of the computing time (Luque and Straub, 2016). Furthermore, BUS with SUS may fail to correctly identify multiple failure domains (Betz, 2017), thus introducing a significant error in the assessment of the cumulative probability of system failure. Ultimately, these limitations may rule out sampling-based methods for the efficient stochastic optimization of heuristic strategies.

Both the DBN model and the BUS-SUS method are flexible with respect to the choice of a-priori probability distributions and transition probabilities, but the performance of the DBN model is not affected by the shape of limit state functions. However, there are still challenges to the application of the DBN framework in practice. Firstly, the translation of the model to a DBN requires careful calibration of the DBN parameters for discretization scheme, including the number of discrete states per variable, the probable domain and a suitable transformation such that the relation between the transformed variable and the state of damage is approximately linear (Straub, 2009). This might be addressed by writing corresponding software tools that automatize this task.

Secondly, the DBN framework has computational limitations with respect to the number of parameters considered in the deterioration model. All CPTs must be established in order to perform exact Bayesian inference, and, ideally, stored in arrays to avoid repeating computations. Besides the fact that the pre-computation of the CPTs can be very demanding, their storage can pose significant memory problems, as the number of elements of one CPT is equal to the product of the number of states of each random variable. Straub (2009) models fatigue deterioration in a hotspot by Equation (5.15), but assumes a correlation of 0.9 between variables C and M. Using this modeling assumption in the Zayas frame example would have entailed the introduction of an additional time-invariant, discretized random variable for C and increasing the size of the CPT for the transition between $D_{i,k}$ and $D_{i+1,k}$. As the storage of this CPT exceeded MATLAB memory capacity, the assumption of full correlation between C and M was retained (see Table 7.1). In the numerical investigations, the time-variant reliability analysis of the Zayas frame for a single I&M history with these assumptions already required 17GB of random-access memory (RAM). However, the DBN algorithm can be sped up and the RAM optimized using the sparsity of the CPTs. Furthermore, the computational cost of the algorithm increases only linearly with the number of components, which makes it suitable for large systems.

Finally, the efficiency of the DBN inference algorithm relies in particular on the conditional independence of the component deterioration processes, given a few hyperparameters. As an example, the deterioration model in the Zayas frame does not enable to explicitly consider time-dependent correlating effects between the components. Here, the evolution of the damage is fixed once the time-invariant deterioration parameters K and M are fixed. If one were to model the fatigue stress-range parameter K as a time-variant parameter, correlated between components through a dynamic environmental effect (e.g., Zhu et al., 2013), the number of conditioning variables to consider each component independently would increase significantly and the algorithm would need to be redesigned in order to handle similar RAM problems as those mentioned previously.

Despite these limitations, the DBN framework enables the flexible modeling of large, multi-component systems. The model can be updated with an increasing amount of observation in a robust manner, without loss of computational performance. The presented DBN approach provides a bound approximation of the queried probability, but its ease of implementation and fast inference algorithm make it suitable to implement within the strategy optimization approach introduced in Chapter 3. Recently, the performance of this algorithm has been exploited by Mendoza et al. (2022) for a parametric study on the influence of fatigue design and system redundancy on the optimal I&M strategy, where the DBN framework is utilized to evaluate the reliability of systems in combination with a generic system representation through equivalent Daniels systems (Straub and Der Kiureghian, 2011).

Part II.

Heuristic methods for infrastructure planning: Applications

Chapter 6

Adaptive I&M planning of a steel frame subject to fatigue

This chapter originates from Bismut, E. and Straub, D. (2021). "Optimal adaptive inspection and maintenance planning for deteriorating structural systems". In: *Reliability Engineering & System Safety* 215, p. 107891.

6.1. Introduction

There are no standard procedures for I&M planning of structures subject to fatigue deterioration. Time-based maintenance is in general not appropriate for this type of deterioration (Jonge et al., 2017). Condition-based maintenance is typically implemented by fixing an inspection interval between inspection campaigns, and inspecting all or selected components, following unknown heuristics.

In this chapter, we apply the heuristic planning methodology of Chapter 3 with its adaptive feature, to the I&M planning of a steel structure representing a jacket support structure of an offshore wind turbine, which is typically subject to fatigue deterioration.

We adopt the Zayas frame model (Zayas, 1980), often used for benchmark studies (e.g., Chen and Sohal, 1988; Luque and Straub, 2016; Schneider et al., 2017; Schneider, 2019), succinctly introduced previously in Section 5.4.1. This model includes correlation among components' deterioration processes. The time-variant reliability of the structural system is evaluated with a DBN model, the details of which are given in previous Section 5.4.6.

We investigate heuristics that combine component characteristics which are closely linked to the VoI. We define a Prioritization Index, PI_k, and study its effect for different combinations of component structural importance, uncertainty and correlation. This Prioritization Index combines component importance within the system and component probability of failure and acts as a ranking index for the heuristic prioritization of components for inspection. A heuristic parameter η weighs the two effects, according to Equation (3.8) and is optimized, along with the other parameters determining the times and location of inspection and repair.

Finally, we improve the strategy obtained through adaptive planning and quantify the resulting expected gain.

6.2. Structural model

The Zayas frame is composed of two vertical legs, braced by 13 tubular members; 22 fatigue hotspots located at the welds are identified as per Figure 6.1 and constitute the model components. The states of deterioration of the components are correlated (see Section 6.3). The frame is loaded laterally with a time-varying load, $S_{max,i}$, which represents the maximum load occurring within one time step, or year. We assume that the maximum annual loads are independently distributed, following a lognormal distribution, with mean 50kN and coefficient of variation 0.53. Failure is determined by the system components deterioration states and the response of the damage structure to the applied load. The pushover analysis for the frame is from Schneider et al. (2017). The ultimate resistance of the undamaged frame is 282kN.

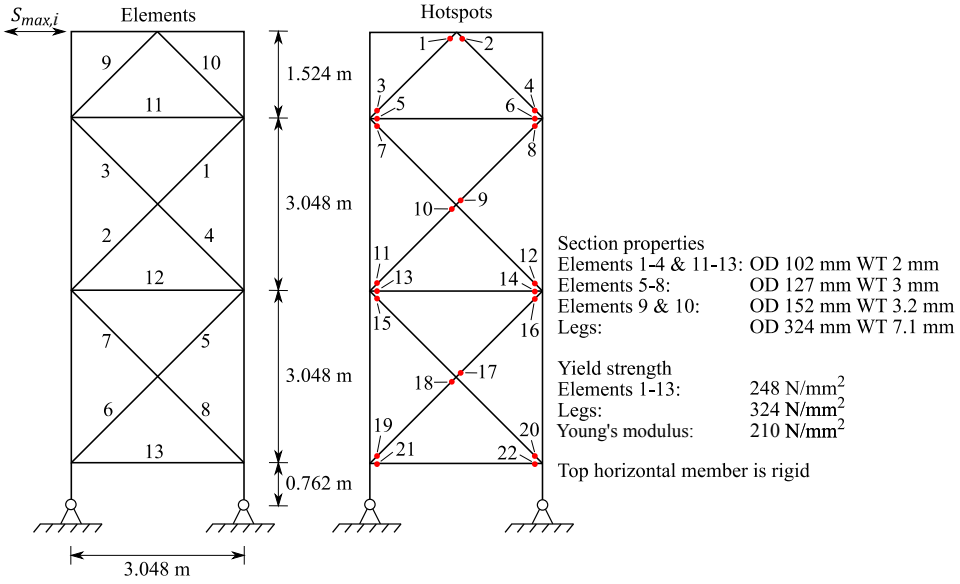

Figure 6.1 Zayas frame. The red dots indicate the locations of 22 fatigue hotspots. The frame is loaded laterally with yearly amplitude $S_{max,i}$. After Schneider et al. (2017)

6.3. Deterioration model

For each component k, $D_{i,k}$ indicates the crack depth at time t_i. The transition from $D_{i,k}$ to $D_{i+1,k}$ is obtained from the fatigue crack growth of Equation (5.15), which gives

$$D_{i+1,k} = \left[\left(1 - \frac{M}{2} \right) C \Delta S_e^M \pi^{\frac{M}{2}} \cdot \nu + D_{i,k}^{1-M/2} \right]^{(1-M/2)^{-1}}, \tag{6.1}$$

where C and M are empirical material parameters and ν is the number of fatigue cycles within one time step. They are correlated with a correlation coefficient close to -1, hence $ln(C)$ is here expressed as a linear function of M (Straub, 2004). The initial crack depth is noted $D_{k,0}$ and failure of a component is defined as the fatigue crack size exceeding a critical depth d_{cr}.

The fatigue stress range ΔS is described by a Weibull distribution with scale and shape parameters K and λ. The distribution of the equivalent fatigue stress range $\Delta S_e = (\mathbf{E}[\Delta S^M])^{\frac{1}{M}}$

is defined by Equation (6.2) (Straub, 2004), as

$$\Delta S_e = K \cdot \Gamma\left(1 + \frac{M}{\lambda}\right)^{\frac{1}{M}}. \tag{6.2}$$

K and M are unknown parameters and are assumed constant during the deterioration process, i.e., for all time steps i, $K_{i,k} = K$ and $M_{i,k} = M$. The distribution of $K_{0,k}$ for each component k is lognormal, and the mean values are calibrated to a chosen fatigue design factor (FDF). The FDFs represent the ratio between the fatigue life of a component and the service life of the structure. The calibration procedure is explained in Appendix F.2. Table F.2 lists the components, their FDFs, and the corresponding means of $K_{0,k}$.

Additionally, the initial crack depths of all components $D_{0,k}$ are equi-correlated with factor ρ_{D_0}, as are the stress and material parameters, K_k and M_k with factors ρ_K and ρ_M respectively. The correlation is reflected in the computation of the probability tables conditional on the hyperparameters $\boldsymbol{\alpha}$ of the DBN, following the procedure of Luque and Straub (2016).

The model parameters and correlations are summarized in Appendix F.1.

6.4. Inspection and repair model

The observation outcome $Z_{i,k}$ is a measure of the crack $D_{i,k}$, and is thus a random variable defined conditionally on $D_{i,k}$. For the considered NDE method, $Z_{i,k}$ can take the value $\{Z_{i,k} = 0\}$, indicating "no crack detected", or values larger than 0, reflecting a measured crack size. The model of NDE quality (see Chapter 4) is defined in two steps. First, the PoD $\Pr(Z_{i,k} > 0 | D_{i,k} = d)$ is:

$$\text{PoD}(d) = 1 - \exp\left(-\frac{d}{\xi}\right) \tag{6.3}$$

Then, in case of detection, the measurement $Z_{i,k}$ has the truncated normal distribution with mean $D_{i,k}$ and standard error σ_ϵ, truncated in 0. The resulting hybrid conditional distribution is defined in Equation (6.4), where $\varphi(.)$ is the standard normal PDF, and $\Phi(.)$ is the standard normal CDF:

$$\begin{cases} \Pr(Z_{i,k} = 0 | D_{i,k} = d) = 1 - \text{PoD}(d) \\ f_{Z_{i,k}|D_{i,k}=d}(Z_{i,k} = z) = \text{PoD}(d) \cdot \frac{1}{1-\Phi\left(\frac{-d}{\sigma_\epsilon}\right)} \cdot \varphi\left(\frac{z-d}{\sigma_\epsilon}\right), \quad \text{for } z > 0. \end{cases} \tag{6.4}$$

We note that this model does not account for the possibility of a false alarm, i.e., the detection of a crack when no crack is present.

In this application, the repair rule is fixed and not optimized. If the damage exceeds a threshold D_{rep}, the component is repaired immediately and completely. This corresponds to restoring it to its initial state, i.e., the probability distribution of the damage after a repair is the one of $D_{0,k}$. The repaired state is assumed to be uncorrelated with the initial state.

Following from DBN model structure described in Section 5.4.6 and in Figure 5.4, the inspection outcome of one component affects the posterior distribution of the crack size of all other components, whether the inspected component is repaired.

6.5. Costs of I&M actions

I&M actions incur mobilization costs, repair costs, costs for material supply, workmanship, inspection techniques, and sometimes downtime. Here, all components are attributed the same cost of inspection and repair, which are constant over time. This choice simplifies the problem specification; alternative cost models do not affect the computation efforts or the accuracy of the method.

The following costs are considered:

- c_C: cost of launching an inspection campaign. It includes the cost of transporting inspection operators to site, and potentially the cost of impairing the operation of the system.
- c_I: cost of inspection per component. It accounts for the time spent to inspect one component during an inspection campaign.
- c_R: cost of repairing one component. It also includes the associated downtime.
- c_F: cost incurred if the structure fails, including full replacement costs and life-cycle costs of the new structure.

All costs are discounted to their present value by the discount factor $\gamma(t) = \frac{1}{(1+r)^t}$, where r is the annually compounded discount rate. The parameters of the cost function and discount factor are provided in Table 6.1.

Table 6.1 Cost parameters

Parameter	c_C	c_I	c_R	c_F	r
Value	1	0.1	0.3	$3 \cdot 10^3$	0.02

6.6. Heuristic parameter choice

In this study, the components are assumed equi-correlated, with equal inspection quality and cost. The question "where" to inspect is therefore divided into two sub-questions, "how many" and "which" components, that result into two different heuristic parameters, n_I which describes a minimum number of components to be inspected, and η which ranks the components in order of priority for inspection, according to the Prioritization Index defined in Equation (3.8).

Figure 6.2 compares two sample inspection histories of the Zayas frame, for two values of η. As expected, more hotspots are inspected during the service life when a lower value for η is fixed. For a higher value of η the inspected hotspots are principally those with the higher SEI values. The effect of η on the Prioritization Index and on the efficiency of the heuristic strategy cannot be assessed without further investigations. For this reason, η is included as a heuristic parameter to be optimized.

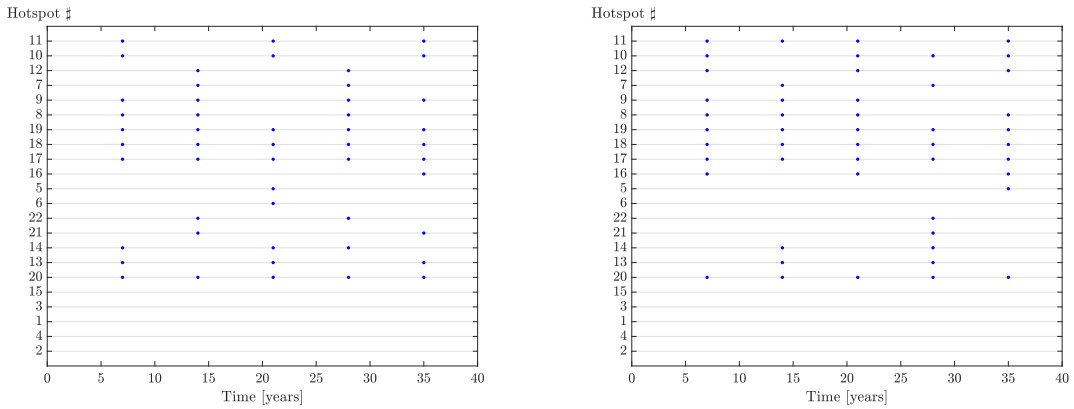

(a) $\eta = 0.84$ (b) $\eta = 2.96$

Figure 6.2 History of hotspots inspected (marked with a blue dot) for a sample deterioration history, following the strategies defined by $\Delta T = 7$[years], $n_I = 10$ and $p_{th} = 5.2 \cdot 10^{-3}$, and a lower (a) and higher (b) prioritization parameter η. The hotspots numbers on the y-axis are sorted according to their calculated SEI.

Therefore, the investigated heuristic includes the following parameters $\boldsymbol{w} = \{\Delta T, p_{th}, n_I, \eta\}$:

(a) Inspection campaigns are carried out at fixed inspection intervals $\Delta T \in \{1, 2, \dots 40\}$ [years].

(b) Additionally, when the annual probability of failure of the system exceeds the probability threshold $p_{th} \in [0, 1]$, an inspection campaign is carried out.

(c) The number of hotspots to be inspected at every inspection campaign is $n_I \in \{1, 2, \dots, 22\}$.

(d) The hotspots are prioritized for inspection following Section 3.4.3 with parameter $\eta \geq 0$.

The repair threshold $D_{rep} \geq 0$ can also be included as a heuristic parameter. For the purpose of this study, a component is repaired if the deterioration exceeds a threshold value $D_{rep} = 0$ at the inspection. This implies that every identified defect is repaired. The results documented in Section 6.8 show that the expected repair costs are low even with this choice, which indicates that optimizing D_{rep} would not significantly affect the expected life-cycle cost.

6.7. Optimization set up and computation

Time-variant analysis using the hierarchical DBN model presented in Section 5.4.6 and illustrated in Figure 5.4 is implemented to approximate the cumulative probability of failure $\Pr(F_i|\boldsymbol{w}, \boldsymbol{Z})$. The annual probabilities of failure are then evaluated with Equation (5.13).

The CE sampling algorithm is run with MATLAB on a 2.6GHz computer with 24 quad-core processors. The algorithm is optimized for the computation of the conditional probability of system failure. One history life-cycle cost is computed in about 20 CPU minutes, but these computations can be run in parallel. In this study, the main obstacle to speeding-up computations is the required 17GB of RAM per simulated history, which limits the number of parallel threads.

For the CE optimization method of Algorithm 3, lognormal sampling distributions are employed for the heuristic parameters p_{th} and η. For the discrete parameters ΔT and n_I, a truncated normal distribution is selected, so that the sampled values are within the acceptable bounds; the sampled values are then rounded to the nearest integer. In this numerical application, all sampling distributions are kept uncorrelated, and the heuristic parameters are optimized one after the other in a recursive manner. This was mainly for ease of graphical representation of the results. Correlating the distributions might lead to more efficient sampling during the optimization and faster convergence towards the optimal parameter values.

We fix $n_{MC} = 1$. About 1600 samples of total life-cycle costs for different strategies are drawn as per Equation (3.11). To obtain a surrogate of the total life-cycle costs, a GPR is performed on the logarithm of the sample costs. This guarantees that the surrogate function stays positive in the original space. The GPR is implemented with the MATLAB 2018 function `fitrgp` and a squared-exponential kernel. The minimum of this surrogate cost function is calculated with the MATLAB 2018 function `surrogateopt`.

GPR can also be performed on all four cost components separately: inspection campaign, component inspection, repair and failure risk. However, it was found that the total cost predictions obtained by summing up the four resulting Gaussian processes are not as stable as the predictions obtained by the GPR on the total life-cycle cost and are therefore not used to find the optimal heuristic parameter values. Figure 6.3 compares the prediction of the expected total life-cycle cost with the two methods, for selected strategies.

We consider one adaptation of the I&M plan after the first inspection campaign. For the adaptation, the deterioration model is updated with the inspection outcomes at the time prescribed by the initial strategy. Then, 1600 deterioration histories are simulated from the posterior distributions, using BUS SUS (Straub and Papaioannou, 2015). Based on these samples, total life-cycle costs are calculated for different strategies, and the strategy optimization is performed as outlined in Section 3.3.

6.8. Results

6.8.1. Optimal heuristic strategy at time $t = 0$

First, we investigate how the expected cost varies in function of the different heuristic parameters. Figure 6.3 shows the total life-cycle cost in function of n_I and ΔT for sample strategies from the CE method. The GPR surrogate estimate is also shown.

As expected, the total life-cycle risk of failure decreases with increasing number n_I of hotspots inspected at every inspection campaign. Similarly, strategies with small inspection intervals ΔT are costly because of the frequency of the inspections; in contrast, strategies with large ΔT suffer from a larger uncertainty and thus an increased risk of failure. Samples drawn in a similar way for varying p_{th} and η show a less clear trend, as can be seen in Figure 6.4.

The minimum of the (continuous) surrogate cost function is achieved for the values $\{\Delta T = 7.0,\ p_{th} = 1.9 \cdot 10^{-3},\ n_I = 9.4,\ \eta = 1.3\}$. The values for ΔT and n_I are rounded to the nearest integer.

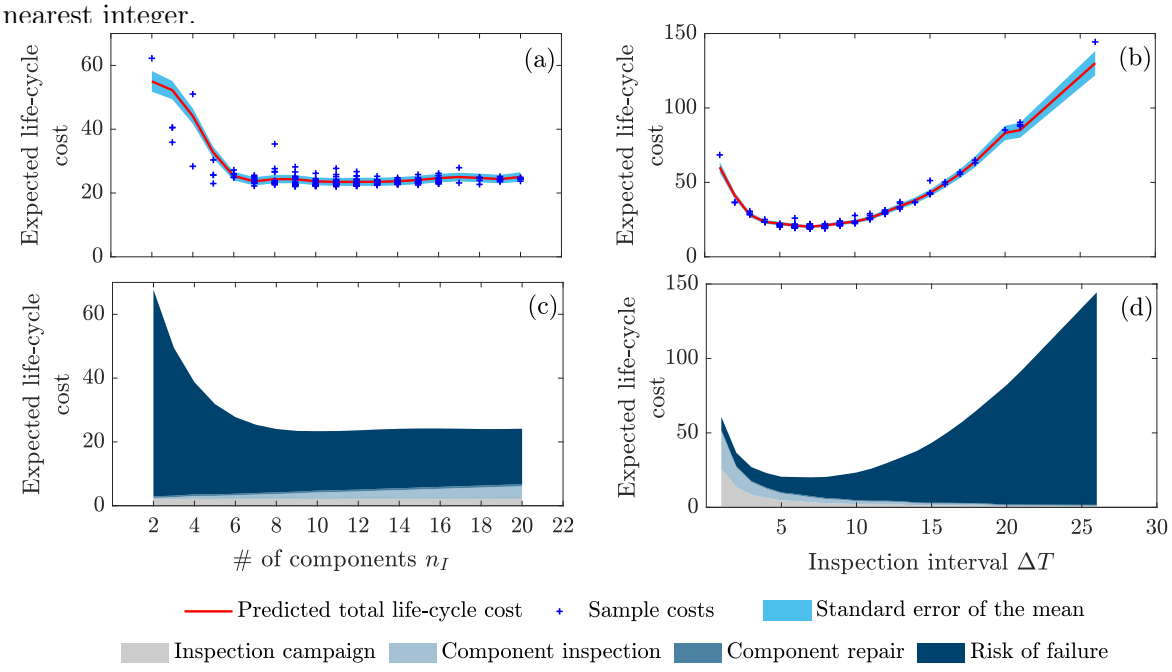

Figure 6.3 Sample total life-cycle cost with corresponding estimated mean value and standard deviation of the prediction (a-b). The prediction for the cost breakdown is shown in (c-d). There is a slight difference in the prediction of the total cost between (a-b) and (c-d), which comes from the GPR. (a) and (c): varying n_I with fixed values $\{\Delta T = 10,\ p_{th} = 1 \cdot 10^{-2},\ \eta = 1\}$; (b) and (d): varying ΔT with fixed values $\{p_{th} = 1 \cdot 10^{-2},\ n_I = 10,\ \eta = 1\}$.

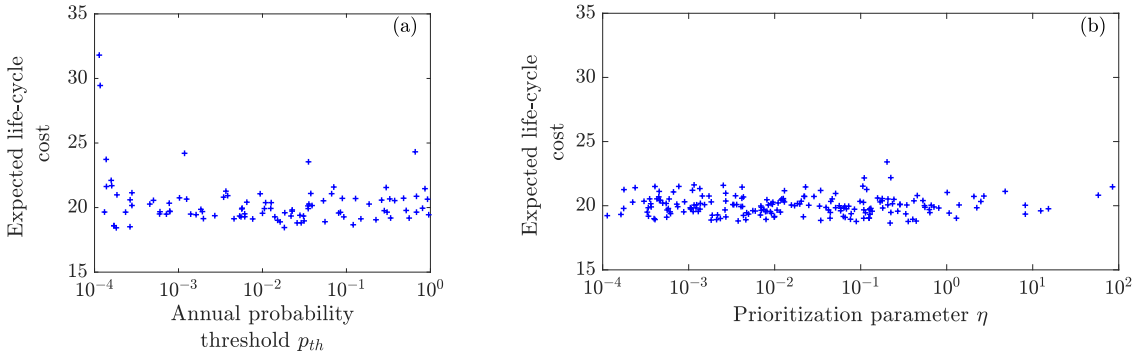

Figure 6.4 Sample total life-cycle costs, for varying probability threshold p_{th} and prioritization parameter η. The risk of failure decreases with the probability threshold. However, for some values of p_{th} (here lower than 10^{-4}), the inspection and repair costs needed to satisfy the threshold requirement increase strongly. Probability thresholds that are too small to meet are assigned an arbitrary cost of 1000. (a): $\Delta T = 7$, $n_I = 9$, $\eta = 1.3$ (b): $\Delta T = 7$, $n_I = 10$, $p_{th} = 5.2 \cdot 10^{-3}$.

Figure 6.5a depicts the contours of the GPR surrogate function, as a function of p_{th} and η, for fixed $\Delta T = 7$[years] and $n_I = 9$. Within a large domain of parameters p_{th} and η, the surrogate cost varies between 19 and 21. Hence the total life-cycle cost is not sensitive to p_{th} and η when the values $\Delta T = 7$[years] and $n_I = 9$ are set. In contrast, Figure 6.5b shows that the value of the inspection interval ΔT has a larger impact on the cost-efficiency of the strategy than the number of inspected components n_I.

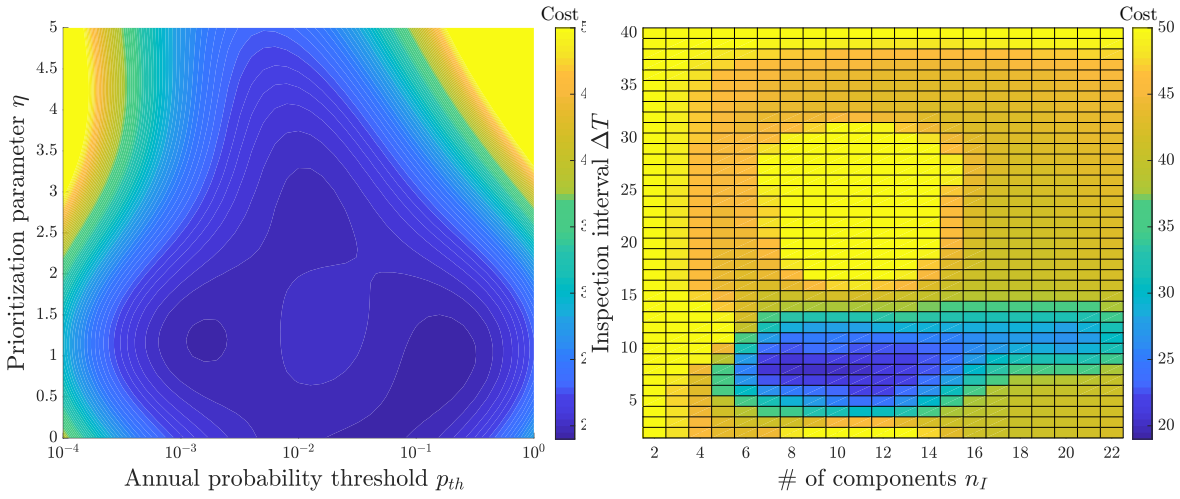

Figure 6.5 (a): Surrogate cost function around the optimum for the prior optimization at $t = 0$ for varying heuristic parameters p_{th} (logarithmic scale) and η, with $\Delta T = 7$[years] and $n_I = 9$. (b): Surrogate cost function around the optimum for the prior optimization at $t = 0$ for varying (integer) heuristic parameters n_I and ΔT, with $p_{th} = 2 \cdot 10^{-2}$ and $\eta = 1.3$.

The GPR only provides an approximation of the underlying function; it reports a standard error of 5% on the estimated expected life-cycle cost at the point minimizing the surrogate. To account for this error, we computed 200 additional MC samples of deterioration histories and inspection outcomes at the point minimizing the surrogate, which yields an expected total life-cycle cost of 21.4. We also evaluated 200 MC samples for a second strategy, increasing the value of p_{th} by an order of magnitude, i.e. $\{\Delta T = 7,\ p_{th} = 2 \cdot 10^{-2},\ n_I = 9,\ \eta = 1.3\}$. This is motivated by Figure 6.5a. For this we obtain an expected total life-cycle cost of 20.1. Both costs are similar, which confirms that the parameter p_{th} does not considerably affect the expected life-cycle cost of a strategy around the optimum. Nevertheless, we adopt the latter strategy as the best strategy, $\mathcal{S}_{\boldsymbol{w}_0^*}$, for the prior model, since it gives the smaller expected cost. We highlight the result in Table 6.2, in which we also include the value given by the surrogate at that point. The corresponding breakdown of the expected total life-cycle cost into its four components is found in Table 6.3.

Table 6.2 Parameters $\boldsymbol{w}_0^*$ and expected total life-cycle cost of the optimal strategy at time $t_0 = 0$.

ΔT	p_{th}	n_I	η	$\mathbf{E}[C_{\text{tot}}\|\boldsymbol{w}_0^*]_{MC}$	$\mathbf{E}[C_{\text{tot}}\|\boldsymbol{w}_0^*]_{\text{surrogate}}$
7	$2 \cdot 10^{-2}$	9	1.3	20.1	20.1

The MC samples also give an estimation of the annual repartition of the cost. Figure 3.3 shows the expected costs associated with the optimal I&M plan. Notably, the annual risk increases in the years before the first inspection and is progressively reduced with each additional inspection campaign, until it reaches a stationary value.

6.8.2. Adaptive strategy at time $t_1 = 7$ years

The adaptive case is now investigated. Following $\mathcal{S}_{\boldsymbol{w}_0^*}$, the first inspection campaign is carried out at year $t_1 = 7$, with inspections of components {8,9,10,11,16,17,18,19,20}, at a cost of

Table 6.3 Breakdown of the expected total life-cycle cost for strategy $\mathcal{S}_{\boldsymbol{w}_0^*}$.

Cost component	Expected cost
System failure	13.0
Inspection campaign	3.3
Component inspection	3.0
Component repair	0.8

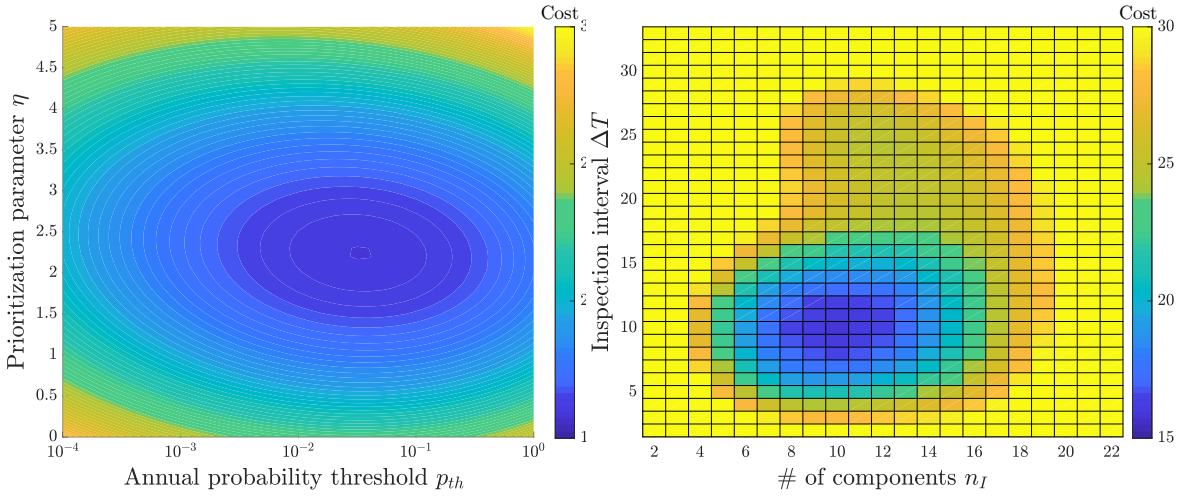

(a) (b)

Figure 6.6 (a): Surrogate cost function around the optimum for the adaptive optimization at $t_1 = 7$ for varying heuristic parameters p_{th} (logarithmic scale) and η, with $\Delta T = 9$[years] and $n_I = 9$. (b): Surrogate cost function around the optimum for the adaptive optimization at $t_1 = 7$ for varying (integer) heuristic parameters n_I and ΔT, with $p_{th} = 3 \cdot 10^{-2}$ and $\eta = 2.2$.

$c_{ini} = 9 * c_I + c_C = 1.9$. No damage is detected. This information is stored as $\mathbf{z}_7$.

At this point, the operator decides to improve the strategy adaptively, rather than continue with strategy $\mathcal{S}_{\boldsymbol{w}_0^*}$.

The optimal strategy $\mathcal{S}_{\boldsymbol{w}_{1|\mathbf{z}_7}^*}$ obtained for the posterior model is characterized by the heuristic parameter values in Table 6.4, with associated expected total life-cycle cost $\mathbf{E}[C_{\text{tot}}|\boldsymbol{w}_{1|\mathbf{z}_7}^*]_{\text{surrogate}} = 15.9$. This value is discounted to time t_1 and excludes the initial cost c_{ini}.

Table 6.4 Parameters $\boldsymbol{w}_1^*$ and expected total life-cycle cost of the optimal strategy at time $t_1 = 7$, after no detection of damage on components {8,9,10,11,16,17,18,19,20}.

ΔT	p_{th}	n_I	η	$\mathbf{E}[C_{\text{tot}}\|\boldsymbol{w}_{1\|\mathbf{z}_7}^*]$
9	$3 \cdot 10^{-2}$	9	2.2	15.9

Figures 6.6a and 6.6b depict the contours of the GPR surrogate cost function around the optimum values of the heuristic parameters at time t_1.

The updated optimal heuristic parameters reflect the information gained at time t_1 and the reduction of uncertainty about the state of the structure. The optimal inspection interval increases to $\Delta T = 9$, as does the optimal threshold on the annual probability of system failure, $p_{th} = 3 \cdot 10^{-2}$. The prescribed number of hotspots to be inspected remains at $n_I = 9$. Furthermore, the updated prioritization component η increases, meaning that it gives more

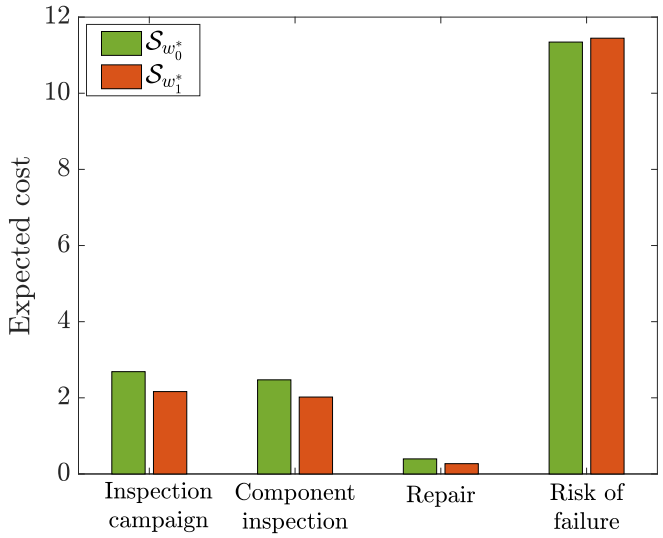

Figure 6.7 Comparison of expected cost for inspection, repair and failure for strategies $\mathcal{S}_{\boldsymbol{w}_0^*}$ and $\mathcal{S}_{\boldsymbol{w}_1^*}$, conditional on $\mathbf{z}_7$.

weight to the components' importance in the system; hence the components with a higher SEI are more likely to be inspected several times during the service life.

In order to compare the initial strategy with the adapted strategy, the expected cost of $\mathcal{S}_{\boldsymbol{w}_0^*}$ conditional on $\mathbf{z}_7$ is evaluated with the surrogate cost function. We find that $\mathbf{E}[C_{\text{tot}}|\boldsymbol{w}_0^*, \mathbf{z}_7]_{\text{surrogate}} = 16.9$, excluding the initial cost c_{ini}. The expected net gain of changing from strategy $\mathcal{S}_{\boldsymbol{w}_0^*}$ to strategy $\mathcal{S}_{\boldsymbol{w}_1^*}$, after detecting no damage at the first inspection is therefore

$$\mathbf{E}\left[C_{\text{tot}}|\boldsymbol{w}_0^*, \mathbf{z}_7\right] - \mathbf{E}[C_{tot}|\boldsymbol{w}_{1|\mathbf{z}_7}^*] = 1.0. \tag{6.5}$$

Figure 6.7 shows that this gain comes from decreasing the number of inspections and repairs, which can be achieved without significantly increasing the risk.

6.9. Summary

We demonstrate the application of the heuristic optimal planning approach and adaptive planning on a benchmark problem.

In the investigated numerical application, the adaptation of the strategy results only in limited cost reductions in the order of $5 - 10\%$. The likely reason for this is that the inspection outcomes are not surprising under the prior model. Were one to consider more unexpected inspection outcomes, the adapted optimal heuristic strategy would differ more significantly from the original strategy.

We introduce a heuristic for prioritizing components for inspections, which is motivated by the value-of-information concept. It accounts for the importance of component in the structural system, but also for the amount of information obtained on other components in the system. Since it is not known a-priori which of these two effects if more important, a heuristic

parameter is optimized to weight them. In the future, the heuristic might be adjusted in cases when components are not equi-correlated. Thereby it must be considered that inspections on components with higher correlation are likely to provide more information on the system overall. Simultaneously, it should also be ensured that components are selected for inspections in way that ensures their representativeness for the entire structure. An adjusted heuristic can also account for varying costs of inspections.

Chapter 7

Reliability-based I&M planning of a nuclear feeder piping system

The paper: Bismut, E., Straub, D., and Pandey, M. (2022). "Inspection and maintenance planning of a feeder piping system". In: *Reliability Engineering & System Safety* 224, p. 108521. constitutes this chapter.

7.1. Introduction

Operation and maintenance of a nuclear power plant (NPP) requires careful planning. Aside from the safety of the plant, which is ensured by a multitude of redundant safety systems, the continued operation of the plant is a major goal of the operator. Regular maintenance of the reactor components is essential to prevent interruptions in energy production and associated loss in revenue.

In a Canada Deuterium Uranium (CANDU) reactor, the feeder piping system consists of inlet pipes that supply coolant to cool the nuclear fuel and of outlet pipes that bring the hot fluid to the steam generators (see Figure 7.1). These hundreds of carbon steel pipes are susceptible to flow accelerated corrosion (FAC), which is largely responsible for wall thinning and leakage, particularly at the bends formed by the outlet feeder pipes (Wu, 1989; Lister et al., 1997; Yuan et al., 2008). Wall thinning and leakage can have serious consequences on the operability of the nuclear reactor. In the event of a leakage, total interruption of plant activity is typically required, at a very high cost. Inspection and maintenance (I&M) planning of feeder pipes is part of the FAC management program. Such planning is especially challenging due to the high number of pipe bends where FAC can occur. Inspecting and/or replacing every single pipe is not economically feasible.

Following a major FAC-related incident at the Surry NPP in 1986 and to address the lack of a unified maintenance practice, guidelines and principles were drafted (Wu, 1989). They are articulated around the following points: (i) piping systems must be inspected regularly; (ii) inspections must measure the wall thickness; (iii) the evolution of the wall thickness must be predicted for every pipe and account for the past inspection outcomes; (iv) pipes that do not comply with a minimum wall thickness must be replaced; (v) pipes selected for the next planned inspection should include pipes never inspected, as well as pipes marked as near-critical during a past inspection (EPRI, 2013).

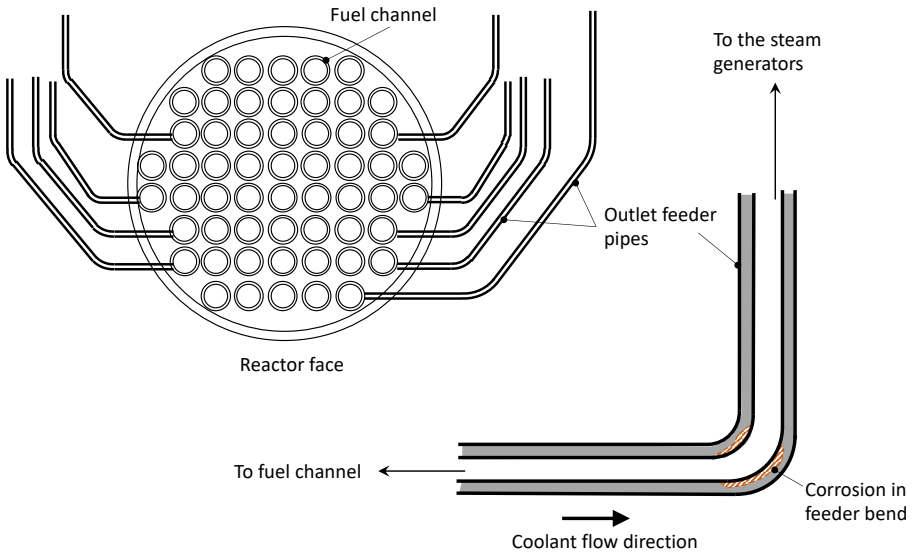

Figure 7.1 Schematic of a CANDU reactor and its feeder piping system. Each fuel channel is connected to inlet and outlet feeders (not all depicted for clarity purposes). The outlet feeders transport the coolant from the fuel channel to the steam generators, where heat is exchanged. The coolant is then transported back to the fuel channels through the inlet feeders. Flow accelerated corrosion is responsible for pipe wall thinning, particularly at the first bend of the outlet feeders. After Lister et al. (1997).

Good I&M planning controls the risk of an unplanned outage due to pipe failures, while keeping the I&M costs (pipe inspection and replacement costs) low. In the current unified practice, the I&M strategies adopted for FAC management in NPPs do not vary widely and have been adapted from past practice. These strategies have not been explicitly optimized to comply to a certain reliability level. Such a level is also not quantified in the guidelines. Therefore, there is an opportunity to optimize the I&M costs while maintaining a specified level of reliability.

To improve current I&M practice and to quantify the potential reduction in I&M costs, we propose a reliability-based planning framework for evaluating and optimizing I&M strategies of a multi-component piping system subject to FAC, under a reliability constraint applied at the system level. The pipes correspond to the system components. The system reliability accounts for the inspection information at component level using Bayesian updating. This framework utilizes a deterioration model, which accounts for the components' interdependence and correlation. The expected cost optimization uses a heuristic description of I&M strategies presented in Chapter 3, which enables the definition of I&M rules based on the reliability of individual components and of the system. The optimization is then performed on a few chosen heuristic parameters. The adopted heuristic notably allows for including eventual operator constraints. The framework proposed in this chapter is designed to handle hidden system failures, which can only be detected through component inspection. Furthermore, it can cope with a large number of deteriorating components, as is typical of a nuclear piping system.

Individual aspects of this reliability-based planning framework have been proposed and implemented in past studies (Alaswad and Xiang, 2017; Jonge and Scarf, 2020) but not in combination. Few studies have considered multi-level decision making for multi-unit systems

(Alaswad and Xiang, 2017; Wang et al., 2022). Several studies have investigated the effect of a reliability requirement on the planning of I&M actions at the system level or at the individual component level (e.g., Frangopol et al., 1997; Sagrilo et al., 1997; Onoufriou, 1999; Onoufriou and Frangopol, 2002; Bressi et al., 2021), a few of which include the cost optimization (Hellevik et al., 1999; Sørensen and Faber, 2001; Gholami et al., 2020; Bressi et al., 2021). In the studies that consider the interaction between the system and its components, the dependence between the component deterioration processes is not accounted for (Barker and Newby, 2008; Flage et al., 2012; Sun et al., 2017; Faddoul et al., 2018), and otherwise the methods are not adapted to a large number of system components (Straub and Faber, 2005; Barone and Frangopol, 2014; Li et al., 2016; Wang et al., 2022). In several studies that enable inspection decisions at the component level, preventive or corrective maintenance actions are limited to a major intervention at the system level (Onoufriou and Frangopol, 2002; Barker and Newby, 2008; Zio and Viadana, 2011), and failures (at the system or component level) are typically assumed to be self-announcing (Flage et al., 2012).

This chapter is organized as follows: Section 7.2 presents the type of nuclear piping system as well as the cost and operational constraints for which the reliability-based framework is developed. Section 7.3 details the simulation-based evaluation of the expected cost of a given I&M strategy under reliability constraint, which is formulated as a threshold p_0 on the system failure rate (see Section 7.3.3). In Section 7.4, we present the associated reliability-based strategy optimization problem, whose solution via the heuristic approach is described in Section 7.4.2. The probabilistic model for FAC at the pipe level is described in Section 7.5. The computation and updating of the reliability of the system and the pipes are detailed in Section 7.6. In Section 7.7, the framework is demonstrated on a 480-feeder piping system subject to FAC. The I&M constrained expected costs of a strategy representative of current I&M practice are evaluated and compared to the optimized heuristic strategies for different values of p_0. The effect of the prior deterioration model parameters is also investigated.

7.2. Inspection and maintenance of a piping system

The presented methodology is applicable in general to I&M planning of nuclear piping system. Nevertheless, to facilitate the description of the reliability-based planning framework in Sections 7.3 and 7.4, we introduce here the configuration and planning constraints of the specific system investigated in Section 7.7.

7.2.1. Piping system

We consider a piping system of a CANDU power reactor. A CANDU piping system typically consists of different pipe geometries (angle of pipe bend, diameter of pipe, thickness of pipe) (Yuan, 2007). However, to restrict the analysis, the piping system considered here consists of N identical large-bore pipes of 2-inch diameter, with initial nominal thickness W_0 (Hazra et al., 2020a).

The pipes are indexed by $1 \leq k \leq N$. The thickness of a pipe k at time t is denoted by $W_k(t)$, with $W_k(0) = W_0$. The loss of wall thickness resulting from FAC, $D_k(t)$, is

$$D_k(t) = W_k(0) - W_k(t). \tag{7.1}$$

To ensure adequate safety and fitness-for-service, the operator must ensure throughout the service life that the wall thickness loss in any of the N pipes does not exceed a certain threshold d_{max}. Piping design standards specify this threshold d_{max} to be 40% of the initial thickness W_0 (ASME, 2013; Hazra et al., 2020a). Failure to comply with this criterion at time t, indicated by the event $F^*(t) = \{\max_k D_k(t) > d_{max}\}$, is here called *system failure* (the point in time failure as in Chapter 5). The event $F_{c,k}(t) = \{D_k(t) > d_{max}\}$ is called *failure of pipe k*. It is $F^*(t) = \cup_k F_{c,k}(t)$.

The threshold d_{max} is based on a regulatory constraint, which typically includes a safety factor. In this case, a non-compliant pipe does not entail a failure (e.g., a leak) as such. Therefore, pipe failure as defined here is not self-announcing and can only be detected through wall-thickness inspection.

Time is measured in effective full-power year (EFPY). To simplify the notation, we refer to 1 EFPY as 1 year (yr). The design service life of the piping system is denoted by T.

7.2.2. I&M actions and cost model

To ensure compliance with the d_{max} criterion , the plant operator performs inspections of the piping system throughout the service life, by measuring the wall thicknesses at the bend of selected pipes with ultrasonic probes. Based on the inspection results, the operator can choose to replace pipes bends by cutting out the old bend and welding in a new pipe bend. In theory, the operator can decide to inspect or repair the pipes at any point in time. In practice, inspection and repair times are typically synchronized with planned maintenance outages, during which the NPP undergoes different types of checks and maintenance operations.

In a practical setting, the costs of pipe inspection and repair depend on the manner they are scheduled. We outline the I&M scheduling constraints and resulting I&M life-cycle costs in Figure 7.2. The I&M campaigns occur at times fixed in advance, typically at regular time intervals ΔT. Pipe inspections and maintenance actions are preferably planned one I&M campaign ahead. Certain pipes are labeled "of interest" (for future inspection). Others are labeled "critical" (for eventual future maintenance) and form the *PM pool*. Maintenance performed on pipes from the PM pool is called *preventive maintenance*. However, the inspections carried out during an I&M campaign can reveal critical pipes among those that have not been scheduled for maintenance during the previous campaign, which form the *CM pool*; critical pipes in the CM pool warrant *corrective maintenance*. This happens for example when an inspected pipe is deemed to deteriorate too fast so that their replacement cannot be postponed until the next outage. The corrective maintenance cost per pipe is typically higher than the cost of preventive maintenance. It is therefore advantageous to plan preventive

maintenance well, so that a minimal amount of corrective maintenance is required. However, labeling too many pipes as critical can result in an unnecessarily large number of inspections.

Note that we do not consider the possibility that maintenance actions occur outside of the predetermined campaign times, for instance during unplanned outages to maintain other parts of the NPP. This also means that what here is labeled as corrective pipe maintenance does not include maintenance actions that occur outside of the planned maintenance times, such as emergency repairs due to an unexpected pipe failure or other incidents. As we discuss in Sections 7.3 and 7.4, system failure is only considered through the system reliability.

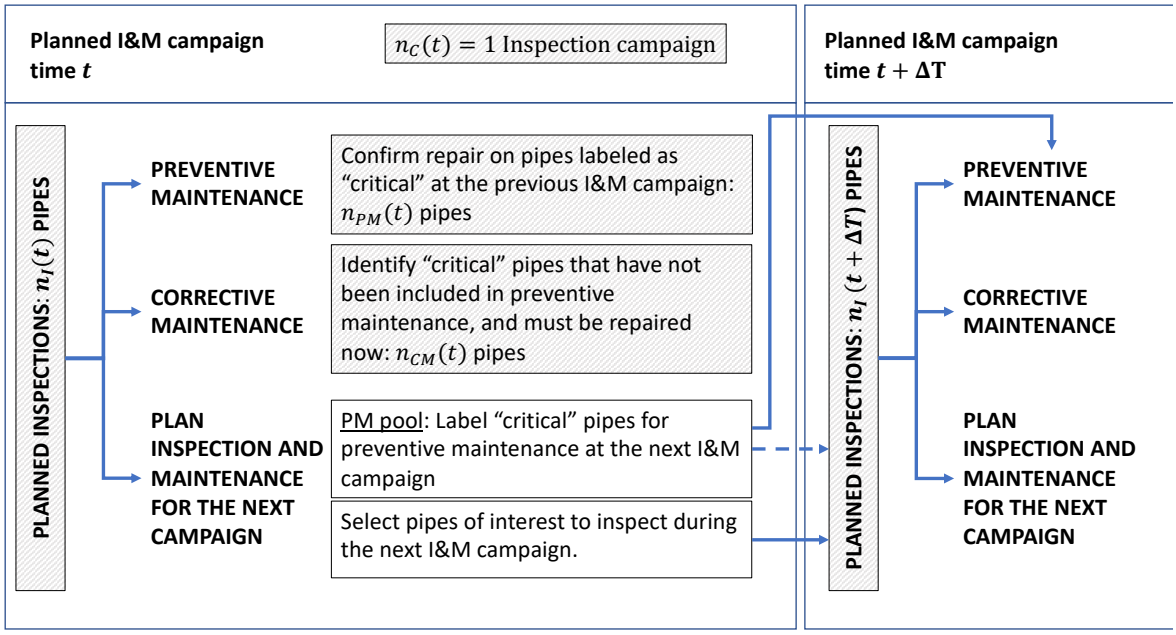

Figure 7.2 Overview on I&M planning. Inspection and maintenance actions occurring at time t are indicated by lightly hatched boxes. Planning of I&M actions for the next I&M campaign are indicated by unhatched boxes. The PM pool consists of the pipes pre-selected for preventive maintenance for the next campaign, the CM pool consists of all other pipes. The plain arrows indicate a scheduling imperative. The dashed arrow indicates possible influences but does not constrain the I&M strategies to follow them. For instance, preventive maintenance or corrective maintenance can be performed on pipes that have not been inspected during the campaign but might have been in the past. This means that the pipes in the PM pool can be, but not necessarily are, inspected at the next campaign, as indicated by the arrow. $n_C(t)$ records the times of I&M campaigns. During an I&M campaign at time t, $n_I(t)$, $n_{PM}(t)$ and $n_{CM}(t)$ are the total number of pipes inspected, and replaced for preventive and corrective maintenance, respectively.

The following costs are considered. The cost of launching an I&M campaign is c_C. It includes mobilization costs and other overheads. The cost of inspecting one pipe is c_I. It accounts for the time needed for one inspection. A unit cost c_{PM} is incurred for each pipe repaired as planned. The corrective maintenance cost per pipe is c_{CM}, which is larger than c_{PM}.

7.3. Reliability-constrained I&M strategy

In this section, we present the framework to evaluate the performance of any operator-defined I&M strategy when constrained by a reliability criterion.

7.3.1. I&M strategies

As discussed in Section 3.4.1, well-defined I&M strategies govern the decision process and must resolve all the questions pertaining to when and where to inspect the system. For the I&M planning problem considered in this study, a strategy defines at which time step the inspection outage takes place, how the PM pool is composed, which pipes are of interest and which pipes are preventively (or correctively) maintained.

A history $\boldsymbol{Z}$ contains all the information gathered during the lifetime of the structure, including inspection outcomes, pipe replacements and eventual system failure. $\boldsymbol{Z}_{0:t^-}$ is the I&M information collected up to time t, and $\boldsymbol{Z}_{k,0:t^-}$ is the information collected on pipe k.

7.3.2. Evaluating a strategy under a reliability criterion

The efficiency of a strategy can be assessed with different metrics. One metric is the total life-cycle expected cost, adding the I&M action expected costs (see Equation (7.8)) to the lifetime risk of failure. This is the risk-based assessment of a strategy, the general formulation of which is presented in Sections 2.3.2 and 3.5. The risk of failure considers explicitly the consequences of failure. These consequences include the cost of an accident (or failure), which entails replacing ruptured feeders but also loss of revenue due to unplanned outage, loss of life, and any other type of financial penalty imposed by the regulator. As an example, the loss incurred after the 1986 Surry NPP incident mentioned in Section 7.1 above amounted to tens of millions of dollars (EPRI, 2013). Correctly appraising the consequences of failure is crucial for a meaningful result using the risk-based approach. Due to the high uncertainty on the magnitude of the consequences of failure, a risk-based assessment is not further pursued here.

In real-life, it has been observed that the current I&M practice implicitly leads to a certain level of reliability (Sagrilo et al., 1997). Most I&M strategies in the nuclear industry are, however, defined in a rule-based approach, without quantifying the system reliability (e.g., EPRI, 2013), and they do not explicitly guarantee a reliability level.

Here, we propose a method to assess any given I&M strategy, such as those described in guidelines, by assessing the life-cycle I&M expected cost associated with this strategy while constraining the system to a fixed reliability level. This method is illustrated by the diagram of Figure 7.3.

The I&M campaigns occur at times prescribed by the considered strategy, for example at regular intervals ΔT. The rules for selecting pipes for inspection, for planning the PM pool and for performing preventive (and eventually corrective) maintenance are applied as prescribed by the strategy.

Then, the reliability criterion is evaluated for the time period until the next campaign and is compared against the required reliability level. If the criterion is violated, maintenance actions are performed such that the piping system is brought to a compliant state. Here, additional pipes are replaced one by one until the failure rate of the system falls under a certain value (see

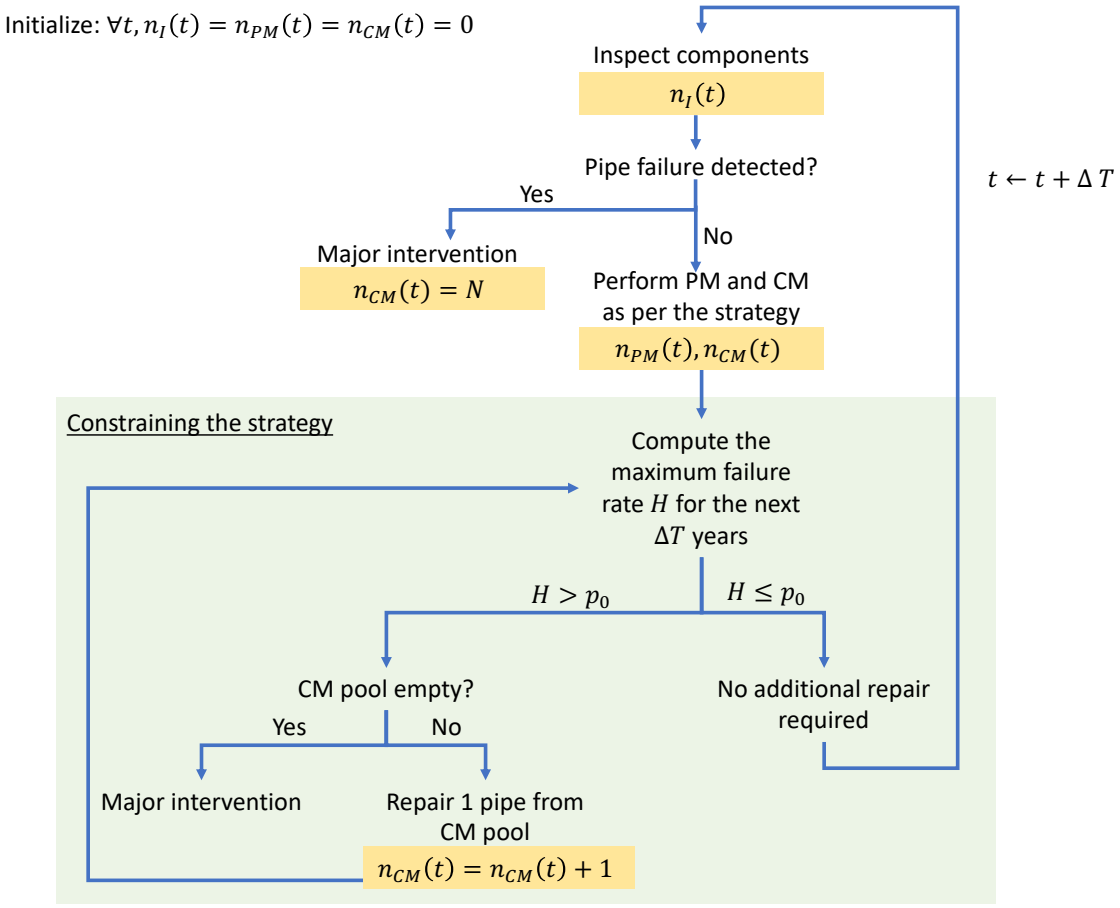

Figure 7.3 Simulation of an I&M history following a given strategy $\mathcal{S}$ constrained to reliability criterion p_0 for the evaluation of a sample life-cycle cost (see Equations (7.4) to (7.9)). The definition of H is given in Section 7.3.3 and Equation (7.3).

Section 7.3.3). The pipes selected for corrective maintenance to satisfy the criterion are those with the highest probability of pipe failure. Since these repairs occur after all I&M actions prescribed by the strategy have taken place, they are accounted for as corrective maintenance, with unit cost c_{CM}.

If system failure is detected, i.e., if an inspection reveals a non-compliant pipe, a major intervention is required and the simulated I&M history is interrupted. As explained above, we do not consider explicitly any costs or further I&M action resulting from system failure. A major intervention is also warranted in the unlikely eventuality that all pipes are replaced and the system is still not compliant, which might occur if the constant deterioration rate μ is too high.

7.3.3. Defining the reliability criterion

In this study, we express the reliability criterion as a threshold p_0 on the system failure rate at time t conditional on past I&M outcomes and actions $\boldsymbol{Z}_{0:t^-}$, which in turn depend on the

chosen I&M strategy $\mathcal{S}$. The failure rate at time t must be such that

$$H(t, \boldsymbol{Z}_{0:t^-}) \leq p_0. \tag{7.2}$$

The failure rate is approximated by

$$H(t, \boldsymbol{Z}_{0:t^-}) = \frac{\Pr\left[F(t+1)|\boldsymbol{Z}_{0:t^-}\right] - \Pr\left[F(t)|\boldsymbol{Z}_{0:t^-}\right]}{1 - \Pr\left[F(t)|\boldsymbol{Z}_{0:t^-}\right]} yr^{-1}. \tag{7.3}$$

$F(t) = \bigcup_{\tau \leq t} F^*(\tau)$ is the accumulated system failure event at time t as previously defined in Section 5.1. $\Pr\left[F(t)|\boldsymbol{Z}_{0:t^-}\right]$ is the filtered cumulative probability of system failure at time t. $\Pr\left[F(t+1)|\boldsymbol{Z}_{0:t^-}\right]$ is the predictive cumulative probability of system failure at time $t+1$.

p_0 can be prescribed explicitly by the regulator. However, in most situations, such a value is not given as such, but is implied by current regulations and constraints. In these cases, a value of the reliability criterion can be extracted from I&M plans that are considered acceptable by the practitioners and the regulators.

7.3.4. Life-cycle I&M cost

For an I&M history $\boldsymbol{Z}$ following a strategy $\mathcal{S}$, the life-cycle cost is calculated by recording the times and numbers of inspection and repair actions during the lifetime and aggregating their cost. To account for the time-value of money, an annual discount rate r is considered, such that all costs incurred at time t are discounted at time 0 by a factor $1/(1+r)^t$. The components of the life-cycle cost are

$$C_{I,T}(\boldsymbol{Z}) = \sum_{t=1}^{T} (c_I n_I(t) + c_C n_C(t)) \frac{1}{(1+r)^t} \tag{7.4}$$

$$C_{PM,T}(\boldsymbol{Z}) = \sum_{t=1}^{T} c_{PM} n_{PM}(t) \frac{1}{(1+r)^t} \tag{7.5}$$

$$C_{CM,T}(\boldsymbol{Z}) = \sum_{t=1}^{T} c_{CM} n_{CM}(t) \frac{1}{(1+r)^t}, \tag{7.6}$$

where $C_{I,T}(\boldsymbol{Z})$, $C_{PM,T}(\boldsymbol{Z})$ and $C_{CM,T}(\boldsymbol{Z})$ are respectively the total life-cycle inspection costs (including I&M campaign costs and pipe inspection costs), the total preventive maintenance costs and the total corrective maintenance costs. $n_C(t) = 1$ if an I&M campaign takes place at time t, 0 otherwise. All unit costs c_C, c_I, c_{PM} and c_{CM} are constant throughout the service life, their values for the numerical investigation are given in Table 7.2.

The life-cycle I&M cost for history $\boldsymbol{Z}$ is therefore

$$C_T(\boldsymbol{Z}) = C_{I,T}(\boldsymbol{Z}) + C_{PM,T}(\boldsymbol{Z}) + C_{CM,T}(\boldsymbol{Z}). \tag{7.7}$$

Before the execution of a strategy, the observation outcomes and eventual maintenance actions are uncertain. Therefore, one can compute the expected life-cycle I&M cost associated with a

strategy $\mathcal{S}$ as

$$C(\mathcal{S}) = C_{I,T}(\mathcal{S}) + C_{PM,T}(\mathcal{S}) + C_{CM,T}(\mathcal{S}), \tag{7.8}$$

where $C_{I,T}(\mathcal{S})$, $C_{PM,T}(\mathcal{S})$ and $C_{CM,T}(\mathcal{S})$ are the expected life-cycle inspection, preventive and corrective maintenance costs, respectively.

7.3.5. Computing the expected cost of a strategy

Following the methodology described in Section 3.5.4, we evaluate the expected life-cycle I&M cost in Equation (7.8) by sample averaging the I&M costs (Equation (7.7)) associated with $1 \leq q \leq n_{MC}$ MC sample observation histories $\boldsymbol{Z}^{(q)}$ following strategy $\mathcal{S}$, as

$$C(\mathcal{S}) \simeq \sum_{q=1}^{n_{MC}} \left[C_{I,T}\left(\boldsymbol{Z}^{(q)}(\mathcal{S})\right) + C_{PM,T}\left(\boldsymbol{Z}^{(q)}(\mathcal{S})\right) + C_{CM,T}\left(\boldsymbol{Z}^{(q)}(\mathcal{S})\right) \right]. \tag{7.9}$$

Furthermore, in the presented reliability-based framework each I&M sample history is generated in two phases: first by following the considered I&M strategy; then by checking if the reliability criterion is complied with and replacing additional pipes if necessary (see Figure 7.3). This procedure requires many computations of the failure rate in Equation (7.3) (one at every time step), for which sampling-based reliability methods are not appropriate. In this case, an efficient reliability computation performed sequentially is needed to generate one sample history $\boldsymbol{Z}^{(q)}$. Section 7.6 describes the procedure for evaluating the probabilities of component and system failure conditional on past observations for the deterioration, inspection and maintenance models presented in Section 7.5.

7.4. Reliability-based heuristic planning

In this section we introduce the reliability-based optimization framework to find an I&M strategy optimized for a fixed reliability level.

7.4.1. Reliability-based optimization

The rule-based approach to I&M planning of nuclear piping systems is the one currently recommended by the regulator. Effectively, it constrains the operator to follow certain principles (see an example below in Section 7.7.2) and leaves little leeway in modifying the prescribed strategy. Risk-based planning, formalized in Chapter 2, prescribes the risk-based assessment of a strategy and, as stated in Section 7.3.2, is not suitable for the considered application.

We therefore implement a reliability-based approach, which is reflected in the form of the considered objective function. In this approach, the optimal strategy minimizes the total I&M costs, while ensuring that the system always complies with a reliability criterion. The

objective function thus excludes any costs associated with all consequences of system failure, as the occurrence of failure is represented through the reliability criterion. The desired I&M strategy $\mathcal{S}^*$ is the solution to this minimization problem:

$$\begin{aligned} \mathcal{S}^* = \arg\min_{\mathcal{S}} \; & \left[C_{I,T}(\mathcal{S}) + C_{PM,T}(\mathcal{S}) + C_{CM,T}(\mathcal{S})\right], \\ \text{s. t. } \forall \text{ I\&M history } & \boldsymbol{Z}, \forall t, \; H(t, \boldsymbol{Z}_{0:t^-}, \mathcal{S}) \leq p_0. \end{aligned} \tag{7.10}$$

Optimal reliability-based planning of the form of Equation (7.10) has been investigated for multi-component systems, however, in this last case, with simplifying assumptions such as non-correlated components or small-sized systems (e.g., Barone and Frangopol, 2014; Li et al., 2016; Sun et al., 2017; Faddoul et al., 2018; Do and Bérenguer, 2020; Wang et al., 2022). One particular challenge of this optimization is the verification of the reliability constraint, which requires to assess the evolution of the system reliability in combination with an I&M strategy. In the section below, we explain how we combine the heuristic formulation of the optimization with a history sampling method to address this challenge.

7.4.2. Heuristic formulation

We employ the heuristic optimization approach introduced in Chapter 3 to obtain an approximate solution for the optimization problem of Equation (7.10). Its appeal resides in the fact that one can explicitly include operational constraints in the definition of a suitable plan. Here, the reliability criterion is directly included in the heuristic description.

The strategy space is thus restricted to a chosen heuristic, associated to a set of parameters $\boldsymbol{w} = \{w_1, ..., w_h\}$, and Equation (7.10) is reduced to an optimization of the parameter values:

$$\begin{aligned} \min_{\boldsymbol{w}} \; & C_{I,T}(\boldsymbol{w}) + C_{PM,T}(\boldsymbol{w}) + C_{CM,T}(\boldsymbol{w}), \\ \text{s. t. } \forall \text{ I\&M history } & \boldsymbol{Z}, \forall t, \; H(t, \boldsymbol{Z}_{0:t^-}, \boldsymbol{w}) \leq p_0. \end{aligned} \tag{7.11}$$

As discussed in Section 3.2, choosing the heuristic is in itself an optimization problem. In the heuristic chosen for the numerical investigation (see Section 7.7.3), we base the pipe inspection prioritization on the potential reduction in uncertainty, linked to the coefficient of variation of the distribution of the pipe thickness at a given time. The selection of the "critical" pipes (PM pool) is based on the probability of pipe failure.

With the heuristic formulation, the reliability constraint is integrated directly into the maintenance rules, which results in the modified history diagram of Figure 7.4, where pipe replacements are carried out specifically to satisfy the reliability criterion. An example of the system failure rate, where the I&M history is such that it follows the strategy and the constraint, is shown in Figure 7.5, for two different strategies. The underlying computations are detailed in Section 7.6. We note that the life-cycle I&M cost associated with a history, for which the system does not comply with the criterion (i.e., the branch "major intervention" is reached at some point during the service life), is high. This ensures that strategies which

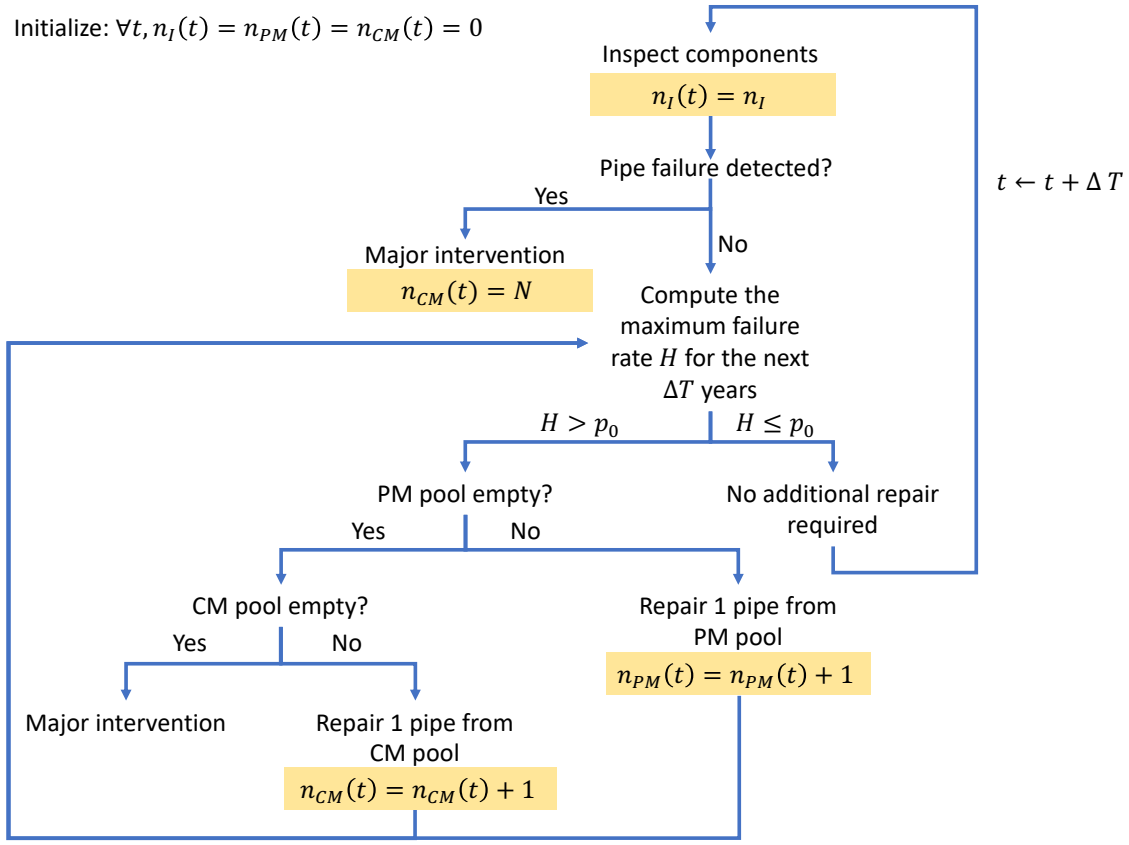

Figure 7.4 Simulation of an I&M history for the evaluation and optimization of heuristic strategies under reliability constraint p_0.

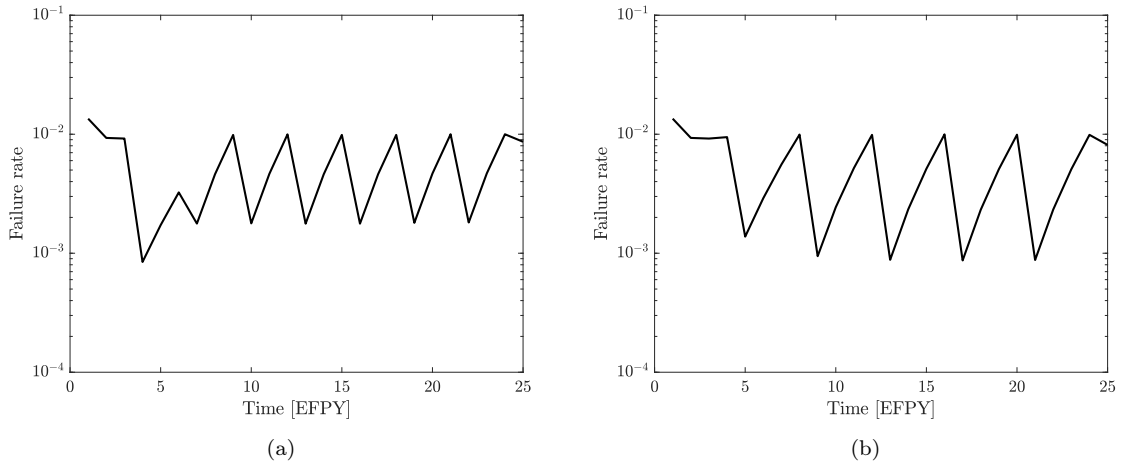

Figure 7.5 Evolution of the failure rate $H(t, \boldsymbol{Z}_{0:t^-})$ for a sample history, following two I&M strategies with different inspection intervals (a) $\Delta T = 3$ and (b) $\Delta T = 4$. In both cases, the strategy ensures that the system complies with the reliability constraint $p_0 = 1.0 \cdot 10^{-2}$, but the second strategy does so in a more efficient manner (see Tables 7.3 and 7.4).

lead to a high number of non-compliant histories are avoided during the optimization process explained in Section 7.4.3 below, without requiring the actual cost of a major intervention to be defined.

7.4.3. Heuristic parameters optimization method

We implement the CE optimization of Algorithm 3. For the numerical investigations, we follow the recommendations from Geyer et al. (2019) and choose the multivariate Gaussian as the sampling density, here truncated to account for the feasible domain of the parameter values. Samples of heuristic parameters corresponding to a probability quantity are obtained indirectly through sampling in the equivalent log-space. We fix $n_{CE} = 100$ and $n_E = 20$. The CE optimization stops after 20 iterations, resulting in a total of 2000 sample strategies. This has proven to allow satisfying convergence of the sampling density. The value of the expected cost evaluated with Equation (7.9) of a strategy is subject to sampling noise. The accuracy depends on the number of sample histories n_{MC} generated to compute the expected cost. Here, we find that $n_{MC} = 10$ provides suitable results for the CE optimization method. The advantage of assigning a small value to n_{MC} is that little computational effort is spent on non-suitable, i.e., expensive, strategies.

The sampling progression of the CE method for this numerical application is shown for two different initial sampling distributions in Figure 3.6. The variation in the obtained optimal heuristic parameter values reflects the sensitivity of the objective function to the parameters, which is further investigated in Section 7.7.6. The computational cost of generating an I&M history depends on the failure rate evaluation loop (see Figure 7.4). The advantage of assigning a small value to n_{MC} is that little computational effort is spent on non-suitable, i.e., expensive, strategies. Here, we find that $n_{MC} = 10$ provides suitable accuracy and results for the CE optimization method.

Finally, the expected cost associated with the identified optimal heuristic parameters is estimated with Equation (7.9) with 2000 MC sample histories.

7.5. Models of pipe deterioration and inspection and repair models

The reliability-based planning framework requires a probabilistic model describing the evolution of the state of the system and its components. Here, FAC in the pipes is modeled with a Gamma process with unknown parameters.

7.5.1. Modeling FAC with a mixed-scale Gamma process

Mechanistic models of FAC have been developed (e.g., Lister and Lang, 2002), but they require the knowledge of numerous parameters characterizing the operating condition of the operator, such as the chemical environment, temperature and pH levels, which typically fluctuate over time. It is therefore appropriate to model the evolution of FAC with a random process. Here, we model the evolution of FAC in the N pipe bends with a mixed-scale Gamma process (Lawless and Crowder, 2004).

The service life between time 0 and T is discretized in n_T time steps. One time step corresponds to 1 year. The loss of thickness in one pipe k due to corrosion is modeled by a Gamma process with stationary increments ΔD_τ, with strictly positive shape and scale parameters $[\alpha, \beta]^\intercal$ (Hazra et al., 2020b). We denote by $\mu = \alpha\beta$ the mean and by $\nu = \frac{1}{\sqrt{\alpha}}$ the coefficient of variation of these increments. μ and ν are population parameters, common to all pipes.

The wall thinning ΔD in Δt time steps is written as the sum of i.i.d yearly increments ΔD_τ

$$\Delta D = \sum_{\tau=1}^{\Delta t} \Delta D_\tau. \tag{7.12}$$

ΔD is Gamma distributed with shape and scale parameters $[\alpha\Delta t, \beta]^\intercal$.

$F_{\Delta D,\Delta t}(d)$ and $f_{\Delta D,\Delta t}(d)$ denote the associated CDF and PDF for a given Δt. It is

$$f_{\Delta D,\Delta t}(d) = \frac{1}{\Gamma(\alpha\Delta t)\,\beta^{\alpha\Delta t}} d^{\alpha\Delta t-1} \exp\left(-\frac{d}{\beta}\right). \tag{7.13}$$

In the mixed-scale Gamma process, ν is a known constant and the mean of the yearly increment μ is modeled as a random variable, with an inverse Gamma distribution, here denoted by $IGa(a, b)$, with prior shape and scale parameters $[a, b]$. The inverse Gamma PDF with parameters $[a, b]$ is

$$f(\mu) = \frac{b^a}{\Gamma(a)} \left(\frac{1}{\mu}\right)^{a+1} \exp\left(-\frac{b}{\mu}\right). \tag{7.14}$$

The distribution of the increment μ is updated through measurements of pipe thicknesses, following Section 7.6.3.

The choice of the prior distribution in a parameter learning context, performed with Bayesian analysis, becomes less important as more inspection data are gathered. In the context of preposterior analysis, where we are interested in computing an expected cost, choosing an appropriate prior has a significant effect on the outcome of the analysis (see Section 2.2.3.2). For a plant-specific optimization, the calibration of the prior distribution of the population parameters can be done by using past inspection data. When no specific information is available, expert knowledge can be a good starting point. The prior parameters a and b of the model are given in Section 7.7.1 for I&M planning of a new plant.

7.5.2. Inspection model

During a I&M campaign, information is collected on the state of deterioration of the pipes through in-situ inspections. The inspections are carried out with an array of ultrasonic probes to measure the wall thickness. In practice, one probe scan measures the thickness of one quadrant of the pipe bend and four scans are required for full inspection of one pipe bend. The minimum wall thickness from those scans is recorded. The recorded wall thickness at

time t of pipe k is $Z_k(t)$. For simplicity, we consider the measurement to be perfect, hence

$$Z_k(t) = W_k(t). \tag{7.15}$$

The presented approach can also be used when the observation likelihood includes measurement error. The associated computational aspects are discussed in Section 7.6.5.

7.5.3. Repair model

Replacing a pipe at time t sets the wall thinning back to 0, i.e., $W_k(t) = W_k(0)$ and $D_k(t) = 0$ immediately after repair at time t. Furthermore, μ is assumed to be remain constant even if the piping system is fully replaced.

7.6. Piping system reliability

In this section, we derive the expressions for the probability of system failure for the FAC model presented in Section 7.5 as well as the characteristics of pipe damage distribution, conditional on past inspection outcomes. These quantities are required for the reliability constraint check and for implementing selected heuristic I&M strategies.

7.6.1. Cumulative probability of system failure

During the execution of the strategy, the reliability constraint must be met. To verify the criterion, one must compute at each step t the failure rate of the system as per Equation (7.3). As per the definitions given in Sections 7.2.1 and 7.3.3, the accumulated system failure event at time t is

$$F(t) = \bigcup_{\tau \leq t} F^*(\tau) = \bigcup_{\tau \leq t} \bigcup_{k} F_{c,k}(\tau). \tag{7.16}$$

The probability of this accumulated failure event must be computed conditional on the inspection outcomes and repair actions up to time t.

We use the notation $D_k(t) = D_{k,t}$, and similarly for all time-variant random variables. At every time t we evaluate the filtered cumulative probability of system failure $\Pr(F(t)|\boldsymbol{Z}_{0:t^-})$.

In the following general derivations, $\boldsymbol{\kappa}$ denotes the unknown model parameters (see Section 2.2.3.2). For the application presented here, $\boldsymbol{\kappa} = \mu$. Using Equation (7.16), one finds

$$P_{max}(t) = 1 - \Pr\left(\bigcap_{\tau \leq t} \bigcap_{k} \{D_{k,\tau} < d_{max}\} | \boldsymbol{Z}_{0:t^-} \right). \tag{7.17}$$

Conditionally on $\boldsymbol{\kappa}$, the deterioration processes and measurements of pipes are independent. Conditioning on $\boldsymbol{\kappa}$, one obtains

$$P_{max}(t) = 1 - \int_{\Omega_{\boldsymbol{\Theta}}} \prod_k \Pr\left(\bigcap_{\tau \leq t} \{D_{k,\tau} < d_{max}\} | \boldsymbol{Z}_{k,0:t^-}, \boldsymbol{\kappa}\right) f_{\boldsymbol{\kappa}|\boldsymbol{Z}_{0:t^-}}(\boldsymbol{\kappa}) \mathrm{d}\boldsymbol{\kappa}, \tag{7.18}$$

where $f_{\boldsymbol{\Theta}|\boldsymbol{Z}_{0:t^-}}(\boldsymbol{\theta})$ is the posterior PDF of $\boldsymbol{\kappa}$ conditional on the measurements $\boldsymbol{Z}_{0:t^-}$.

The posterior distribution of $\boldsymbol{\kappa}$ is obtained with Bayes' rule:

$$f_{\boldsymbol{\kappa}|\boldsymbol{Z}_{0:t^-}}(\boldsymbol{\kappa}) \propto \mathcal{L}(\boldsymbol{\kappa}; \boldsymbol{Z}_{0:t^-}) f_{\boldsymbol{\kappa}}(\boldsymbol{\kappa}). \tag{7.19}$$

$\mathcal{L}(\boldsymbol{\kappa}; \boldsymbol{Z}_{0:t^-})$ is the likelihood of $\boldsymbol{Z}_{0:t^-}$ conditional on $\boldsymbol{\kappa}$. The normalizing constant is $c = \int_{\Omega_{\boldsymbol{\kappa}}} f_{\boldsymbol{\kappa}}(\boldsymbol{\kappa}) \mathcal{L}(\boldsymbol{\kappa}; \boldsymbol{Z}_{0:t^-}) \mathrm{d}\boldsymbol{\kappa}$. The measurements are independent conditionally on κ. This is an approximation, due to the selection bias (Nie et al., 2018). We will not correct this bias, as it does not significantly affect our results (see Section 3.5.5).

Thus

$$\mathcal{L}(\boldsymbol{\kappa}; \boldsymbol{Z}_{0:t^-}) = \prod_k \mathcal{L}(\boldsymbol{\kappa}; \boldsymbol{Z}_{k,0:t^-}). \tag{7.20}$$

$\mathcal{L}(\boldsymbol{\theta}; \boldsymbol{Z}_{k,0:t^-})$ is the likelihood of $\boldsymbol{Z}_{k,0:t^-}$ conditional on $\boldsymbol{\kappa}$.

As stated in Section 7.5.2, we consider that there is no uncertainty in the measurement. Hence for $\tau < T$ we have $Z_{k,\tau} = W_{k,0} - D_{k,\tau}$, where the initial thickness $W_{k,0}$ is also known. The conditional probability of pipe failure and the posterior distribution of parameter $\boldsymbol{\kappa}$ are derived in the paragraphs below.

7.6.2. Conditional cumulative probability of pipe survival

For a fixed time t, we denote by $\mathcal{I}_k = \{t_{I,1} < ... < t_{I,p}\}$ the inspection times and by $\mathcal{R}_k = \{t_{R,1} < ... < t_{R,q}\}$ the repair times of pipe k up to and not including time t. If no inspection occurred, $\mathcal{I}_k = \emptyset$. If no repair occurred prior to time t, $q = 1$ and $t_{R,1} = 0$.

For a given pipe, the deterioration process $D_{k,\tau}$ is monotonously increasing in the interval between two consecutive replacements. Therefore, the intersection of pipe survival events in Equation (7.18) is equivalent to

$$\bigcap_{\tau \leq t} \{D_{k,\tau} < d_{max}\} = \{D_{k,t} < d_{max}\} \bigcap \{\cap_{1 \leq j \leq q} \{D_{k,t_{R,j}} < d_{max}\}\}. \tag{7.21}$$

where $D_{k,t_{R,j}}$ is the deterioration of pipe k just before it is replaced at time $t_{R,j}$. The state of pipe deterioration is furthermore independent of all states and measurements before the last repair time. This and the above simplification allow writing the conditional cumulative

probability of pipe survival as

$$\Pr\left(\bigcap_{\tau\le t}\{D_{k,\tau} < d_{max}\}|\boldsymbol{Z}_{k,0:t^-},\boldsymbol{\kappa}\right) = \Pr\left(D_{k,t} < d_{max}|\boldsymbol{Z}_{k,t_{R,q}:t^-},\boldsymbol{\kappa}\right) \cdot \prod_{1\le j\le q}\Pr\left(D_{k,t_{R,j}} < d_{max}|\boldsymbol{Z}_{k,t_{R,j-1}:t_{R,j}},\boldsymbol{\kappa}\right), \quad (7.22)$$

where $t_{R,0} = 0$.

The distribution of state $D_{k,\tau}$ conditional on measurement and repair actions up to but not including time τ is fully determined either by the time of the last repair before τ or by the last pipe thickness measurement, whichever occurred last. Let τ_k be the larger of these times of last repair and last measurement.

– If repair occurred at time τ_k,

$$\Pr(D_{k,\tau} < d_{max}|\boldsymbol{Z}_{k,0:\tau^-},\boldsymbol{\kappa}) = F_{\Delta D,\tau-\tau_k|\boldsymbol{\kappa}}(d_{max}). \quad (7.23)$$

– If a measurement Z_{k,τ_k} was obtained at time τ_k,

$$\Pr(D_{k,\tau} < d_{max}|\boldsymbol{Z}_{k,0:\tau^-},\boldsymbol{\kappa}) = \Pr(D_{k,\tau} < d_{max}|\boldsymbol{Z}_{k,\tau_k},\boldsymbol{\kappa}) = F_{\Delta D,\tau-\tau_k|\boldsymbol{\kappa}}(d_{max}-(W_{k,0}-Z_{k,\tau_k})). \quad (7.24)$$

The distribution of state $D_{k,\tau}$ conditional on inspection outcome $Z_{k,\tau}$ at time τ is simply the Dirac density in $Z_{k,\tau}$.

$$\Pr(D_{k,\tau} < d_{max}|Z_{k,\tau},\boldsymbol{\kappa}) = \mathbb{1}_{W_{k,0}-Z_{k,\tau}\le d_{max}}, \quad (7.25)$$

where $\mathbb{1}_{W_{k,0}-Z_{k,\tau}\le d_{max}}$ takes the value 1 if $W_{k,0} - Z_{k,\tau} \le d_{max}$, 0 otherwise.

7.6.3. Likelihood and posterior distribution of deterioration parameters

Using the chain rule and the Markovian assumption, the likelihood $\mathcal{L}(\boldsymbol{\kappa};\boldsymbol{Z}_{k,0:t^-})$ can be computed sequentially. For each $t_j \in \mathcal{I}_k$, we compute the time interval $\Delta t_j = \min(t_j - t_l,\ s.t.\ t_l \in \mathcal{R}_k\ and\ t_l < t_j)$ between inspection time t_j and the time of last repair (0 if the pipe has never been repaired). The likelihood describing measurements on pipe k is

$$\mathcal{L}(\boldsymbol{\kappa};\boldsymbol{Z}_{k,0:t^-}) = \prod_{j\in\mathcal{I}_k} f_{\Delta D,\Delta t_j|\boldsymbol{\kappa}}(W_{k,0} - Z_{k,t_j}). \quad (7.26)$$

The rate parameter $1/\beta = 1/(\mu\nu^2)$ of the Gamma process (see Section 7.5.1) is also Gamma distributed. Making use of the self-conjugacy of the Gamma distribution (Robert, 2007), the posterior (filtered) distribution of $\boldsymbol{\kappa} = \mu$ can be obtained by updating the parameters of

the inverse gamma distribution with the (perfect) measurements $\boldsymbol{Z}_{0:t^-}$, such that $\boldsymbol{\kappa}|\boldsymbol{Z}_{0:t^-} \sim IGa(a_{post}, b_{post})$, with

$$a_{post} = a + \frac{\sum_{k=1}^{N}\sum_{j\in\mathbb{J}_k}\Delta t_j}{\nu^2}, \tag{7.27}$$

$$b_{post} = b + \frac{\sum_{k=1}^{N}\sum_{j\in\mathbb{J}_k}(W_{k,0} - Z_{k,t_j})}{\nu^2}. \tag{7.28}$$

7.6.4. Posterior distribution of pipe deterioration state

The scaled deterioration state at time t conditional on past history $\boldsymbol{Z}_{0:t^-}$, $(D_{k,t} - d_Z)/\xi$, with $\xi = \frac{b_{post}(t-\tau_k)}{a_{post}}$, follows the Fisher–Snedecor distribution with degrees of freedom $\frac{2(t-\tau_k)}{\nu^2}$ and $2a_{post}$ (Lawless and Crowder, 2004; Yuan, 2007). The CDF of this distribution is denoted by $F_{\frac{2(t-\tau_k)}{\nu^2},2a_{post}}(\cdot)$. τ_k is defined as in Section 7.6.2 above as the larger of the times of last repair and last measurement before the considered time t and $d_Z = 0$ if repair occurred at τ_k, $d_Z = W_0 - Z_{k,\tau_k}$ otherwise.

The posterior distribution of $D_{k,t}$ is characterized by its mean $\frac{b_{post}(t-\tau_k)}{a_{post}-1} + d_Z$ and its standard deviation $\frac{b_{post}(t-\tau_k)}{a_{post}-1}\sqrt{\frac{\frac{(t-\tau_k)}{\nu^2}+a_{post}-1}{\frac{(t-\tau_k)}{\nu^2}(a_{post}-2)}}$. The associated coefficient of variation is

$$c.o.v.(D_{k,t}|\boldsymbol{Z}_{0:t^-}) = \frac{1}{1+\frac{d_Z(a_{post}-1)}{b_{post}(t-\tau_k)}}\sqrt{\frac{\frac{(t-\tau_k)}{\nu^2}+a_{post}-1}{\frac{(t-\tau_k)}{\nu^2}(a_{post}-2)}}. \tag{7.29}$$

The probability of pipe failure is

$$\Pr(D_{k,t} > d_{max}|\boldsymbol{Z}_{0:t^-}) = 1 - F_{\frac{2(t-\tau_k)}{\nu^2},2a_{post}}\left((d_{max} - d_Z)/\xi\right). \tag{7.30}$$

The evolution of probability of pipe failure and expected value of pipe thickness and the resulting system probability of failure and failure rate are depicted in Figure 7.6 for sample histories.

7.6.5. Computation details

As the observation likelihood does not include measurement error, the integrand of Equation (7.18) has a closed form, and a numerical integration is appropriate to evaluate $\Pr(F(t)|\boldsymbol{Z}_{0:t^-})$.

7.7. Numerical investigation: I&M planning at the beginning of service life.

We apply the framework to evaluate I&M strategies for the piping system in a new NPP described in Section 7.2.1, at the beginning of its service life, with $N = 480$, $W_0 = 5.5$[mm], $d_{max} = 2.2$[mm] and $T = 25yr$.

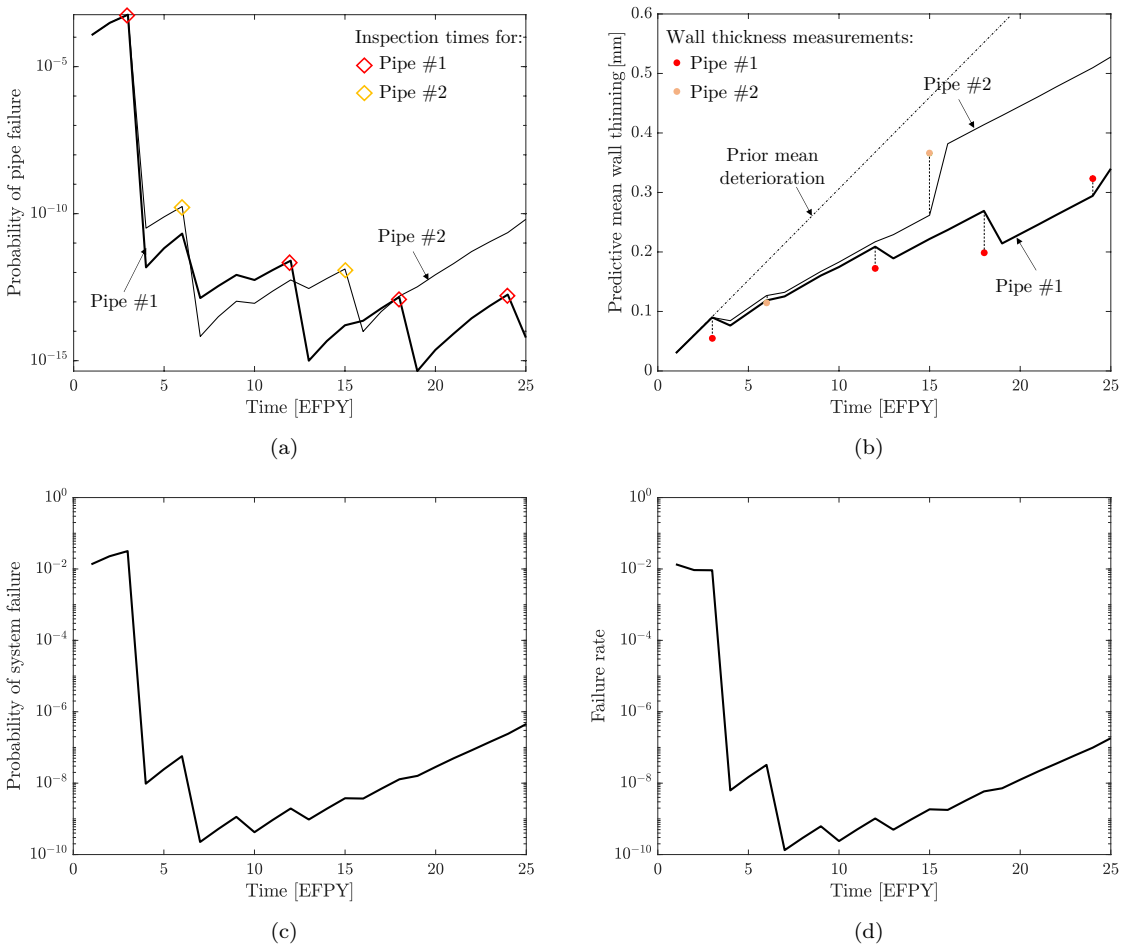

Figure 7.6 a) Filtered probability of pipe failure $\Pr(D_{k,t} > d_{max}|\boldsymbol{Z}_{0:t^-})$, for pipes number $k = 1$ and $k = 2$. Pipe inspection times are indicated. b) Evolution of the predictive mean wall thinning D_k for pipes number $k = 1$ and $k = 2$. Wall thickness measurements are indicated for these two pipes. In the assumed deterioration model, the predicted mean deterioration rate is the same for all pipes, hence the change of slope occurs also for non-inspected pipes. c) Filtered cumulative probability of system failure $\Pr(F(t)|\boldsymbol{Z}_{0:t^-})$. d) Failure rate computed with Equation (7.3).

7.7.1. Planning setup

The model used for simulating sample histories for evaluating strategies is described in Section 7.5. Its prior parameters are summarized in Table 7.1. The costs are found in Table 7.2 below.

Table 7.1 Prior deterioration model parameters

Parameter	Type	Value / Distribution	Unit
μ	Random variable	$IGa(a, b)$	mm
ν	Deterministic	2	
a	Deterministic	3	
b	Deterministic	0.06	
W_0	Deterministic	5.5	mm
$D_i(0)$	Deterministic	0	mm
d_{max}	Deterministic	2.2	mm

The prior distribution parameters of μ in Table 7.1 result in a prior expected value of

Table 7.2 Cost model parameters

Campaign	c_C	1
Pipe inspection	c_I	0.1
Preventive maintenance	c_{PM}	1
Corrective maintenance	c_{CM}	5
Discount rate	r	0.05

$0.03[\text{mm}/yr]$ and a c.o.v. of 100%. The choice of this prior model is based on the analysis of historical events: Lister et al. (1997) states that wear rates at 0.02[mm/yr] are "acceptable". There is however a high variability in the wear rate. Indeed, wear rates between 0.07[mm/yr] and 0.2[mm/yr] have been recorded (Lister et al., 1997; Hazra et al., 2020a). Usually, the reported wear rates in the literature are obtained from "lead feeders", i.e., feeders which experience larger rate of degradation than an average feeder in the population and are therefore not representative of the average degradation rate. This high uncertainty in the prior FAC wear rate is here reflected in the high c.o.v. This may be a pessimistic assumption about the state of knowledge about the deterioration process in NPP piping systems. The probability that the mean wear rate exceeds 0.08[mm/yr] is 5%. The value of $\nu = 2$ is such that the probability of pipe failure at the end of service life is $4 \cdot 10^{-2}$. The resulting system failure rate for the non-maintained system is shown in Figure 7.7. The maximum failure rate of $1.6 \cdot 10^{-2}$ is reached at the end of the service life. It is clear that for any constraint p_0 larger than this value, the optimal strategy according to Equation (7.10) is to do nothing.

We investigate the following reliability criteria: $p_0 \in \{0.1, 0.5, 1.0, 1.5, 5.0\} \cdot 10^{-2}$.

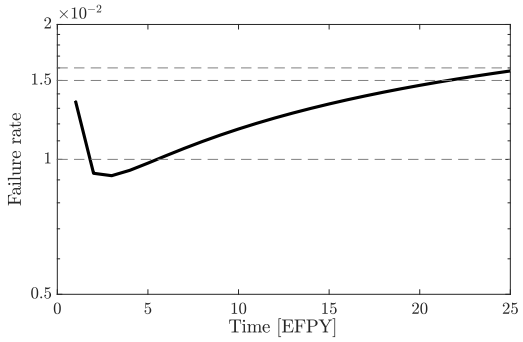

Figure 7.7 Failure rate for the non-maintained, non-inspected system. The levels $\{0.5, 1.0, 1.5, 1.6\} \cdot 10^{-2}$ are also indicated.

7.7.2. Constrained representative strategy $\mathcal{S}_{REP}$

7.7.2.1. Description of the strategy and associated FAC prediction model

To test the reliability-constrained strategy approach of Section 7.3, we construct a strategy $\mathcal{S}_{REP}$ representative of the current I&M practice. (EPRI, 2013; Walker, 2017) provide guidelines for implementing I&M programs specifically targeted to avoid FAC-related failures. The current approach to I&M of piping system typically assumes deterministic prediction models for FAC. The inspection data is processed with basic statistical tools. Uncertainty is

addressed in a semi-probabilistic manner, with safety factors applied to the predicted wear rate.

The inspection plan follows the logic of inspecting critical pipes, which have a small predicted remaining service life, as well as pipes that have not yet been inspected (EPRI, 2013; Walker, 2017). At each I&M campaign, 30% of pipes are inspected, here 140 pipes. As previously stated, this I&M strategy does not allow for I&M campaigns outside of the fixed times. The maintenance interval is fixed at 3 years. Preventive and corrective maintenance prescribed by the strategy are only carried out on pipes which have been inspected.

The strategy S_{REP} is summarized below. $W_{k,pred}$ is computed using the FAC-predictive model (see Appendix G) and $W_{accept} = W_0 - d_{max}$.

Strategy $\mathcal{S}_{REP}$ - 140 pipes are inspected at each campaign and $\Delta T = 3$yr is fixed.

- The interval between I&M campaigns is $\Delta T = 3$yr.
- Pipe inspections: Inspect pipes that have been labeled "of interest" and those labeled as "critical" for preventive maintenance at the previous I&M campaign. The two groups of pipes are not necessarily mutually exclusive.
- Preventive maintenance: pipes that have been previously labeled critical and therefore have just been inspected are considered. The pipes k for which the predicted thickness at the next I&M campaign $W_{k,pred}(t + \Delta T) < W_{accept}$ are repaired, at a unit cost c_{PM}.
- Corrective maintenance: the predicted wall thickness $W_{k,pred}(t + \Delta T)$ at the next I&M campaign at time $t+\Delta T$ is computed for each inspected pipe (which has not been already repaired during preventive maintenance) k. All pipes for which $W_{k,pred}(t+\Delta T) < W_{accept}$ are replaced now (at time t).

Planning for the next campaign

- Plan predictive maintenance for campaign at time $t + \Delta T$: Pipes for which $W_{k,pred}(t + 2\Delta T) < W_{accept} < W_{k,pred}(t + \Delta T)$ are labeled as "critical" for the next I&M campaign.
- Plan inspections for next campaign: a total of $n_I = 140$ pipes are selected for inspection. A proportion of 70%, i.e., 98 pipes, are selected in decreasing order of time to last inspection, and the remaining 30%, i.e., 42 pipes, are selected according to their estimated remaining service life (Equation (G.3)).

7.7.2.2. Unconstrained vs constrained strategy

Figure 7.8a depicts samples of the evolution of the failure rate H following the unconstrained strategy $\mathcal{S}_{REP}$. It is clear that for a fixed reliability level, say $p_0 = 1.5 \cdot 10^{-2}$, many trajectories exceed the threshold. On the other hand, for the trajectories that do comply with the criterion, it is possible that some of the inspections or pipe replacement prescribed by the strategy are not necessary to comply with the reliability criterion. Figure 7.8b shows samples of the

evolution of the failure rate following the constrained strategy. Only the histories which would have exceeded the criterion are affected by the reliability constraint.

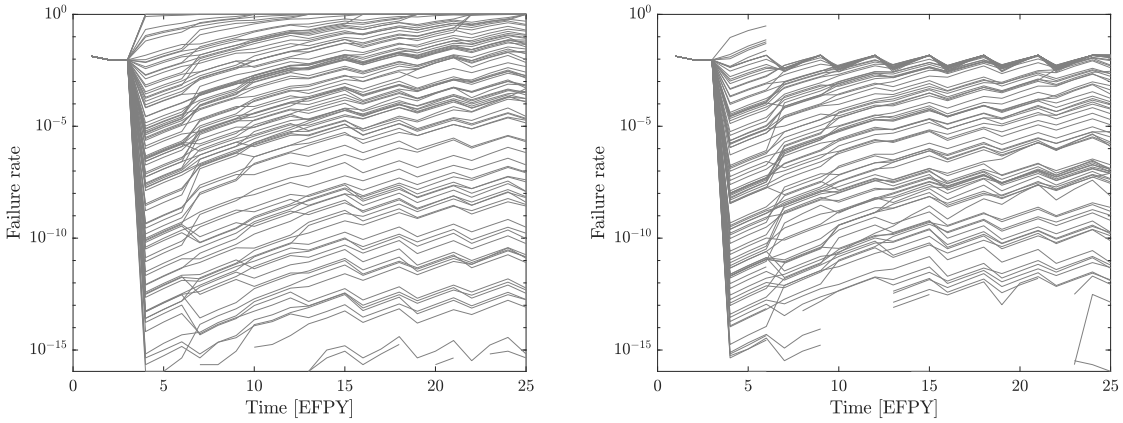

Figure 7.8 a) Failure rate $H(t, \boldsymbol{Z}_{0:t^-})$, following unconstrained strategy $\mathcal{S}_{REP}$ for 100 sample I&M histories. b) Failure rate for 100 sample I&M histories following the strategy $\mathcal{S}_{REP}$ constrained to $p_0 = 1.5 \cdot 10^{-2}$. The histories are interrupted when the constraint on the failure rate cannot be met (i.e., a major intervention is required).

7.7.3. Heuristic investigated

For the reliability-based heuristic planning, we investigate the following Heuristic A. The selection rule for pipe inspection is done by ranking the pipes according to their coefficient of variation of the wall thickness loss. This reflects the primary goal of an inspection, which is to reduce the uncertainty about the state of the system. The PM pool is composed of pipes for which the probability of pipe failure exceeds a fixed threshold. PM and CM actions are furthermore carried out as outlined in Figure 7.4.

7.7.4. Computational cost

Each optimization was performed in parallel on a 2.2 GHz, 10 cores, 128 GB of RAM computer and took in the order of 3.5 hours.

7.7.5. Results

We evaluate the expected costs of strategy $\mathcal{S}_{REP}$ constrained to the reliability thresholds p_0 and we optimize the heuristic parameters.

First, we fix $\Delta T = 3$yr to match the I&M campaign interval specified by strategy $\mathcal{S}_{REP}$ above (see Section 7.7.2). The optimal parameter values obtained for Heuristic A for different values of p_0 are summarized in Table 7.3. The expected costs of the optimal strategies and of the constrained strategy $\mathcal{S}_{REP}$ are estimated with $n_{MC} = 2000$ MC sample histories. The standard error on the estimation of the expected cost is around $3 - 4\%$.

Heuristic A - Parameters ΔT, n_I, p_{th}

- ΔT is the constant inspection interval. The only I&M opportunities are at the planned inspection times.
- Pipe inspection at first campaign: n_I pipes are randomly selected and inspected.
- Pipe inspection at next campaigns: n_I is the number of pipes selected for inspection (labeled "of interest") at each campaign, according to the prioritization rule (see point below). To these pipes are added those that have been labeled as "critical" for preventive maintenance [at the previous I&M campaign]. An overlap between these two groups is possible. Hence, there is a minimum of n_I pipes inspected at each campaign.

Planning for the next campaign

- Pipes are selected for preventive maintenance at time $t + \Delta T$ (labeled as "critical") based on their probability of failure $\Pr(D_k(t + \Delta T) > d_{max}|\boldsymbol{Z}_{0:t^-})$ (Equation (7.30)) exceeding a threshold p_{th}.
- The pipes are prioritized for inspection as the ones with the highest coefficient of variation of $D_k(t + \Delta T)$, given by Equation (7.29).

Table 7.3 Optimized heuristic parameters n_I and p_{th} of Heuristic A (see Section 7.7.3) for fixed $\Delta T = 3$yr and associated expected life-cycle I&M cost for different values of p_0. The expected cost of the constrained strategy $\mathcal{S}_{REP}$, for which the total number of inspected pipes per campaign is 140, is indicated for comparison. For p_0 above $1.6 \cdot 10^{-2}$, the best I&M strategy is that which prescribes no inspections or replacements of pipes.

	Optimal heuristic strategy ($\Delta T = 3$[EFPY])		Constrained strategy $\mathcal{S}_{REP}$
p_0 ($\times 10^{-2}$)	Parameters	Expected I&M cost	Expected I&M cost
5.0	$n_I = 0$, $p_{th} = 1$	0	634.6
1.5	$n_I = 152$, $p_{th} = 5.1 \cdot 10^{-7}$	351.4	721.4
1.0	$n_I = 195$, $p_{th} = 5.6 \cdot 10^{-7}$	379.1	840.7
0.5	$n_I = 167$, $p_{th} = 2.0 \cdot 10^{-6}$	399.9	890.7
0.1	$n_I = 147$, $p_{th} = 1.6 \cdot 10^{-4}$	628.5	1137.6

We find that the more stringent the criterion is, the higher the expected cost of the optimized I&M plan from Equation (7.11) and of the constrained strategy $\mathcal{S}_{REP}$. For $p_0 > 1.6 \cdot 10^{-2}$, the non-maintained system complies to the reliability level (see Figure 7.7), thus the optimal I&M costs is 0. For $p_0 < 1.6 \cdot 10^{-2}$, we find that the preventive maintenance planning parameter p_{th} increases with decreasing value of p_0.

Figure 7.9 shows the average annual number of pipe replacements during the service life for the optimized heuristic strategy for $p_0 = 10^{-2}$, as an example. The peak at time $t = 3$yr is due to corrective replacement (and eventual non-compliance of the plant) associated with a rate μ sampled from the tail of the distribution (see Section 7.7.1 above), which can lead to early system failure. This effect is also reflected in the higher failure rate of the non-maintained system in the first years of service, as depicted in Figure 7.7. If the system does not fail in the early years, the number of expected replacements is of the order of magnitude of what is observed in the industry, i.e., that not more than 15 to 20 pipes are replaced, and

that the replacements typically occur at the mid-life of the reactor. In addition, we see that the expected number of preventive replacements is in general higher than that of corrective replacement, which indicates that the optimized strategy is efficient in planning preventive maintenance. The corresponding cost breakdown is displayed in Figure 7.10.

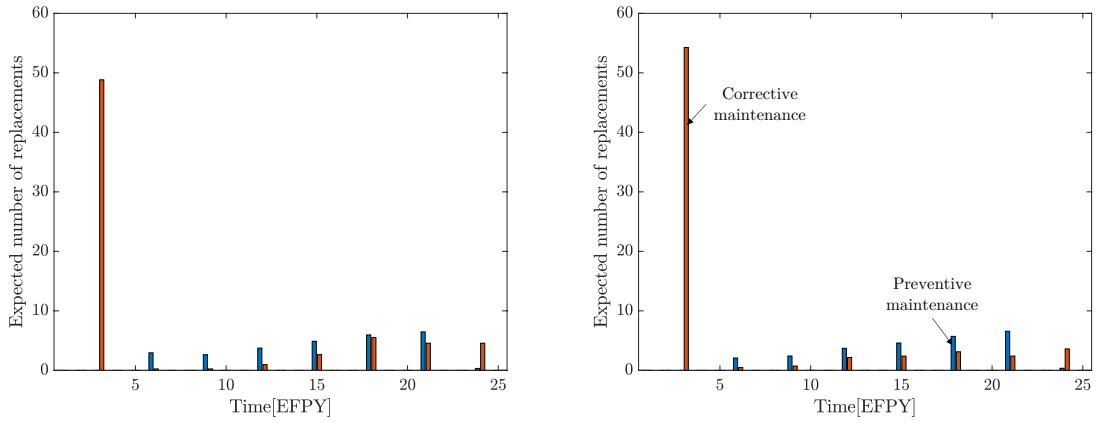

(a) $p_0 = 1.5 \cdot 10^{-2}$ (b) $p_0 = 10^{-2}$

Figure 7.9 Average number of pipes preventively or correctively replaced, following the optimal heuristic strategy found for a) $p_0 = 1.5 \cdot 10^{-2}$ and b) $p_0 = 10^{-2}$. The initial peak of pipe maintenance is due to the early failure stage identified on Figure 7.7.

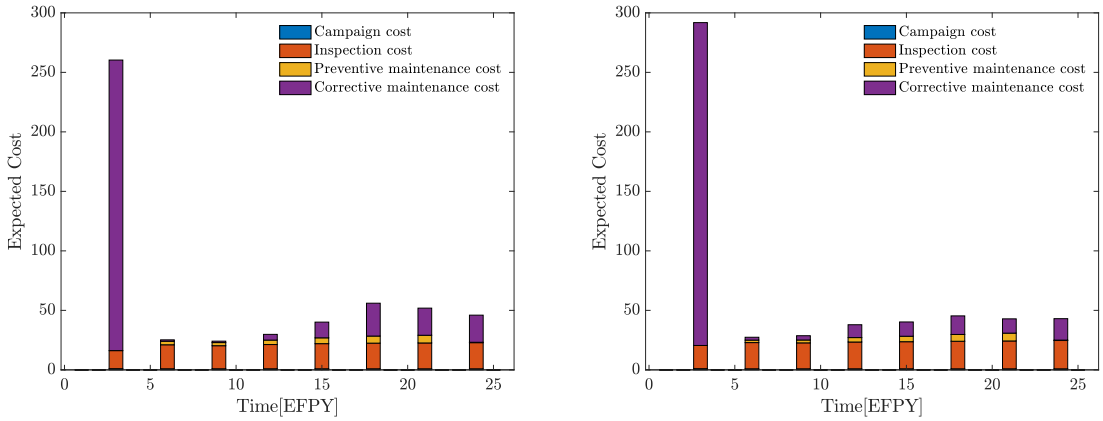

(a) $p_0 = 1.5 \cdot 10^{-2}$ (b) $p_0 = 10^{-2}$

Figure 7.10 Undiscounted annual breakdown of the life-cycle I&M costs, for the optimal heuristic strategy found for a) $p_0 = 1.5 \cdot 10^{-2}$ and b) $p_0 = 10^{-2}$.

We can compare these costs and actions with the constrained representative strategy $\mathcal{S}_{REP}$, shown in Figure 7.11. This shows that this strategy does not efficiently plan for preventive maintenance. This can also be due to the fact that the pipes inspected are not optimally selected to reduce the uncertainty in the deterioration rate. The strategy $\mathcal{S}_{REP}$ performs much worse than the optimized heuristic strategies but can be improved by adapting the selection rules as per the heuristic.

Heuristic A also allows one to vary the campaign interval ΔT. The resulting optimal heuristic parameters are given in Table 7.4. The added freedom of varying parameter ΔT yields lower

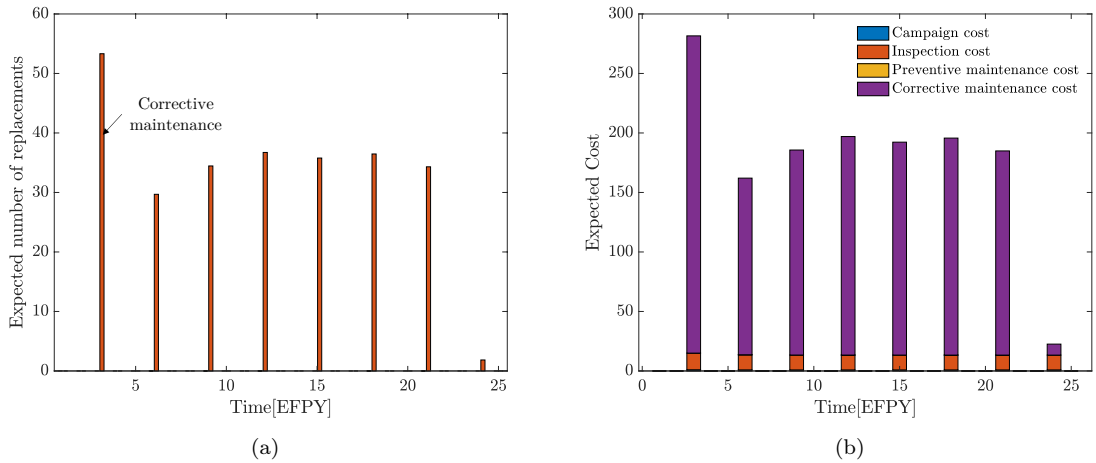

Figure 7.11 a) Average number of pipes preventively or correctively replaced for constrained strategy $\mathcal{S}_{REP}$ for $p_0 = 10^{-2}$. b) Undiscounted annual breakdown of the life-cycle I&M costs, for the optimal heuristic strategy found for $p_0 = 10^{-2}$.

optimal expected costs than those found in Table 7.3. We identify a clear trend on the optimal interval ΔT, which decreases with decreasing p_0. This is not surprising, as a more stringent reliability criterion will warrant more frequent inspections. The optimal value for p_{th} follows the trend identified above for fixed ΔT. For $p_0 = 1.5 \cdot 10^{-2}$, we note that the strategy recommends to inspect in fact almost all pipes once during the service life.

Table 7.4 Optimized heuristic parameters n_I, p_{th} and I&M campaign interval ΔT. For each value of p_0, the obtained optimal expected cost is lower than that calculated for fixed $\Delta T = 3$yr in Table 7.3.

	Optimal heuristic strategy (varying ΔT)	
p_0 ($\times 10^{-2}$)	Parameters	Expected I&M cost
1.5	$n_I = 349$, $p_{th} = 7.9 \cdot 10^{-12}$, $\Delta T = 18$	258.7
1.0	$n_I = 119$, $p_{th} = 2.5 \cdot 10^{-7}$, $\Delta T = 4$	377.5
0.5	$n_I = 117$, $p_{th} = 7.0 \cdot 10^{-6}$, $\Delta T = 2$	392.7
0.1	$n_I = 144$, $p_{th} = 2.9 \cdot 10^{-1}$, $\Delta T = 2$	540.6

7.7.6. Sensitivity of expected cost to the heuristic parameters

Here, we investigate the shape of the expected life-cycle I&M cost function for Heuristic A over the domain of parameters n_I and p_{th}, with fixed $\Delta T = 3$yr, for $p_0 = 10^{-2}$. To do so, we estimate the expected cost with Equation (7.9) and $n_{MC} = 1000$ sample histories for heuristic strategies defined by the pair (n_I,p_{th}) on a 408-point grid over the domain $p_{th} \in [10^{-16}, 1]$ and $n_I \in [0, 480]$. The estimation of the cost thus obtained at each point is not exact with a standard error of $4 - 7\%$, hence, we fit a Gaussian process to the 408 estimated values to obtain a surrogate of the cost function. The resulting Gaussian field provides the predicted expected cost at for each parameter value set.

Figure 7.12a depicts the resulting Gaussian field and the predicted expected life-cycle I&M cost for any pair (n_I, p_{th}).

The surrogate of the expected cost function thus obtained confirms the location of the optimum

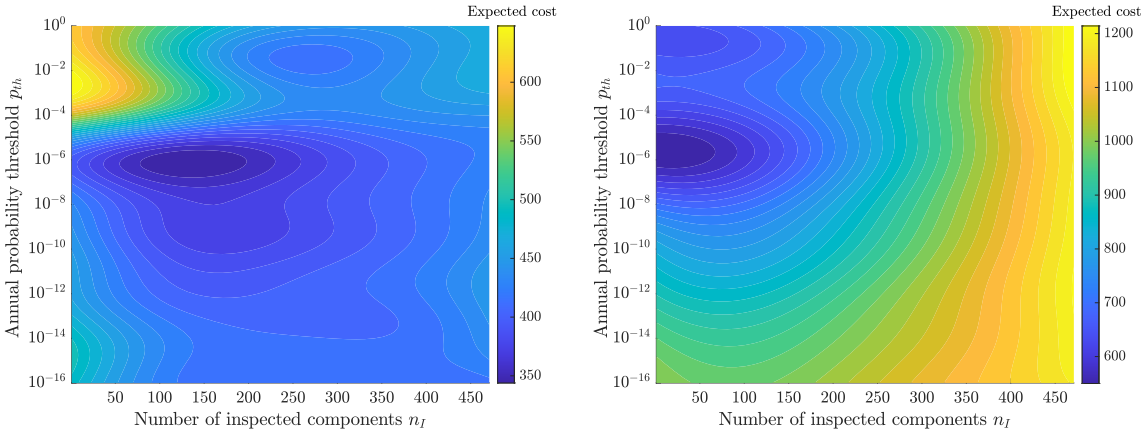

Figure 7.12 Expected I&M life-cycle cost in function of p_{th} and n_I, parameters of Heuristic A, for $p_0 = 10^{-2}$. The cost function is estimated by fitting a Gaussian process to values estimated with Equation (7.9) and $n_{MC} = 1000$, at 408 grid points with coordinates $p_{th} \in \{10^{-16}, 10^{-15}, ..., 10^{0}\}$ and $n_I \in \{20, 40, 60, ..., 480\}$. (a) for the cost model of Table 7.2; (b) with increased unit inspection cost $c_I = 0.5$.

point found with the CE method (Table 7.3). It should be noted that finding the optimal heuristic parameter values by fitting a Gaussian process to point estimates arranged in a grid here has 20 times the computation cost of the CE optimization method. The more efficient combination of the two methods suggested in Chapter 6 can be applied instead.

We observe that in the vicinity of the found optimum, the expected cost is not highly sensitive to the number of pipes to be inspected at each campaign, n_I. This can reflect two things: first, the cost of pipe inspection is low compared to the cost of maintenance, therefore a variation of the order of 50 pipes inspected does not significantly affect the expected cost; second, the optimal number of inspected pipes is related to the amount of information that is provided by inspecting an additional pipe, which is in turn related to the efficiency of the inspection rule. This low sensitivity to the number of pipes inspected is also observed in Table 7.3.

It is also possible to see the effect of the cost parameters on the resulting expected cost function and optimal heuristic parameters. We increase 5-fold the unit cost of inspection, such that $c_I = 0.5$, and the expected life-cycle costs are evaluated again by applying Equation (7.9) with the modified cost parameters. A Gaussian process is fitted again to the 408 grid points. The resulting Gaussian field is depicted in Figure 7.12b. The effect of a higher inspection cost can be seen in the lower optimal parameter value of n_I, and an increased sensitivity to n_I and p_{th}.

7.7.7. Effect of the prior

We investigate the sensitivity of the expected cost and optimal heuristic parameters to the choice of the prior. More specifically, we modify the distribution of μ such that the c.o.v. is reduced to 20% from 100%. The failure rate for the non-maintained system is depicted in Figure 7.13. We note that the curve does not possess a bathtub curve shape as in Figure 7.7.

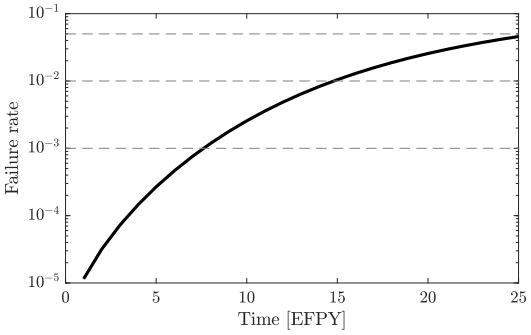

Figure 7.13 Failure rate for the non-maintained, non-inspected system, with a modified prior where the c.o.v of μ is 20%. The levels $\{0.1, 1.0, 5.0\} \cdot 10^{-2}$ are also indicated.

We evaluate strategy $\mathcal{S}_{REP}$ and optimize the heuristic parameters with fixed $\Delta T = 3$yr.

Table 7.5 Results for modified prior.

	Optimal heuristic strategy		Constrained strategy $\mathcal{S}_{REP}$
p_0 ($\times 10^{-2}$)	Parameters	Expected I&M cost	Expected I&M cost
5.0	$n_I = 0$, $p_{th} = 1$	0	315.7
1.0	$n_I = 122$, $p_{th} = 1.1 \cdot 10^{-2}$	190	744.4
0.1	$n_I = 154$, $p_{th} = 1.4 \cdot 10^{-6}$	214.9	1773.4

The expected number of pipe replacement and expected annual life-cycle I&M cost for the optimized strategy and the constrained strategy $\mathcal{S}_{REP}$ are detailed in Figure 7.14. For $p_0 = 10^{-2}$, we note that the optimal heuristic strategy does not plan for preventive maintenance and relies only on corrective maintenance to maintain the reliability level. This balance is likely to change with a different cost model. It also shows that the heuristic chosen might not be appropriate for this reliability level.

For lower $p_0 = 10^{-3}$, the heuristic strategy is efficient in collecting information about the system and planning preventive maintenance. The constrained representative strategy $\mathcal{S}_{REP}$ performs noticeably worse. This can be attributed to the fact that it does not allow for more than 140 pipes to be inspected, regardless of the condition of the system, and therefore fails to reduce the uncertainty about the state of the system.

7.8. Summary

In this study, we propose a reliability-based planning framework to improve standard I&M plans for nuclear feeder piping systems. This framework provides the means to assess the performance of any given I&M strategy under a specified reliability constraint. It does not require the consequences of failure to be explicitly quantified, which makes it suitable for applications in NPP maintenance. Additionally, a heuristic description of the I&M strategies can be chosen, which opens the possibility to explore different decision rules and to integrate regulatory constraints.

The framework includes a probabilistic predictive model for the deterioration process at the

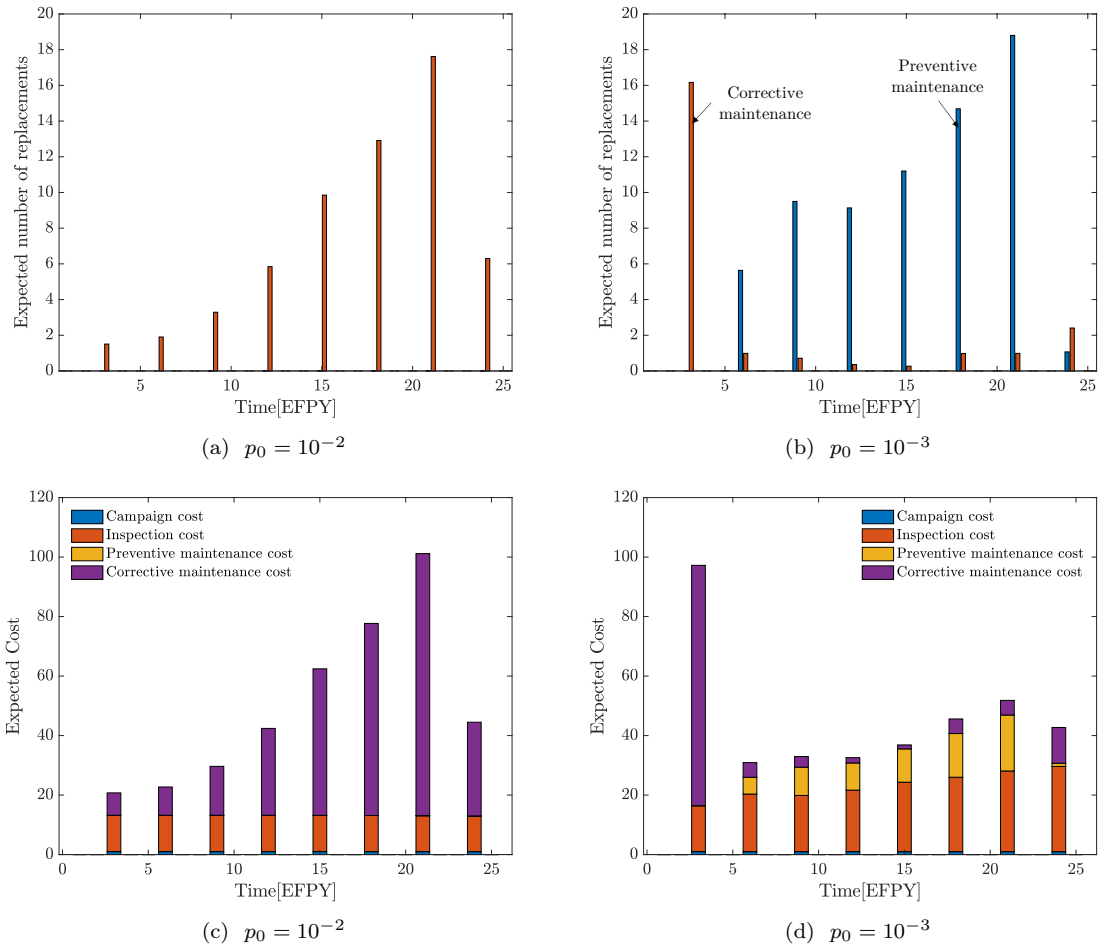

(a) $p_0 = 10^{-2}$ (b) $p_0 = 10^{-3}$

(c) $p_0 = 10^{-2}$ (d) $p_0 = 10^{-3}$

Figure 7.14 Top: Average number of pipes preventively or correctively replaced, following the optimal heuristic strategy found for (a) $p_0 = 10^{-2}$ and (b) $p_0 = 10^{-3}$. The initial peak of pipe maintenance is due to the early failure stage identified on Figure 7.7. Bottom: Undiscounted annual breakdown of the life-cycle I&M costs, for the optimal heuristic strategy found for (c) $p_0 = 10^{-2}$ and (d) $p_0 = 10^{-3}$.

pipe level, with which the piping system reliability can be evaluated over time, including all the past inspection outcomes and maintenance actions.

The numerical application shows that integrating reliability computations in the decision process leads to better decisions and lower life-cycle I&M expected cost, compared to a strategy based on a deterministic prediction model.

This study shows that the choice of a cost model influences the outcome of strategy assessment and optimization. Other aspects must be considered by the analyst for the implementation of this reliability-based planning and optimizing framework in practice, such as the fact that the uncertainty in the model affects the outcome of the assessment and heuristic optimization. The values of the prior model parameters can be calibrated based on expert knowledge and similar plant data. This uncertainty in the model parameters can be also addressed through adaptive planning (see Section 3.3), whereby the heuristic I&M plan is modified as new information through inspections and monitoring becomes available. The effect of information gain on the improved strategy will be considered in future research.

The deterioration model can be altered to reflect various probabilistic dependence structures. Here, the model for FAC assumes a constant mean deterioration rate μ across all pipes and enables the evaluation of the system reliability at a low computational cost. Plant data suggest that there are lead feeders in which the deterioration rate is higher than for other pipes (Hazra et al., 2020a). This is likely due to geometry aspects, which are not considered here. A future improvement of this framework will include the efficient modeling of pipe groups with correlated wear rates, and will integrate uncertainty on the measurement data. Increasing the complexity of the deterioration and observation models comes at a cost, since the generation of a sample I&M history requires the system reliability to be evaluated at every time step. To ensure the efficient and fast computation of the system reliability, a discretized hierarchical DBN model (see Section 5.4.6) can be utilized to model correlated deterioration rates μ.

Finally, while the presented framework has been developed for a specific type of system and a specific application, it can be extended to systems with different configurations, dependence structures and deterioration processes.

Chapter 8

Conclusion and outlook

8.1. Conclusion

Risk-based and reliability-based inspection and maintenance planning(I&M) for large infrastructure is a challenging problem, in which the expected life-cycle cost of the I&M actions must be balanced against the life-cycle risk of failure, through an appropriate I&M strategy. In Chapter 2, we showed how this problem can be analyzed within the class of stochastic sequential decision problems. Dynamic programming algorithms developed in the 1960s to solve for Markovian decision processes (MDPs), later extended to include uncertainty in the inspection information through partially observable MDPs (POMDPs), provide, in theory, the complete solution of the I&M planning problem. However, the computational complexity increases with the dimensionality of the problem, such that, in general, it is intractable. When the POMDP framework has been applied to I&M planning of civil infrastructure, the studies have either considered the system as a single entity, or, if sub-systems or components were explicitly included, their interaction and interdependence have not been accounted for in order to make the solution computable. These simplifying assumptions (a) limit the type of structures and deterioration that can be modeled, (b) the resulting I&M strategies cannot account for information propagation through the system and (c) these strategies under perform in comparison with the case where components' interdependence is modeled.

In Chapter 3, we presented an integral framework for planning inspections and maintenance actions in deteriorating multi-component systems. The framework, which draws upon earlier works (Luque and Straub, 2016, 2019), for the first time enables such a planning for a general system as a whole. The framework is based on the use of *heuristics* for prescribing inspection and maintenance strategies. The strategy explores a sub-space of all possible strategies described by a few rules (the heuristics) and associated heuristic parameters. The values of these parameters are then optimized, such that the expected total life-cycle cost is minimized.

This heuristic approach only results in an approximately optimal strategy. When new information is available, an improved heuristic may be found, which is more optimal under the a-posteriori model. This motivated us to propose an adaptive approach, in which a new optimal heuristic is identified after inspection results are obtained. As we proved in Section 3.3, this adapted strategy is always at least as good as the original strategy.

The framework relies on explicitly modeling the deterioration process at component level and on including the dependencies among multiple components. The structure of the probabilistic

model proposed in Chapter 5 accounts for the interaction among the components within the structural system and their effect on the system reliability. We highlighted in particular the advantages and limitations of using a hierarchical dynamic Bayesian network (DBN) model. With such a model, the framework propagates the information collected at individual component inspections, according to the considered I&M strategy, to the rest of the system.

In general, the proposed approach is flexible with respect to adding new heuristic rules and parameters, for instance to include operational constraints (e.g., constant inspection intervals) or to comply with fixed reliability criteria as illustrated in Chapter 7. While there is no guarantee that any given heuristic is optimal, the computed expected total life-cycle cost allows to select the best heuristic among the investigated ones. Hence, the more heuristics are investigated, the better. In addition, the framework enables the evaluation of the expected total life-cycle cost of any given strategy, which may be preferred by the operator and can be then compared to the resulting optimal heuristic strategy.

This flexibility constitutes a significant advantage over traditional POMDP approaches. The heuristic strategies explored are interpretable, in the sense that the I&M actions are prescribed following explicit rules, which the operator can understand and, in turn, control and influence. This interpretability is maintained by a dichotomy characteristic of the heuristic philosophy: The chosen heuristic should be designed to approximate the theoretical optimal I&M strategy, while remaining simple enough (i.e., with a reasonable number of rules and parameters) to be accessible and understandable.

The heuristic approach provides valuable insights into the maintainability of a system with regards to the deterioration processes, the associated uncertainties and the costs of inspection and mitigating actions. The flexibility in the heuristic description led us to identify a proxy for the value of information (VoI) of inspecting a component, which combines the importance of the component towards the reliability of the system with its probability of failure.

The numerical investigations demonstrated that the proposed heuristic I&M planning framework is applicable to large systems. Two case studies were presented: an offshore support structure subject to fatigue (Chapter 6); and the feeder piping system of a nuclear power plant subject, where the thickness of its 480 pipes decrease due to flow-accelerated corrosion (Chapter 7).

In the numerical investigations, we did not include model uncertainty with regards to the inspection likelihood. In both case studies, we considered standard non-destructive evaluation (NDE) techniques, and we assumed either no measurement error (Chapter 7) or we adopted standard likelihood function, which we found in the literature to be typical of the considered NDE method (Chapter 6). However, the quality and the interpretation of the information collected is key to the optimality of an I&M strategy, and this led us to research and analyze the context in which models of NDE quality are developed. We reviewed in Chapter 4 the main types of models of NDE quality and interpreted them, for the first time, within a unifying framework. This study revealed that experimental design can hide important information about the quality of the NDE method and that the resulting model (a PoD or ROC curve) can

misrepresent the performance and reliability of NDE. Through VoI analysis, we also illustrated how data interpretation affects the optimal decision process.

8.2. Originality of work

The original material presented in this thesis includes:

- A rigorous formulation of the decision problem with heuristic parametrization for I&M planning problems.
- An extension to include adaptive planning, as well as the proof of strategy improvement.
- The definition of a new proxy for the VoI of component inspection, the Prioritization Index, for multi-component systems.
- The development, extension and parallelization of an algorithm for Bayesian inference and time-variant reliability evaluation with a hierarchical DBN.
- The adaptation and tuning of the cross-entropy method for the noisy optimization of the expected life-cycle cost of an I&M strategy.
- A sensitivity analysis of heuristic and cost parameters on the optimality of an I&M strategy using Gaussian process regression to obtain a surrogate of the expected cost of a strategy as a function of the heuristic parameter values.
- A unifying framework for models of NDE quality and recommendations on the way they should be learned, calibrated, and applied.
- A reliability-based planning framework incorporating the reliability constraints in the chosen heuristics. This framework includes the evaluation of any given strategy under a reliability constraint. It does not require the consequences of system failure to be quantified.

8.3. Outlook

There are still challenges to the application of the proposed framework in practice. Aside from the limitations mentioned in the above sections and chapters, the optimization problem is only meaningful when reasonable cost estimations for the mitigating actions and consequences of failure are available, which is difficult because of the lack of data (Schöbi and Chatzi, 2016). While a reliability-based approach offers a way to get around evaluating the cost of failure, this challenge highlights the need to implement an industry-wide data sharing scheme. Alternatively, this framework can be utilized to investigate the sensitivity of the optimized I&M heuristic strategy to these costs.

In Chapter 3, we provided starting points for defining suitable heuristics for I&M planning. A systematic, parametric study investigating the suitability of different inspection and repair rules in different systems could lead to improved recommendations on heuristic choice, such

that the strategies explored are close to the optimal strategy. In particular, these heuristics could account for varying costs of inspection among components, or non-equi-correlated deterioration processes, such that the information obtained on one component and its impact on the reduction of uncertainty in other components is reflected in a modified proxy for the VoI.

An extension of the DBN framework to include component-level monitoring data seems straightforward, as long as a Bayesian analysis of the structural system with the monitoring data is possible. Monitoring data can then be treated in the same way as inspection data. With such an extension, the framework can be utilized to optimize monitoring systems. One of the main limitations of the DBN model explicitly representing a multi-component system for time-variant reliability analysis is the need to fully define the functional relationship between the states of the system and its components. Preliminary works by Straub and Der Kiureghian (2011) and Mendoza et al. (2022) could open the way to a concise representation of larger systems, which still accounts for component interdependence and their effect on the system reliability.

The optimization methods applied in this work to heuristic I&M planning have not been formally analyzed in terms of their convergence properties. In this field, alternative methods are being investigated specifically for the I&M planning problem (Holdorf Lopez et al., 2022).

Finally, it is undeniable that the optimization capabilities of deep reinforcement learning (RL) for complex sequential decision problems with high dimensions will expand in the coming decade. As forecasted in numerous studies (e.g., Andriotis and Papakonstantinou, 2019), deep RL algorithms will be able to handle I&M planning for large infrastructure. The optimal strategies will be able to finely react to information collected on the components, the environment, and even live input from the operator. However, strategies produced by such algorithms will almost certainly escape the understanding of the analyst, of the decision-maker and of the operator. This will feed skepticism towards the capability of these advanced methods, in the same way that Bellman (1958) does not agree that a computer can "think and create". This misunderstanding between the machine, which does not justify its prompts, and the human will need to be bridged by an interface, such that optimized strategies are not only generated, but also explained. To that aim, the heuristic approach can provide the structure to extract features from the deep RL strategies and link them to the characteristics of the planning problem, in analogy with the finite-state-controller extraction implemented by Kaelbling et al. (1998). In this manner, the underlying mechanisms of complex, POMDP-oriented strategies obtained with deep RL will be revealed and explained. This will ensure that expert knowledge is still relevant and validated through heuristic-enhanced problem solving (see Simon and Newell (1958)), and that trust towards artificial intelligence is fostered.

Part III.

Appendices

Appendix A

Prioritization Index for component inspection

This appendix can also be found in Bismut, E. and Straub, D. (2021). "Optimal adaptive inspection and maintenance planning for deteriorating structural systems". In: *Reliability Engineering & System Safety* 215, p. 107891.

This section outlines the reasoning behind the expression for the Prioritization Index (PI) in Equation (3.8), proposed as a proxy for the VoI. Here F_s is used to denote the interval failure event F_i^* for a given time step i. The following derivations omit the conditioning on $\boldsymbol{Z}_{1:i-1}$. The SEI_k are nonetheless independent of any observation, by definition. We express the certain event as $\{\Omega\} = \{\{F_{c_1} \cup \overline{F_{c_1}}\} \cap ... \cap \{F_{c_N} \cup \overline{F_{c_N}}\}\}$, and obtain that

$$\begin{aligned}\Pr(F_s) = &\ \Pr(F_s \cap \{\{F_{c_1} \cup \overline{F_{c_1}}\} \cap ... \cap \{F_{c_N} \cup \overline{F_{c_N}}\}\}) \\ &= \Pr(F_s, \overline{F_{c_1}}, \dots, \overline{F_{c_N}}) + \Pr(F_s, F_{c_1}, \overline{F_{c_2}}, \dots, \overline{F_{c_N}}) + \Pr(F_s, \overline{F_{c_1}}, F_{c_2}, \dots \overline{F_{c_N}}) \\ &+ \dots + \Pr(F_s, \overline{F_{c_1}}, \overline{F_{c_2}}, \dots, \overline{F_{c_{N-1}}}, F_{c_N}) + \sum_{\mathcal{J}} \Pr(F_s, F_{c_\mathcal{J}} \cap \overline{F_{c_{\setminus \mathcal{J}}}})\end{aligned} \tag{A.1}$$

The last term in Equation (A.1) corresponds to the joint probabilities of F_s and failed components belonging to the subsets $\mathcal{J}$ of $\{1..N\}$, with $|\mathcal{J}| \geq 2$.

By introducing conditional probabilities and writing $a = \Pr(F_s|\overline{F_{c_1}}, \dots, \overline{F_{c_N}})$, the probability of failure of the system is

$$\begin{aligned}\Pr(F_s) = &\ a \cdot \Pr(\overline{F_{c_1}}, \dots, \overline{F_{c_N}}) + \Pr(F_s|F_{c_1}, \overline{F_{c_2}}, \dots, \overline{F_{c_N}}) \cdot \Pr(F_{c_1}, \overline{F_{c_2}}, \dots, \overline{F_{c_N}}) + \dots \\ &+ \Pr(F_s|\overline{F_{c_1}}, \overline{F_{c_2}}, \dots, F_{c_N}) \cdot \Pr(\overline{F_{c_1}}, \overline{F_{c_2}}, \dots, F_{c_N}) + \sum_{\mathcal{J}} \Pr(F_s|F_{c_\mathcal{J}} \cap \overline{F_{c_{\setminus \mathcal{J}}}}) \cdot \Pr(F_{c_\mathcal{J}} \cap \overline{F_{c_{\setminus \mathcal{J}}}})\end{aligned} \tag{A.2}$$

From Equation (3.7), we have that $\Pr(F_s|\overline{F_{c_1}}, \dots, \overline{F_{c_{k-1}}}, F_{c_k}, \overline{F_{c_{k+1}}}, \dots, \overline{F_{c_N}}) = a + SEI_k$, and similarly we can express each $\Pr(F_s|F_{c_\mathcal{J}} \cap \overline{F_{c_{\setminus \mathcal{J}}}}) = a + MEI_\mathcal{J}$, where $MEI_\mathcal{J}$ is the multiple elements importance of components in $\mathcal{J}$. By factorizing a, we obtain Equation (A.3):

$$\Pr(F_s) = a + SEI_1 \cdot \Pr(F_{c_1}, \overline{F_{c_2}}, ..., \overline{F_{c_N}}) + ... + SEI_N \cdot \Pr(\overline{F_{c_1}}, \overline{F_{c_2}}, ..., F_{c_N}) + b, \tag{A.3}$$

where b represents the contribution of simultaneous component failure. Equation (A.4) introduces the marginal probabilities of component failure:

$$\begin{aligned}\Pr(F_s) = &\ a + SEI_1 \cdot \Pr(F_{c_1}) \cdot \Pr(\overline{F_{c_2}}, ..., \overline{F_{c_N}}|F_{c_1}) + ... \\ &+ SEI_N \cdot \Pr(F_{c_N}) \cdot \Pr(\overline{F_{c_1}}, ..., \overline{F_{c_{N-1}}}|F_{c_N}) + b.\end{aligned} \tag{A.4}$$

From Equation (A.4), we approximate $\Pr(F_s)$ with

$$\Pr(F_s) \simeq a + SEI_1 \cdot \Pr(F_{c_1}) + ... + SEI_N \cdot \Pr(F_{c_N}) + b, \tag{A.5}$$

Equation (A.5) is not actually used to calculate the interval failure probability of the system, $\Pr(F_i^*)$, but shows that the probability of system failure is a function of the terms $SEI_k \cdot \Pr(F_{c_k})$ defined for each component, hence by the VoI for component k is a linear function of $SEI_k \cdot \Pr(F_{c_k})$. Furthermore, the amount of information learned on other components is related to the probability of failure $\Pr(F_{c_k})$, through the components' interdependence.

Appendix B

Estimation of the annual risk of failure

This appendix can also be found in Bismut, E. and Straub, D. (2021). "Optimal adaptive inspection and maintenance planning for deteriorating structural systems". In: *Reliability Engineering & System Safety* 215, p. 107891.

The efficiency of the optimization method described in Section 3.2 depends on the sampling uncertainty of the expectation with MCS (Equation (3.17)), with $n_{MC} = 1$ as the limiting case.

In theory, Equation (3.13) coupled with Equation (3.17), implies that the probabilities at every time step should be conditioned on the full observation history $\boldsymbol{Z}_{1:n_T}$, which includes the future inspection outcomes. In this section, we show that one can replace the smoothed probability $\Pr(F_i|\boldsymbol{w}, \boldsymbol{Z}_{1:n_T})$ in Equation (3.13) by the filtered probability $\Pr(F_i|\boldsymbol{w}, \boldsymbol{Z}_{1:i-1})$ when estimating the expected risk of failure. Furthermore, we show that the corresponding MC estimator of the risk has a smaller sample variance.

We consider the actions that affect the system reliability $\boldsymbol{A} = \{A_1 ... A_{n_T}\}$ during the service life, such as repair or other maintenance actions. In this derivation, we consider only deterministic policies, insofar the actions are deterministic for given inspection history $\boldsymbol{Z}_{1:n_T}$ and strategy $\mathcal{S}_{\boldsymbol{w}}$, i.e., $\boldsymbol{A} = \boldsymbol{A}(\boldsymbol{w}, \boldsymbol{Z}_{1:n_T})$. Here we explicitly include them in the expression of the expected cumulative probability of failure:

$$\mathbf{E}_{\boldsymbol{Z}_{1:n_T}}\left[\Pr(F_i|\boldsymbol{w}, \boldsymbol{Z}_{1:n_T})\right] = \mathbf{E}_{\boldsymbol{Z}_{1:n_T}}\left[\Pr(F_i|\boldsymbol{A}(\boldsymbol{w}, \boldsymbol{Z}_{1:n_T}), \boldsymbol{w}, \boldsymbol{Z}_{1:n_T})\right] \tag{B.1}$$

We recall two key principles in a sequential decision process. Firstly, a policy at time step i that assigns an action A_i can only consider information $\boldsymbol{Z}_{1:i}$ about the system up to that time, or in other terms, decisions cannot be based on specific knowledge acquired in the future, i.e., $A_i = A_i(\boldsymbol{w}, \boldsymbol{Z}_{1:i})$. Secondly, the cumulative failure event F_i never depends on the actions after time step i, $\boldsymbol{A}_{i:n_T}$, neither unconditionally nor conditionally on $\boldsymbol{Z}_{1:n_T}$. Hence, we obtain Equation (B.2):

$$\mathbf{E}_{\boldsymbol{Z}_{1:n_T}}\left[\Pr(F_i|\boldsymbol{w}, \boldsymbol{Z}_{1:n_T})\right] = \mathbf{E}_{\boldsymbol{Z}_{1:n_T}}\left[\Pr(F_i|\boldsymbol{A}_{1:i-1}(\boldsymbol{w}, \boldsymbol{Z}_{1:i-1}), \boldsymbol{w}, \boldsymbol{Z}_{1:n_T})\right] \tag{B.2}$$

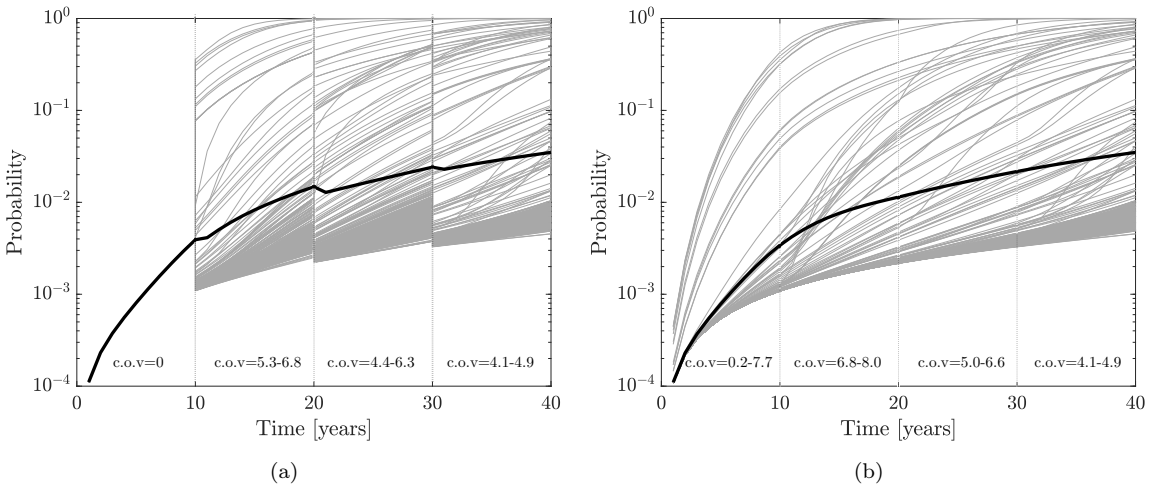

Figure B.1 Strategy defined by $\boldsymbol{w} = \{\Delta T = 10, p_{th} = 1, n_i = 5, \eta = 1, D_{rep} = \infty\}$: the components are inspected but never repaired. (a): Filtered conditional probability of failure $\Pr(F_i|\boldsymbol{w}, \boldsymbol{Z}_{1:i-1})$ for 500 sample histories $\boldsymbol{z}^{(q)}$, and resulting mean (bold line); (b) Smoothed conditional probability of failure $\Pr(F_i|\boldsymbol{w}, \boldsymbol{Z}_{1:n_T})$ for 500 sample histories $\boldsymbol{z}^{(q)}$, and resulting mean (bold line). The estimated range of the coefficient of variation (c.o.v) is indicated for each decade.

From there, we can split the expectation of the right-hand term of Equation (B.2):

$$\begin{aligned}\mathbf{E}_{\boldsymbol{Z}_{1:n_T}}\left[\Pr(F_i|\boldsymbol{w}, \boldsymbol{Z}_{1:n_T})\right] &= \mathbf{E}_{\boldsymbol{Z}_{1:i-1}}\left[\mathbf{E}_{\boldsymbol{Z}_{i:n_T}|\boldsymbol{Z}_{1:i-1}}\left[\Pr(F_i|\boldsymbol{A}_{1:i-1}(\boldsymbol{w}, \boldsymbol{Z}_{1:i-1}), \boldsymbol{w}, \boldsymbol{Z}_{1:i-1}, \boldsymbol{Z}_{i:n_T})\right]\right] \\ &= \mathbf{E}_{\boldsymbol{Z}_{1:i-1}}\left[\Pr(F_i|\boldsymbol{A}_{1:i-1}(\boldsymbol{w}, \boldsymbol{Z}_{1:i-1}), \boldsymbol{w}, \boldsymbol{Z}_{1:i-1})\right].\end{aligned} \tag{B.3}$$

Finally we obtain,

$$\mathbf{E}_{\boldsymbol{Z}_{1:n_T}}\left[\Pr(F_i|\boldsymbol{w}, \boldsymbol{Z}_{1:n_T})\right] = \mathbf{E}_{\boldsymbol{Z}_{1:i-1}}\left[\Pr(F_i|\boldsymbol{w}, \boldsymbol{Z}_{1:i-1})\right]. \tag{B.4}$$

Therefore for a sample observation history $\mathbf{z}_{1:n_T}$, the conditional filtered probability, $\Pr(F_i|\boldsymbol{w}, \mathbf{z}_{1:i-1})$, and the smoothed probability, $\Pr(F_i|\boldsymbol{w}, \mathbf{z}_{1:n_T})$, are two valid unbiased estimators of the expected value $\mathbf{E}_{\boldsymbol{Z}_{1:n_T}}\left[\Pr(F_i|\boldsymbol{w}, \boldsymbol{Z}_{1:n_T})\right]$. Furthermore, Equation (B.3) shows that the filtered probability is equal to the expectation of the smoothed probability over the inspection results $\boldsymbol{Z}_{i:n_T}$. This implies that the filtered probability is an estimator with a smaller variance than the smoothed probability, hence, is better suited as estimator of the noisy objective function in the optimization method described in Section 3.2.

To illustrate this effect, we consider the case study investigated in Chapter 6. The variances of these two estimators and the standard error of the mean are compared for the I&M strategies that prescribe only inspections but no repair or maintenance actions to be carried out, i.e., for any $\boldsymbol{Z}_{1:n_T}$, and at any time step i, $A_i(\boldsymbol{Z}_{1:i})$ = "do nothing". For instance, the strategy parametrized by $\boldsymbol{w} = \{\Delta T = 10, p_{th} = 1, n_i = 5, \eta = 1, D_{rep} = \infty\}$ satisfies this condition. The expectations $\mathbf{E}_{\boldsymbol{Z}_{1:i-1}}\left[\Pr(F_i|\boldsymbol{w}, \boldsymbol{Z}_{1:i-1})\right]$ and $\mathbf{E}_{\boldsymbol{Z}_{1:n_T}}\left[\Pr(F_i|\boldsymbol{w}, \boldsymbol{Z}_{1:n_T})\right]$ are equal to $\Pr(F_i)$ calculated with the prior model assumptions. The variance of these estimators is evaluated

for the numerical application described in Chapter 6, with $n_{MC} = 500$ sample histories (see Figure B.1).

The variance of the smoothed estimator is indeed larger than of the filtered estimator: for the times between 1 and 10 years, the filtered estimator is exact, and the coefficient of variation of the smoothed estimator is of the order of 500%. For the subsequent time steps, up to year 30, the coefficient of variation of the smoothed estimator is up to 1.3 times that of the filtered estimator.

Appendix C

Solution of the two-step decision problem

This appendix constitutes the supplemental material of Bismut, E. and Straub, D. (2022). "A unifying review of NDE models towards optimal decision support". In: *Structural Safety* 97, p. 102213.

C.1. A priori optimal actions

There are four possible courses of action (A_1, A_2). We compute the four corresponding expected costs $\mathbf{E}[C_T(A_1, A_2, e_0)]$. We use the notation: $\Pr(Y_1 = 1) = p'_{Y_1}$.

$$\mathbf{E}[C_T(a_0, a_0, e_0)] = c_F \left\{ p'_{Y_1} [1 + \Pr(Y_2 = 1|Y_1 = 1)] + (1 - p'_{Y_1}) \Pr(Y_2 = 1|Y_1 = 0) \right\} = \text{€}12.25 \text{ million}. \tag{C.1}$$

$$\mathbf{E}[C_T(a_R, a_0, e_0)] = c_R + c_F \Pr(Y_2 = 1|Y_1 = 0) = \text{€}7.5 \text{ million}. \tag{C.2}$$

$$\mathbf{E}[C_T(a_0, a_R, e_0)] = c_F p'_{Y_1} + c_R = \text{€}10 \text{ million}. \tag{C.3}$$

$$\mathbf{E}[C_T(a_R, a_R, e_0)] = 2c_R = \text{€}10 \text{ million}. \tag{C.4}$$

Hence, the prior optimal actions are to first repair and then do nothing, $(A_1, A_2)_{e_0} = (a_R, a_0)$.

C.2. A posteriori optimal actions considering the continuous signal

Because the number of states of $Y_{1,2}$ and $Y'_{1,2}$ and the number of decision opportunities is small, we resolve the decision problem at the belief space level (see Figure C.1). We use the following notations: $\Pr(Y_1 = 1|S_1) = p''_{Y_1}$, $\Pr(Y'_1 = 1|S_1, A_1) = p_{Y'_1}$, $\Pr(Y_2 = 1|S_1, A_1) = p'_{Y_2}$, and $\Pr(Y_2 = 1|S_1, S_2, A_1) = p''_{Y_2}$.

We first determine the transition function between p''_{Y_1} and p''_{Y_2}. Applying Bayes' theorem,

$$p''_{Y_1} = \frac{f_{S_1|Y_1=1}(S_1) p'_{Y_1}}{f_{S_1|Y_1=1}(S_1) p'_{Y_1} + f_{S_1|Y_1=0}(S_1)(1 - p'_{Y_1})}. \tag{C.5}$$

The total probability theorem yields

$$p_{Y'_1} = p''_{Y_1} \Pr(Y'_1 = 1|Y_1 = 1, A_1) + (1 - p''_{Y_1}) \Pr(Y'_1 = 1|Y_1 = 0, A_1) = \mathbb{1}_{A_1 = a_0} p''_{Y_1} \tag{C.6}$$

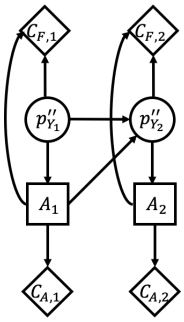

Figure C.1 Equivalent two-step MDP at the belief space level.

and

$$p'_{Y_2} = p_{Y'_1} \Pr(Y_2 = 1|Y'_1 = 1) + (1 - p_{Y'_1}) \Pr(Y_2 = 1|Y'_1 = 0)$$
$$= \mathbb{1}_{A_1=a_0} p''_{Y_1} \Pr(Y_2 = 1|Y'_1 = 1) + (1 - \mathbb{1}_{A_1=a_0} p''_{Y_1}) \Pr(Y_2 = 1|Y'_1 = 0). \tag{C.7}$$

Applying Bayes' theorem,

$$p''_{Y_2} = \frac{f_{S_2|Y_2=1}(S_2) p'_{Y_2}}{f_{S_2|Y_2=1}(S_2) p'_{Y_2} + f_{S_2|Y_2=0}(S_2)(1 - p'_{Y_2})}. \tag{C.8}$$

By combining Equations (C.5) to (C.8), one obtains a relationship between p''_{Y_1} and p''_{Y_2} that explicitly includes the observations $S1$ and $S2$. By taking the expected value with respect to $S1$ and $S2$, one can transform this relationship into a probabilistic one, to find the distribution of p''_{Y_2} conditional on p''_{Y_1} and actions A_1 and A_2.

The conditional distribution of S_2 given A_1 and S_1 is a Gaussian mixture with mixture coefficients p'_{Y_2} and $1 - p'_{Y_2}$. Hence, we can write S_2 as a function of two independent random variables, $U_2 \sim \mathcal{U}(0, 1)$ and $Z_2 \sim \mathcal{N}(0, 1)$, as

$$S_2 = \mathbb{1}_{U_2 > p'_{Y_2}} (\mu_0 + \sigma_0 Z_2) + \mathbb{1}_{U_2 < p'_{Y_2}} (\mu_1 + \sigma_1 Z_2). \tag{C.9}$$

We find the distribution of p''_{Y_2} conditional on p''_{Y_1} given $A_1 = a_0$. For $0 < q < 1$, and given $0 < p_{Y'_2} < 1$, we obtain from Equation (C.8)

$$\Pr(p''_{Y_2} \leq q|p''_{Y_1}, A_1 = a_0) = \Pr\left[f_{S_2|Y_2=1}(S_2) p'_{Y_2}(1 - q) \leq q f_{S_2|Y_2=0}(S_2)(1 - p'_{Y_2})\right]$$
$$= \Pr\left[\frac{f_{S_2|Y_2=1}(S_2)}{f_{S_2|Y_2=0}(S_2)} \frac{p'_{Y_2}(1 - q)}{q(1 - p'_{Y_2})} \leq 1\right]. \tag{C.10}$$

We take the logarithm of the terms of the inequality. After simplification,

$$\Pr(p''_{Y_2} \leq q|p''_{Y_1}, A_1 = a_0) = \Pr\left[\left(\frac{S_2 - \mu_0}{\sigma_0}\right)^2 - \left(\frac{S_2 - \mu_1}{\sigma_1}\right)^2 - 2 \log\left(\frac{\sigma_0}{\sigma_1} \frac{q(1 - p'_{Y_2})}{p'_{Y_2}(1 - q)}\right) \leq 0\right]. \tag{C.11}$$

From Equation (C.9), we can write

$$\left(\frac{S_2-\mu_0}{\sigma_0}\right)^2 = \mathbb{1}_{U_2>p'_{Y_2}} Z_2^2 + \mathbb{1}_{U_2<p'_{Y_2}} \left(\frac{\mu_1-\mu_0}{\sigma_0} + \frac{\sigma_1}{\sigma_0} Z_2\right)^2, \tag{C.12}$$

$$\left(\frac{S_2-\mu_2}{\sigma_2}\right)^2 = \mathbb{1}_{U_2>p'_{Y_2}} \left(\frac{\mu_0-\mu_1}{\sigma_1} + \frac{\sigma_0}{\sigma_1} Z_2\right)^2 + \mathbb{1}_{U_2<p'_{Y_2}} Z_2^2. \tag{C.13}$$

Hence,

$$\begin{aligned}\Pr(p''_{Y_2} \le q | p''_{Y_1}, A_1 = a_0) = \Pr\Bigg[& \mathbb{1}_{U_2>p'_{Y_2}} \frac{1}{\sigma_1^2}\left[(\sigma_1^2-\sigma_0^2)Z_2^2 - 2\sigma_0(\mu_0-\mu_1)Z_2 - (\mu_0-\mu_1)^2\right] \\ & + \mathbb{1}_{U_2<p'_{Y_2}} \frac{1}{\sigma_0^2}\left[(\sigma_1^2-\sigma_0^2)Z_2^2 - 2\sigma_1(\mu_0-\mu_1)Z_2 + (\mu_0-\mu_1)^2\right] \\ & - 2\log\left(\frac{\sigma_0}{\sigma_1}\frac{q(1-p'_{Y_2})}{p'_{Y_2}(1-q)}\right) \le 0\Bigg].\end{aligned} \tag{C.14}$$

As U_2 and Z_2 are independent, we obtain

$$\begin{aligned}&\Pr(p''_{Y_2} \le q | p''_{Y_1}, A_1 = a_0) = \\ &(1-p'_{Y_2}) \Pr\left[\frac{1}{\sigma_1^2}\left((\sigma_1^2-\sigma_0^2)Z_2^2 - 2\sigma_0(\mu_0-\mu_1)Z_2 - (\mu_0-\mu_1)^2\right) - 2\log\left(\frac{\sigma_0}{\sigma_1}\frac{q(1-p'_{Y_2})}{p'_{Y_2}(1-q)}\right) \le 0\right] \\ &+ p'_{Y_2} \Pr\left[\frac{1}{\sigma_1^2}\left((\sigma_1^2-\sigma_0^2)Z_2^2 - 2\sigma_1(\mu_0-\mu_1)Z_2 + (\mu_0-\mu_1)^2\right) - 2\log\left(\frac{\sigma_0}{\sigma_1}\frac{q(1-p'_{Y_2})}{p'_{Y_2}(1-q)}\right) \le 0\right].\end{aligned} \tag{C.15}$$

The roots of the two polynomial expressions in Z_2 of Equation (C.15) are derived. We indicate by index $> p'_{Y_2}$ the quantities referring to the polynomial in the first term and by index $< p'_{Y_2}$ the quantities referring to the polynomial in the second term. We compute the determinants.

$$\Delta_{<p'_{Y_2}} = \frac{4}{\sigma_0^2}\left[(\mu_0-\mu_1)^2 + 2(\sigma_1^2-\sigma_0^2)\log\left(\frac{\sigma_0}{\sigma_1}\frac{q(1-p'_{Y_2})}{p'_{Y_2}(1-q)}\right)\right], \tag{C.16}$$

$$\Delta_{>p'_{Y_2}} = \frac{4}{\sigma_1^2}\left[(\mu_0-\mu_1)^2 + 2(\sigma_1^2-\sigma_0^2)\log\left(\frac{\sigma_0}{\sigma_1}\frac{q(1-p'_{Y_2})}{p'_{Y_2}(1-q)}\right)\right]. \tag{C.17}$$

The polynomials do not admit roots if $\delta(q) = (\mu_0-\mu_1)^2 + 2(\sigma_1^2-\sigma_0^2)\log\left(\frac{\sigma_0}{\sigma_1}\frac{q(1-p'_{Y_2})}{p'_{Y_2}(1-q)}\right) < 0$. Note that when $q \to 0$ or $q \to 1$, $\delta \to \pm\infty$. If $\delta \ge 0$, the two roots $z_a \le z_b$ for each polynomial are

$$z_{a,<p'_{Y_2}} = \frac{\operatorname{sign}(\sigma_1^2-\sigma_0^2)\sigma_1(\mu_0-\mu_1) - \sigma_0\sqrt{\delta}}{|\sigma_1^2-\sigma_0^2|}, \tag{C.18}$$

$$z_{b,<p'_{Y_2}} = \frac{\operatorname{sign}(\sigma_1^2-\sigma_0^2)\sigma_1(\mu_0-\mu_1) + \sigma_0\sqrt{\delta}}{|\sigma_1^2-\sigma_0^2|}, \tag{C.19}$$

$$z_{a,>p'_{Y_2}} = \frac{\operatorname{sign}(\sigma_1^2-\sigma_0^2)\sigma_0(\mu_0-\mu_1) - \sigma_1\sqrt{\delta}}{|\sigma_1^2-\sigma_0^2|}, \tag{C.20}$$

$$z_{b,>p'_{Y_2}} = \frac{\operatorname{sign}(\sigma_1^2 - \sigma_0^2)\sigma_0(\mu_0 - \mu_1) + \sigma_1\sqrt{\delta}}{|\sigma_1^2 - \sigma_0^2|}. \tag{C.21}$$

Finally,

$$\begin{aligned}\Pr(p''_{Y_2} \leq q | p''_{Y_1}, A_1 = a_0) = \mathbb{1}_{\delta\geq 0}\Bigg\{(1-p'_{Y_2})\Bigg(\mathbb{1}_{\sigma_1<\sigma_0} + \operatorname{sign}(\sigma_1^2-\sigma_0^2)\left[\Phi\left(z_{b,>p'_{Y_2}}\right) - \Phi\left(z_{a,>p'_{Y_2}}\right)\right]\Bigg) \\ + p'_{Y_2}\Bigg(\mathbb{1}_{\sigma_1<\sigma_0} + \operatorname{sign}(\sigma_1^2-\sigma_0^2)\left[\Phi\left(z_{b,<p'_{Y_2}}\right) - \Phi\left(z_{a,<p'_{Y_2}}\right)\right]\Bigg)\Bigg\} \\ + \mathbb{1}_{\delta<0}\mathbb{1}_{\sigma_1<\sigma_0},\end{aligned} \tag{C.22}$$

where $\Phi(.)$ denotes the standard normal CDF. This reduces to

$$\begin{aligned}\Pr(p''_{Y_2} \leq q | p''_{Y_1}, A_1 = a_0) = \mathbb{1}_{\sigma_1<\sigma_0} + \mathbb{1}_{\delta\geq 0}\operatorname{sign}(\sigma_1^2-\sigma_0^2)\Bigg\{(1-p'_{Y_2})\left[\Phi\left(z_{b,>p'_{Y_2}}\right) - \Phi\left(z_{a,>p'_{Y_2}}\right)\right] \\ + p'_{Y_2}\left[\Phi\left(z_{b,<p'_{Y_2}}\right) - \Phi\left(z_{a,<p'_{Y_2}}\right)\right]\Bigg\}.\end{aligned} \tag{C.23}$$

The conditional probability density function of p''_{Y_2} is obtained by differentiating $\Pr(p''_{Y_2} \leq q | p''_{Y_1}, A_1 = a_0)$ with respect to q. The derivative of δ is

$$\frac{\mathrm{d}\delta}{\mathrm{d}q} = 2(\sigma_1^2 - \sigma_0^2)\frac{1}{q(1-q)}. \tag{C.24}$$

The derivatives of the roots are

$$\frac{\mathrm{d}z_{a,<p'_{Y_2}}}{\mathrm{d}q} = -\operatorname{sign}(\sigma_1^2-\sigma_0^2)\sigma_0\frac{1}{q(1-q)\sqrt{\delta}}, \tag{C.25}$$

$$\frac{\mathrm{d}z_{b,<p'_{Y_2}}}{\mathrm{d}q} = \operatorname{sign}(\sigma_1^2-\sigma_0^2)\sigma_0\frac{1}{q(1-q)\sqrt{\delta}}, \tag{C.26}$$

$$\frac{\mathrm{d}z_{a,>p'_{Y_2}}}{\mathrm{d}q} = -\operatorname{sign}(\sigma_1^2-\sigma_0^2)\sigma_1\frac{1}{q(1-q)\sqrt{\delta}}, \tag{C.27}$$

$$\frac{\mathrm{d}z_{b,>p'_{Y_2}}}{\mathrm{d}q} = \operatorname{sign}(\sigma_1^2-\sigma_0^2)\sigma_1\frac{1}{q(1-q)\sqrt{\delta}}. \tag{C.28}$$

The indicator function $\mathbb{1}_{\delta\geq 0}$ is constant on segments of q for a given p'_{Y_2}, hence its derivative is zero. The PDF of p''_{Y_2} conditional on p''_{Y_1} and $A_1 = a_0$ has the following expression:

$$\begin{aligned}f_{p''_{Y_2}|p''_{Y_1},A_1=a_0}(q) = \mathbb{1}_{\delta\geq 0}\frac{1}{q(1-q)\sqrt{\delta}}\Bigg\{(1-p'_{Y_2})\sigma_0\left[\varphi\left(z_{b,>p'_{Y_2}}\right) + \varphi\left(z_{a,>p'_{Y_2}}\right)\right] \\ + p'_{Y_2}\sigma_1\left[\varphi\left(z_{b,<p'_{Y_2}}\right) + \varphi\left(z_{a,<p'_{Y_2}}\right)\right]\Bigg\}.\end{aligned} \tag{C.29}$$

The expected cost for a given value of p''_{Y_1} and A_1 is given by

$$\mathbf{E}[C_1(p''_{Y_1}, A_1)] = \mathbb{1}_{A_1=a_0} c_F p''_{Y_1} + \mathbb{1}_{A_1=a_R} c_R + c_F \int_0^{\frac{c_R}{c_F}} q f_{p''_{Y_2}|p''_{Y_1}}(q)\mathrm{d}q + c_R \int_{\frac{c_R}{c_F}}^1 f_{p''_{Y_2}|p''_{Y_1}}(q)\mathrm{d}q. \tag{C.30}$$

If $p''_{Y_1} < 0.08$, action $A_1 = a_0$ is optimal, otherwise action $A_1 = a_R$ is optimal. The threshold on S_1 corresponding to $p''_{Y_1} = 0.08$ is $s_{th,1} = -0.27$[Volt]. The threshold on S_2 is determined by the value taken by the posterior probability of failure $p''_{Y_2} = \Pr(Y_2|S_1, S_2, A_1)$ being above or below the ratio $\frac{c_R}{c_F}$.

C.3. A posteriori optimal actions for a binary observed signal with a fixed threshold

We define events $\{I_{1,2} = 1\} = \{S_{1,2} < s_{th}\}$ and denote $\Pr(I_1 = 1)$ by p_{I_1}. We have $\mathrm{PoD} = \Pr(I_{1,2} = 1|Y_{1,2} = 1)$ and $\mathrm{PFA} = \Pr(I_{1,2} = 1|Y_{1,2} = 0)$. We use the notations p''_{Y_1}, p'_{Y_2} and p''_{Y_2} in analogy to Appendix C.2 above, replacing $S_{1,2}$ by $I_{1,2}$.

We first find the expected cost at time step 2, for a fixed PoD and PFA, given the posterior probability p''_{Y_2}. The first term corresponds to optimal action $A_2 = a_0$, while the second term corresponds to optimal action $A_2 = a_R$.

$$\mathbf{E}[C_2(p''_{Y_2})] = \mathbb{1}_{p''_{Y_2} < \frac{c_R}{c_F}} c_F p''_{Y_2} + \mathbb{1}_{p''_{Y_2} > \frac{c_R}{c_F}} c_R. \tag{C.31}$$

For a binary observed signal, the posterior probability of failure p''_{Y_2} can take two values, with probabilities $p_{I_2|p'_{Y_2}} = \mathrm{PoD}p'_{Y_2} + \mathrm{PFA}(1 - p'_{Y_2})$ and $1 - p_{I_2|p'_{Y_2}}$. As a function of p'_{Y_2}, these values are respectively

$$p''_{Y_{2,a}} = \frac{\mathrm{PoD}p'_{Y_2}}{\mathrm{PoD}p'_{Y_2} + \mathrm{PFA}(1 - p'_{Y_2})}, \tag{C.32}$$

$$p''_{Y_{2,b}} = \frac{(1 - \mathrm{PoD})p'_{Y_2}}{(1 - \mathrm{PoD})p'_{Y_2} + (1 - \mathrm{PFA})(1 - p'_{Y_2})}. \tag{C.33}$$

Similarly, the posterior probability of failure p''_{Y_1} can take two values, with probabilities $p_{I_1} = \mathrm{PoD}p'_{Y_1} + \mathrm{PFA}(1 - p'_{Y_1})$ and $1 - p_{I_1}$. As a function of p'_{Y_1}, these are respectively

$$p''_{Y_{1,a}} = \frac{\mathrm{PoD}p'_{Y_1}}{\mathrm{PoD}p'_{Y_1} + \mathrm{PFA}(1 - p'_{Y_1})}, \tag{C.34}$$

$$p''_{Y_{1,b}} = \frac{(1 - \mathrm{PoD})p'_{Y_1}}{(1 - \mathrm{PoD})p'_{Y_1} + (1 - \mathrm{PFA})(1 - p'_{Y_1})}. \tag{C.35}$$

In Equations (C.32) and (C.33), p'_{Y_2} can be expressed as a function of p''_{Y_1} using Equation (C.7).

The expected cost at time step 1, given p''_{Y_1} and action A_1, is

$$\begin{aligned}\mathbf{E}[C_1(p''_{Y_1}, A_1)] =& \mathbb{1}_{A_1=a_0} c_F p''_{Y_1} + \mathbb{1}_{A_1=a_R} c_R + p_{I_2|p'_{Y_2}(p''_{Y_1},A_1)} \mathbf{E}\left[C_2(p''_{Y_{2,a}}(p'_{Y_2}(p''_{Y_1}, A_1)))\right] \\ &+ (1 - p_{I_2|p'_{Y_2}(p''_{Y_1},A_1)}) \mathbf{E}\left[C_2(p''_{Y_{2,b}}(p'_{Y_2}(p''_{Y_1}, A_1)))\right]. \end{aligned} \tag{C.36}$$

By minimizing the expected cost of Equation (C.36), we obtain the optimal action $a_{1,opt}(I_1)$. The optimal action $a_{2,opt}(I_2, I_1)$ is deduced from Equation (C.31). The expected cost for fixed PoD and PFA is

$$\begin{aligned}\mathbf{E}[C_T] =& p_{I_1} \min\left\{\mathbf{E}\left[C_1(p''_{Y_{1,a}}, A_1 = a_0)\right], \mathbf{E}\left[C_1(p''_{Y_{1,a}}, A_1 = a_R)\right]\right\} \\ &+ (1 - p_{I_1}) \min\left\{\mathbf{E}\left[C_1(p''_{Y_{1,b}}, A_1 = a_0)\right], \mathbf{E}\left[C_1(p''_{Y_{1,b}}, A_1 = a_R)\right]\right\}. \end{aligned} \tag{C.37}$$

Appendix D

Hierarchical DBN inference algorithm

This section describes the inference algorithms for the hierarchical DBN. The algorithm is described here for the Zayas frame example (see Section 5.4.1.2 and chapter 6). The algorithm computes at every time step the filtered, predicted and smoothed interval probabilities of system failure.

D.1. Discretization of variables

The variables D, M, K and $\boldsymbol{\alpha}$ are discretized following Straub (2009) and Luque and Straub (2016). We discuss the impact of the discretization in Appendix E. The inspection outcome variables Z are discretized with the same scheme as for variable D, with 2 additional states to represent "no inspection" and "no detection".

D.2. Pre-computed conditional probability tables

We denote the number of states for variables D, M, K, Z and $\boldsymbol{\alpha} = \alpha_M, \alpha_K, \alpha_D$ by n_D, n_M, n_K, $n_Z = 2 + n_D$, and $n_\alpha = n_{\alpha_D} = n_{\alpha_M} = n_{\alpha_K}$, respectively. The CPTs for the hierarchical DBN and their dimensions are listed in Table D.1 below. They are pre-computed according to Straub (2009).

Table D.1 Pre-computed conditional probability tables and their dimensions

CPT	Dimensions	Reference
$CPT_D = \Pr(D_{i+1,k} \mid D_{i,k}, M_{i+1,k}, K_{i+1,k})$	$n_D \times n_D \times n_M \times n_K$	see eq. (6.1)
$CPT_M = \Pr(M_{i+1,k} \mid M_{i,k})$	$n_M \times n_M$ (identity matrix)	see section 6.3
$CPT_K = \Pr(K_{i+1,k} \mid K_{i,k})$	$n_K \times n_K$ (identity matrix)	see section 6.3
$CPT_{D_0} = \Pr(D_{0,k} \mid \alpha_D)$	$n_D \times n_\alpha$	see table F.1
$CPT_{M_0} = \Pr(M_{0,k} \mid \alpha_M)$	$n_M \times n_\alpha$	see table F.1
$CPT_{K_0} = \Pr(K_{0,k} \mid \alpha_K)$	$n_K \times n_\alpha$	see table F.1
$CPT_Z = \Pr(\boldsymbol{Z}_{i,k} \mid D_{i,k}, I_{i,k})$	$n_Z \times n_D \times 2$	see eq. (6.4)
$CPT_{\alpha_D} = \Pr(\alpha_D)$	$n_\alpha \times 1$	Standard normal (table F.1)
$CPT_{\alpha_M} = \Pr(\alpha_M)$	$n_\alpha \times 1$	Standard normal (table F.1)
$CPT_{\alpha_K} = \Pr(\alpha_K)$	$n_\alpha \times 1$	Standard normal (table F.1)

D.3. Bayesian inference algorithm

The following describe the Bayesian inference algorithm for the time-dependent probability of failure at the system and at the component level.

At every time step i, for each component k, the multi-dimensional matrices $A_{0:i,k,q=1,2}$ are computed recursively, using the pre-computed CPTs (Table D.1). Each $A_{j,k,q}$ contains $n_D n_M n_K n_\alpha^3$ elements. The index $q = 1$ indicates that the effect of a repair on the component is included, $q = 2$ is before repair.

The matrices Gj, k, q store in memory stages of computation of $A_{j,k,q}$ throughout the algorithm execution. $q = 1$ is the probability at time i after repair occurred at time step i, $q = 2$ is the probability at time $i + 1$ conditional on observations and repairs up to time i, $q = 3$ is the probability at time i conditional on observations up to time i, but before repair occurred at time i. Note that in case there is no repair at time i, $q = 1$ corresponds to the probability at time step i conditional on observations up to time i, and $q = 3$ is not defined.

We use the following notation:

- $DMK_{i,k} = D_{i,k}, M_{i,k}, K_{i,k}$
- $CPT_{XY} \times CPT_{YZ}$ is an element-wise multiplication of multi-dimensional CPTs along their common dimensions (here, along variable X). The resulting array is of dimension $n_X \cdot n_Y \cdot n_Z$.
- $\sum_X(\cdot)$ marginalizes (i.e., sums the elements of) the input multi-dimensional array with respect to the variable X.

Steps	**Operations on CPTs**
Initializing at $i = 0$	
`For each component` k`, do`	
$A_{0,k,1} = \Pr(DMK_{0,k}\|\boldsymbol{\alpha})$	$A_{0,k,1} \leftarrow CPT_{D_0} \times CPT_{M_0} \times CPT_{K_0}$
`Store for smoothing operation`	$G_{0,k,1} \leftarrow A_{0,k,1}$
$G_{0,k,2} = \Pr(DMK_{1,k}\|\boldsymbol{\alpha})$	
$= \sum_{DMK_{0,k}} \Pr(DMK_{1,k}\|DMK_{0,k}) \Pr(DMK_{0,k}\|\boldsymbol{\alpha})$	$G_{0,k,2} \leftarrow \sum_{DMK_{0,k}} CPT_D \times CPT_M \times CPT_K \times G_{0,k,1}$

Steps	**Operations on CPTs**
Forward operation at time step i	
`For each component` k`, do`	
– `if no repair at time` i	
$A_{i,k,1} = \Pr(DMK_{i,k}, \mathbf{z}_{1:i,k}\|\boldsymbol{\alpha})$	$A_{i,k,1} \leftarrow CPT_Z \times G_{i-1,k,2}$
– `if repair occurs at` i	
$A_{i,k,2} = \Pr(DMK_{i,k}, \mathbf{z}_{1:i,k}\|\boldsymbol{\alpha})$	$A_{i,k,2} \leftarrow CPT_Z \times G_{i-1,k,2}$
$A_{i,k,1} = \Pr(D_{i,k,R}, MK_{i,k}, \mathbf{z}_{1:i,k}\|\boldsymbol{\alpha})$	
$= \Pr(D_{0,k}\|\|\boldsymbol{\alpha}) \Pr(MK_{i,k}, \mathbf{z}_{1:i,k}\|\boldsymbol{\alpha})$	$A_{i,k,1} \leftarrow CPT_{D_0} \times \sum_{D_{i,k}} A_{i,k,2}$
`Store for smoothing operation`	$G_{i,k,1} \leftarrow A_{i,k,1}$
	$G_{i,k,3} \leftarrow A_{i,k,2}$ if it exists
$G_{i,k,2} = \Pr(DMK_{i+1,k}, \mathbf{z}_{1:i,k}\|\boldsymbol{\alpha})$	
$= \sum_{DMK_{i,k}} \Pr(DMK_{i+1,k}\|DMK_{i,k})$	
$\cdot \Pr(DMK_{i,k}, \mathbf{z}_{1:i,k}\|\boldsymbol{\alpha})$	$G_{i,k,2} \leftarrow \sum_{DMK_{i,k}} CPT_D \times CPT_M \times CPT_K \times G_{i,k,1}$
Smoothing operation (backward) for all $j < i$, where $q = 1$ if there was no repair at time $j+1$, or $q = 2$ otherwise	
$A_{j,k,1} = \Pr(DMK_{j,k}, \mathbf{z}_{1:i,k}\|\boldsymbol{\alpha})$	
$= \sum_{DMK_{j+1,k}} \Pr(DMK_{j,k}\|DMK_{j+1,k}, \mathbf{z}_{1:j,k}, \boldsymbol{\alpha})$	
$\cdot \Pr(DMK_{j+1,k}, \mathbf{z}_{1:i,k}\|\boldsymbol{\alpha})$	
$= \sum_{DMK_{j+1,k}} \frac{\Pr(DMK_{j+1,k}\|DMK_{j,k})}{\Pr(DMK_{j+1,k}, \mathbf{z}_{1:j,k}\|\boldsymbol{\alpha})}$	$A_{j,k,1} \leftarrow \sum_{DMK_{j+1,k}} \frac{CPT_D \times CPT_M \times CPT_K \times G_{j,k,1}}{G_{j,k,2}}$
$\cdot \Pr(DMK_{j,k}, \mathbf{z}_{1:j,k}\|\boldsymbol{\alpha})$	$\times A_{j+1,k,q}$

Steps	**Operations on CPTs**
if there was a repair at time step j, $A_{j,k,2}$ gives the probability distribution before repair Note that if there is a repair following time j, then $D_{j,k}$, conditional on $M_{j+1,k}$ and $K_{j+1,k}$, is independent of all observations occurring after time step j.	
$A_{j,k,2} = \Pr(DMK_{j,k}, \mathbf{z}_{1:i,k}\|\boldsymbol{\alpha})$ $= \sum_{DMK_{j+1,k}} \Pr(DMK_{j,k}, DMK_{j+1,k}, \mathbf{z}_{1:i,k}\|\boldsymbol{\alpha})$ $= \sum_{MK_{j+1,k}} \Pr(DMK_{j,k}\|MK_{j+1,k}, \mathbf{z}_{1:j,k}, \boldsymbol{\alpha})$ $\cdot \sum_{D_{j+1,k}} \Pr(DMK_{j+1,k}, \mathbf{z}_{1:i,k}\|\boldsymbol{\alpha})$ $= \sum_{MK_{j+1,k}} \Bigg(\frac{\Pr(MK_{j+1,k}\|DMK_{j,k}, \mathbf{z}_{1:j,k}, \boldsymbol{\alpha})}{\Pr(MK_{j+1,k}\|\mathbf{z}_{1:j,k}, \boldsymbol{\alpha})}$ $\cdot \Pr(DMK_{j,k}\|\mathbf{z}_{1:j,k}, \boldsymbol{\alpha}) \cdot \sum_{D_{j+1,k}} A_{j+1,k,m} \Bigg)$	$A_{j,k,2} \leftarrow \sum_{MK_{j+1,k}} \left(\frac{CPT_M \cdot CPT_K \cdot G_{j,k,3}}{\sum_{D_{j+1,k}} G_{j,k,2}} \cdot \sum_{D_{j+1,k}} A_{j+1,k,m} \right)$

At this point, we have obtained the joint probability $\Pr(D_{j,k}, M_{tj,k}, K_{j,k}, \mathbf{z}_{1:i,k}|\boldsymbol{\alpha})$ for all $j \leq i$, for all components k, including before and after eventual repairs. The probability of the hyperparameters is obtained as follows.

$$B = \Pr(\boldsymbol{\alpha}|\mathbf{z}_{1:i,1:N}) = \frac{\Pr(\mathbf{z}_{1:i,1:N}|\boldsymbol{\alpha}) \cdot \Pr(\boldsymbol{\alpha})}{\Pr(\mathbf{z}_{1:i,1:N})} = \frac{\prod_{k=1}^{N} \Pr(\mathbf{z}_{1:i,k}|\boldsymbol{\alpha}) \cdot \Pr(\boldsymbol{\alpha})}{\Pr(\mathbf{z}_{1:i,1:N})}$$

$\Pr(\mathbf{z}_{1:i,k}|\boldsymbol{\alpha})$ is obtained by marginalizing $A_{i,k,1}$ and $\Pr(\boldsymbol{\alpha}) = CPT_{\alpha_D} \cdot CPT_{\alpha_M} \cdot CPT_{\alpha_K}$. We can compute:

$$\begin{aligned} C = \Pr(DMK_{j,k}, \boldsymbol{\alpha}|\mathbf{z}_{1:i,1:N}) &= \Pr(DMK_{j,k}|\mathbf{z}_{1:i,k}, \boldsymbol{\alpha}) \cdot \Pr(\boldsymbol{\alpha}|\mathbf{z}_{1:i,1:N}) \\ &= \frac{A_{j,k,1}}{\sum_{DMK_{j,k}} A_{j,k,1}} \times B. \end{aligned}$$

The probability of failure of each component k at time j conditional on all components observations up to time i is therefore:

$$\Pr(D_{j,k}|\mathbf{z}_{1:i,1:N}) = \sum_{MK_{j,k},\boldsymbol{\alpha}} C$$

The corresponding interval probability of system failure at time j conditional on all components observations up to time step i is:

$$\Pr(F_j^*|\mathbf{z}_{1:i,1:N}) = \sum_{\boldsymbol{D}_{j,1:N}} \Pr(F_s(j)|\boldsymbol{D}_{j,1:N}) \cdot \Pr(\boldsymbol{D}_{j,1:N}|\mathbf{z}_{1:i,1:N})$$

$$= \sum_{\boldsymbol{D}_{j,1:N}} \Pr(F_s(j)|\boldsymbol{D}_{j,1:N}) \cdot \sum_{\boldsymbol{\alpha}} \prod_{k=1}^{N} \Pr(D_{j,k}|\mathbf{z}_{1:i,k}, \boldsymbol{\alpha}) \cdot \Pr(\boldsymbol{\alpha}|\mathbf{z}_{1:i,1:N})$$

Note that we use the probabilities after repair (i.e., $A_{j,k,1}$). Finally, the cumulative probability of failure at time step i, $\Pr(F_i|\mathbf{z}_{1:i,1:N})$ is approximated by $1 - \prod_{j \leq i} \Big[1 - \Pr(F_j^*)|\mathbf{z}_{1:i,1:N})\Big]$.

Appendix E

Effect of the discretization scheme on the accuracy of the DBN

To illustrate the effect of the discretization of the component states on the accuracy of the exact Bayesian inference with the discrete DBN, we consider a simple DBN model of the deterioration of a single component. The component resistance decreases linearly with a constant and unknown rate A, such that the resistance at time step i, R_i, $R_i = R_0 - A \cdot i$, with unknown initial resistance R_0. Component failure is defined as $R(t) < r_{crit}$. R_0 and A are assumed normal distributed. Z_i is the imperfect measurement of R_i, such that $Z_i \sim \mathcal{N}(R_i, \sigma_e)$. The parameters of the distributions are summarized in Table E.1. The DBN model is depicted in Figure E.1.

Table E.1 Parameters of the deterioration model

Parameter	Distribution type	mean	standard deviation
R_0	normal	$\mu_0 = 10$	$\sigma_0 = 1$
A	normal	$\mu_A = 1$	$\sigma_A = 0.1$
σ_e	deterministic	0.5	-
r_{crit}	deterministic	-1.5	-

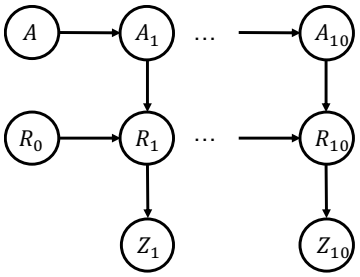

Figure E.1 DBN model of the deterioration at component level, with a single invariant parameter A, here duplicated by state-space augmentation (see Section 2.4.3.2).

In this DBN, the distributions of the unknown parameters follow a Gaussian and the dynamics are linear, hence all marginal and conditional distributions are also Gaussian. Hence, the predicted, filtered and smoothed probability of component failure can be written in a closed form expression with the standard normal CDF Φ, the distribution parameters of Table E.1 and the inspection results $\boldsymbol{Z}$.

These probabilities can also be computed with the associated discrete DBN and using exact Bayesian inference as explained in Section 5.4.6. The discretization of variable A is shown in Figure E.2.

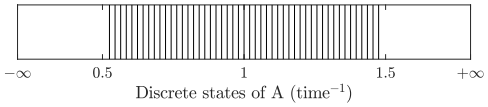

Figure E.2 Discretization scheme for variable A.

We investigate two discretization schemes for variable $R_{i\geq 0}$, the same scheme is applied to Z_i. The schemes are shown in Figure E.3. The CPTs of the DBN are derived following the procedure by Straub (2009), with no variable transformation. In general, (Straub, 2009) recommends to transform the variables of the DBN before discretization so that the relationship between the transformed variable is linear with the damage.

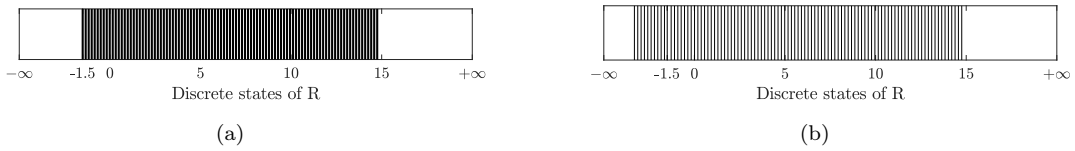

Figure E.3 Possible discretization schemes for variables $R_{i\geq 0}$. (a) The failure domain $R_i \leq r_{crit} = -1.5$ is represented by a single state. (b) The failure domain is represented by 12 discrete states.

We consider the case when the component is inspected at time step $i = 5$ and $Z_5 = 1.5$, and we compute the smoothed and predicted probability of failure for time steps $0 \leq i \leq 10$ including this observation.

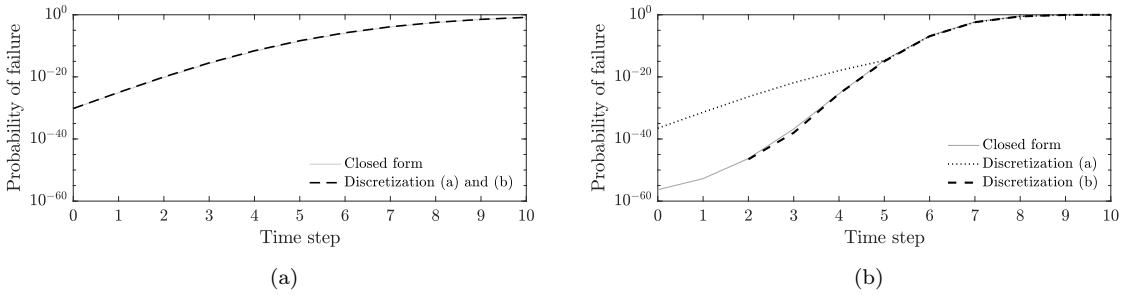

Figure E.4 Comparison of the discretization schemes with the closed form expression. (a): Evolution of the probability of failure with no observation. (b): Smoothed and predicted probability of failure including observation $Z_5 = 1.5$ at time step $i = 5$. The discontinuity observed at time $i = 5$ in the probability for discretization scheme (a) is due to the rough discretization of the component failure domain.

The study shows that the discretization of the failure domain affects the accuracy of the BN approximation when the probabilities are conditioned on observation outcomes. The smoothed probability of failure for time steps $j \leq 5$ is overestimated for discretization scheme (a). Using discretization scheme (b), the computed probabilities match the reference closed form evaluation. This example confirms the results of Zhu and Collette (2015).

We also studied the impact at the system level of the discretization scheme for the multi-component system of the Zayas frame presented in Section 5.4.1.2. Predicted, filtered and smoothed probability were computed for different discretization schemes of the component failure domain. The results showed that the curve for the system interval probability of failure

$\Pr(F_i^*|\boldsymbol{Z})$ presents the same kink as shown in Figure E.4b when the component failure domain is not discretized. Consequently, we find that the annual probability of system failure of Equation (5.13) is slightly overestimated. For the Zayas frame application in Chapter 6, the effect of this error, within the context of the approximation of the calculation of the cumulative probability of failure is, however, minor, and is further mitigated by the discounting factor on the later years.

Appendix F

Parameters of the fatigue deterioration model

This appendix can also be found in Bismut, E. and Straub, D. (2021). "Optimal adaptive inspection and maintenance planning for deteriorating structural systems". In: *Reliability Engineering & System Safety* 215, p. 107891.

F.1. General model parameters

The parameters of deterioration model are obtained from (Straub, 2009; Luque and Straub, 2016). The relationship between $\ln(C)$ and M is defined after (Ditlevsen and Madsen, 1996), such that the joint distribution of $(\ln(C), M)$ is normally distributed with mean value $(-33, 3.5)$, standard deviations $(0.47, 0.3)$ and correlation coefficient -1.

Here, a time step t corresponds to $\nu = 10^5$ fatigue cycles, after (Straub, 2009). For each fatigue hotspots, the stress scale factor K is assumed lognormally distributed. The standard deviation of $\ln(K)$ is 0.22 for all hotspots, after (Moan and Song, 2000). The mean of $\ln(K)$ varies with the assumed fatigue life for each component (see Appendix F.2).

Table F.1 Parameters of the fatigue crack growth model.

Variable	Type	Mean	Std. Deviation
α_{a_0}	Normal dist.	0	1
α_K	Normal dist.	0	1
α_M	Normal dist.	0	1
$D_{0,k}$ [mm]	Exponential dist.	1	1
$M_{0,k}$	Normal dist.	3.5	0.3
$M_{i,k}$	Function	$M_{i,k} = M_{i-1,k}$	-
$\ln(C_{i,k})$	Function	$\ln(C_{i,k}) = -1.5667 * M_{i,k} - 27.5166$	-
$\ln K_{0,k}$	Normal dist.	Obtained from Table F.2	0.22
$K_{i,k}$	Function	$K_{i,k} = K_{i-1,k}$	-
λ_i	Deterministic	0.8	-
d_{cr} [mm]	Deterministic	50	-
ξ [mm]	Deterministic	10	-
ν [cycles]	Deterministic	10^5	-
T [years]	Deterministic	40	-
ρ_{D_0}	Deterministic	0.5	-
ρ_M	Deterministic	0.6	-
ρ_K	Deterministic	0.8	-

F.2. Calibration of the fatigue stress range parameter to the fatigue life

Different approaches for the calibration of deterioration models to the assumed component FDF are discussed in detail in (Straub, 2004). The FDF is defined as the ratio between the component fatigue life, T_{FL}, and the system service life, $T_{SL} = T = 40$[years]. Here, the mean value of the random stress scale parameter K in Equation (6.2) is calibrated to the FDF in two steps, through two damage models, so that they output the same probability of component failure after T_{SL} years.

The first model is the Palmgren-Miner damage accumulation law (Palmgren, 1924; Miner, 1945). It defines damage as a unitless quantity increasing with the number of fatigue stress cycles. The damage increment $\Delta\delta$ due to one stress cycle at stress level S is

$$\Delta\delta = \frac{1}{N_F(S)}, \tag{F.1}$$

where N_F is the number of cycles to failure of constant stress amplitude S. Here, we adopt the S-N curve D from the Department of Energy (DoE), UK, after (Straub, 2004). This curve is bilinear in logarithmic scale and is described by the stochastic Equation (F.2).

$$\begin{cases} \frac{1}{N_F} = \frac{1}{C_1} B_s^{m_1} S^{m_1} & \text{for } B_s \cdot S \geq S_q, \\ \frac{1}{N_F} = \frac{1}{C_1} B_s^{m_2} S^{m_2} S_q^{m_1 - m_2} & \text{for } 0 \leq B_s \cdot S \leq S_q, \end{cases} \tag{F.2}$$

where $m_1 = 3$ and $m_2 = 5$ are empirical material parameters. S_q is defined from $N_q = \frac{1}{C_1^D} S_q^{m_1} = 10^7$. In this model, it is assumed that the fatigue stress S has a Weibull distribution with scale parameter k_S and shape parameter $\lambda_S = 0.8$. The epistemic uncertainty on the stress range S is included in a multiplicative factor B_s, lognormally distributed with moments $(1,\ 0.25)$ (Straub, 2004). C_1 is lognormally distributed with moments $(3.99 \cdot 10^{12},\ 2.03 \cdot 10^{12})$.

For n stress cycles, the total damage δ_n is the sum of the damages due to each stress cycles. For high-cycle fatigue, δ_n is approximated in Equation (F.3),

$$\delta_n = \sum_{i=1}^{n} \Delta\delta_i \simeq n \cdot \mathbf{E}_S[\Delta\delta] = n \cdot \mathbf{E}_S\left[\frac{1}{N_F(S)}\right]. \tag{F.3}$$

Failure occurs when the total damage exceeds a critical threshold, Δ, lognormally distributed with moments $(1, 0.3)$ (Faber et al., 2000; JCSS, 2001). The resulting limit state function after n cycles is written:

$$g_{SN}(\Delta, B_s, C_1) = \Delta - n \cdot \mathbf{E}_S\left[\frac{1}{N_F(S)}\right]. \tag{F.4}$$

The scale parameter k_S is first calibrated to the assumed FDF by replacing the S-N curves of Equation (F.2) with the corresponding characteristic design S-N curve, given by Equa-

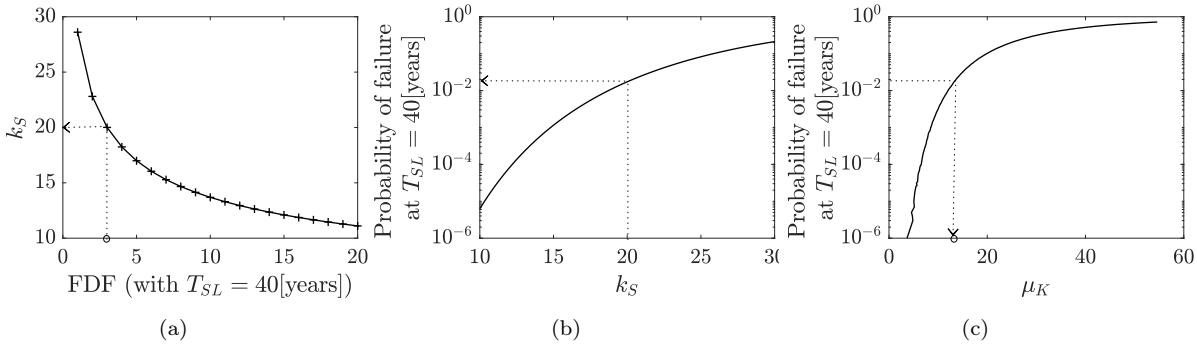

Figure F.1 (a): S-N model parameter k_S in function of the FDF. (b): Probability of hotspot failure calculated from the S-N model with parameter k_S. (c): Probability of hotspot failure according to the FM model, in function of μ_K.

Table F.2 Fatigue design factors (FDFs) and corresponding mean of random variable K at each hotspot.

Hotspot index k	FDF	Mean of $K_{k,0}$
$\{1, 2, 3, 4\}$	10	7.58
$\{5, 6, 13, 14, 17, 18, 21, 22\}$	2	16.26
$\{7, 8, 9, 10, 11, 12, 19, 20\}$	3	13.29
$\{15, 16\}$	7	8.88

tion (F.5).

$$\begin{cases} \frac{1}{N_F^D} = \frac{1}{C_1^D} S^{m_1} & \text{for } S \geq S_q \\ \frac{1}{N_F^D} = \frac{1}{C_1^D} S^{m_2} S_q^{m_1 - m_2} & \text{for } 0 \leq S \leq S_q, \end{cases} \tag{F.5}$$

with $C_1^D = 1.53 \cdot 10^{12}$. The fatigue life $FDF \cdot T$, with a yearly cycle rate ν, is such that the total accumulated damage δ_n, with $n = \nu \cdot FDF \cdot T$, assuming the design S-N curve reaches the critical value 1:

$$\delta_n = \nu \cdot FDF \cdot T \cdot \mathbf{E}\left[\frac{1}{N_F^D}\right] = 1. \tag{F.6}$$

The expectation in Equation (F.6) can be expressed in function k_S, λ_S, m_1, m_2, C_1^D and N_q, hence a mapping between FDF and k_S is established, and depicted in Figure F.1a. Additionally, for a fixed value of k_S, the probability $\Pr(g_{SN} < 0)$ at the end of the lifetime T, i.e., $n = \nu \cdot T$, is approximated with FORM (Figure F.1b).

The second model is the fracture mechanics (FM) model of Equation (6.1). By integrating between time steps 0 and T, assuming an initial crack depth D_0.

$$D_T = \left[\left(1 - \frac{M}{2}\right) C \cdot \Delta S_e(K, M)^M \pi^{M/2} \nu \cdot T + D_0^{(1-M/2)}\right]^{1-M/2)^{-1}} \tag{F.7}$$

The limit state function defined with the FM approach is therefore:

$$g_{FM} = d_{cr} - D_T. \tag{F.8}$$

The probability of failure $\Pr(g_{FM} < 0)$ in function of the assumed mean value of K, μ_K, is shown in Figure F.1c.

Finally, the mean value of variable K in the FM model corresponding to the chosen FDF is such that the limit state functions in Equations (F.4) and (F.8) result in the same probability of failure at the end of service life T, and is obtained by jointly reading Figures F.1a to F.1c. The FDF values and corresponding means of K for all hotspots for the numerical application are summarized in Table F.2.

Appendix G

Simplified flow accelerated corrosion predictive model

This appendix can also be found in Bismut, E., Straub, D., and Pandey, M. (2022). "Inspection and maintenance planning of a feeder piping system". In: *Reliability Engineering & System Safety* 224, p. 108521.

For this representative strategy $\mathcal{S}_{REP}$, the pipe replacement criterion is based on a simplified FAC-predictive model, in which the evolution of the wall thickness is described by a linear model with a constant wear rate for each pipe, as recommended by EPRI (2013). The wear rate for pipe k is estimated as $\hat{R}_k$, based on the thickness measurements of this pipe. For simplicity, it is assumed that the replacement pipe retains the estimated wear rate of the pipe it replaces. For each inspected pipe k, this wear rate at time t is estimated by linear regression with quadratic loss using all measurements on pipe k until time t (Hazra et al., 2020a). With initial wall thickness $W_k(0)$, the wear rate estimate $\hat{R}_k(t)$ is

$$\hat{R}_k(t) = \frac{\sum_{j\in\mathcal{J}} (t_j - t_R) \cdot (W_k(0) - Z_k(t_j))}{\sum_{j\in\mathcal{J}} (t_j - t_R)^2}. \tag{G.1}$$

t_j are the inspection times of pipe k up to and including time t, and t_R is the time of last repair of pipe k before time t_j.

$W_{k,pred}(t + \Delta t)$ is the predicted thickness at time $t + \Delta t$ of pipe k, and is calculated for all pipes inspected at time t:

$$W_{k,pred}(t + \Delta t) = W_k(\tau_k) - SF_k \cdot \hat{R}_k(t) \cdot (t + \Delta t - \tau_k), \tag{G.2}$$

$\tau_k < t$ being the time of last inspection or repair up to an including time t, and $W_k(\tau_k) = Z_k(\tau_k)$ if the pipe is inspected but not repaired, $W_k(\tau_k) = W_0$ if it is repaired. As in Section 7.5.2, $Z_k(t)$ is the measured wall thickness at time t.

A safety factor $SF_k = 1.1$ is applied to the prediction wear rates $\hat{R}_k(t)$ until the next I&M campaign at time $t + \Delta T$. For the pipes for which the measured wall thickness at time t $Z_k(t)$ is lower than the predicted wall thickness from the previous I&M campaign, $W_{k,pred}(t)$, we postulate that the safety factor is increased to $SF_k = 1.5$. The choice of the safety factors affects the planning of preventive maintenance and inspection. Here we have not chosen the factors in a particular way that would optimize the strategy for the problem considered.

The remaining service life of the inspected pipes is calculated as

$$T_{k,SL} = \frac{Z_k(t) - W_{accept}}{\hat{R}_k \cdot SF_k} \tag{G.3}$$

Appendix H

Nomenclature

H.1. Symbols

$\boldsymbol{A}$	maintenance actions
C_{tot}, C_T	total life cycle cost
$C_{I\&M}$	total life cycle I&M cost
$\boldsymbol{e}$	see $\boldsymbol{I}$
F_i^*	interval failure event
F_i	cumulative failure event
$\boldsymbol{I}, I_i$	inspection decisions
$IGa(a, b)$	inverse Gamma distribution with shape parameter a and scale parameter b
i, j	time step index
k	system component index
$\mathcal{N}(\mu, \sigma)$	normal distribution with parameters μ and σ
n_T	number of time steps in horizon T
$\boldsymbol{R}$	see $\boldsymbol{A}$
r	discount rate
$\mathscr{S}$	space of strategies
$\mathcal{S}$	strategy
$\mathcal{S}_{\boldsymbol{w}}$	heuristic strategy described by parameters $\boldsymbol{w}$
T	time horizon
T_F	time to failure
$u(\cdot)$	utility function
$\boldsymbol{w}$	heuristic parameter vector
w_l	heuristic parameter
$\boldsymbol{Z}$	inspection outcomes
γ	discount factor
π_i	policy at time step i
φ	standard normal PDF
Φ	standard normal CDF

H.2. Acronyms

BN	Bayesian network

BUS	Bayesian updating with structural reliability methods
CDF	cumulative distribution function
CANDU	Canada Deuterium Uranium
CE	cross-entropy
CM	corrective maintenance
CPT	conditional probability table
DBN	dynamic Bayesian network
EFPY	effective full power year
FAC	flow accelerated corrosion
FORM	first order reliability method
GPR	Gaussian process regression
I&M	inspection and maintenance
LSF	limit state function
MC	Monte Carlo
MCMC	Markov chain Monte Carlo
MCS	Monte Carlo simulation
MCTS	Monte Carlo tree search
MDP	Markov decision process
MPC	model predictive control
NDE	non-destructive evaluation
NDT	non-destructive testing, see NDE
NPP	nuclear power plant
OR	operations research
PBVI	point based value iteration
PDF	probability density function
PFA	probability of false alarm
PI	prioritization index
PM	preventive maintenance
PMF	probability mass function
PoD	probability of detection
POMDP	partially observable Markov decision process
RAM	random access memory
RBI	risk-based inspection
ROC	receiver operating characteristic
SDP	sequential decision problem
SEGO	stochastic efficient global optimization
SEI	Single element importance
SHM	structural health monitoring
SUS	subset simulation
USFOS	Ultimate Strength for Offshore Structures software
VoI	value of information

References

Alaswad, S. and Xiang, Y. (2017). "A review on condition-based maintenance optimization models for stochastically deteriorating system". In: *Reliability Engineering & System Safety* 157, pp. 54–63. ISSN: 0951-8320. (Cited on pp. 130, 131).

Aldrin, J. C., Knopp, J. S., and Sabbagh, H. A. (2013). "Bayesian methods in probability of detection estimation and model-assisted probability of detection evaluation". In: *AIP Conference Proceedings*. Vol. 1511. American Institute of Physics, pp. 1733–1740. ISBN: 0735411298. (Cited on pp. 66, 72).

Amiri, M. and Modarres, M. (2014). "An entropy-based damage characterization". In: *Entropy* 16.12, pp. 6434–6463. (Cited on p. 96).

Andriotis, C. P. and Papakonstantinou, K. G. (2019). "Managing engineering systems with large state and action spaces through deep reinforcement learning". In: *Reliability Engineering & System Safety* 191, p. 106483. ISSN: 0951-8320. (Cited on pp. 3, 31, 35–37, 160).

Annis, C. (2009). *Nondestructive evaluation system reliability assessment*. Report MIL-HDBK-1823A. Department of Defense. (Cited on pp. 66, 67, 72).

Arnold, M. (1883). *Literature & dogma*. Vol. 8. Macmillan. (Cited on p. 2).

Askar, M. and Derin, H. (1981). "A recursive algorithm for the Bayes solution of the smoothing problem". In: *IEEE Transactions on Automatic Control* 26.2, pp. 558–561. ISSN: 0018-9286. (Cited on p. 110).

Askar, M. and Derin, H. (1983). "Recursive algorithms for the Bayes solution of the fixed-point and fixed-lag smoothing problems". In: *IEEE Transactions on Automatic Control* 28.10, pp. 996–998. ISSN: 0018-9286. (Cited on p. 110).

ASME (2013). *ASME Boiler and Pressure Vessel Code*. American Society of Mechanical Engineers (ASME). ISBN: 9780791869741. (Cited on p. 132).

Åström, K. J. (1965). "Optimal control of Markov processes with incomplete state information". In: *Journal of mathematical analysis and applications* 10.1, pp. 174–205. (Cited on pp. 3, 25).

Barker, C. and Newby, M. (2008). "Nonperiodic inspections to guarantee a prescribed level of reliability". In: *Statistical models and methods for biomedical and technical systems*. Springer. Chap. 9, pp. 109–125. (Cited on p. 131).

Barlow, R. and Hunter, L. (1960). "Optimum preventive maintenance policies". In: *Operations research* 8.1, pp. 90–100. ISSN: 0030-364X. (Cited on p. 47).

Barone, G. and Frangopol, D. M. (2014). "Reliability, risk and lifetime distributions as performance indicators for life-cycle maintenance of deteriorating structures". In: *Reliability Engineering & System Safety* 123, pp. 21–37. ISSN: 0951-8320. (Cited on pp. 40, 100, 131, 138).

Bellman, R. (1953). *An introduction to the theory of dynamic programming*. Report. RAND Corp Santa Monica CA. (Cited on p. 20).

Bellman, R. (1957a). "A Markovian decision process". In: *Journal of Mathematics and Mechanics* 6.5, pp. 679–684. ISSN: 0095-9057. (Cited on pp. 3, 22, 25, 29).

Bellman, R. (1957b). *Dynamic Programming*. Princeton University Press, p. 360. ISBN: 9780691146683. (Cited on pp. 3, 25, 29, 30, 86).

Bellman, R. (1958). "Letter to the Editor—On "Heuristic Problem Solving," by Simon and Newell". In: *Operations Research* 6.3, pp. 448–449. ISSN: 0030-364X. (Cited on p. 160).

Benjamin, J. R. and Cornell, C. A. (1970). *Probability, statistics, and decision for civil engineers*. McGraw-Hill. (Cited on pp. 2, 10, 13).

Berens, A. P. (2000). *Probability of Detection (POD) Analysis for the Advanced Retirement for Cause (RFC)/Engine Structural Integrity Program (ENSIP) Nondestructive Evaluation (NDE) System-Volume 1: Pod Analysis*. Report. University of Dayton Research Institute. (Cited on pp. 63, 66, 67, 73).

Berens, A. P. and Hovey, P. W. (1981). "Evaluation of NDE Reliability Characterisation". In: *Air Force Wright Aeronautical Laboratories, AFWAL-TR-81-4160, November 1981*. (Cited on pp. 62, 63, 66, 67, 70, 72, 73).

Bernoulli, D. (1954). "Exposition of a New Theory on the Measurement of Risk". In: *Econometrica* 22.1, pp. 23–36. (Cited on pp. 2, 16).

Bertovic, M. (2016). "A human factors perspective on the use of automated aids in the evaluation of NDT data". In: *AIP Conference Proceedings*. Vol. 1706. AIP Publishing LLC, p. 020003. ISBN: 0735413533. (Cited on pp. 89, 90).

Betz, W. (2017). "Bayesian inference of engineering models". Thesis. (Cited on p. 113).

Bismut, E., Luque, J., and Straub, D. (2017). "Optimal prioritization of inspections in structural systems considering component interactions and interdependence". In: *12th International Conference on Structural Safety & Reliability, ICOSSAR 2017*, pp. 2260–2269. (Cited on pp. vii, 3, 37).

Bismut, E. and Straub, D. (2018a). "Adaptive Direct Policy Search for Inspection and Maintenance Planning in Structural Systems". In: *Sixth International symposium on Life-Cycle Civil Engineering 2018, IALCCE*. (Cited on p. vii).

Bismut, E. and Straub, D. (2018b). "Inspection and maintenance planning in large monitored structures". In: *Proc 6th International Symposium on Reliability and Engineering Risk Management (ISRERM)*. (Cited on p. vii).

Bismut, E. and Straub, D. (2019). "Direct policy search as an alternative to POMDP for sequential decision problems in infrastructure planning". In: *13th International Conference on Applications of Statistics and Probability in Civil Engineering, ICASP13*. ISBN: 9791196712501. (Cited on pp. vii, 21, 28, 31, 41, 59).

Bismut, E. and Straub, D. (2021). "Optimal adaptive inspection and maintenance planning for deteriorating structural systems". In: *Reliability Engineering & System Safety* 215, p. 107891. (Cited on pp. vii, 9, 39, 43, 51, 55, 58, 86, 93, 117, 163, 165, 185).

Bismut, E. and Straub, D. (2022). "A unifying review of NDE models towards optimal decision support". In: *Structural Safety* 97, p. 102213. (Cited on pp. vii, 61, 169).

Bismut, E., Straub, D., and Pandey, M. (2022). "Inspection and maintenance planning of a feeder piping system". In: *Reliability Engineering & System Safety* 224, p. 108521. (Cited on pp. vii, 44, 56, 129, 189).

Bloch, A., Sørensen, J. D., and Faber, M. H. (2000). "Simplified approach to inspection planning". In: *8th ASCE Specialty Conference on Probabilistic Mechanics and Structural Reliability*. (Cited on p. 39).

Bocchini, P., Saydam, D., and Frangopol, D. M. (2013). "Efficient, accurate, and simple Markov chain model for the life-cycle analysis of bridge groups". In: *Structural Safety* 40, pp. 51–64. ISSN: 0167-4730. (Cited on pp. 101, 105).

Boero, J., Schoefs, F., and Capra, B. (2009). "Effect on Risk Based Inspection of spatio-temporal dependence of ROC curves: Study of the corrosion of steel harbour structures". In: *NDTCE 09*. (Cited on pp. 69, 72).

Botev, Z. I., Kroese, D. P., Rubinstein, R. Y., and L'Ecuyer, P. (2013). "The cross-entropy method for optimization". In: *Handbook of statistics*. Vol. 31. Elsevier, pp. 35–59. ISBN: 0169-7161. (Cited on p. 108).

Brennan, F. (2013). "Risk based maintenance for offshore wind structures". In: *Procedia CIRP* 11, pp. 296–300. ISSN: 2212-8271. (Cited on p. 66).

Bressi, S., Santos, J., and Losa, M. (2021). "Optimization of maintenance strategies for railway track-bed considering probabilistic degradation models and different reliability levels". In: *Reliability Engineering & System Safety* 207, p. 107359. ISSN: 0951-8320. (Cited on p. 131).

Calmon, P. (2012). "Trends and stakes of NDT simulation". In: *Journal of Nondestructive evaluation* 31.4, pp. 339–341. ISSN: 0195-9298. (Cited on p. 66).

Calmon, P., Chapuis, B., Jenson, F., and Sjerve, E. (2016). "The use of simulation in POD curves estimation: An overview of the IIW best practices proposal". In: *19th World Conference on Non-Destructive Testing*. Munich, Germany. (Cited on p. 66).

Chebotar, Y., Kalakrishnan, M., Yahya, A., Li, A., Schaal, S., and Levine, S. (2017). "Path integral guided policy search". In: *Robotics and Automation (ICRA), 2017 IEEE International Conference on*. IEEE, pp. 3381–3388. ISBN: 150904633X. (Cited on p. 35).

Chen, C.-H. and Lee, L. H. (2011). *Stochastic simulation optimization: an optimal computing budget allocation*. Vol. 1. World scientific. ISBN: 9814282642. (Cited on p. 58).

Chen, W.-F. and Sohal, I. S. (1988). "Cylindrical members in offshore structures". In: *Thin-Walled Structures* 6.3, pp. 153–285. ISSN: 0263-8231. (Cited on p. 117).

Clark, R., Dover, W. D., and Bond, L. J. (1987). "The effect of crack closure on the reliability of NDT predictions of crack size". In: *NDT international* 20.5, pp. 269–275. ISSN: 0308-9126. (Cited on p. 65).

Colmer, J. (2020). "What is the meaning of (statistical) life? Benefit–cost analysis in the time of COVID-19". In: *Oxford Review of Economic Policy*. PMC7499700[pmcid], graa022. ISSN: 0266-903X 1460-2121. (Cited on p. 24).

Coquelin, P.-A., Deguest, R., and Munos, R. (2008). "Particle filter-based policy gradient for POMDPs". In: *Advances in Neural Information Processing Systems*. (Cited on pp. 30, 31, 36).

Covello, V. T. and Mumpower, J. (1985). "Risk analysis and risk management: an historical perspective". In: *Risk analysis* 5.2, pp. 103–120. ISSN: 1539-6924. (Cited on pp. 1, 2).

De Boer, P.-T., Kroese, D. P., Mannor, S., and Rubinstein, R. Y. (2005). "A tutorial on the cross-entropy method". In: *Annals of operations research* 134.1, pp. 19–67. ISSN: 0254-5330. (Cited on p. 54).

Deisenroth, M. P., Neumann, G., and Peters, J. (2013). "A survey on policy search for robotics". In: *Foundations and Trends® in Robotics* 2.1–2, pp. 1–142. ISSN: 1935-8253. (Cited on p. 35).

Deming, D. (2020). "The aqueducts and water supply of Ancient Rome". In: *Ground water* 58.1, p. 152. (Cited on p. 2).

Der Kiureghian, A. (2004). "First-and second-order reliability methods". In: *Engineering design reliability handbook*. CRC Press LLC. Chap. 14. (Cited on p. 96).

Der Kiureghian, A. and Liu, P.-L. (1986). "Structural reliability under incomplete probability information". In: *Journal of Engineering Mechanics* 112.1, pp. 85–104. ISSN: 0733-9399. (Cited on p. 102).

Det Norske Veritas (2010). *Fatigue design of offshore steel structures - DNV Recommended Practice*. Report DNV-RP-C203. (Cited on p. 98).

Deutsches Institut für Normung (2014). *In-service inspections for primary coolant circuit components of light water reactors - Part 6: Eddy current testing of steam generator heating tubes*. Report DIN 25435-6:2014-01. (Cited on p. 62).

Diaz, G. I., Fokoue-Nkoutche, A., Nannicini, G., and Samulowitz, H. (2017). "An effective algorithm for hyperparameter optimization of neural networks". In: *IBM Journal of Research and Development* 61.4, 9:1–9:11. ISSN: 0018-8646. (Cited on p. 41).

Ditlevsen, O. and Madsen, H. O. (1996). *Structural reliability methods*. Vol. 178. Wiley New York. (Cited on pp. 95, 105, 185).

Do, P. and Bérenguer, C. (2020). "Conditional reliability-based importance measures". In: *Reliability Engineering & System Safety* 193, p. 106633. ISSN: 0951-8320. (Cited on p. 138).

Duff, M. O. (2002). "Optimal learning: Computational procedures for Bayes-adaptive Markov decision processes". Thesis. (Cited on pp. 2, 32, 33).

Durango, P. L. and Madanat, S. M. (2002). "Optimal maintenance and repair policies in infrastructure management under uncertain facility deterioration rates: an adaptive control approach". In: *Transportation Research Part A: Policy and Practice* 36.9, pp. 763–778. ISSN: 0965-8564. (Cited on pp. 3, 35–37, 101).

Efroni, Y., Dalal, G., Scherrer, B., and Mannor, S. (2018). "Multiple-step greedy policies in approximate and online reinforcement learning". In: *Advances in Neural Information Processing Systems*, pp. 5238–5247. (Cited on p. 43).

Elsener, B., Andrade, C., Gulikers, J., Polder, R., and Raupach, M. (2003). "Half-cell potential measurements—Potential mapping on reinforced concrete structures". In: *Materials and Structures* 36.7, pp. 461–471. ISSN: 1359-5997. (Cited on p. 82).

Enright, M. P. and Frangopol, D. M. (1999). "Condition prediction of deteriorating concrete bridges using Bayesian updating". In: *Journal of Structural Engineering* 125.10, pp. 1118–1125. ISSN: 0733-9445. (Cited on p. 1).

EPRI (2013). *Recommendations for an Effective Flow-Accelerated Corrosion Program*. Report NSAC- 202L-R4. (Cited on pp. 129, 134, 147, 148, 189).

European Commission (2020). *Harmonised Transport Infrastructure Monitoring in Europe for Optimal Maintenance and Safety*. Web Page. URL: https://cordis.europa.eu/project/id/958171. (Cited on p. 2).

Faber, M. H., Engelund, S., Sørensen, J. D., and Bloch, A. (2000). "Simplified and Generic Risk Based Inspection Planning". English. In: *Proceedings of OMAE2000, New Orleans, 2000*. Paper 6143. (Cited on pp. 4, 40, 45, 99, 186).

Faber, M. H. and Sorensen, J. D. (2002). "Indicators for inspection and maintenance planning of concrete structures". In: *Structural Safety* 24.2-4, pp. 377–396. ISSN: 0167-4730. (Cited on pp. 82, 83, 85, 88, 89).

Faddoul, R., Raphael, W., and Chateauneuf, A. (2018). "Maintenance optimization of series systems subject to reliability constraints". In: *Reliability Engineering & System Safety* 180, pp. 179–188. ISSN: 0951-8320. (Cited on pp. 131, 138).

Faddoul, R., Soubra, A. H., Raphael, W., and Chateauneuf, A. (2013). "Extension of dynamic programming models for management optimisation from single structure to multi-structures level". In: *Structure and Infrastructure Engineering* 9.5, pp. 432–447. ISSN: 1573-2479. (Cited on p. 105).

Fatemi, A. and Yang, L. (1998). "Cumulative fatigue damage and life prediction theories: a survey of the state of the art for homogeneous materials". In: *International journal of fatigue* 20.1, pp. 9–34. ISSN: 0142-1123. (Cited on pp. 97, 99, 100).

Feistkorn, S. and Taffe, A. (2011). "Die POD-eine Vorgehensweise zum qualitativen Gütenachweis zerstörungsfreier Prüfverfahren im Bauwesen am Beispiel des Impulsradars". In: *DGZfP-Jahrestagung 2011, Bremen, Germany*. (Cited on p. 66).

Fick, A. (1855). "Ueber diffusion". In: *Annalen der Physik* 170.1, pp. 59–86. ISSN: 0003-3804. (Cited on p. 100).

Finney, D. J. (1978). *Statistical method in biological assay*. 3rd. High Wycombe: Griffin, p. 508. (Cited on pp. 62, 66).

Flage, R., Coit, D. W., Luxhøj, J. T., and Aven, T. (2012). "Safety constraints applied to an adaptive Bayesian condition-based maintenance optimization model". In: *Reliability Engineering & System Safety* 102, pp. 16–26. ISSN: 0951-8320. (Cited on p. 131).

Fluss, R., Faraggi, D., and Reiser, B. (2005). "Estimation of the Youden Index and its associated cutoff point". In: *Biometrical Journal: Journal of Mathematical Methods in Biosciences* 47.4, pp. 458–472. ISSN: 0323-3847. (Cited on pp. 68, 69).

Frangopol, D. M., Lin, K.-Y., and Estes, A. C. (1997). "Life-cycle cost design of deteriorating structures". In: *Journal of Structural Engineering* 123.10, pp. 1390–1401. ISSN: 0733-9445. (Cited on pp. 62, 101, 131).

Fu, M. C. (2016). "AlphaGo and Monte Carlo tree search: The simulation optimization perspective". In: *Proceedings of the 2016 Winter Simulation Conference*. IEEE Press, pp. 659–670. ISBN: 1509044841. (Cited on p. 36).

Geyer, S., Papaioannou, I., and Straub, D. (2019). "Cross entropy-based importance sampling using Gaussian densities revisited". In: *Structural Safety* 76, pp. 15–27. ISSN: 0167-4730. (Cited on pp. 56, 140).

Gholami, H., Asgarian, B., and Asil Gharebaghi, S. (2020). "Practical Approach for Reliability-Based Inspection Planning of Jacket Platforms Using Bayesian Networks". In: *ASCE-ASME Journal of Risk and Uncertainty in Engineering Systems, Part A: Civil Engineering* 6.3, p. 04020029. ISSN: 2376-7642. (Cited on p. 131).

Gittins, J. C. (1979). "Bandit processes and dynamic allocation indices". In: *Journal of the Royal Statistical Society: Series B (Methodological)* 41.2, pp. 148–164. ISSN: 0035-9246. (Cited on pp. 22, 45).

Giuffrida, A. (May 26, 2021). "Italian cable car brakes 'tampered with', say prosecutors". In: *The Guardian*. URL: `https://www.theguardian.com/world/2021/may/26/italian-cable-car-brakes-tampered-with-say-prosecutors` (visited on 10/22/2021). (Cited on p. 3).

Goulet, J.-A., Der Kiureghian, A., and Li, B. (2015). "Pre-posterior optimization of sequence of measurement and intervention actions under structural reliability constraint". In: *Structural Safety* 52, pp. 1–9. ISSN: 0167-4730. (Cited on p. 66).

Graham, T. and Tetelman, A. (1974). "The use of crack size distribution and crack detection for determining the probability of fatigue failure". In: *15th Structural Dynamics and Materials Conference*, p. 394. (Cited on p. 62).

Grall, A., Dieulle, L., Bérenguer, C., and Roussignol, M. (2002). "Continuous-time predictive-maintenance scheduling for a deteriorating system". In: *IEEE transactions on reliability* 51.2, pp. 141–150. ISSN: 0018-9529. (Cited on p. 45).

Granville, R. and Charlton, P. (2016). "Detection and sizing of baffle plate erosion and fretting using eddy current array technology". In: *ndt. net* 21.09. ISSN: 1435-4934. (Cited on p. 66).

Green, D. M. and Swets, J. A. (1966). *Signal detection theory and psychophysics*. Vol. 1. John Wiley & Sons, Inc. (Cited on pp. 75, 84).

Greiner, M., Pfeiffer, D., and Smith, R. D. (2000). "Principles and practical application of the receiver-operating characteristic analysis for diagnostic tests". In: *Preventive veterinary medicine* 45.1-2, pp. 23–41. ISSN: 0167-5877. (Cited on p. 69).

Gurney, T. R. (1976). "Fatigue Design Rules for Welded Steel Joins". In: *Welding Institute Research Bulletin* 17, pp. 115–124. (Cited on p. 98).

Hamida, Z. and Goulet, J.-A. (2020). "Modeling infrastructure degradation from visual inspections using network-scale state-space models". In: *Structural Control and Health Monitoring* 27.9, e2582. ISSN: 1545-2255. (Cited on p. 72).

Harris, D. O. and Lim, E. Y. (1983). "Applications of a probabilistic fracture mechanics model to the influence of in-service inspection on structural reliability". In: *Probabilistic Fracture Mechanics and Fatigue Methods: Applications for Structural Design and Maintenance*. ASTM International, pp. 19–41. (Cited on p. 62).

Hayward, G., Pearson, J., and Stirling, G. (1993). "An intelligent ultrasonic inspection system for flooded member detection in offshore structures". In: *IEEE transactions on ultrasonics, ferroelectrics, and frequency control* 40.5, pp. 512–521. ISSN: 0885-3010. (Cited on p. 70).

Hazra, I., Pandey, M. D., and Jyrkama, M. I. (2020a). "Estimation of Flow-Accelerated Corrosion Rate in Nuclear Piping System". In: *Journal of Nuclear Engineering and Radiation Science* 6.1. ISSN: 2332-8983 2332-8975. (Cited on pp. 131, 132, 147, 156, 189).

Hazra, I., Pandey, M. D., and Manzana, N. (2020b). "Approximate Bayesian computation (ABC) method for estimating parameters of the gamma process using noisy data". In: *Reliability Engineering & System Safety* 198, p. 106780. ISSN: 09518320. (Cited on p. 141).

He, D., Lee, L. H., Chen, C.-H., Fu, M. C., and Wasserkrug, S. (2010). "Simulation optimization using the cross-entropy method with optimal computing budget allocation". In: *ACM Transactions on Modeling and Computer Simulation (TOMACS)* 20.1, p. 4. ISSN: 1049-3301. (Cited on p. 58).

Heasler, P. G. and Doctor, S. R. (1996). *Piping inspection round robin*. Report. U.S. Nuclear Regulatory Commission, Washington, DC (United States).. (Cited on p. 67).

Hellevik, S., Langen, I., and Sørensen, J. D. (1999). "Cost optimal reliability based inspection and replacement planning of piping subjected to CO2 corrosion". In: *International Journal of Pressure Vessels and Piping* 76.8, pp. 527–538. ISSN: 0308-0161. (Cited on p. 131).

Hill, S. D. (2013). "Discrete Optimization with Noisy Objective Function Measurements". In: *Wiley Encyclopedia of Operations Research and Management Science*. ISSN: 0470400536. (Cited on p. 54).

Hobbacher, A. (2015). *Recommendations for fatigue design of welded joints and components*. Springer. ISBN: 3319237578. (Cited on p. 98).

Hohenbichler, M. and Rackwitz, R. (1981). "Non-normal dependent vectors in structural safety". In: *Journal of the Engineering Mechanics Division* 107.6, pp. 1227–1238. ISSN: 0044-7951. (Cited on p. 107).

Holdorf Lopez, R., Bismut, E., and Straub, D. (2022). "Stochastic efficient global optimization with high noise variance and mixed design variables". In: *Journal of the Brazilian Society of Mechanical Sciences and Engineering* 45.1, p. 7. ISSN: 1806-3691. (Cited on pp. vii, 57, 58, 160).

Hong, H. P. (1997). "Reliability analysis with nondestructive inspection". In: *Structural Safety* 19.4, pp. 383–395. ISSN: 0167-4730. (Cited on p. 62).

Hovey, P. W. and Berens, A. P. (1988). "Statistical evaluation of NDE reliability in the aerospace industry". In: *Review of Progress in Quantitative Nondestructive Evaluation*. Springer, pp. 1761–1768. (Cited on pp. 61, 62, 66).

Howard, R. A. (1960). *Dynamic programming and Markov Processes*. Technology Press and Wiley New York, VII, 136 S.. (Cited on pp. 3, 20, 25).

Hu, J., Fu, M. C., and Marcus, S. I. (2008). "A model reference adaptive search method for stochastic global optimization". In: *Communications in Information & Systems* 8.3, pp. 245–276. ISSN: 1526-7555. (Cited on pp. 56, 58).

Hu, J., Fu, M. C., and Marcus, S. I. (n.d.). "A model reference adaptive search method for stochastic optimization with applications to Markov decision processes". In: *2007 46th IEEE Conference on Decision and Control*. IEEE, pp. 975–980. ISBN: 1424414970. (Cited on p. 56).

International Atomic Energy Agency (1965). *Non-Destructive Testing in Nuclear Technology Vol I Proceedings of a Symposium on Non-Destructive Testing in Nuclear Technology*.

(Austria). International Atomic Energy Agency (IAEA): IAEA. ISBN: 0074-1884. (Cited on p. 62).

Irving, P. E. and McCartney, L. N. (1977). "Prediction of fatigue crack growth rates: theory, mechanisms, and experimental results". In: *Metal Science* 11.8-9, pp. 351–361. ISSN: 0306-3453. (Cited on pp. 1, 100).

Jarvis, R., Cawley, P., and Nagy, P. B. (2018). "Permanently installed corrosion monitoring using magnetic measurement of current deflection". In: *Structural Health Monitoring* 17.2, pp. 227–239. ISSN: 1475-9217. (Cited on p. 68).

JCSS (2001). "Probabilistic model code". In: *Joint Committee on Structural Safety*. (Cited on pp. 24, 99, 186).

Jensen, F. V., Nielsen, T. D., and Nielsen, T. D. (2007). *Bayesian Networks and Decision Graphs*. 2nd ed. Information Science and Statistics. Springer New York. (Cited on pp. 14, 21).

Jonge, B. de, Teunter, R., and Tinga, T. (2017). "The influence of practical factors on the benefits of condition-based maintenance over time-based maintenance". In: *Reliability Engineering & System Safety* 158, pp. 21–30. ISSN: 0951-8320. (Cited on p. 117).

Jonge, B. de and Scarf, P. A. (2020). "A review on maintenance optimization". In: *European journal of operational research* 285.3, pp. 805–824. ISSN: 0377-2217. (Cited on p. 130).

Kaelbling, L. P., Littman, M. L., and Cassandra, A. R. (1998). "Planning and acting in partially observable stochastic domains". In: *Artificial intelligence* 101.1-2, pp. 99–134. ISSN: 0004-3702. (Cited on pp. 3, 25, 27, 28, 35, 160).

Kahn, G., Zhang, T., Levine, S., and Abbeel, P. (2017). "Plato: Policy learning using adaptive trajectory optimization". In: *2017 IEEE International Conference on Robotics and Automation (ICRA)*, pp. 3342–3349. ISBN: 150904633X. (Cited on p. 43).

Kamariotis, A., Chatzi, E., and Straub, D. (2022). "Value of information from vibration-based structural health monitoring extracted via Bayesian model updating". In: *Mechanical Systems and Signal Processing* 166, p. 108465. ISSN: 0888-3270. (Cited on pp. 25, 44, 73).

Ken-Iti, S. (1999). *Lévy processes and infinitely divisible distributions*. Cambridge university press. ISBN: 0521553024. (Cited on p. 100).

Kerntechnischer Ausschuss (2016). *Safety Standards of the Nuclear Safety Standards Commission (KTA)*. Standard. (Cited on p. 73).

Kessler, S. and Gehlen, C. (2017). "Reliability evaluation of half-cell potential measurement using POD". In: *Journal of Infrastructure Systems* 23.2, B4016007. ISSN: 1076-0342. (Cited on p. 82).

King, R. N. (1998). *A review of fatigue crack growth rates in air and seawater*. Health and Safety Executive Norwich, UK. ISBN: 0717624137. (Cited on p. 1).

Knight, F. H. (1921). *Risk, uncertainty and profit*. Boston; New York: Houghton Mifflin Company. (Cited on p. 16).

Kochenderfer, M. J. (2015). *Decision making under uncertainty: theory and application*. MIT press. ISBN: 0262029251. (Cited on pp. 2, 3, 14, 19, 23, 25, 29, 31–33, 35, 36, 54).

Konakli, K. and Faber, M. H. (2014). "Value of information analysis in structural safety". In: *Vulnerability, Uncertainty, and Risk: Quantification, Mitigation, and Management*, pp. 1605–1614. (Cited on p. 19).

Kübler, O. and Faber, M. H. (2004). "Optimality and Acceptance Criteria in Offshore Design". In: *Journal of Offshore Mechanics and Arctic Engineering* 126.3, pp. 258–264. ISSN: 0892-7219. (Cited on p. 49).

Kumar, P. R. (1985). "A survey of some results in stochastic adaptive control". In: *SIAM Journal on Control and Optimization* 23.3, pp. 329–380. ISSN: 0363-0129. (Cited on p. 36).

Kurniawati, H., Hsu, D., and Lee, W. S. (2008). "SARSOP: Efficient point-based POMDP planning by approximating optimally reachable belief spaces". In: *Robotics: Science and systems*. Citeseer. (Cited on p. 33).

Kurz, J. H., Jüngert, A., Dugan, S., and Dobmann, G. (2012). "Probability of Detection (POD) determination using ultrasound phased array for considering NDT in probabilistic damage assessments". In: *South-African Institute for Non-destructive Testing: World Conference on Nondestructive Testing (18), WCNDT*. Citeseer. (Cited on pp. 64, 66, 72, 90).

Lam, C. T. and Yeh, R. H. (1994). "Optimal maintenance-policies for deteriorating systems under various maintenance strategies". In: *IEEE Transactions on reliability* 43.3, pp. 423–430. ISSN: 0018-9529. (Cited on pp. 4, 40, 101).

Lavender, J. D. (1976). *Ultrasonic testing of steel castings*. Steel Founders' Society of America. (Cited on p. 65).

Lawless, J. and Crowder, M. (2004). "Covariates and random effects in a gamma process model with application to degradation and failure". In: *Lifetime data analysis* 10.3, pp. 213–227. ISSN: 1380-7870. (Cited on pp. 140, 145).

Lentz, A., Faber, M. H., and Johnsen, T. (2002). "Half-cell potential measurements for condition assessment". In: *Proceeding of 1st International Conference on Bridge Maintenance*. (Cited on pp. 61, 82, 83).

Li, H., Deloux, E., and Dieulle, L. (2016). "A condition-based maintenance policy for multi-component systems with Lévy copulas dependence". In: *Reliability Engineering & System Safety* 149, pp. 44–55. ISSN: 0951-8320. (Cited on pp. 131, 138).

Lin, Y. K. and Yang, J. N. (1985). "A stochastic theory of fatigue crack propagation". In: *AIAA journal* 23.1, pp. 117–124. ISSN: 0001-1452. (Cited on p. 100).

Lister, D. H. and Lang, L. C. (2002). "A mechanistic model for predicting flow-assisted and general corrosion of carbon steel in reactor primary coolants". In: *Proc. Chimie*, pp. 22–26. (Cited on p. 140).

Lister, D. H., Slade, J., and Arbeau, N. (1997). "Accelerated corrosion of CANDU outlet feeders- observations, possible mechanisms and potential remedies". In: *Proceedings- Annual Conference, Canadian Nuclear Association*. ISBN: 0227-1907. (Cited on pp. 129, 130, 147).

Luce, R. D. and Raiffa, H. (1989). *Games and decisions: Introduction and critical survey*. Dover Publications Inc. ISBN: 0486659437. (Cited on pp. 2, 12, 13, 16, 17).

Luque, J. and Straub, D. (2013). "Algorithms for optimal risk-based planning of inspections using influence diagrams". In: *Proceedings of the 11th International Probabilistic Workshop*. (Cited on pp. 4, 37, 45).

Luque, J. and Straub, D. (2016). "Reliability analysis and updating of deteriorating systems with dynamic Bayesian networks". In: *Structural Safety* 62, pp. 34–46. ISSN: 0167-4730. (Cited on pp. 4, 5, 32, 40, 101, 102, 107–110, 112, 113, 117, 119, 157, 175, 185).

Luque, J. and Straub, D. (2019). "Risk-based optimal inspection strategies for structural systems using dynamic Bayesian networks". In: *Structural Safety* 76, pp. 68–80. ISSN: 0167-4730. (Cited on pp. 4, 40, 48, 54, 108, 157).

Madsen, H. O. (1987). "Model updating in reliability theory". In: *Proc. ICASP5*. Vancouver, Canada, pp. 565–577. (Cited on p. 16).

Madsen, H. O., Skjong, R. K., and Tallin, A. G. (1987). "Probabilistic fatigue crack growth analysis of offshore structures, with reliability updating through inspection". In: *Marine Structural Reliability Engineering Symposium*, pp. 45–55. (Cited on pp. 62, 100, 101).

Malings, C. and Pozzi, M. (2016). "Conditional entropy and value of information metrics for optimal sensing in infrastructure systems". In: *Structural Safety* 60, pp. 77–90. ISSN: 0167-4730. (Cited on p. 19).

Mansour, A., Wirsching, P., White, G., and Ayyub, B. (1996). *Probability-Based Ship Design: Implementation of Design Guidelines*. Report. Ship Structure Committee. (Cited on p. 99).

Melchers, R. E. (2003a). "Modeling of marine immersion corrosion for mild and low-alloy steels—Part 1: Phenomenological model". In: *Corrosion* 59.4, pp. 319–334. ISSN: 0010-9312. (Cited on pp. 1, 2, 100).

Melchers, R. E. (2003b). "Probabilistic model for marine corrosion of steel for structural reliability assessment". In: *Journal of Structural Engineering* 129.11, pp. 1484–1493. ISSN: 0733-9445. (Cited on p. 97).

Melchers, R. E. and Beck, A. T. (2018). *Structural reliability analysis and prediction*. John Wiley & Sons. ISBN: 1119265991. (Cited on p. 95).

Memarzadeh, M. and Pozzi, M. (2016). "Value of Information in Sequential Decision Making: component inspection, permanent monitoring and system-level scheduling". In: *Reliability Engineering & System Safety* 154, pp. 137–151. ISSN: 0951-8320. (Cited on pp. 3, 36).

Memarzadeh, M., Pozzi, M., and Kolter, J. Z. (2016). "Hierarchical modeling of systems with similar components: A framework for adaptive monitoring and control". In: *Reliability Engineering & System Safety* 153, pp. 159–169. ISSN: 0951-8320. (Cited on p. 37).

Mendoza, J., Bismut, E., Straub, D., and Köhler, J. (2021). "Risk-Based Fatigue Design Considering Inspections and Maintenance". In: *ASCE-ASME Journal of Risk and Uncertainty in Engineering Systems, Part A: Civil Engineering* 7.1, p. 04020055. ISSN: 2376-7642. (Cited on pp. viii, 24).

Mendoza, J., Köhler, J., Bismut, E., and Straub, D. (2019). "Integrated Life-cycle Decision Framework for Structural Systems". In: *Structural Health Monitoring 2019*. (Cited on p. viii).

Mendoza, J., Bismut, E., Straub, D., and Köhler, J. (2022). "Optimal life-cycle mitigation of fatigue failure risk for structural systems". In: *Reliability Engineering & System Safety* 222, p. 108390. ISSN: 0951-8320. (Cited on pp. viii, 114, 160).

Miner, M. A. (1945). "Cumulative fatigue damage". In: *Journal of applied mechanics* 12.3, A159–A164. (Cited on pp. 98, 99, 186).

Mnih, V., Kavukcuoglu, K., Silver, D., Graves, A., Antonoglou, I., Wierstra, D., and Riedmiller, M. (2013). "Playing Atari with Deep Reinforcement Learning". In: *arXiv preprint arXiv:1312.5602*. (Cited on pp. 31, 34, 36).

Moan, T. (2005). "Reliability-based management of inspection, maintenance and repair of offshore structures". In: *Structure and Infrastructure Engineering* 1.1, pp. 33–62. ISSN: 1573-2479. (Cited on pp. 4, 40, 101, 102).

Moan, T. and Song, R. (2000). "Implications of inspection updating on system fatigue reliability of offshore structures". In: *Journal of Offshore Mechanics and Arctic Engineering* 122.3, pp. 173–180. ISSN: 0892-7219. (Cited on p. 185).

Montgomery, W. H. and Levine, S. (2016). "Guided policy search via approximate mirror descent". In: *Advances in Neural Information Processing Systems*, pp. 4008–4016. (Cited on p. 35).

Morgese, M., Ansari, F., Domaneschi, M., and Cimellaro, G. P. (2020). "Post-collapse analysis of Morandi's Polcevera viaduct in Genoa Italy". In: *Journal of Civil Structural Health Monitoring* 10.1, pp. 69–85. ISSN: 2190-5479. (Cited on pp. 3, 99).

Murakami, Y., Takagi, T., Wada, K., and Matsunaga, H. (2021). "Essential structure of SN curve: Prediction of fatigue life and fatigue limit of defective materials and nature of scatter". In: *International Journal of Fatigue* 146, p. 106138. ISSN: 0142-1123. (Cited on pp. 98, 99).

Nath, S. (2021). "Estimates of probability of detection and sizing of flaws in ultrasonic time of flight diffraction inspections for complex geometry components with grooved surfaces". In: *Journal of Nondestructive Evaluation, Diagnostics and Prognostics of Engineering Systems* 4.2, p. 021003. ISSN: 2572-3901. (Cited on p. 66).

National Center for Environmental Economics (2010). *Guidelines for Preparing Economic Analyses*. Government Document. (Cited on p. 24).

National Materials Advisory Board (1969). *Nondestructive evaluation*. Report NMAB-252. (Cited on p. 62).

Nelson, W. B. (2009). *Accelerated testing: statistical models, test plans, and data analysis*. Vol. 344. John Wiley & Sons. ISBN: 0470317477. (Cited on p. 98).

Newman Jr, J. C. (1998). "The merging of fatigue and fracture mechanics concepts: a historical perspective". In: *Progress in Aerospace Sciences* 34.5-6, pp. 347–390. ISSN: 0376-0421. (Cited on pp. 1, 2).

Ng, A. Y., Parr, R., and Koller, D. (2000). "Policy search via density estimation". In: *Advances in Neural Information Processing Systems*, pp. 1022–1028. (Cited on p. 34).

Nie, X., Tian, X., Taylor, J., and Zou, J. (2018). "Why adaptively collected data have negative bias and how to correct for it". In: *International Conference on Artificial Intelligence and Statistics*. PMLR, pp. 1261–1269. ISBN: 2640-3498. (Cited on pp. 52, 143).

Nielsen, J. J. and Sørensen, J. D. (2010a). "Bayesian networks as a decision tool for O&M of offshore wind turbines". In: *Proceedings of the 5th international ASRANet conference*. (Cited on p. 45).

Nielsen, J. J. and Sørensen, J. D. (2010b). "Risk-based operation and maintenance planning for offshore wind turbines". In: *Proceedings of the Reliability and Optimization of Structural Systems*, pp. 7–10. (Cited on pp. 1, 45, 47).

Nielsen, J. J. and Sørensen, J. D. (2011). "Risk-based operation and maintenance of offshore wind turbines using Bayesian networks". In: *The 11th International Conference on Applications of Statistics and Probability in Civil Engineering*. CRC Press, pp. 311–317. ISBN: 0415669863. (Cited on p. 4).

Nielsen, J. S. and Sørensen, J. D. (2014). "Methods for risk-based planning of O&M of wind turbines". In: *Energies* 7.10, pp. 6645–6664. (Cited on pp. 3, 4, 40, 42, 101).

Nielsen, J. S. and Sørensen, J. D. (2015). "Risk-based decision making for deterioration processes using POMDP". In: *ICASP12 International Conference on Applications of Statistics and Probability in Civil Engineering*. (Cited on pp. 1, 31, 36, 37, 40).

Nielsen, J. S. and Sørensen, J. D. (2018). "Computational framework for risk-based planning of inspections, maintenance and condition monitoring using discrete Bayesian networks". In: *Structure and Infrastructure Engineering* 14.8, pp. 1082–1094. ISSN: 1573-2479. (Cited on p. 108).

Noortwijk, J. M. van (2009). "A survey of the application of gamma processes in maintenance". In: *Reliability Engineering & System Safety* 94.1, pp. 2–21. ISSN: 0951-8320. (Cited on p. 100).

Olin, B. D. and Meeker, W. Q. (1996). "Applications of statistical methods to nondestructive evaluation". In: *Technometrics* 38.2, pp. 95–112. ISSN: 0040-1706. (Cited on p. 67).

Onoufriou, T. and Frangopol, D. M. (2002). "Reliability-based inspection optimization of complex structures: a brief retrospective". In: *Computers & Structures* 80.12, pp. 1133–1144. ISSN: 0045-7949. (Cited on pp. 16, 131).

Onoufriou, T. (1999). "Reliability based inspection planning of offshore structures". In: *Marine structures* 12.7-8, pp. 521–539. ISSN: 0951-8339. (Cited on p. 131).

Packman, P. F., Pearson, H. S., Owens, J. S., and Marchese, G. B. (1968). *The Applicability of a Fracture Mechanics-Nondestructive Testing Design Criterion*. Report. Lockheed-Georgia Company Material Sciences Research Laboratory. (Cited on pp. 61–63, 67).

Pakrashi, V., Schoefs, F., Memet, J. B., and O'Connor, A. (2010). "ROC dependent event isolation method for image processing based assessment of corroded harbour structures". In: *Structures & Infrastructure Engineering* 6.3, pp. 365–378. ISSN: 1573-2479. (Cited on p. 68).

Palmgren, A. (1924). "Die Lebensdauer von Kugellagern". In: *Zeitschrift des Vereines Deutscher Ingenieure* 68.4, pp. 339–341. (Cited on pp. 97, 98, 186).

Pandey, M. D., Yuan, X.-X., and Van Noortwijk, J. M. (2009). "The influence of temporal uncertainty of deterioration on life-cycle management of structures". In: *Structure and Infrastructure Engineering* 5.2, pp. 145–156. ISSN: 1573-2479. (Cited on p. 100).

Papadimitriou, C. H. and Tsitsiklis, J. N. (1987). "The complexity of Markov decision processes". In: *Mathematics of operations research* 12.3, pp. 441–450. ISSN: 0364-765X. (Cited on pp. 3, 29, 35).

Papakonstantinou, K. G., Andriotis, C. P., and Shinozuka, M. (2018). "POMDP and MOMDP solutions for structural life-cycle cost minimization under partial and mixed observability". In: *Structure and Infrastructure Engineering* 14.7, pp. 869–882. ISSN: 1573-2479. (Cited on pp. 3, 37).

Papakonstantinou, K. G. and Shinozuka, M. (2014). "Optimum inspection and maintenance policies for corroded structures using partially observable Markov decision processes and stochastic, physically based models". In: *Probabilistic Engineering Mechanics* 37, pp. 93–108. ISSN: 0266-8920. (Cited on pp. 3, 30, 36, 37, 112).

Paris, P. and Erdogan, F. (1963). "A critical analysis of crack propagation laws". In: ISSN: 0021-9223. (Cited on p. 100).

Pavlovic, M., Takahashi, K., Müller, C., Boehm, R., and Ronneteg, U. (2008). *Reliability in non-destructive testing (NDT) of the canister components. NDT Reliability — Final Report.* Report. SKB Technical report R-08-129, ISSN 1402-3091, Swedish Nuclear Fuel and Waste Management Co. (Cited on p. 62).

Peterson, W. W. and Birdsall, T. G. (1953). *The theory of signal detectability: Part I. The general theory.* Report. Technical Report 13, June 1953. Electronic Defense Group, University of Michigan. (Cited on pp. 62, 75).

Pineau, J., Gordon, G., and Thrun, S. (2006). "Anytime point-based approximations for large POMDP". In: *Journal of Artificial Intelligence Research* 27, pp. 335–380. ISSN: 1076-9757. (Cited on pp. 27, 29, 33).

Polya, G. (2004). *How to solve it: A new aspect of mathematical method.* Vol. 85. Princeton university press. ISBN: 069111966X. (Cited on p. 59).

Pooya, A. and Pakdaman, M. (2018). "Optimal control model for finite capacity continuous MRP with deteriorating items". In: *Journal of Intelligent Manufacturing* 30.5, pp. 1–13. ISSN: 0956-5515. (Cited on p. 43).

Porta, J. M., Spaan, M. T. J., and Vlassis, N. (2004). *Value iteration for continuous-state POMDPs.* Report Technical report IAS-UVA-04-04. University of Amsterdam, Amsterdam, Netherlands. (Cited on pp. 31, 36).

Porta, J. M., Spaan, M. T. J., and Vlassis, N. (2005). "Robot planning in partially observable continuous domains". In: *Proc. Robotics: Science and Systems*, pp. 217–224. (Cited on pp. 31, 36).

Poupart, P., Vlassis, N., Hoey, J., and Regan, K. (2006). "An analytic solution to discrete Bayesian reinforcement learning". In: *Proceedings of the 23rd international conference on Machine learning*, pp. 697–704. (Cited on p. 32).

Pourmoayed, R. and Nielsen, L. R. (2019). "An approximate dynamic programming approach for sequential pig marketing decisions at herd level". In: *European Journal of Operational Research* 276.3, pp. 1056–1070. ISSN: 0377-2217. (Cited on pp. 10, 59).

Powell, W. B. (2011). *Approximate dynamic programming: Solving the curses of dimensionality.* Hoboken, United States: John Wiley & Sons, Incorporated. ISBN: 9781118029152. (Cited on pp. 2, 33, 34).

Pozzi, M. and Der Kiureghian, A. (2011). "Assessing the value of information for long-term structural health monitoring". In: *Health monitoring of structural and biological systems 2011.* Vol. 7984. International Society for Optics and Photonics, 79842W. (Cited on p. 17).

Prigogine, I. (1978). "Time, structure, and fluctuations". In: *Science*, pp. 777–785. ISSN: 0036-8075. (Cited on p. 96).

Quirk, L., Matos, J., Murphy, J., and Pakrashi, V. (2018). "Visual inspection and bridge management". In: *Structure and Infrastructure Engineering* 14.3, pp. 320–332. ISSN: 1573-2479. (Cited on pp. 63, 70).

Raiffa, H. and Schlaifer, R. (1961). *Applied Statistical Decision Theory*. Harvard Business Review Press. (Cited on pp. 1–3, 10, 12, 13, 16, 17, 19, 20, 25, 73).

Rajesh, S. N. (1993). *Probability of detection models for eddy current NDE methods*. Report. Ames Lab., IA (United States). (Cited on pp. 69, 72).

Rasmussen, C. E. (2004). "Gaussian processes in machine learning". In: *Advanced lectures on machine learning*. Springer, pp. 63–71. (Cited on pp. 54, 57).

Rausand, M. and Høyland, A. (2004). *System reliability theory: models, statistical methods, and applications*. Vol. 396. John Wiley & Sons. ISBN: 047147133X. (Cited on pp. 47, 93, 94, 105).

Ritz, C., Baty, F., Streibig, J. C., and Gerhard, D. (2015). "Dose-response analysis using R". In: *PloS ONE* 10.12. (Cited on pp. 62, 66).

Robert, C. P. (2007). *The Bayesian choice: from decision-theoretic foundations to computational implementation*. 2nd. Springer texts in statistics. Springer. (Cited on p. 144).

Röckmann, C., Lagerveld, S., and Stavenuiter, J. (2017). "Operation and Maintenance Costs of Offshore Wind Farms and Potential Multi-use Platforms in the Dutch North Sea". In: *Aquaculture Perspective of Multi-Use Sites in the Open Ocean: The Untapped Potential for Marine Resources in the Anthropocene*. Cham: Springer International Publishing, pp. 97–113. ISBN: 978-3-319-51159-7. (Cited on p. 1).

Rosenfield, D. (1976). "Markovian deterioration with uncertain information—a more general model". In: *Naval Research Logistics Quarterly* 23.3, pp. 389–405. ISSN: 0028-1441. (Cited on p. 105).

Rosenstein, M. T. and Barto, A. G. (2001). "Robot weightlifting by direct policy search". In: *International Joint Conference on Artificial Intelligence*. Vol. 17. Citeseer, pp. 839–846. ISBN: 1045-0823. (Cited on p. 34).

Ross, S., Chaib-draa, B., and Pineau, J. (2007). "Bayes-Adaptive POMDPs". In: *NIPS*, pp. 1225–1232. (Cited on p. 32).

Ross, S., Pineau, J., Chaib-draa, B., and Kreitmann, P. (2011). "A Bayesian Approach for Learning and Planning in Partially Observable Markov Decision Processes". In: *Journal of Machine Learning Research* 12.5. ISSN: 1532-4435. (Cited on pp. 18, 30).

Rouhan, A. and Schoefs, F. (2003). "Probabilistic modeling of inspection results for offshore structures". In: *Structural Safety* 25.4, pp. 379–399. ISSN: 0167-4730. (Cited on p. 72).

Roy, N., Gordon, G., and Thrun, S. (2005). "Finding approximate POMDP solutions through belief compression". In: *Journal of artificial intelligence research* 23, pp. 1–40. ISSN: 1076-9757. (Cited on pp. 31, 36).

Rubinstein, R. Y. and Kroese, D. P. (2004). *The cross-entropy method: a unified approach to combinatorial optimization, Monte-Carlo simulation and machine learning*. Springer Science & Business Media. ISBN: 1475743211. (Cited on pp. 54, 55).

Rubinstein, R. Y. and Kroese, D. P. (2017). *Simulation and the Monte Carlo method*. 3rd ed. Wiley series in probability and statistics. Hoboken, New Jersey: Wiley, xvii, 414 pages. ISBN: 9781118632161. (Cited on pp. 5, 40).

Rudemo, M., Ruppert, D., and Streibig, J. (1989). "Random effect models in nonlinear regression with applications to bioassay". In: *Biometrics* 45.2, pp. 349–362. (Cited on pp. 62, 66).

Rummery, G. A. and Niranjan, M. (1994). *On-line Q-learning using connectionist systems*. Vol. 37. Citeseer. (Cited on p. 34).

Russell, S. J. and Norvig, P. (2016). *Artificial intelligence: a modern approach*. Malaysia; Pearson Education Limited. (Cited on p. 59).

Sagrilo, L. V. S., Castro Prates de Lima, E., Cunha Dias Henriques, C., and Hormazabal Rodriguez, S. G. (1997). "Reliability-based fatigue inspection planning of fixed offshore structures". In: *WIT Transactions on The Built Environment* 32. ISSN: 1853125377. (Cited on pp. 131, 134).

Sarkar, P., Meeker, W. Q., Thompson, R. B., Gray, T. A., and Junker, W. (1998). "Probability of detection modeling for ultrasonic testing". In: *Review of Progress in Quantitative Nondestructive Evaluation*. Ed. by D. C. D.O. Thompson. Vol. 17. Springer, pp. 2045–2052. (Cited on pp. 61, 66, 67).

Särkkä, S. (2013). *Bayesian filtering and smoothing*. Vol. 3. Cambridge University Press. ISBN: 110703065X. (Cited on p. 110).

Schneider, R. (2019). "Effect of repair models on risk based optimal inspection strategies for support structures of offshore wind turbines". In: *Fifth Conference on Smart Monitoring, Assessment and Rehabilitation of Civil Structures (SMAR19)*. (Cited on pp. 52, 117).

Schneider, R., Thöns, S., and Straub, D. (2017). "Reliability analysis and updating of deteriorating systems with subset simulation". In: *Structural Safety* 64, pp. 20–36. ISSN: 0167-4730. (Cited on pp. 52, 102, 107, 112, 113, 117, 118).

Schöbi, R. and Chatzi, E. N. (2016). "Maintenance planning using continuous-state partially observable Markov decision processes and non-linear action models". In: *Structure and Infrastructure Engineering* 12.8, pp. 977–994. ISSN: 1573-2479. (Cited on pp. 3, 31, 33, 36, 37, 159).

Schoefs, F., Boéro, J., Clément, A., and Capra, B. (2012). "The αδ method for modelling expert judgement and combination of non-destructive testing tools in risk-based inspection context: application to marine structures". In: *Structure and Infrastructure Engineering* 8.6, pp. 531–543. ISSN: 1573-2479. (Cited on pp. 68, 69).

Schoefs, F. and Clement, A. (2004). "Multiple inspection modeling for decision making and management of jacket off-shore platforms: effect of false alarms". In: *International Forum on Engineering Decision Making, Switzerland*. (Cited on p. 78).

Shafiee, M., Finkelstein, M., and Bérenguer, C. (2015). "An opportunistic condition-based maintenance policy for offshore wind turbine blades subjected to degradation and environmental shocks". In: *Reliability Engineering & System Safety* 142, pp. 463–471. ISSN: 0951-8320. (Cited on pp. 99, 100).

Shani, G., Pineau, J., and Kaplow, R. (2013). "A survey of point-based POMDP solvers". In: *Autonomous Agents and Multi-Agent Systems* 27.1, pp. 1–51. ISSN: 1387-2532. (Cited on p. 33).

Shannon, C. E. (1948). "A mathematical theory of communication". In: *Bell system technical journal* 27.3, pp. 379–423. ISSN: 0005-8580. (Cited on pp. 62, 63).

Sheils, E., O'Connor, A., Schoefs, F., and Breysse, D. (2012). "Investigation of the effect of the quality of inspection techniques on the optimal inspection interval for structures". In: *Structure and Infrastructure Engineering* 8.6, pp. 557–568. ISSN: 1573-2479. (Cited on pp. 62, 67, 71).

Sheils, E., O'Connor, A., Breysse, D., Schoefs, F., and Yotte, S. (2010). "Development of a two-stage inspection process for the assessment of deteriorating infrastructure". In: *Reliability Engineering & System Safety* 95.3, pp. 182–194. ISSN: 0951-8320. (Cited on pp. 63, 68, 70, 72).

Silva, R. R. da and Padua, G. X. de (2012). "Nondestructive inspection reliability: state of the art". In: *Nondestructive Testing Methods and New Applications*, p. 1. ISSN: 9535101080. (Cited on pp. 66, 70, 90).

Silver, D. and Veness, J. (2010). "Monte-Carlo planning in large POMDPs". In: *Advances in neural information processing systems*, pp. 2164–2172. (Cited on pp. 31, 33, 34, 36, 43).

Silver, D. et al. (2017). "Mastering the game of Go without human knowledge". In: *Nature* 550.7676, pp. 354–359. ISSN: 1476-4687. (Cited on p. 34).

Simon, H. A. and Newell, A. (1958). "Heuristic problem solving: The next advance in operations research". In: *Operations research* 6.1, pp. 1–10. ISSN: 0030-364X. (Cited on p. 160).

Sindel, R. and Rackwitz, R. (1996). "Calculation of the failure probability and inspection optimization for cracks in ships". In: *Technische Universität München*. (Cited on p. 16).

Singh, R. (2000). "Three decades of NDI reliability assessment". In: *Contract* 41608.99-C, p. 404. (Cited on p. 62).

Smallwood, R. D. and Sondik, E. J. (1973). "The optimal control of partially observable Markov processes over a finite horizon". In: *Operations research* 21.5, pp. 1071–1088. ISSN: 0030-364X. (Cited on pp. 30, 36).

Somoza, E., Mossman, D., and McFeeters, L. (1990). "The INFO-ROC technique: a method for comparing and optimizing inspection systems". In: *Review of Progress in Quantitative Nondestructive Evaluation*. Springer, pp. 601–608. (Cited on p. 61).

Sondik, E. J. (1971). *The optimal control of partially observable Markov processes*. Report. Stanford Univ Calif Stanford Electronics Labs. (Cited on pp. 27, 29).

Sørensen, J. D. and Faber, M. H. (2001). "Reliability-based optimal planning of maintenance and inspection". In: *Life-Cycle Cost Analysis and Design of Civil Infrastructure Systems*, pp. 271–298. (Cited on p. 131).

Southwell, C. R., Bultman, J. D., and Hummer, C. W. (1979). "Estimating service life of steel in seawater". In: *Seawater corrosion handbook* 87, p. 374. (Cited on p. 2).

Spall, J. C. (2012). "Stochastic optimization". In: *Handbook of computational statistics*. Springer, pp. 173–201. (Cited on p. 54).

Strack, G. and Pochet, Y. (2010). "An integrated model for warehouse and inventory planning". In: *European Journal of Operational Research* 204.1, pp. 35–50. ISSN: 0377-2217. (Cited on pp. 10, 59).

Straub, D. (2004). *Generic approaches to risk based inspection planning for steel structures*. Vol. 284. vdf Hochschulverlag AG. ISBN: 3728129690. (Cited on pp. 1–4, 13, 24, 40, 62, 67, 72, 99, 101, 102, 105, 118, 119, 186).

Straub, D. (2009). "Stochastic modeling of deterioration processes through dynamic Bayesian networks". In: *Journal of Engineering Mechanics* 135.10, pp. 1089–1099. ISSN: 0733-9399. (Cited on pp. 4, 40, 101, 106, 108–110, 113, 175, 182, 185).

Straub, D. (2011). "Reliability updating with equality information". In: *Probabilistic Engineering Mechanics* 26.2, pp. 254–258. ISSN: 0266-8920. (Cited on p. 16).

Straub, D. (2014). "Value of information analysis with structural reliability methods". In: *Structural Safety* 49, pp. 75–85. ISSN: 0167-4730. (Cited on p. 73).

Straub, D. and Bismut, E. (2019). *Lecture slides: Probabilistic life cycle analysis and integrity management of infrastructures*. Audiovisual Material. (Cited on p. 47).

Straub, D., Bismut, E., Depina, I., and Papaioannou, I. (2021). "Stochastische Optimierung mittels Cross Entropy: Methodik und Anwendungen". In: *Proc. Baustatik-Baupraxis 14*. (Cited on p. viii).

Straub, D. and Der Kiureghian, A. (2011). "Reliability acceptance criteria for deteriorating elements of structural systems". In: *Journal of Structural Engineering* 137.12, pp. 1573–1582. ISSN: 0733-9445. (Cited on pp. 46, 114, 160).

Straub, D. and Faber, M. H. (2004). "On the relation between inspection quantity and quality". In: *e-Journal of Nondestructive Testing*. Vol. 9, pp. 1–14. (Cited on p. 19).

Straub, D. and Faber, M. H. (2005). "Risk based inspection planning for structural systems". In: *Structural safety* 27.4, pp. 335–355. ISSN: 0167-4730. (Cited on pp. 1, 4, 40, 45, 46, 101, 131).

Straub, D. and Faber, M. H. (2006). "Computational aspects of risk-based inspection planning". In: *Computer-Aided Civil and Infrastructure Engineering* 21.3, pp. 179–192. ISSN: 1467-8667. (Cited on pp. 1, 45).

Straub, D. and Papaioannou, I. (2015). "Bayesian updating with structural reliability methods". In: *Journal of Engineering Mechanics* 141.3, p. 04014134. ISSN: 0733-9399. (Cited on pp. 52, 122).

Straub, D., Schneider, R., Bismut, E., and Kim, H.-J. (2020). "Reliability analysis of deteriorating structural systems". In: *Structural Safety* 82, p. 101877. ISSN: 0167-4730. (Cited on pp. viii, 94, 95, 103, 107, 108, 110, 112).

Straub, D., Chatzi, E., Bismut, E., Courage, W., Döhler, M., Faber, M. H., Köhler, J., Lombaert, G., Omenzetter, P., and Pozzi, M. (2017). "Value of information: A roadmap to quantifying the benefit of structural health monitoring". In: *12th International Conference on Structural Safety & Reliability, ICOSSAR 2017*. (Cited on p. viii).

Sun, Q., Ye, Z.-S., and Chen, N. (2017). "Optimal inspection and replacement policies for multi-unit systems subject to degradation". In: *IEEE Transactions on Reliability* 67.1, pp. 401–413. ISSN: 0018-9529. (Cited on pp. 131, 138).

Sutton, R. S. and Barto, A. G. (2018). *Reinforcement learning: An introduction*. MIT press. ISBN: 0262352702. (Cited on p. 2).

Sutton, R. S., McAllester, D. A., Singh, S. P., and Mansour, Y. (2000). "Policy gradient methods for reinforcement learning with function approximation". In: *Advances in neural information processing systems*, pp. 1057–1063. (Cited on pp. 35, 36).

Swets, J. A. (1983). "Assessment of NDT systems. I. The relationship of true and false detections. II. Indices of performance". In: *Materials Evaluation* 41.11, pp. 1294–1303. ISSN: 0025-5327. (Cited on p. 67).

Swets, J. A. (1992). "The science of choosing the right decision threshold in high-stakes diagnostics". In: *American Psychologist* 47.4, p. 522. ISSN: 1935-990X. (Cited on pp. 70, 72).

Szita, I. and Lörincz, A. (2006). "Learning Tetris using the noisy cross-entropy method". In: *Neural computation* 18.12, pp. 2936–2941. ISSN: 0899-7667. (Cited on p. 56).

Taner, T. and Antony, J. (2000). "The assessment of quality in medical diagnostic tests: a comparison of ROC/Youden and Taguchi methods". In: *International Journal of Health Care Quality Assurance*. (Cited on p. 69).

Tang, W. H. (1973). "Probabilistic updating of flaw information". In: *Journal of Testing and Evaluation* 1.6, pp. 459–467. ISSN: 0090-3973. (Cited on p. 16).

Thoft-Christensen, P. and Sørensen, J. D. (1987). "Optimal strategy for inspection and repair of structural systems". In: *Civil Engineering Systems* 4.2, pp. 94–100. ISSN: 0263-0257. (Cited on pp. 1, 4, 40, 45).

Tsang, A. H. C. (1995). "Condition-based maintenance: tools and decision making". In: *Journal of quality in maintenance engineering* 1.3, pp. 3–17. ISSN: 1355-2511. (Cited on p. 42).

Tschöke, K., Mueller, I., Memmolo, V., Moix-Bonet, M., Moll, J., Lugovtsova, Y., Golub, M., Venkat, R. S., and Schubert, L. (2021). "Feasibility of Model-Assisted Probability of Detection Principles for Structural Health Monitoring Systems based on Guided Waves for Fibre-Reinforced Composites". In: *IEEE Transactions on Ultrasonics, Ferroelectrics, and Frequency Control*. ISSN: 0885-3010. (Cited on p. 67).

Virkkunen, I., Koskinen, T., Papula, S., Sarikka, T., and Hänninen, H. (2019). "Comparison of â Versus a and Hit/Miss POD-Estimation Methods: A European Viewpoint". In: *Journal of Nondestructive Evaluation* 38.4, p. 89. ISSN: 0195-9298. (Cited on p. 67).

Viscusi, W. K. and Aldy, J. E. (2003). "The value of a statistical life: a critical review of market estimates throughout the world". In: *Journal of risk and uncertainty* 27.1, pp. 5–76. ISSN: 1573-0476. (Cited on p. 24).

Visser, W. P. (2002). *POD/POS Curves for Non-Destructive Examination*. Report Offshore Technology Report 2000/018. HSE Books, Norwich, United Kingdom. (Cited on pp. 66, 70).

Von Neumann, J. and Morgenstern, O. (1953). *Theory of games and economic behavior*. Princeton university press. (Cited on p. 13).

Vora, J. A. (1974). "Heuristics and Optimizing Techniques Applied to Long Range Facility Planning for Hospital Ancillary Departments". In: *Management Science* 21.4, pp. 409–417. ISSN: 0025-1909 1526-5501. (Cited on pp. 10, 59).

Wald, A. (1947). *Sequential analysis*. John Wiley and Sons. ISBN: 0486439127. (Cited on p. 2).

Walker, Z. (2017). *Third Party Review of EPRI Recommendations for an Effective flow Accelerated Corrosion Program and Their Applicability to CANDU Reactors*. Generic. (Cited on pp. 147, 148).

Wall, M. and Wedgwood, F. (1994). "NDT-value for money". In: *Insight* 36.10, pp. 782–90. ISSN: 1354-2575. (Cited on p. 72).

Walraven, E. and Spaan, M. T. J. (2019). "Point-based value iteration for finite-horizon POMDPs". In: *Journal of Artificial Intelligence Research* 65, pp. 307–341. ISSN: 1076-9757. (Cited on pp. 33, 36).

Wang, T., Lizotte, D., Bowling, M., and Schuurmans, D. (2005). "Bayesian sparse sampling for on-line reward optimization". In: *Proceedings of the 22nd international conference on Machine learning*, pp. 956–963. (Cited on p. 36).

Wang, Y., Li, X., Chen, J., and Liu, Y. (2022). "A condition-based maintenance policy for multi-component systems subject to stochastic and economic dependencies". In: *Reliability Engineering & System Safety* 219, p. 108174. ISSN: 0951-8320. (Cited on pp. 131, 138).

Watkins, C. J. C. H. (1989). "Learning from delayed rewards". In. (Cited on: p. 34).

Webb, G. T., Vardanega, P. J., and Middleton, C. R. (2015). "Categories of SHM deployments: technologies and capabilities". In: *Journal of Bridge Engineering* 20.11, p. 04014118. ISSN: 1084-0702. (Cited on pp. 64, 72).

Wen, Y. K. and Chen, H. C. (1987). "On fast integration for time variant structural reliability". In: *Probabilistic Engineering Mechanics* 2.3, pp. 156–162. ISSN: 0266-8920. (Cited on p. 107).

Williams, R. J. (1992). "Simple statistical gradient-following algorithms for connectionist reinforcement learning". In: *Machine learning* 8.3-4, pp. 229–256. ISSN: 0885-6125. (Cited on p. 34).

Wirsching, P. H. and Chen, Y. N. (1988). "Considerations of probability-based fatigue design for marine structures". In: *Marine Structures* 1.1, pp. 23–45. ISSN: 0951-8339. (Cited on p. 1).

Wood, H. A. and Engle Jr, R. M. (1979). *USAF Damage Tolerant Design Handbook: Guidelines for the analysis and Design of Damage Tolerant Aircraft Structures. Revision A*. Report. Air Force Flight Dynamics Lab Wright-Patterson Air Force Base, Ohio. (Cited on pp. 67, 72).

Woodward, P. M. and Davies, I. L. (1952). "Information theory and inverse probability in telecommunication". In: *Proceedings of the IEE-Part III: Radio and Communication Engineering* 99.58, pp. 37–44. ISSN: 2054-0442. (Cited on p. 62).

Wu, P. C. (1989). *Erosion/corrosion-induced pipe wall thinning in Us nuclear power plants*. Report. US Nuclear Regulatory Commission (NRC), Washington, DC (United States). (Cited on pp. 3, 129).

Xu, J., Huang, E., Chen, C.-H., and Lee, L. H. (2015). "Simulation optimization: A review and exploration in the new era of cloud computing and big data". In: *Asia-Pacific Journal of Operational Research* 32.03, p. 1550019. ISSN: 0217-5959. (Cited on p. 56).

Yang, J. N. (1994). "Application of reliability methods to fatigue, quality assurance and maintenance". In: *Proceedings of ICOSSAR'93, Innsbruck*, pp. 1–21. (Cited on p. 2).

Yang, J. N. and Chen, S. (1985). "Fatigue reliability of gas turbine engine components under scheduled inspection maintenance". In: *Journal of Aircraft* 22.5, pp. 415–422. ISSN: 0021-8669. (Cited on p. 62).

Yang, J.-N. and Trapp, W. J. (1974). "Reliability analysis of aircraft structures under random loading and periodic inspection". In: *AIAA journal* 12.12, pp. 1623–1630. ISSN: 0001-1452. (Cited on p. 62).

Yaron, D. and Horowitz, U. (1972). "Short-and-long run farm planning under uncertainty; Integration of linear programming and decision tree analysis". In: *Canadian Journal of Agricultural Economics/Revue canadienne d'agroéconomie* 20.2, pp. 17–30. ISSN: 0008-3976. (Cited on pp. 10, 59).

Youden, W. J. (1950). "Index for rating diagnostic tests". In: *Cancer* 3.1, pp. 32–35. ISSN: 0008-543X. (Cited on p. 69).

Yuan, X. (2007). "Stochastic modeling of deterioration in nuclear power plant components". Thesis. University of Waterloo, Ontario, Canada. (Cited on pp. 131, 145).

Yuan, X.-X., Pandey, M., and Bickel, G. (2008). "A probabilistic model of wall thinning in CANDU feeders due to flow-accelerated corrosion". In: *Nuclear Engineering and Design* 238.1, pp. 16–24. ISSN: 0029-5493. (Cited on p. 129).

Zayas, V. A. (1980). "Ultimate Earthquake Resistance of Steel Offshore Structures". Thesis. (Cited on p. 117).

Zhou, J., Arshad, S. Z., Luo, S., and Chen, F. (2017). "Effects of uncertainty and cognitive load on user trust in predictive decision making". In: *IFIP conference on human-computer interaction*. Springer, pp. 23–39. (Cited on p. 39).

Zhu, J. and Collette, M. (2015). "A dynamic discretization method for reliability inference in Dynamic Bayesian Networks". In: *Journal of Reliability Engineering System Safety* 138, pp. 242–252. ISSN: 0951-8320. (Cited on pp. 110, 182).

Zhu, W., Fouladirad, M., and Bérenguer, C. (2013). "A predictive maintenance policy based on the blade of offshore wind turbine". In: *IEEE Proceedings of Reliability and Maintainability Symposium (RAMS)*, pp. 1–6. ISBN: 1467347116. (Cited on pp. 105, 114).

Zio, E. and Viadana, G. (2011). "Optimization of the inspection intervals of a safety system in a nuclear power plant by Multi-Objective Differential Evolution (MODE)". In: *Reliability Engineering & System Safety* 96.11, pp. 1552–1563. ISSN: 0951-8320. (Cited on p. 131).